Vysoké učení technické v Brně
Brno University of Technology

Fakulta strojního inženýrství
Ústav konstruování / Odbor tribologie

Faculty of Mechanical Engineering
Institute of Machine and Industrial Design / Department of Tribology

Effect of surface texturing on friction and film thickness under starved lubrication conditions

[Dizertační práce]
[PhD thesis]

Autor práce:Ing.Fadi Ali

Author

Brno 2015

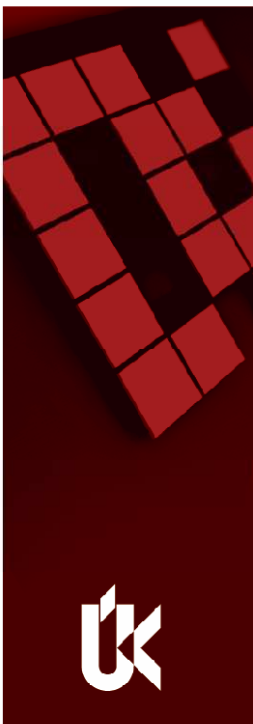

Vysoké učení technické v Brně
Brno University of Technology

Fakulta strojního inženýrství
Ústav konstruování / Odbor tribologie
Faculty of Mechanical Engineering
Institute of Machine and Industrial Design / Department of Tribology

Effect of surface texturing on friction and film thickness under starved lubrication conditions

[Dizertační práce]
[PhD thesis]

Autor práce: **Ing. Fadi Ali**
Author

Vedoucí práce: **prof. Ing. Martin Hartl, Ph.D.**
Supervisor

Brno 2015

ústav konstruování

STATEMENT

I confirm that this PhD thesis is a representation of my original research work, and I have not made use of the work of any other authors without acknowledgement or referencing. The work was done under the supervision of prof. Ing. **Martin Hartl**, Ph.D.

Brno, 15/ 04/ 2015 .....

Fadi ALI

ACKNOWLEDGMENT

I would like to thank my supervisor prof. Martin Hartl and prof. Ivan Křupka for their support and advice during my PhD study. Also, I would like to thank all my colleagues in the Institute of Machine and Industrial Design for their kindness and friendship. Heartfelt thanks for my dear wife Ola. Finally, I express my sincere thanks to prof. Motohiro Kaneta from Japan for his nice contribution in the numerical simulation presented in the thesis.

BIBLIOGRAPHIC CITATION

Fadi Ali, *Effect of surface texturing on friction and film thickness under starved lubrication conditions*. Brno University of Technology, Faculty of Mechanical Engineering, 2015. PhD Thesis 134 pp. Supevisor: prof. Ing. Martin Hartl, Ph.D.

BIBLIOGRAPHICKÁ CITACE

Fadi Ali, *Vliv cílené modifikace topografie na velikost tření a tloušťku filmu za podmínek nedostatečného mazání*. Vysoké učení technické v Brně, Fakulta strojního inženýrství, 2015. Disertační práce 134 s. Vedoucí práce prof. Ing. Martin Hartl, Ph.D.

ABSTRACT

This PhD thesis focuses on studying the effects of shallow micro-textures on friction and film thickness of lubricated non-conformal contacts under extreme and starved conditions. Measurements were carried out using a ball-on-disc tribometer equipped with high speed camera and torque sensor. Two types of micro-textures have been assessed in this study, micro-dents and transverse micro-grooves. The results reveal that micro-dents are helpful in reducing friction under starved conditions due to the film thickness enhancement. The mechanism of filling the depleted micro-dents with fresh lubricant is probably attributed to the capillary effect in the inlet zone under starvation. On the other hand, the rubbing surfaces with transverse shallow micro-grooves with a length less than the diameter of the Hertzian contact have an improved tribological performance in comparison with smooth surfaces. Indeed, transverse shallow micro-grooves showed a significant enhancement of film thickness under starvation and under extreme operating condition (reverse motion). The numerical simulation of the transient behavior of transverse limited micro-grooves showed accepted agreement with experimental results.

KEYWORDS

Micro-textures, Friction, Film thickness, EHL, Starved lubrication

ABSTRAKT

Tato disertační práce se zabývá vlivem mělkých mikro-textur na tření a tloušťku filmu v mazaných nekonformních kontaktech za extrémních podmínek a za podmínek hladovění kontaktu. Měření byla realizována na tribometru v konfiguraci ball-on-disk. Kontakt byl pozorován pomocí vysokorychlostní kamery. Pro stanovení součinitele tření byl využit snímač krouticího momentu. V této studii byly popsány dva typy mikrotextur – mikrovtisky a příčné mikrodrážky. Výsledky naznačují, že za podmínek hladovění vedou mikrovtisky ke snížení tření a to díky nárůstu tloušťky mazacího filmu. Mechanismus doplňování mikrovtisků čerstvým mazivem je pravděpodobně způsoben kapilárními jevy ve vstupní oblasti. Třecí plochy s příčnými mikrodrážkami, jejichž délka byla menší než průměr Hertzova kontaktu, potom obecně vykazovaly lepší tribologické parametry ve srovnání s hladkými povrchy. Příčné mikrodrážky vedly k výraznému nárůstu tloušťky mazacího filmu za podmínek hladovění i za extrémních provozních podmínek (protisměrný pohyb). Numerické simulace přechodových jevů příčných mikrodrážek ukázaly dobrou shodu s experimentálními výsledky.

KLÍČOVÁ SLOVA

Mikro-textury, tření, tloušťka filmu, EHL, mazání za podmínek hladovění

CONTENTS

1 INTRODUCTION

Lubrication is necessary in industrial and economic applications to extend the life cycle of machine components and to reduce friction, wear and the loss of energy between rubbing surfaces. Concentrated non-conformal surfaces are common in machine components such as gears, rolling-element bearings, cams, etc. The formation of lubricating films in concentrated contacts is subjected to the theory of elastohydrodynamic lubrication (EHL) [1]. In the EHL regime, the area of contact between mating surfaces is very small (point or line contact) resulting in a high concentrated pressure associated with elastic deformations and contact fatigue even under low loads. Moreover, the value of lubricant viscosity increases significantly within the contact due to the high pressure.

Rolling/sliding concentrated contacts are designed to operate under full film regime where the pressure buildup starts relatively far upstream of the Hertzian contact. However, a lot of machine components with non-conformal contacts operate under starved lubrication especially in cases of high speeds and high viscosities or in cases where grease is used to lubricate bearings. Indeed, starved lubrication leads to a sharp reduction in film thickness within EHL contacts which is one of the most common reasons of fatigue failures of contacting surfaces.

The modification of surface topography by artificially produced micro-features is introduced as a promising approach to reduce friction and wear between rubbing surfaces. However, the obtained benefits depend quantitatively and qualitatively on the proper design of the shape and the size of micro-features. Also, the regime of lubrication in combination with the operating conditions should be taken into account to optimize the design of micro-textures. In recent years, a lot of efforts have been exerted by many researchers to study the effect of artificial micro-features on the film thickness profile and the pressure distribution in fully flooded EHL contacts. But there is still a need to clarify and to observe the direct effect of surface micro-textures on the friction and film thickness in non-conformal contacts under starved lubrication and severe conditions such as reverse motion.

This thesis presents an experimental and numerical study on the effects of shallow micro-textures (micro-dents and micro-grooves) on the coefficient of friction and film thickness in EHL contacts under extreme operating conditions and starved lubrication. Furthermore, the understanding of starvation phenomenon was necessary to carry out the solution of the topic presented in this thesis. Therefore, the correlation between friction and the degree of starvation has been investigated theoretically and experimentally. Also the effect of lubricant replenishment on friction and film thickness in EHL contacts has been briefly highlighted as a secondary aim of this thesis.

The content of this thesis is not only unpublished results, but also the sum of author’s publications in prestigious impact journals (see appended papers) which are in relevant to the topic of thesis. In other words, this thesis provides an extended and detailed explanation of the results published by the author during the last five years (2010 − 2015).

2 STATE OF THE ART

2.1 Stribeck curve and lubrication regimes

The separation between lubricated surfaces in the relative motion determines the value of friction and the role of asperities in carrying the load .Under low speeds, the separation between surfaces is small and the nature of friction is nearly Columbian where the most part of load is carried by asperities resulting in high values of friction between rubbing surfaces. Such regime of lubrication is called Boundary Lubrication (BL) where the film thickness (h) tends to zero ($h \to 0$). Increasing the velocity increases the separation between lubricated surfaces in the relative motion and the part of load which is carried by asperities becomes less due to the increase of the hydrodynamic effect in the contact. This regime of lubrication is called Mixed Lubrication (ML). In this case, the film thickness becomes in the scale of surface roughness ($h \simeq R$). Under high velocities and low loads, the separation in the contact becomes large enough to create full film lubrication. Thus, the effect of asperities becomes negligible and the most part of load is carried by the hydrodynamic effect and the regime of lubrication is called the Hydrodynamic Lubrication (HL) with film thickness explicitly larger than surface roughness ($h \gg R$). For lubricated non-conformal contacts, the value of elastic deformation of surfaces has a significant effect on the film thickness; this regime is called the Elastohydrodynamic Lubrication (EHL). Figure 2.1 shows a generalized Stribeck curve. The coefficient of friction is presented as a function of Hersey number (ηN/p), where η is the oil viscosity in Pas, N is the speed in rpm, and P is the average pressure in Pa. It is clear from Figure 2.1 that the film thickness (h) increases strongly with increasing the Hersey number.

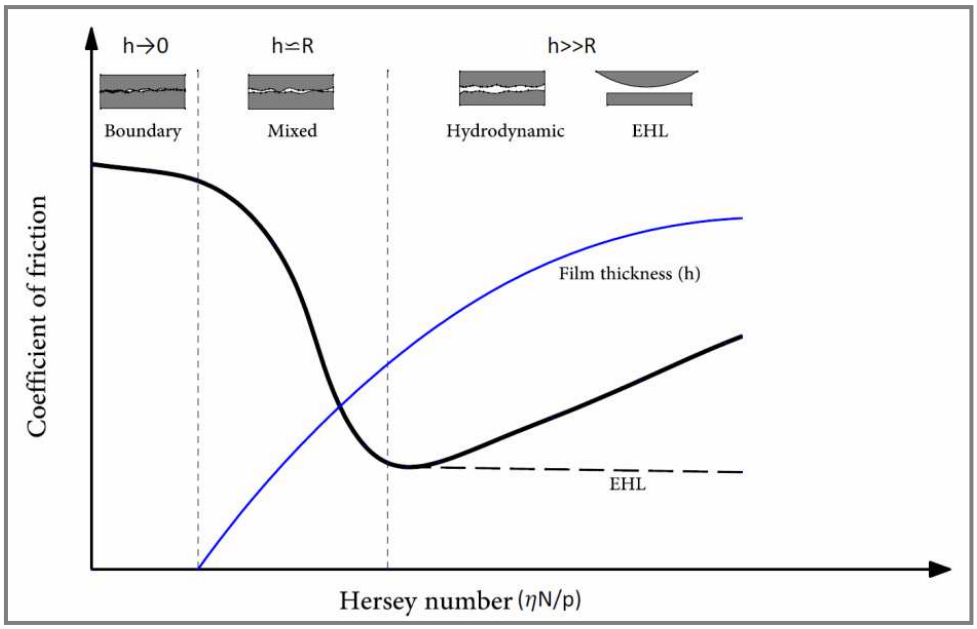

Fig. 2.1 Generalized Stribeck curve and lubrication regimes.

Indeed, lubricated non-conformal contacts are subjected to high pressures which results in high values of lubricant viscosity and increased shear stress especially in the sliding motion. However, friction of EHL contacts is governed by many factors such as operating conditions, roughness and material properties, viscosity and temperature.

The effect of surface roughness on the coefficient of friction was investigated by Wang et al. [2-3]. Experiments were performed for ball on disc with different values of roughness R_a, see Figure 2.2 The study revealed that a higher friction coefficient corresponds to the higher roughness within all the regime of lubrication.

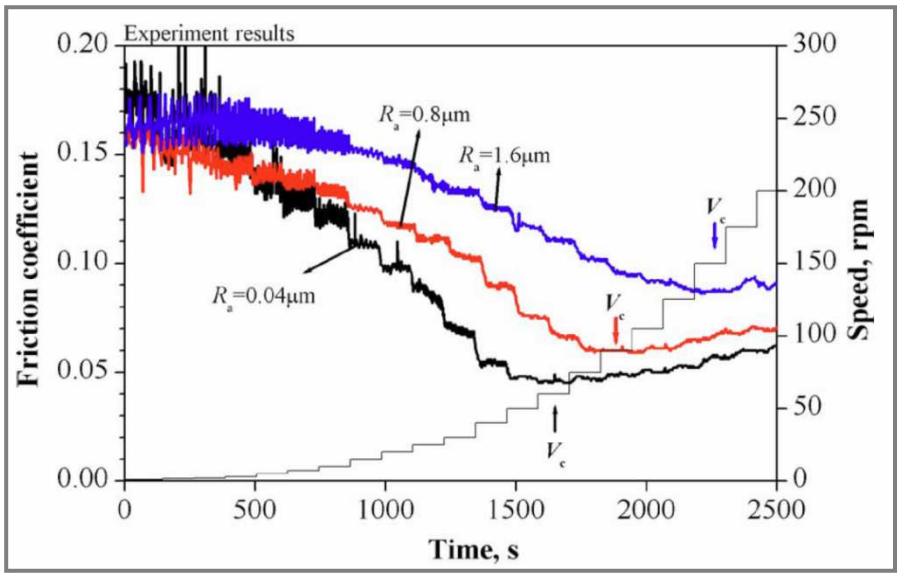

Fig. 2.2 Effect of surface roughness on Stribeck curve [3].

Sojoudi et al. [4] studied the behavior of friction for lubricated point contacts under sliding conditions. The results show that the Stribeck curve is influenced by the physical properties of lubricant such as the viscosity. However, the effect of viscosity is pronounced particularly in the range of mixed lubrication, see Figure 2.3.

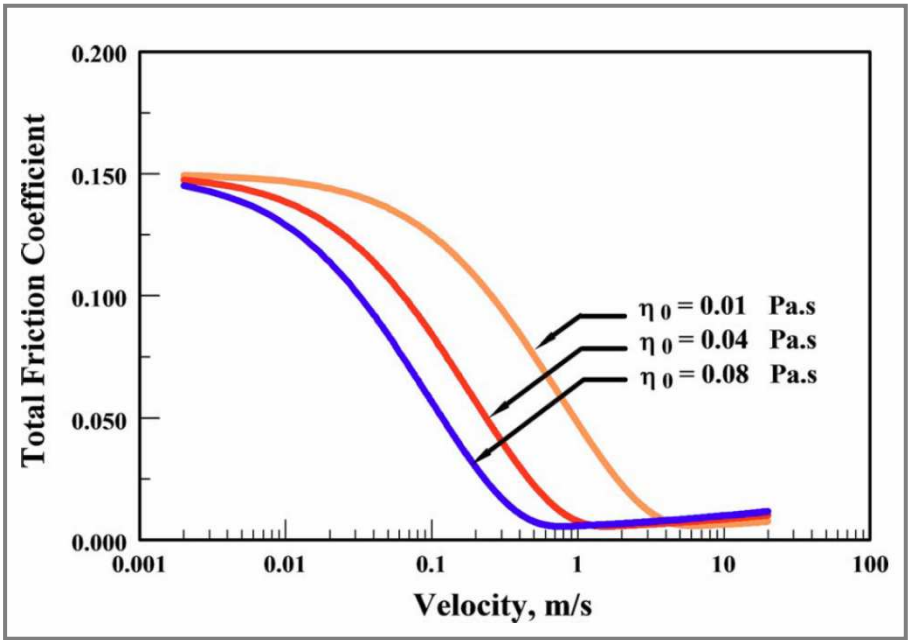

Fig. 2.3 Effect of oil viscosity on Stribeck curve [4].

2.2 Surface texturing in tribology

Improving the tribological performance of mechanical interfaces is required to reduce the frictional loss of energy. Different techniques are used to enhance the surface properties against the wear and failure of machine components. The modification of surface topography by artificially produced micro-features is a recent technique to control friction and wear between rubbing surfaces [5]. However, the beneficial effects are significantly related to the proper design (shape and size) of micro-features [6]. Moreover, the performance of micro-features is influenced by the regime of lubrication and operating conditions [7]. The mechanisms of how micro-cavities can bring benefits to the lubricated contacts are explained in the literature by the following:

- Entrapment of wear debris: This mechanism operates efficiently in the boundary or dry regime where the micro-cavities help in minimizing the plowing friction caused by the wear particles [8-10]. Generally, a pattern of transversely oriented fine micro-grooves are helpful to get benefits in the boundary lubrication [8-12].
- Increasing the load-carrying capacity: This effect can be observed basically in the hydrodynamic regime where the artificially produced micro-features (dents, grooves or dimples) generate additional separating forces and a hydrodynamic lift between sliding surfaces resulting in reducing the friction and enhancing the film thickness [13-22].
- Acting as oil reservoirs: Shallow micro-cavities can store the lubricant to be extracted into the contact under the effect of the sliding motion and the elastic deformation. Consequently, a significant increase in the film thickness has been investigated in the EHL regime. However, micro-features with improper design can aggravate the tribological performance of rubbing surfaces [23-33].

Two opposing effects related to film thickness and pressure can be observed with lubricated textured surfaces [34]:

- Enhancement in the lubricant film thickness in the contact resulting in a larger separation and less interaction between asperities. Thus, the coefficient of friction is reduced in the mechanical contacts.
- Micro-textures cause a turbulent of lubricant flow and pressure fluctuation increasing the flow resistance and the coefficient of friction.

Andersson et al. [35] investigated experimentally the behavior of friction and wear for smooth and laser-textured surfaces in oscillating sliding motion. They revealed that a significant improvement in the tribological performance can be achieved with the low density of micro-textures combined with an oil of high viscosity. Oils with a low viscosity are proper for lubricating surfaces with a high density of micro-textures at low sliding velocities.

Wakuda et al. [36] investigated the frictional properties of textured ceramic surfaces using pin-on-disc test rig under a very high contact pressure. Figure 2.4 shows the dimensions and distribution of micro-dimples on the surface of ceramic plate. Figure 2.5 shows the schematic diagram of pin-on-disc friction testing method. They found that an appropriate surface modification can lead to a significant reduction of friction under boundary and mixed lubrication conditions at the line contact in sliding motion. Figure 2.6 depicts the reduction of friction after introducing micro-dents on the surface of ceramic. On the other hand, Wakuda's study revealed that the tribological characteristics depend strongly on the size and

density of micro-dimples. The dimple size of approximately 100µm at a density of 5–20% is recommended. However, micro-textures are not effective when the size is equivalent to, or smaller than, the contact line width between the mating elements. Indeed, this last conclusion by Wakuda is in contradiction with many studies bout surface texturing in concentrated contacts.

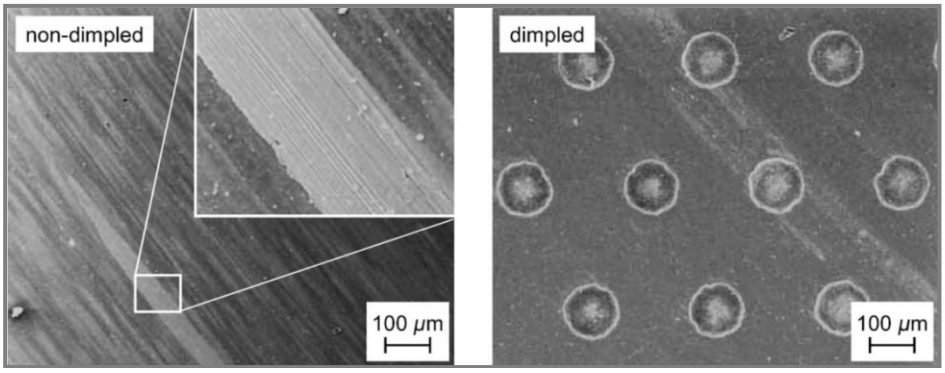

Fig.2. 4 Dimpled and non-dimpled surfaces [36].

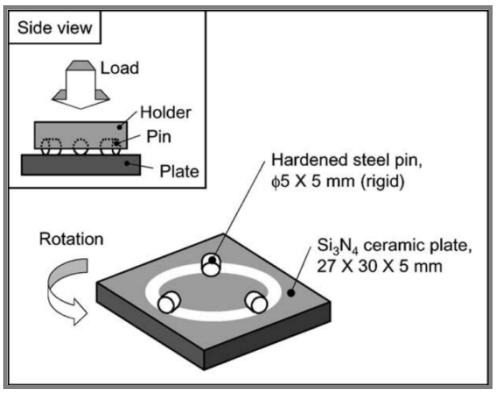

Fig.2. 5 Schematic diagram of pin-on-disc friction testing method [36].

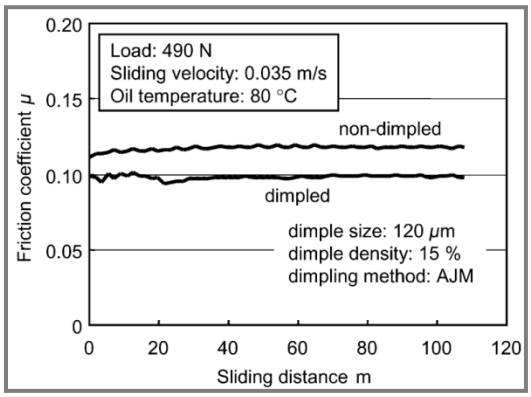

Fig.2. 6 Coefficient of friction of dimpled and non-dimpled surfaces [36].

Kovalchenko et al. [7] carried out an experimental comparison of Stribeck curves for smooth surfaces and different types of textured surfaces. Experiments were performed using a pin-on-disc apparatus at sliding speeds in the range of 0.015-0.75 m/s and pressures from 0.16 to 1.6 MPa. The micro-cavities formed by laser texturing have surface densities 7%, 12 % and 15 %. The conclusion of this study is that the beneficial effects of laser surface texturing are more pronounced at higher speeds and loads and with higher oil viscosity.

Galda et al. [37, 38, 39] studied the influence of geometrical characteristics of surface textures on friction and wear resistance using the test assembly shown in Figure 2.7. The test was carried out under unidirectional sliding for a conformal contact block-on-ring. Figure 2.8 shows the shapes and distribution of dimples used in the test. A significant reduction of friction has been observed by introducing the textures compared to untextured surfaces. Also, it was found that the shape, the size of oil pockets and density strongly affect the coefficient of friction. However, dimples density smaller than 20% is beneficial to reduce friction of sliding pairs in the mixed lubrication regime. Figure 2.9 shows the variation of friction for different

dimples densities. It is clear from Figure2.9 that the density 20% causes the highest friction while density 12.5% results in the lowest friction. On the other hand, the textured block showed a significant improvement in wear resistance in comparison to untextured samples.

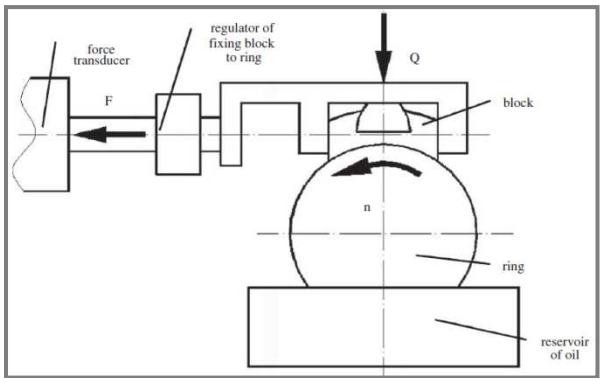

Fig. 2.7 The schema of test assembly [37].

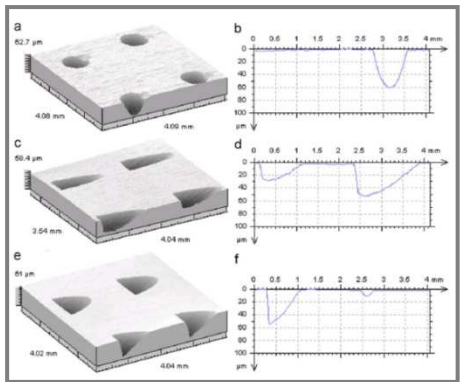

Fig. 2.8 Examples of surface topographies of textured samples [37].

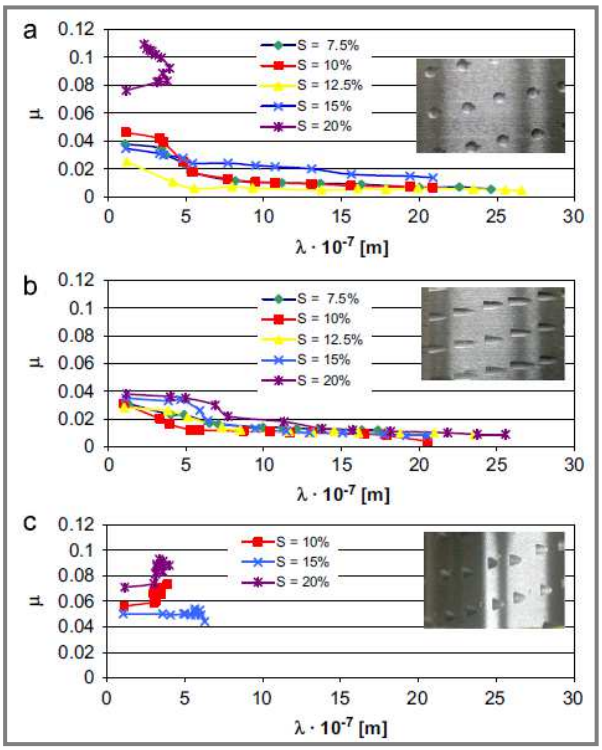

Fig. 2.9 Variation of the coefficient of friction [37].

Schreck et al. [40] examined, using a cylinder/plate tribometer, the effects of different topographies on friction and wear behavior for water lubricated and reversed sliding contact. Micro-channels and micro-pits were generated on 100Cr6 and alumina surfaces mated to 100Cr6 cylinders by a laser ablation process. However, all textured samples showed a reduction of friction compared to smooth surfaces. The decrease of friction was explained by the fact that the micro-cavities act as wear particles traps. Figure 2.10 shows the friction reduction obtained for surfaces textured by crossed channels in comparison with smooth polished surfaces.

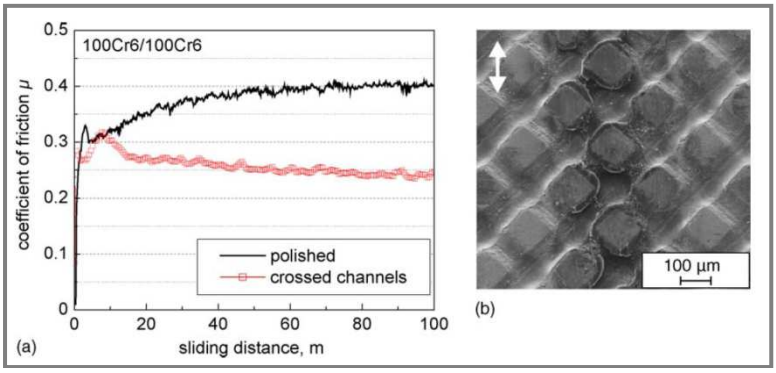

Fig. 2.10 (a) Coefficient of friction vs. sliding distance up to 100 m for a polished and a structured (crossed channels) 100Cr6 surface under water lubrication, (b) SEM-micrograph of a worn 100Cr6 plate (structured) after 100 m sliding distance (the arrow displays sliding direction) [40].

Also, crossed micro-channels have been used by Wahl et al. [41] as deterministic surface micro-texturing to control friction coefficient and wear. Micro-textures have been generated by laser-assisted process in different sizes. Figure 2.11 shows the three different textures with crossed micro channels. The channels have a depth of 50 μm while the width was chosen as 60, 100 and 300 μm. The tribological behavior was investigated for friction coefficient and film thickness using the pin-on-disc setup. Figure 2.12 shows the results under sliding conditions. Increasing channel or plateau width results in less friction and higher film thickness under different loads.

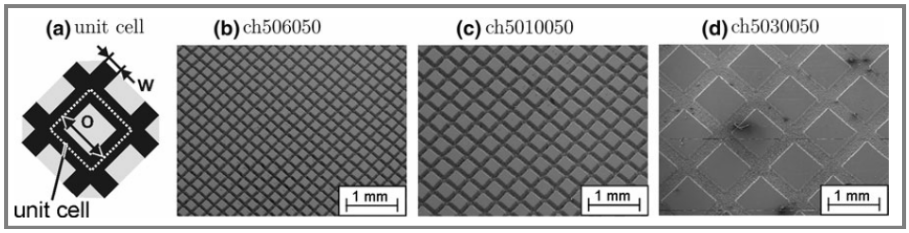

Fig. 2.11 The unit cell of the texture element and b–d SEM images of the textured steel surfaces with constant coverage fraction and depth of 50 % and 50 μm of the different channel widths (b) w = 60 μm, (c) w = 100 μm, and (d) w = 300 μm [41].

Implementation of surface texturing for some mechanical parts with parallel or conformal surfaces, for example, seals and thrust bearings, leads to decrease friction and improve the lifecycle of operating contacts. Etsion et al. [43-45] studied experimentally and theoretically the effect of surface texturing on friction and it was proven that the application of laser surface texturing (LST) with piston rings provides benefits in reducing friction about 30% in comparison with non-textured rings. On the other hand, the performance of thrust bearings can be improved by using a proper micro-texturing because of the increasing of the hydrodynamic pressure, load capacity and wear resistance.

Indeed, the hydrodynamic effect of micro-textures has been profoundly and intensively studied by many investigators, for example, Wang et al. [16], Costa et al. [17], Ramesh et al. [18] and Han et al. [19]. There is a consensus that the proper design of micro-cavities results in enhancing the load-carrying capacity of sliding

surfaces. However, the beneficial effect of micro-textures is related also to other factors such as operating conditions and oil prosperities.

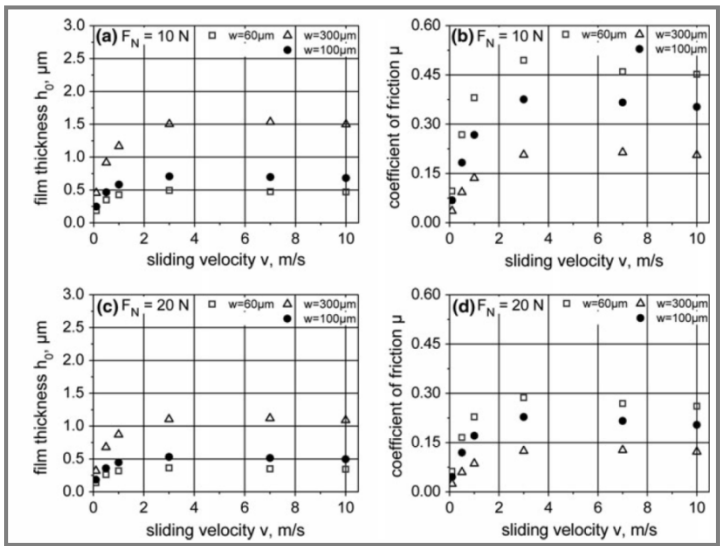

Fig. 2.12 Film thickness friction coefficient as a function of sliding velocity for different channel widths 60, 100 and 300 µm [41].

2.2.1 Effect of surface texturing on wear

Reducing wear of lubricated mechanical interfaces is crucial for increasing service life of mating surfaces. Extreme operating conditions with high friction values and thin lubrication films aggravate the wear rate over time. Usually, wear begins when there is a plastic deformation due to metal-to-metal contacts. The modification of surface topography by artificially produced micro-textures patterns influence significantly the behavior of wear and friction of rubbing surfaces. However, the plowing friction caused by wear particles produced during sliding becomes a principal mechanism of friction and wear in the boundary lubrication [8]. Saka et al. [9] showed that undulated surfaces minimize the plowing effect due to wear debris resulting in reduced friction and wear. Pettersson et al. [12] investigated wear behavior of sliding smooth and textured surfaces. 20 µm wide groove textures and 20 µm wide square depression textures were produced by lithography and anisotropic etching of silicon wafers. The results showed that wear rate of textured DLC coated surfaces after 20000 cycles is less than for flat DLC coated surfaces under boundary lubrication conditions. Similar study was carried out by Chouquet et al. [42] where surface texturing was used in order to improve the tribological properties of a DLC coating in lubricated sliding contacts. Experiments were conducted by means of a ball-on-disc Tribometer with different sliding speeds from 5.5cm/s to 68.5cm/s. The contact was lubricated by oil amount of (8 µl) with oil viscosity of 0.12 Pa.s (at 25 °C). The behavior of friction and wear was analyzed depending on the cavity dimensions. Figure 2.13 shows the results of the tribological performance of the reference DLC coating and three samples textured with different dimple sizes. It is clear from Figure 2.13 that the textured sample 1 with the cavity diameter of 65 µm and depth of 1.3 µm has a significant increase of friction and wear compared to the non-textured reference DLC coating. On the other hand, reducing the cavity depth for sample 2 and reducing the cavity diameter and depth for sample 3 resulted in friction and wear reduction compared to the non-textured reference DLC coating.

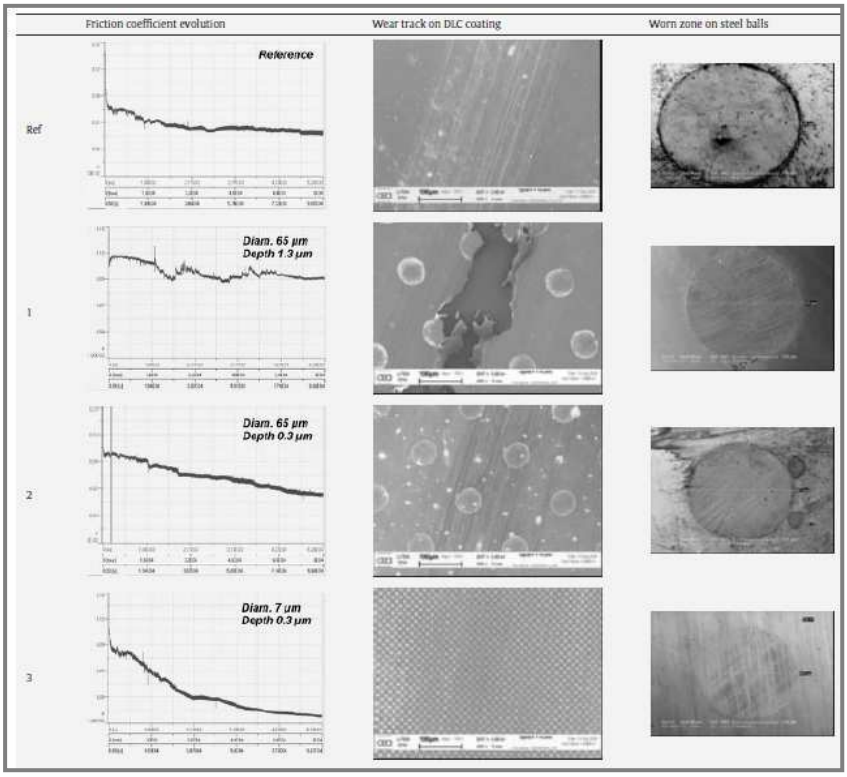

Fig. 2.13 Evolution of friction coefficient and SEM images of worn zones on DLC coatings and steel balls as a function of the DLC surface texture [42].

2.2.2 Effect of micro-textures orientation

Pettersson et al. [11-12] found that the ability of micro-textures to extract the lubricant into the interface of sliding contacts and to trap wear particles is related to the shape, size and orientation of the texture patterns. Under starved boundary lubrication conditions, surfaces with micro-textures showed very low and stable friction and much better wear resistance than non-textured surfaces. The successful textures were those having the smallest tested grooves or squares and an orientation perpendicular to the sliding direction, see Figures. 2.14 and 2.15.

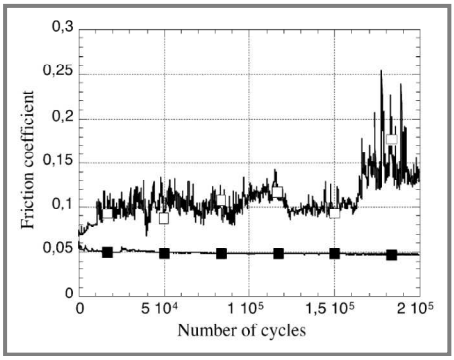

Fig. 2.14 The influence of texture orientation on the friction behavior under starved boundary lubrication [12].

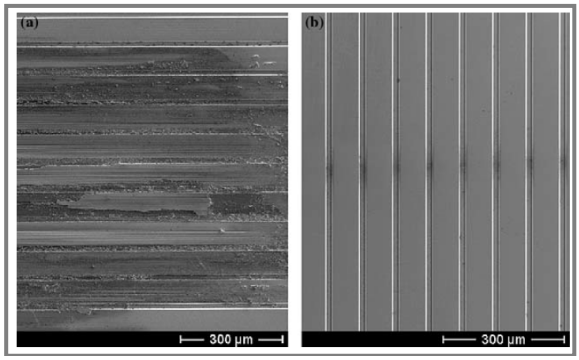

Fig. 2.15 The influence of orientation on wear under starved boundary lubrication [12].

2.3 Micro-textures in EHL contacts

Elastohydrodynamic lubrication (EHL) can be encountered in many mechanical interfaces with non-conformal contacts such as gear teeth, rolling-element bearings, cams, etc. EHL contacts are highly loaded with contact pressure about 0.5 -3 GPa. Therefore, the elastic deformation of mating surfaces has a significant role on the film thickness. On the other hand, the viscosity of lubricant is pressure dependant in the elastohydrodynamic regime due to the high pressure. As a result, the effects of micro-textures in EHL contacts reflect the interaction between film thickness, pressure, oil viscosity, operating conditions and the geometry of micro-textures.

The utilization of micro-textures to improve the tribological properties of rubbing surfaces is not limited for conformal surfaces, but also with non-conformal contacts some benefits can be obtained. Many papers were published about the effects of surfaces texturing on the film thickness and pressure profile for non-conformal contacts. There is a consensus that micro-textures with proper dimensions and operating conditions can enhance the tribological performance of concentrated contacts. Wang et al. [24] investigated experimentally the effect of dimple size on friction under line contact condition. The patterns of dimples were fabricated on the surface of brass discs with area density of 7% and the dimple diameter varies from 20 to 60 μm. They stated that only the pattern with dimple diameter of 20 μm produced the effect of friction reduction because small dimples are able to obtain hydrodynamic pressure higher than untextured surface. Blatter et al. [25] compared the frictional behavior and sliding life of the laser-patterned samples with the non-patterned one using a pin-on-disc tribometer. A copper-vapor laser emitting at 510 nm wavelength was used to produce microgrooves on the surface of sapphire plates. The life of lubricated sliding increased considerably for the laser-patterned sapphire. Moreover, fine-patterned surfaces showed less friction than original highly polished surfaces. Nakatsuji et al. [46] evaluated the effects of micro-pockets on lubrication by using a roller with a small number of micro-dents marked by a diamond pyramid. The results revealed that micro-dents can prevent metal to metal contacts and scuffing under high load. Nanbu et al. [47] established a model-based virtual texturing for simulating the effects of micro-textures bottom shape on the elastohydrodynamic lubrication interface. The study provided an explanation of micro-texturing mechanisms in improving the performance of lubrication and film thickness. Micro-textures have been investigated under three different relative motions: textured surface moving, un-textured surface moving, and both moving. They showed that dimples with flat bottom and those that form a convergent wedge can bring additional flow into the interface resulting in enhanced lubrication film thickness. The sliding speed determines the degree of the texture effect on film thickness while the rolling speed controls the level of the film thickness. However, the faster moving textured surface should bring additional flow into the contact. Some shapes of textures are able to produces micro-hydrodynamic lifting mechanism or micro-bearing. Also, an inlet suction mechanism may exist in a moving texture. This mechanisms work with other factors and other mechanisms such as, the elastic deformation and the volume of dimples. Since the pressure outside of the dimple is much larger than that inside the dimple, a larger elastic deformation is localized at dimple edges. On the other hand, the volume of the deformed dimple becomes smaller and the lubricant may be squeezed out of the dimple providing additional lubricant supply. Similar virtual texturing simulations have been conducted by Ren et

al. [48] and Zhu [49] to investigate the geometric shape effects of surface textures by means of numerical approach.

2.3.1 Pressure distribution in dented non-conformal surfaces

The analysis of the pressure contact and subsurface stress tensor of dented surfaces is crucial for failure and lifecycle prediction. Coulon et al. [50] studied a non-conformal dented contact under sliding conditions using a ball-on-disc tribometer. The dent characteristics are: depth = 3.5µm, diameter = 90µm and the shoulder height = 0.5µm. They observed a high value of pressure in the place where lubricant leaves the dent which results in very high pressure gradients. Figure 2.16 shows the pressure profile for dented and smooth surfaces at 25 mm/s sliding speed. One can notice that there are two pressure peaks in the area of the left and right dent shoulders. The pressure collapses down to a very low value between peaks. However, this demonstrates that no cavitation occurs after the first shoulder and that a significant part of the initial lubricant volume remains entrapped inside the dent. The presence of geometrical defects on the mating surfaces modifies the normal distribution of pressure. Figure 2.17 shows a pressure concentration on the edges of micro-dent and the resulting shear stress. The maximum shear stress is localized in places of pressure peaks.

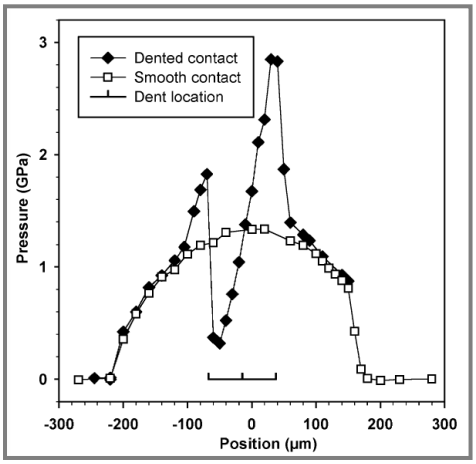

Fig. 2.16 Pressure profiles for dented and smooth surfaces under sliding motion [50].

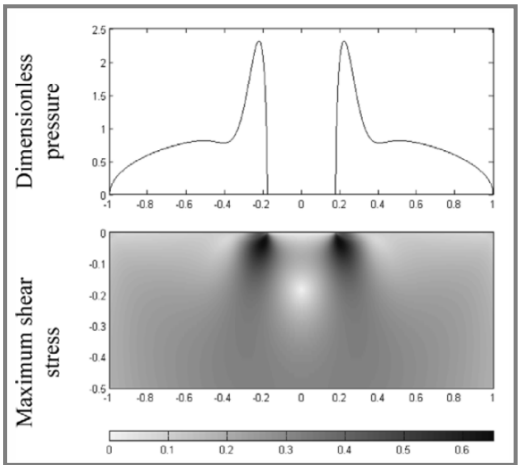

Fig. 2.17 Pressure profile and maximum shear stress for dented surfaces [50].

Nélias et al. [51] performed numerical simulations on the effects of debris dents on rolling contact fatigue through an EHL contact**.** They defined three different lubrication regimes corresponding to the size of surface defects. The results show that the dent (or bump) has effects on the pressure distribution and film thickness profile, only when the depth of dent is larger than the amplitude of surface roughness. Consequently, the regime of lubrication becomes different according to the size of defects on the surface. For small size, the dent will be totally absorbed by the elastic deformation and the film thickness of lubrication will be the same such as in the case of smooth surfaces and the lubrication regime is the quasi-smooth EHL regime, Figure 2.18-a.

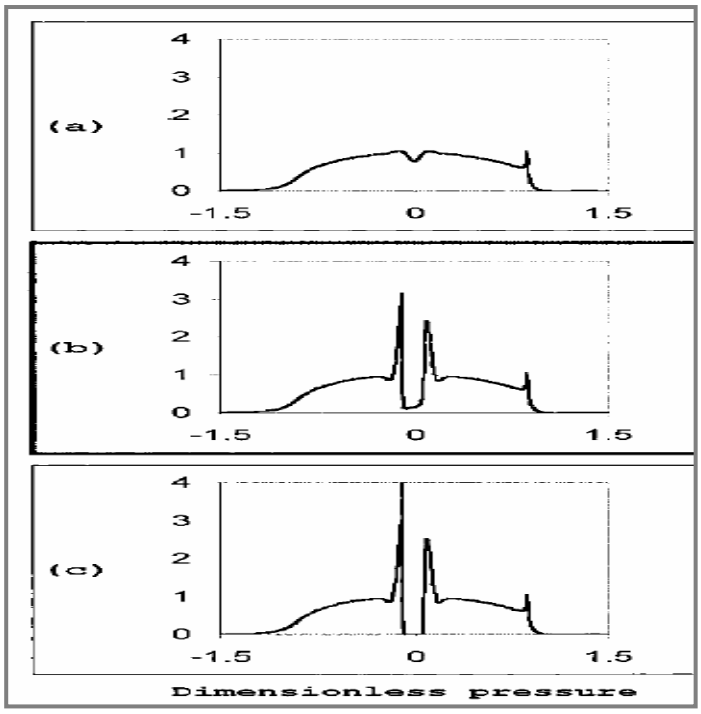

Fig. 2.18 Definition of three lubrication regimes corresponding to three typical sizes of dents [51].

Defects (dents) of intermediate size will be partially absorbed by the deformation and the micro-EHL regime without cavitation occurs, Figure 2.18-b. The large size of dent leads to create a zone of cavitation and the micro-EHL regime with cavitation occurs, Figure 2.18-c.The same study of Nélias demonstrated the effect of slide-to-roll ratio on the shear stress in the vicinity of the dent. Figure 2.19 shows that the maximum shear stress increases for higher ratios of slide-to-roll with Hertzian pressure of 1.5 GPa and mean rolling speed of 40 m/s.

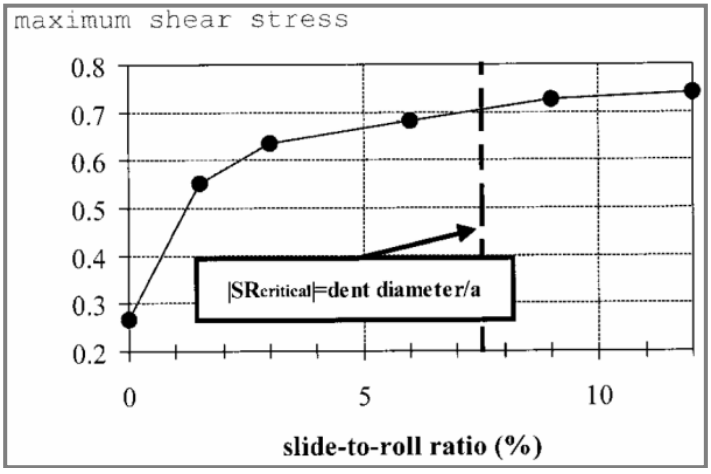

Fig. 2.19 Maximal local shear stress calculated in the vicinity of the dent (with shoulder) vs. slide-to-roll ratio [51].

Cann and Spikes [52] developed a method using optical interferometer to measure the pressure in the EHL contact zone. This method is limited to static contacts. The calibration was carried out by measuring the compression at a single position in the center of the contact of a smooth steel ball against a flat disc. Figure 2.20 shows the

measured pressure profiles for a dent, 80 µm diameter and 500 nm deep, under loads of 20 and 40 N. The corresponding smooth-surface Hertzian profiles are also shown in Figure 2.20. The two pressure peaks are clear on dent edges even under static load.

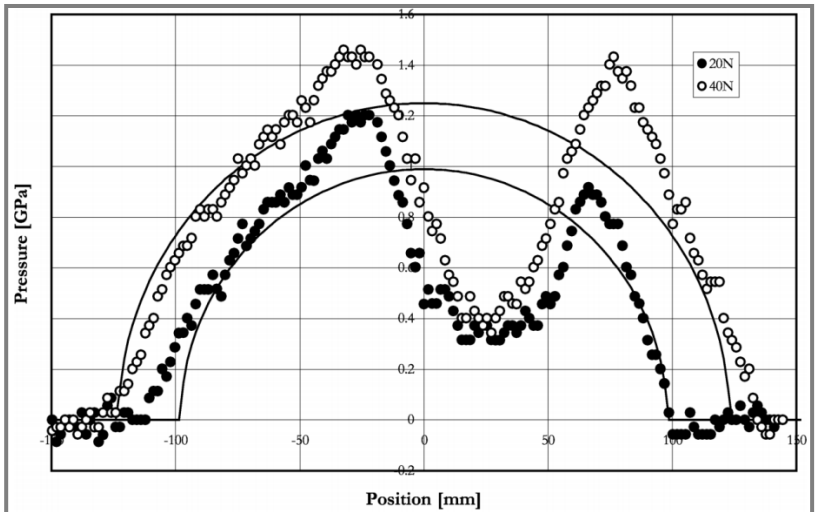

Fig. 2.20 Measured pressure profiles for a dent, 80µm diameter and 500 nm deep, for loads of 20 and 40 N. The corresponding smooth-surface Hertzian profiles are also shown [52].

2.3.2 Film thickness profile in dented non-conformal surfaces

Film thickness prediction is necessary to improve the performance and durability of machine components. However, introducing artificial micro-textures on rubbing surfaces influences significantly the pressure distribution within the contact. Consequently, textured EHL conjunctions demonstrate a transient behavior of the lubricant flow and film thickness. The transient behavior of micro-textures in EHL contacts has been widely studied by many researchers.

Křupka et al. [53, 54] observed the behavior of shallow micro-dents within mixed lubricated non-conformal contacts (ball-on-disc) by using the thin film colorimetric interferometry. Their study showed that an array of shallow micro-dents reduces asperity interactions of mating surfaces and the lubricant emitted by shallow micro-dents provides a local increase in lubrication film thickness. In addition, they referred to the effect of surface texturing in case of reversal motion where starvation of lubricant is dominated. The results show that micro-textures help in reducing the negative influence of starvation by emitting additional lubricant from the dents which can lead to avoid the collapse of film thickness due to starvation. However, the emitted lubricant from the shallow dent improves the film thickness in case the disc moves faster than the dented ball. At the same time, the micro-cavities localized around the border of the Hertzian contact had a negative effect on the film thickness and the hydrodynamic pressure because of the side leakage of lubricant. Křupka and Hartl [26, 27] performed an experimental study for the effect of micro-dents on the thin EHD lubrication films for non-conformal surfaces. Figure 2.21 depicts the effect of a row of shallow micro-dents on thin film thickness through an EHL contact. It is clear that micro-dents act as oil reservoirs and the emitted lubricant upstream or downstream depends on the direction of sliding. On the other hand, the results showed that in case of positive slide-to-roll ratio, deep micro-dents can lead to reduce the lubricant film thickness.

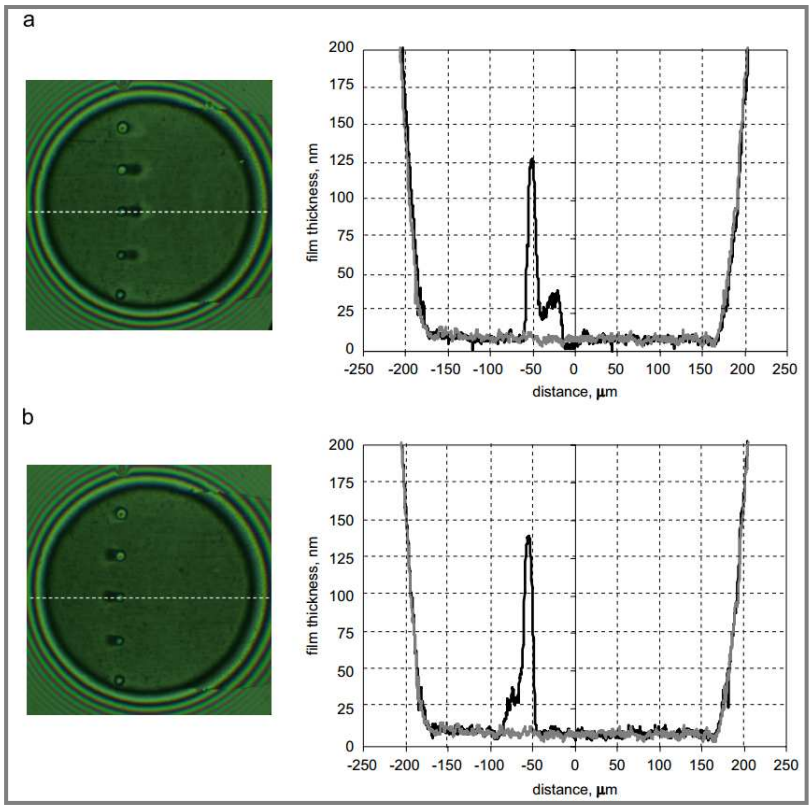

Fig. 2.21 Interferograms and film thickness profiles depicting the effect of shallow micro-dents on thin EHD lubricated contact, SRR=0.5 for a) and SRR=-0.5 for b) [53].

Moreover, the study presented in references [26, 27] showed that the minimizing of micro-dents depth can improve the film thickness of lubrication at slide-to-roll ratio SRR=0.5. Indeed, minimizing the depth of micro-dents from 1180nm to 560 nm led to increase the film thickness from 20 nm to 49 nm. In case of the negative slide-to-roll ratio, the depth of micro-dents has not a significant effect in reducing the film thickness. Furthermore, when dents are introduced on the slower moving surface, push the lubricant in the direction of flow, otherwise, dents on faster surface push the lubricant in the opposite direction of flow. Figure 2.22 shows a comparison of film thickness for smooth and dented surfaces. The local enhancement of film thickness is formed just downstream of the leading edge of the micro-dent and this local enhancement becomes more pronounced as the slide-to-roll ratio increases.

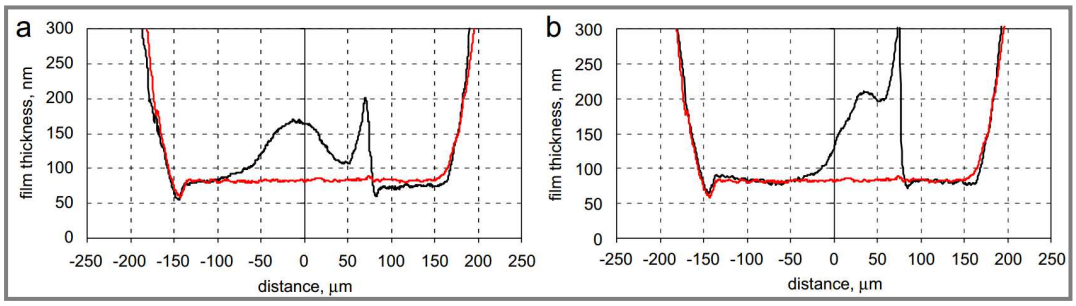

Fig. 2.22 Comparison of film thickness for smooth and dented non-conformal surfaces, SRR = 0.5 for b) and SRR=1 for a) [26].

2.3.3 Effect of micro-cavities depth

Lubrecht [55] investigated the influence of local and global features in EHL contacts. The local features such as indentation influence significantly the pressure contact when these local features have amplitude (depth) larger than the global roughness. In his study, the pressure distribution of concentrated contacts has been approximated by the pressure distribution of the dry contact because the results showed that the difference in pressure and stress field is small for dry and lubricated contact with artificially created defects. Moreover, the dent geometry influences strongly the life reduction of non-conformal contacts. In general, micro-features with amplitudes larger than the overall film thickness aggravate the life expectancy of mating surfaces. Mourier et al. [23, 33, 56] investigated experimentally and numerically the effect of micro-cavities depth on the film thickness for a lubricated contact between steel ball and silica disc. The conclusion of work showed that the micro-cavities do not significantly influence the oil film thickness under pure rolling conditions. On the other hand, micro-cavities have a positive or a negative effect in case of sliding motion according to the depth of micro-cavities. Deep cavities cause a local decrease and failure in film thickness. While shallow micro-cavities increase significantly the film thickness. The local lubricant film reinforcement is proportional to the slide-to-roll ratio, and to the time spent by the micro-dimple into the contact zone because the oil is pushed out from the micro-cavity under the combined effect of sliding motion and the elastic deformation of contacting surfaces. Figure 2.23 shows the profile of film thickness for a smooth surface and a dented surface with deep micro-cavity (25 μm diameter and a depth exceeding 100 μm). It is clear that there is a collapse of the lubricant film near the moving micro-geometry. On the contrary, Figure 2.24 shows an important increase of film thickness locally generated by the passing of the shallow micro-cavity through the contact zone.

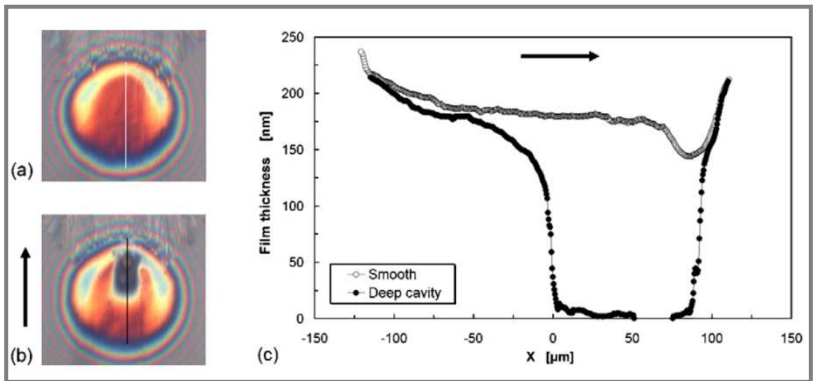

Fig. 2.23 Effect of deep micro-cavity on film thickness [33].

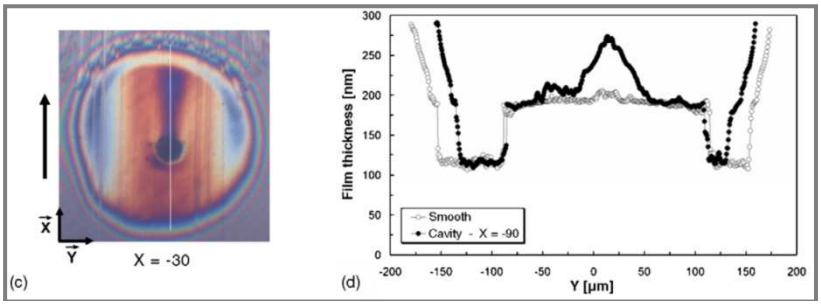

Fig. 2.24 Effect of shallow micro-dimple on film thickness [33].

The numerical solution of elastohydrodynamic lubrication using multigrid methods enabled to predict the film thickness and the corresponding pressure as a function of the micro-cavity amplitude [23]. Numerical solution was carried out for entraining velocity of 4 m/s and slide-to-roll ratio SRR=0.5. The film thickness increases almost linearly when the micro-cavities amplitude increases from 25 nm to 300 nm, see Figure 2.25. However, in reference [23] the amplitude of micro-cavities is considered shallow until value of 300 nm. Figure 2.26 shows a significant pressure reduction in the micro-cavity. Indeed, as the depth of micro-cavity becomes large the pressure tends to zero. Consequently, the lubricant will flow into the cavity instead of being emitted out of the cavity by the shear flow. Thus, deep micro-cavities cause a film thickness reduction in EHL contacts.

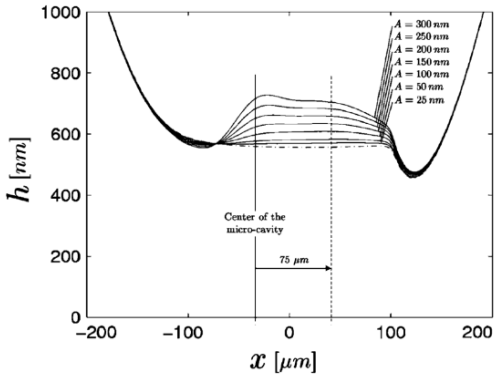

Fig. 2.25 Transient increase of film thickness as a function of the micro-cavities amplitude [33].

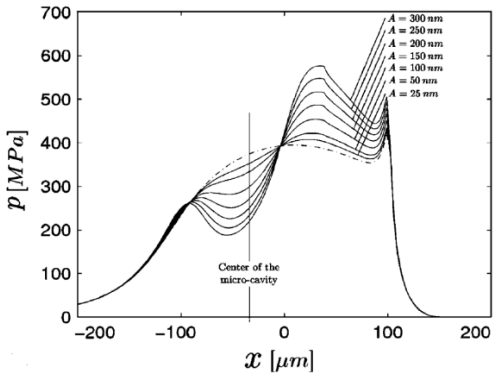

Fig. 2.26 Corresponding pressure profiles as a function of the micro-cavity amplitude [33].

2.3.4 Effect of slide-to-roll ratio on the behavior of micro-dents

Wedeven et al. [32] used the optical interferometry to measure the film thickness induced by artificially produced dents and grooves under rolling and sliding conditions. A reduction in film thickness and pressure was observed at the leading edge of the dent due to the local modification of EHD pressure created by the dent through its passage in the contact. The significant increase of pressure and film occurred on the trailing edge of the dent. However, under pure rolling conditions, the film thickness distribution remained the same as the dent passed the Hertzian region. Micro-EHD pressures were observed as the dent passes the Hertzian region under sliding conditions. Grooves, which are perpendicularly oriented on the direction of flow, cause a substantial increase in film thickness , while the parallel grooves to the direction of flow have not a significant effect on the film thickness under pure rolling and pure sliding.

Figure 2.27 shows an experimental and numerical simulation to the passage of micro-dent in EHL contact under pure rolling conditions. It is clear that the micro-cavity does not induce a significant film thickness variation and a small local pressure decrease accompanies the micro-geometry during its passage. This pressure reduction increases with the depth of the micro-cavity, whereas it does not seem to depend on the diameter and profile of the micro-cavity [23].

When sliding is introduced in the elastohydrodynamic lubrication regime, two different types of film thickness distributions can be observed as a function of the micro-cavity depth:

- Local collapse of fluid film attributed to the deep micro-cavity

- Transient increase of lubricant film thickness induced by the shallow micro-cavity.

Figure 2.28 shows the transient effect of passing micro-cavity through a circular EHL contact under rolling-sliding conditions. In this case, a significant increase in lubricant film thickness is induced by a shallow micro-cavity in the elastohydrodynamic lubrication regime.

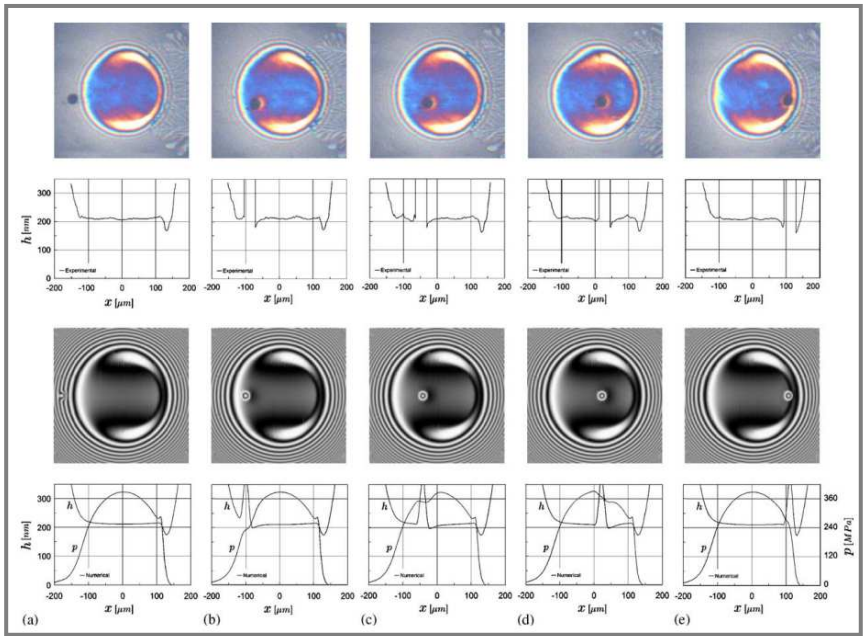

Fig. 2.27 Micro-cavity passing through a circular EHL contact under pure rolling [23].

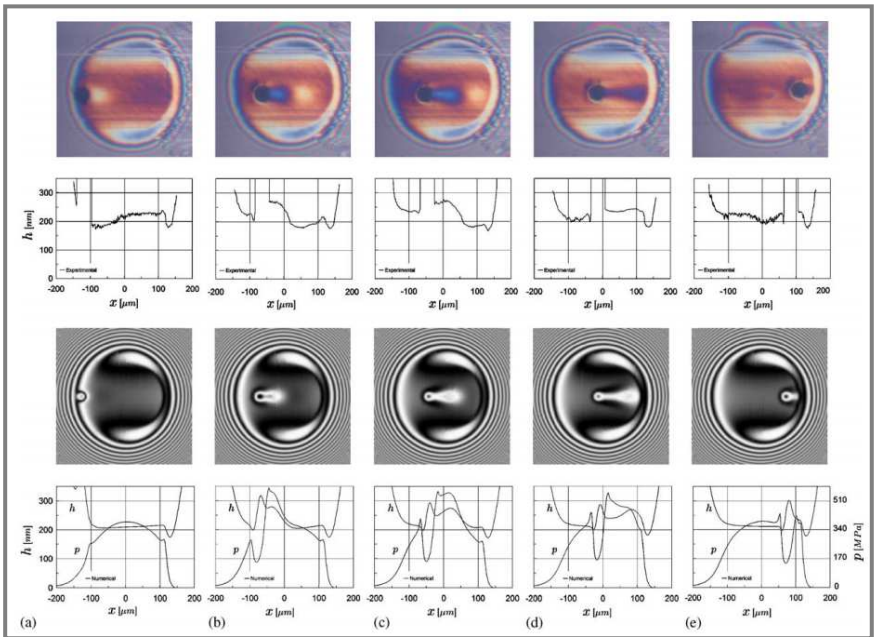

Fig. 2.28 Micro-cavity passing through a circular EHL contact under rolling-sliding conditions [23].

Figure 2.29 shows a numerical simulation of the central film thickness profiles for slide-to-roll ratios SRR from 0% to -50%. The micro-cavity diameter is 120 μm and its depth is 200 nm. The sliding velocity increases proportionally the length of the elastic deformation on the trailing edge of the micro-cavity.

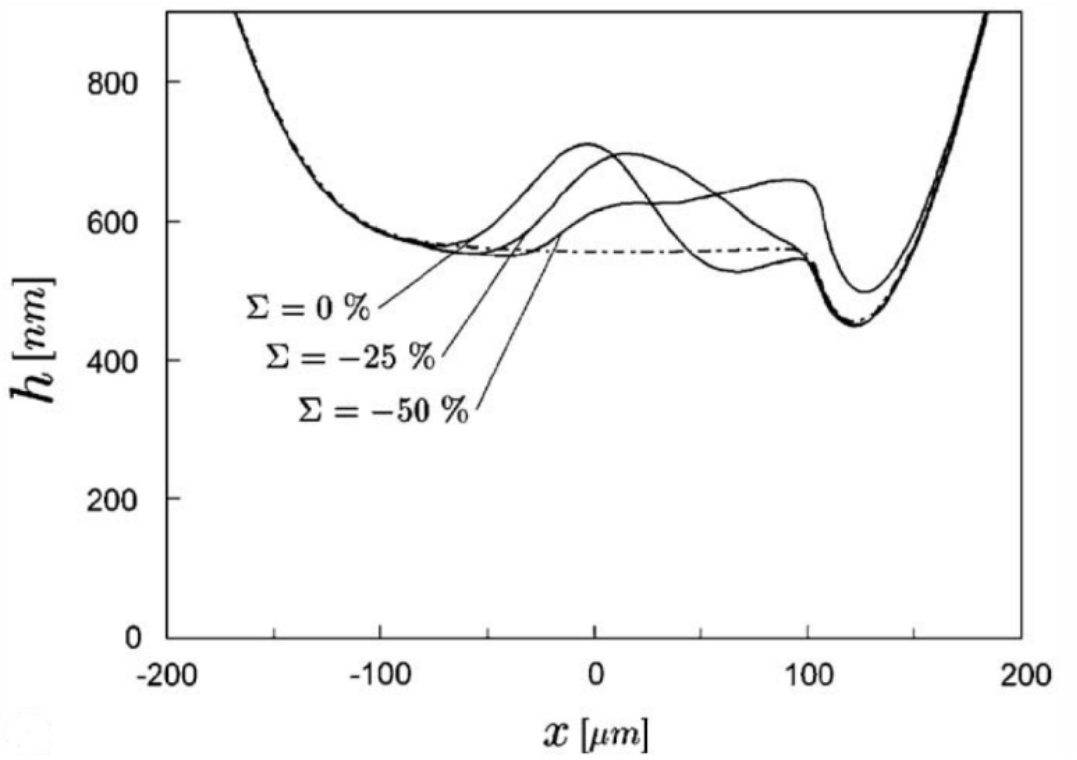

Fig. 2.29 Influence of the slide-to-roll ratio SRR on the elastic deformation propagation [23].

The effect of operating conditions on the behavior of surface irregularity was also investigated by Yang et al. [59] and Kaneta et al. [60]. They revealed that the film thickness distribution or the elastic deformation of the bump is influenced significantly by the surface kinematic conditions and the orientation of the bump. Under simple sliding conditions (SRR= 2), surface irregularity has a negative effect on the film thickness.

Ai et al. [29-62] studied numerically the influence of moving dent on point EHL contacts. The results show that under pure rolling conditions, the effect of dents on the pressure distribution is very limited and localized in the vicinity of the dent. See Figure 2.30. On the other hand, the presence of sliding motion results in a pressure ridge at the trailing edge as the dent moves faster than the opposite surface and at the leading edge as the dent is slower than the opposite surface. The pressure and film thickness profile become more influenced by the dent as the slide-to-roll ratio increases. Increasing the slide-to-roll ratio and the depth of dent is generally associated with increasing the fluctuation of fluid in the vicinity of the dent. However, the pressure fluctuation becomes larger when the dent is localized on the slower or stationary surface. Otherwise, increasing the dent width in x and y direction reduces the fluctuation. Figures 2.31 and 2.32 show a numerical simulation of pressure distribution and the corresponding film thickness in the vicinity of micro-dimple under positive and negative slide-to-roll ratio (SRR).

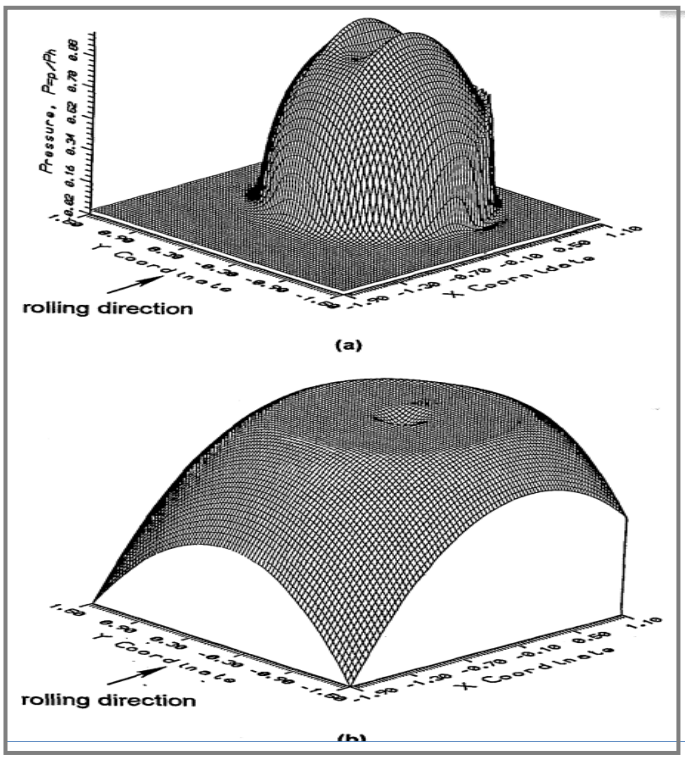

Fig. 2.30 Effect of micro-dent on pressure distribution (a) and film thickness profile (b) under pure rolling conditions SRR=0 [29].

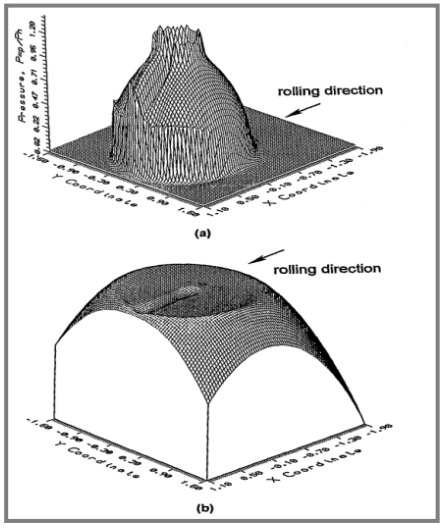

Fig. 2.31 Effect of micro-dent on pressure distribution (a) and film thickness profile (b) under sliding conditions SRR=-2 [29].

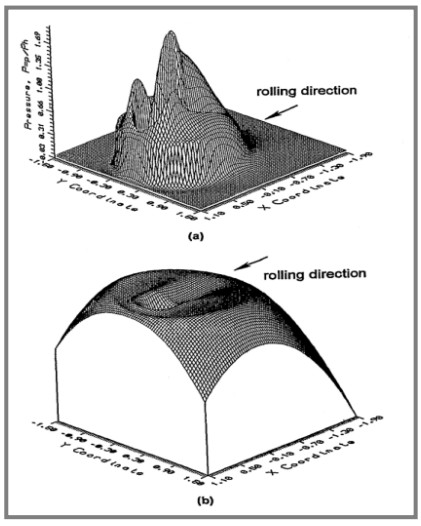

Fig. 2.32 Effect of micro-dent on pressure distribution (a) and film thickness profile (b) under sliding conditions SRR=+2 [29].

2.4 Behavior of transverse and longitudinal irregularities in EHL contacts

2.4.1 Effect on pressure, film thickness and traction

Kaneta et al. [57, 58] investigated optically a local reduction in film thickness due to the passage of transverse micro-grooves though EHL contacts. The local reduction in film thickness is essentially caused by the side leakage along the groove because of the relative low viscosity in the groove. However, the amount of the side leakage decreases with reducing the size (width and depth of micro-groove) and increasing the overall film thickness. Yang et al. [59] proved numerically the results of Kaneta. However the longitudinal groove divides the contact into two parts and it does not reduce the minimum film thickness too much. Figure 2.33 demonstrates film thickness contour maps and pressure and film thickness distributions by the numerical solutions for a transversely oriented groove at various locations. Figure 2.34 shows numerical results for the EHL contact with a centrally located longitudinal groove.

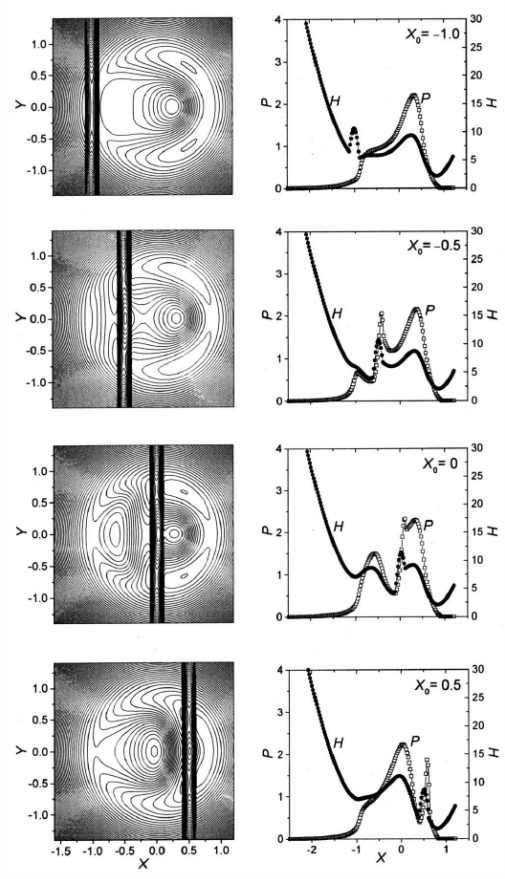

Fig. 2.33 Film thickness contour maps and pressure and film thickness distributions by the numerical solutions for a transversely oriented groove at various locations [59].

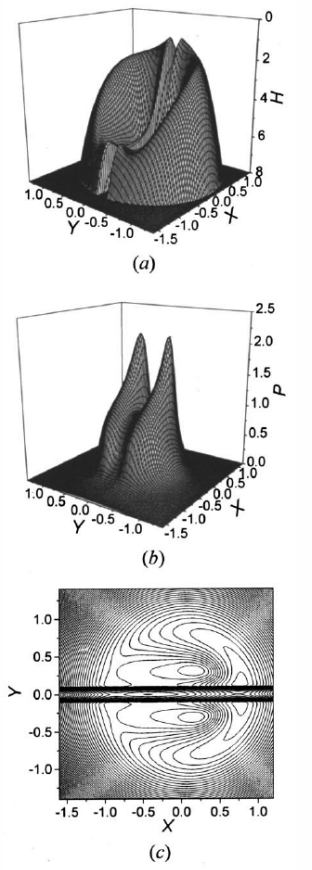

Fig. 2.34 Numerical results for the EHL contact with a centrally located longitudinal groove a. film thickness, .b. pressure, and .c. map of the film thickness contours [59].

Jiang et al. [61] studied numerically the effect of asperity orientation as well as the effect of rolling-sliding condition on the film thickness and pressure in the mixed

EHL. Figure 2.35 shows the dimensions of the elliptical asperity. The study simulated the behavior of asperity under sliding conditions for longitudinal and transverse orientation with respect to the rolling direction. From Figure 2.36, for the longitudinal asperity, at the trailing side of the contact, a lubricant pressure spike was generated due to the wedge effect of the film shape. On the other hand, at the leading side of the contact area, the lubricant pressure dropped sharply with the diverging shape of the film. For the transverse asperity, the lubricant pressure spike at the trailing side of the contact was more pronounced than that of the longitudinal asperity.

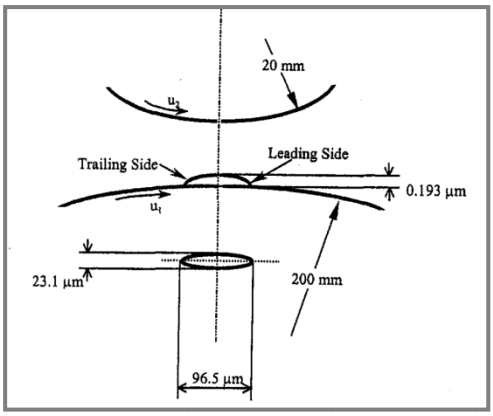

Fig. 2.35 Sketch of geometry and elliptical asperity [60].

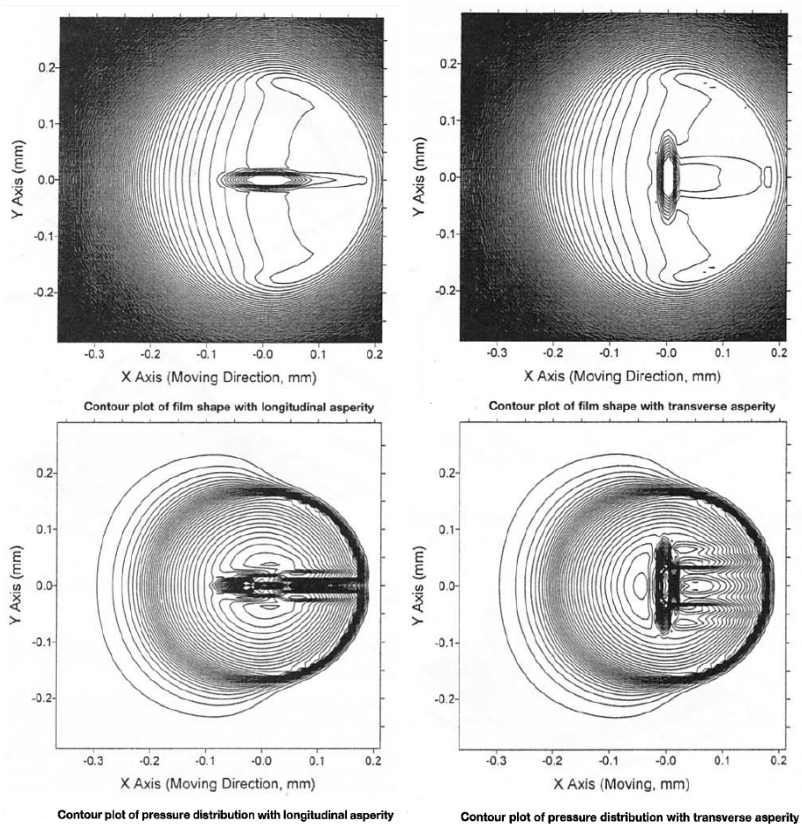

Fig. 2.36 Comparison of longitudinal and transverse elliptical asperity under sliding condition [60].

Wedeven and Cusano [32] used optical EHD rig to investigate the passage of parallel and longitudinal grooves through EHL point contacts under rolling and sliding conditions. They revealed that both types of grooves reduce the film thickness compared to a smooth surface under pure rolling conditions. Also by using of optical interferometry, Jackson and Cameron [63] observed cavitation between transverse asperity pairs in the elastohydrodynamic lubrication. Scaraggi et al. [64] showed by means of pin-on-disc test rig that the regular array of micro-holes reduces friction in the different lubrication regimes. On the contrary, the parallel microgrooves lead to an increase of friction compared to the flat control surface because the oil easily flows along the parallel microgrooves leading to increased friction. Nanbu et al. [65] used 4-roller tester to show the influence of the surface micro-texture orientation on the traction coefficient. Their experiments were performed under high pressure and rolling speed conditions. Figure 2.37 shows examples of used micro-textures and the resulting traction coefficient and film thickness. However, it was found that the grooves with orientation parallel to the rolling direction reduce the metal-to-metal contact and increase the traction coefficient.

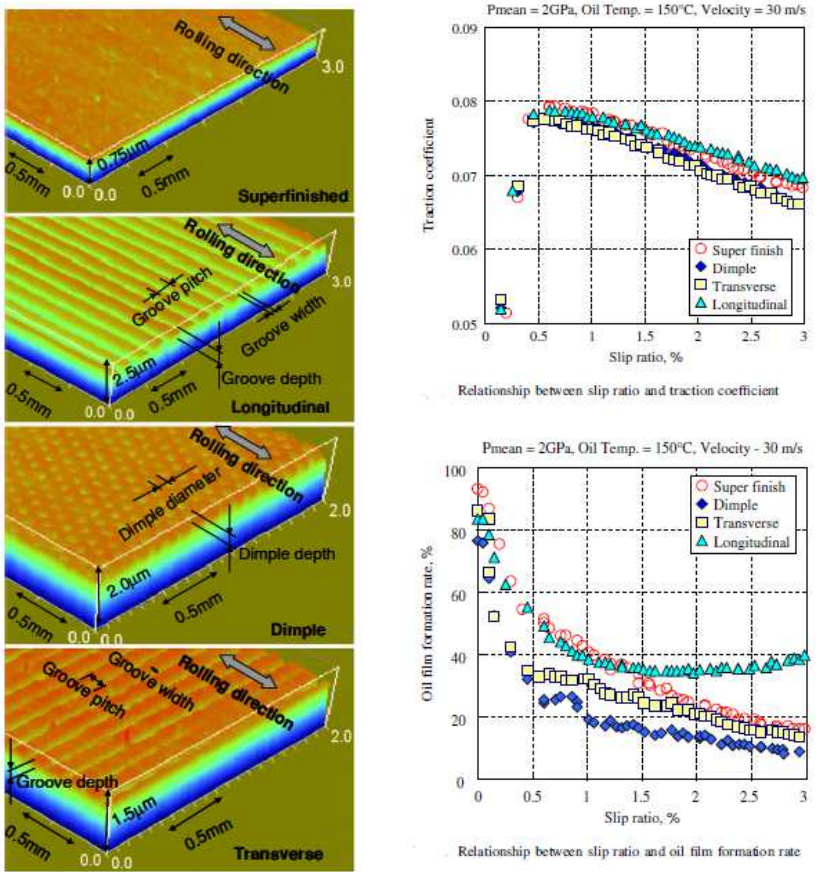

Fig. 2.37 Examples of micro-texture and resulting traction coefficient and film thickness [65].

2.4.2 Thermal effects of transverse and longitudinal irregularities

Yang et al. [66] studied the influence of surface waviness on the EHL behavior of point contacts .The results show that the thermal and non-Newtonian effects can be enlarged significantly by the surface waviness. The worst configuration of the

surface topography is that both surfaces are with longitudinal waviness, see Figure2.38.

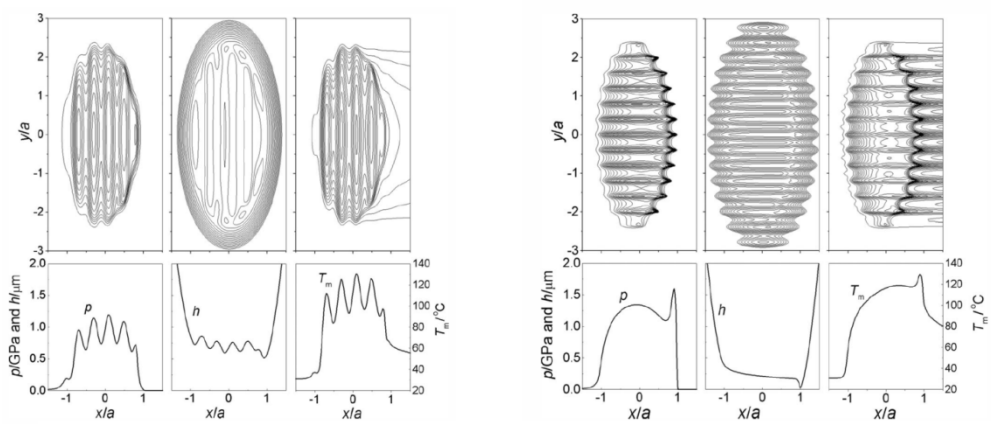

Fig. 2.38 Contour maps of pressure, film thickness and temperature for a) transverse waviness b) longitudinal waviness [66].

Yagi et al. [67] studied the effect of longitudinal grooves on the temperature field in the EHL conjunction between steel ball and a sapphire disc under high slip conditions. An infrared technique has been used to measure the temperatures of the oil film. The results show that the temperature of the grooved ball surface increased considerably compared with that of a non-grooved ball. Figure 2.39 shows the temperature distribution field of the ball, oil film, and disc surface in the direction perpendicular to the sliding direction. There are fluctuations of the temperatures in the inlet zone for the temperature profiles along the sliding direction. The temperature rise of the oil film and disc surface in the land zones is higher than those in the grooved zones.

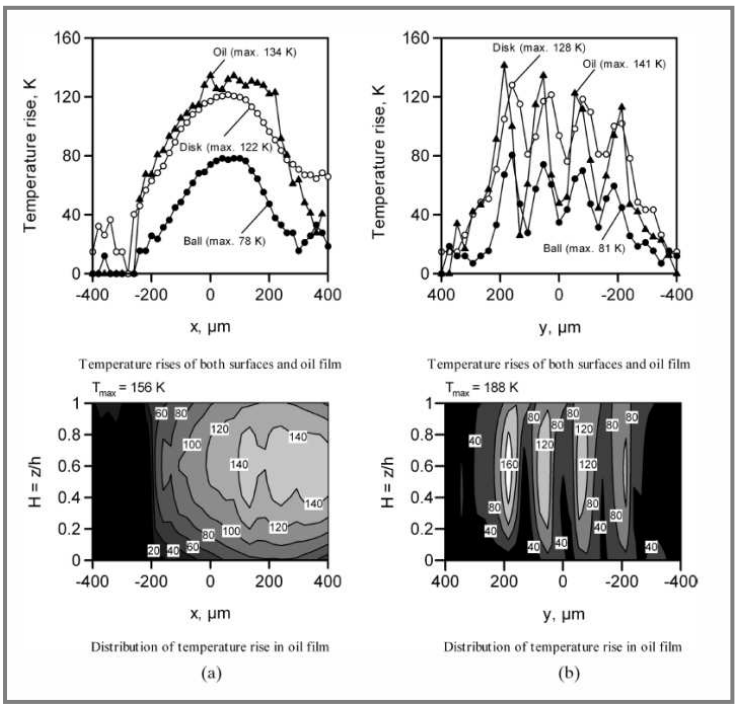

Fig. 2.39 (a) the temperature rise distributions along the sliding direction, (b) the temperature rise distributions in the direction perpendicular to the sliding direction [67].

2.5 Surface texturing under starved lubrication

2.5.1 Starved EHL contacts

Starvation occurs in case of insufficient amount of lubricant in the inlet region of the contact or in cases where greases are used for lubricating. Figure2.40 shows a schematic comparison of film thickness and pressure in a fully flooded and starved EHL contact [68, 69]. However, starved EHL contacts show a thinner film thickness in comparison with the fully flooded lubrication. Consequently, starvation increases friction and the risk of metal-to-metal contacts. Extreme operating conditions such as high speeds and viscosities aggravate starvation in EHL contacts [70]. The behavior of starved film thickness cannot be predicted by Hamrock and Dowson formula [71] as shown in Figure 2.41. Therefore, many experimental efforts have been exerted by Wedeven et al. [72], Chiu [73] and Pemberton and Cameron [74] to investigate the phenomenon of starvation. They also observed optically the emergence of the oil-air meniscus at the inlet zone of the contact in starved EHL contacts. As the oil-air meniscus approaches the contact, the pressure build-up is delayed leading to a film thickness reduction. Indeed, the delay in pressure build-up for EHL contacts leads to reduce the rolling friction and to increase the sliding friction [72]. Figure 2.40 shows that the starved contact has the onset of the pressure buildup closer to the contact compared to the flooded contact.

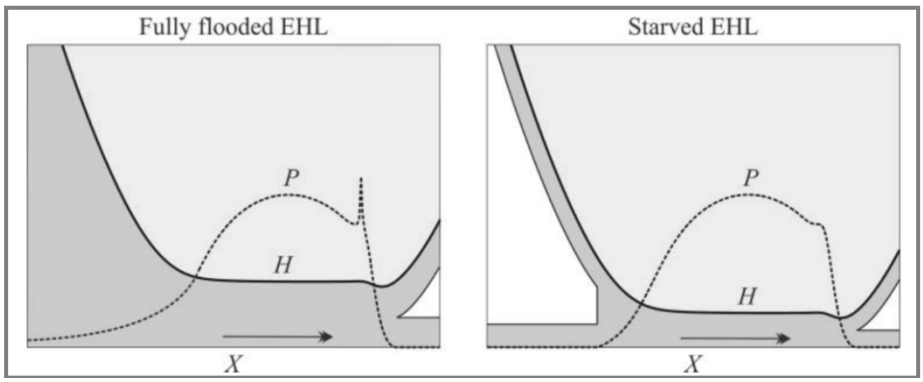

Fig. 2.40 Schematic representation of film thickness and pressure in a fully flooded and starved EHL contact [68] and [69].

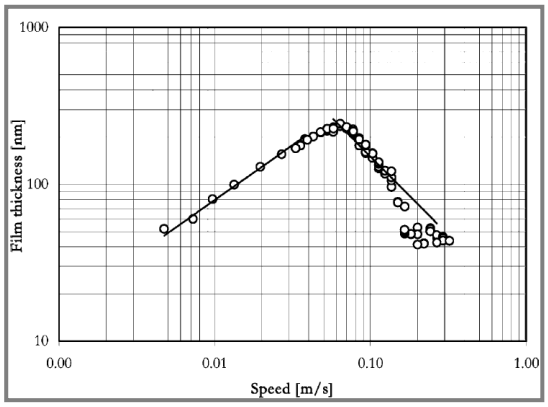

Fig. 2.41 Film thickness under starved conditions as a function of speed [70].

Chevalier et al. [75] and Damiens et al. [76] used the Elrod algorithm to describe the starved EHL point contacts. Their numerical model is applicable for circular and elliptical contacts under steady state and non-steady state conditions. The effect of starvation on the lubrication of rigid non-conformal contacts was studied by Ghosh et al. [77] and it was revealed that the dynamic load capacity of the contact reduces with the increase of starvation in comparison with the fully flooded dynamic load capacity. Nevertheless, starvation has not a valuable effect on the peak of pressure in the contact.

2.5.2 Effect of starvation on the coefficient of friction

Schipper et al. [78-79] introduced a theoretical model supported by experiments to predict the friction of starved line contacts. Calculations are presented for different oil supply layer thickness by means of the Stribeck curve from boundary lubrication to Elasto-Hydrodynamic lubrication. The numerical model depends on the fact that friction of lubricated contacts is the sum of asperities friction and the hydrodynamic action. Thus, the load is carried by the interacting asperities and by the hydrodynamic component. Figure 2.42 shows the effect of starvation on the coefficient of friction and the separation in line contact. As the degree of starvation is low, the coefficient of friction does not change strongly in comparison with the fully flooded condition. On the other hand, friction starts to increase when the separation between mating surfaces becomes lower and the oil amount on the track is less. Indeed, the starved Stribeck curve tends to be flat under severe starvation which means that the coefficient of friction through the different lubrication regimes is similar to boundary friction. Surely, such high value of friction is not preferred for machine components.

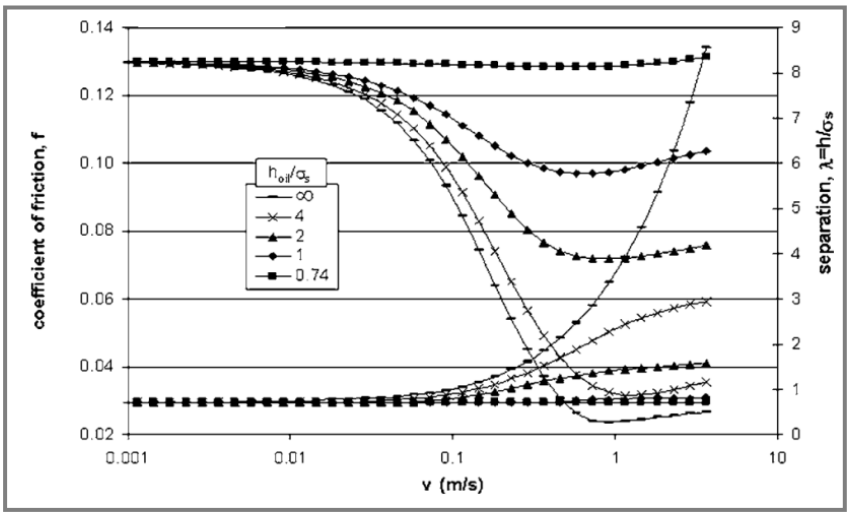

Fig. 2.42 Effect of starvation on the coefficient of friction and the separation of line contact [78].

Querlioz et al. [80] studied the influence of starvation on the traction coefficient for point contacts using Mini Traction Machine (MTM). The study proved that the traction depends strongly on the amount of lubricant and operating conditions. However, starvation increases the thermal effects and scuffing-type failures in the contacts. Figure 2.43 shows the effect of oil amount on the traction coefficient compared to fully flooded conditions.

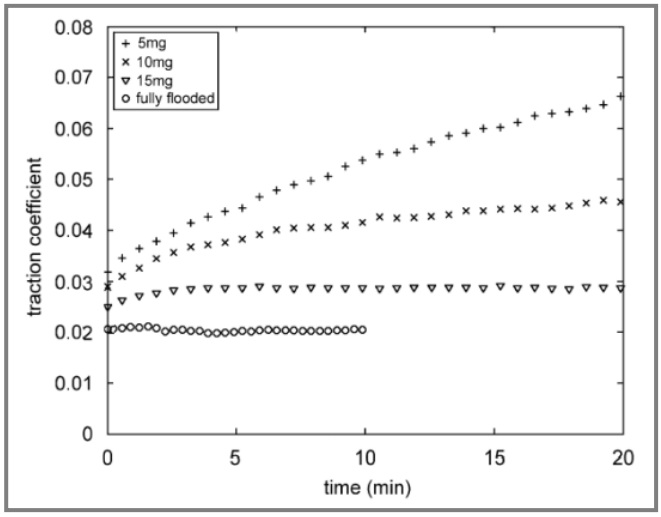

Fig. 2.43 Traction coefficient versus time for different amounts of lubricant [80].

2.5.3 Behavior of micro-features under starved lubrication

Dumont et al. [81] described numerically the behavior of micro- pits in fully flooded and starved EHL point contacts. The reduction of micro-pit amplitude is similar for fully flooded and starved conditions since in both cases the pressure distributions are quite similar. Consequently, the quantity of oil squeezed out of the pit is approximately the same in both cases. Indeed, the pit deformation is delayed in the starved case because the pressure buildup is delayed under starvation. However, the film profile around the micro-pit is similar to the smooth film profile for fully flooded conditions but for starved conditions there is a change in film profile on the sides and behind the pit. In the starved case, the height of the film behind the pit is almost 3 times larger than the height in front of the pit. Also, the benefits of pits decrease as the degree of starvation decreases because the overall film thickness becomes larger and the relative effect of emitted oil from the pits becomes less.

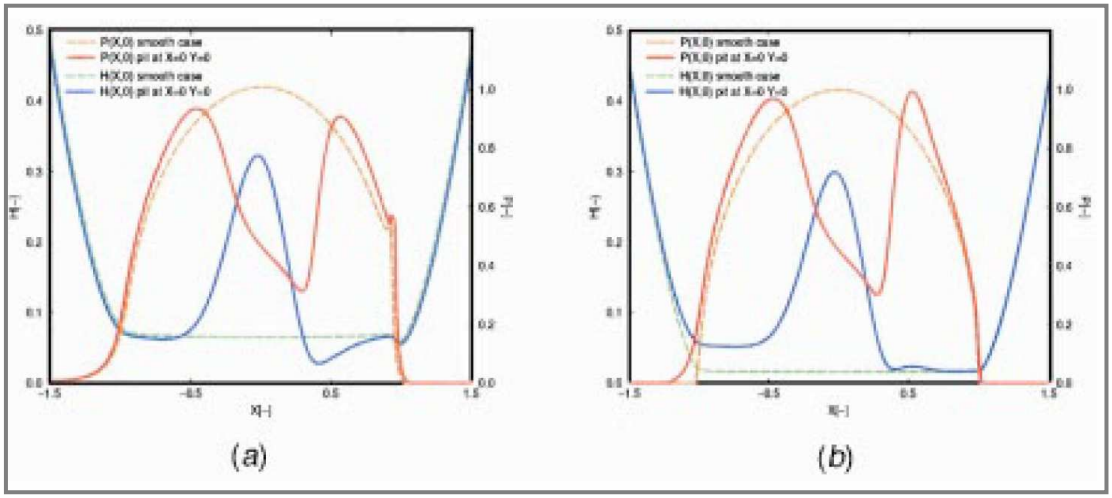

Fig. 2.44 Gap and pressure profiles along the X axis, (a) fully flooded contact, (b) starved contact [81].

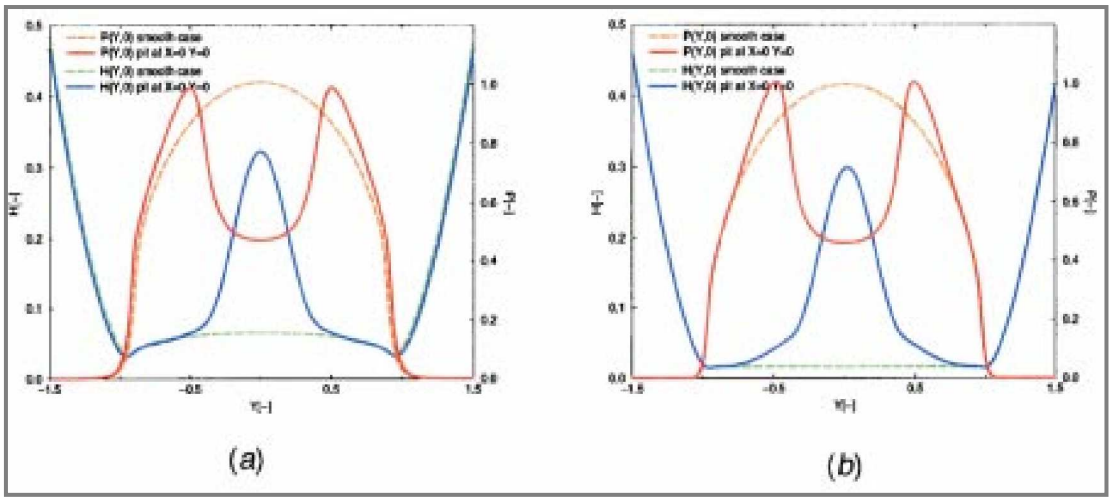

Fig. 2.45 Gap and pressure profiles along the X axis, (a) fully flooded contact, (b) starved contact [81].

Figures 2.44 and 2.45 show a numerical comparison of the film thickness and pressure profiles along the X and Y axes under fully flooded and starved contact. On the other hand, if the filled pits are on the moving surface, they bring more oil into the contact than would a moving smooth surface. The supply of additional lubricant is attributed to the elastic deformation of pits in the high pressure region. Figure 2.46 shows a 3-D simulation to the effect of micro-pits under severe starvation and the increase of film thickness behind the pit is clear.

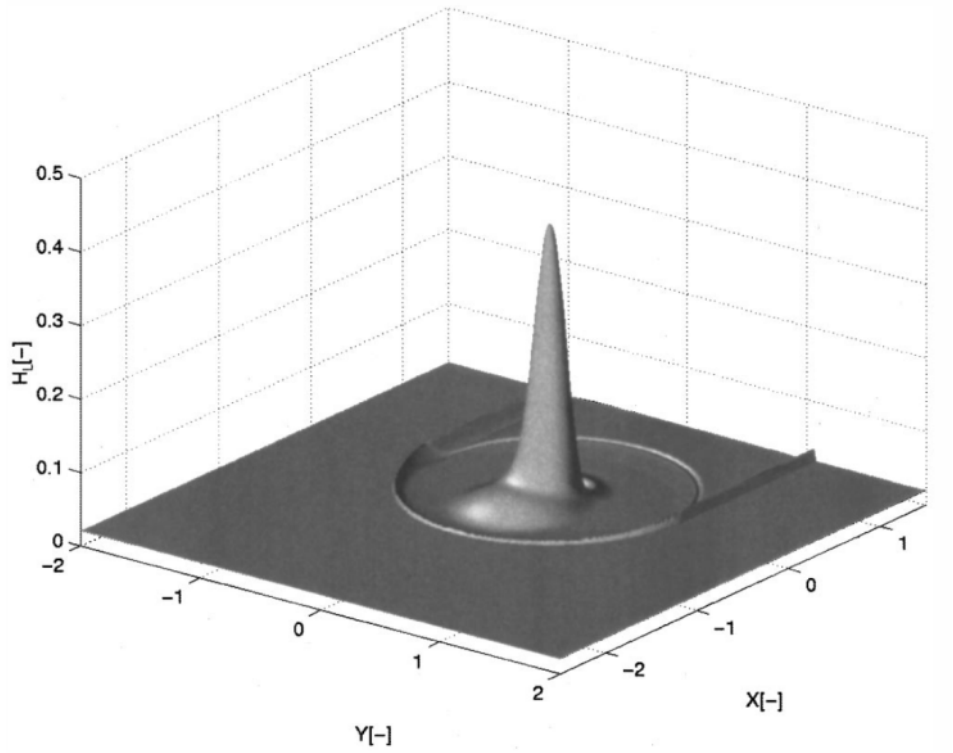

Fig. 2.46 Lubricant layer in a severely starved contact [81].

2.6 Effect of surface texturing on the contact fatigue

Contact fatigue is the major reason of machine components failure. The initiation of fatigue is usually induced by micro-cracks and the propagation of cracks which leads later to the fracture.

Cheng et al. [82] investigated experimentally the contact fatigue and crack initiation due to artificial defects. Transverse and longitudinal furrows and conical and spherical dents were made on specimen surface. They revealed by the study that the direction of friction force determines the position of cracks initiation. Furthermore, the propagation of crack is strongly influenced by the roughness hardness and temperature. The size of the defect doesn't influence significantly the crack initiation, but the height of the edge buildup is the dominant parameter on surface crack initiation.

Nelias et al. [51] performed fatigue tests with discs made of AISI 52100 steel under a slide-to-roll ratio of 61.5% and Hertzian pressure of 3 GPa. Micro-dent had a diameter of 50 μm and depth about 4 μm. The results showed that dent originated RCF starts ahead of the surface defect according to the sliding (or friction) direction. Numerical simulations have been carried out at 3 GPa as shown in Figure 2.47. The upper row in Figure 2.47 shows the pressure distribution and film thickness while the dent is travelling through the EHL contact. The middle row shows the position of the maximum shear stress in the vicinity of the dent. The lower row gives dent micrographs after 200 $x10^6$ cycles at 3 GPa and a rolling speed of 40 m/s under opposite slide-to-roll ratios. It is clear that the spike of pressure, shear stress and the initiation of fatigue are localized on the trailing edge of micro dent according to the direction of sliding.

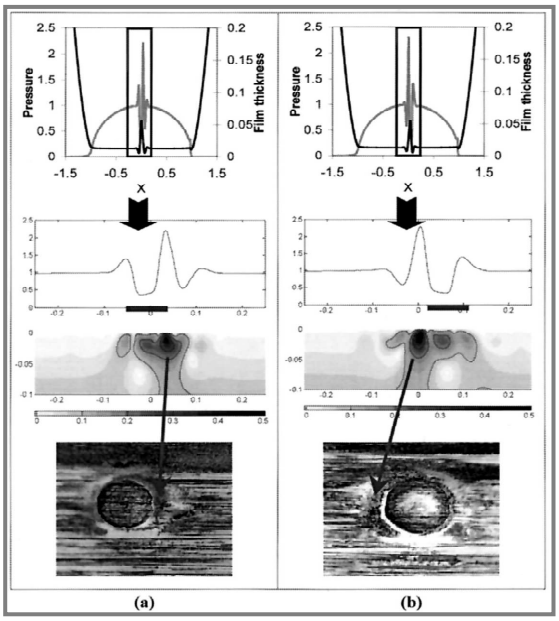

Fig. 2.47 Pressure, Film thickness and stress field in the vicinity of micro-dent (a) Slide-to-roll ratio of +1.5%; (b) Slide-to-roll ratio of -1.5% [51].

Querlioz et al. [80] determined the influence of surface defects under staved conditions. Experiments were carried out using twin disc fatigue machine as shown

in Figure 2.48. The test rig simulates the contact between gear teeth or between rolling elements under Hertzian pressure of 3.5 GPa and mean rolling speeds of 11 m/s with a constant slide-to-roll ratio of 7%. Micro-dents with diameter of 250 μm were made using a Rockwell indenter. The results demonstrated that for a relative lubricant flow rate of 50%, the fatigue life is significantly shortened (almost divided by two). Thus, the rolling contact fatigue life depends strongly on the degrees of starvation. Figure 2.49 shows dented surfaces (a) before test, (b) after test. It is clear the propagation of damage around the micro-dent.

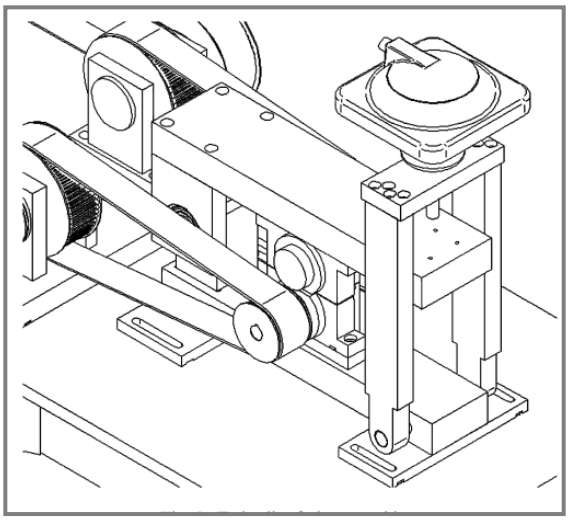

Fig. 2.48 Twin disc fatigue machine [80].

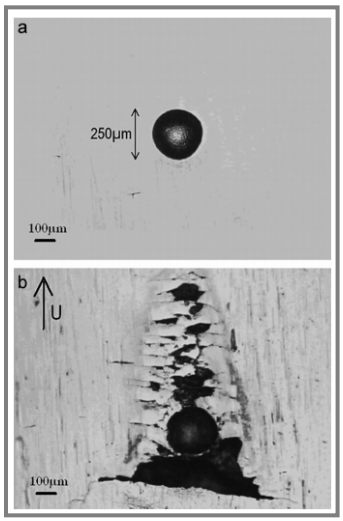

Fig. 2.49 Dented surfaces (a) Before test, (b) after test [80].

Volchok et al. [86] studied the possibility of increasing fretting fatigue life of EHL line contacts by laser surface texturing. Cylinder-on-flat contact geometry was chosen to investigate the effect of laser surface texturing on fretting contact. Schematic diagram of the experimental apparatus is shown in Figure 2.50. The results show that the laser texturing of a surface can extend the fatigue life due to the ability of micro-dimples to collect wear debris from the fretted zone. Figure 2.51 shows the beneficial effect of micro-dimples on the mean fretting fatigue life. However, maximal beneficial effect of micro-topography on the fretting fatigue resistance is strongly related to geometry parameters of micro-pores (diameter, density and depth).

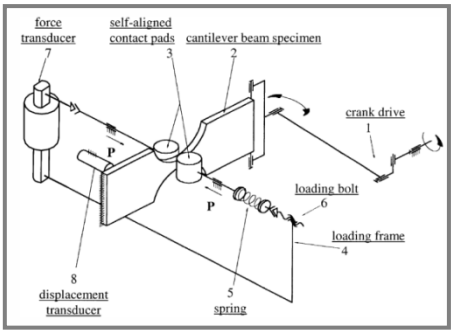

Fig. 2.50 Schematic diagram of the experimental apparatus [86].

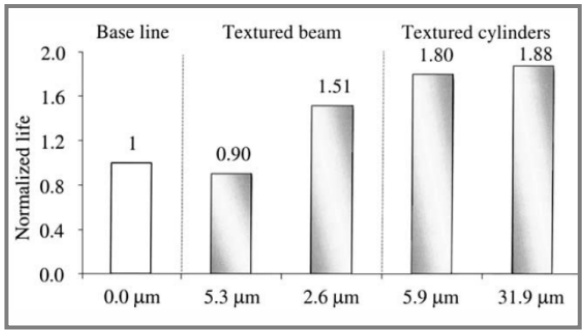

Fig. 2.51 The effect of micro-dimples on the mean fretting fatigue life [86].

Enhancing the fatigue life of rolling line contacts was investigated by Zhai et al. [83]. The significance of their study shows that the effect of micro-dents on the fatigue life depends on the lubrication regime. However, micro-dents are more active in enhancing the fatigue life under poor lubrication conditions than under fully flooded lubrication.

Vrbka et al. [87] studied the effects of surface texturing on RCF (Rolling Contact Fatigue) within non-conformal rolling/sliding contacts operated under mixed lubrication conditions. Experiments were carried out using two discs made from AISI 52100 loaded and running against cylindrical test specimen (roller). The corresponding maximum Hertzian pressure of contact is 5 GPa. Figure 2.52 shows Experimental apparatus for RCF measurements and test specimen (roller), while Figure 2.53 shows the texturing patterns used in the experiments. Different surface texture densities have been used, T1 area density: 9.2%; T2 area density: 31.6%; T3, T4 area density: 18.4%.

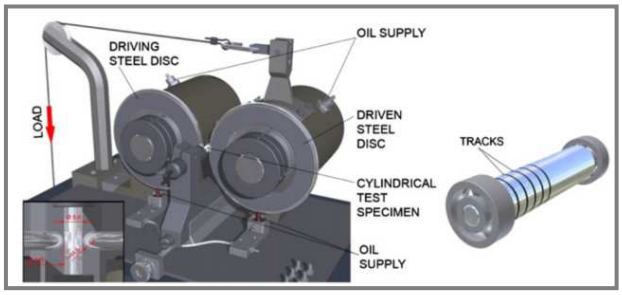

Fig. 2.52 Experimental apparatus for RCF measurements and test specimen (roller) [87].

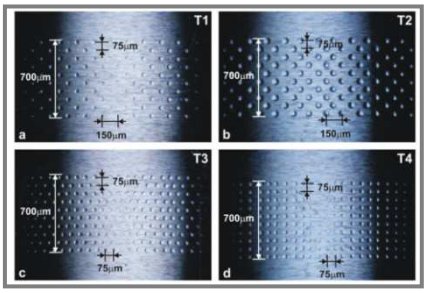

Fig. 2.53 Types of created textures on ground surfaces of rollers before RCF test [87].

The results demonstrated that lubricant emitted from micro-dents could effectively lift off the real roughness features that provided an increase in average fatigue life. See Figure2.54.

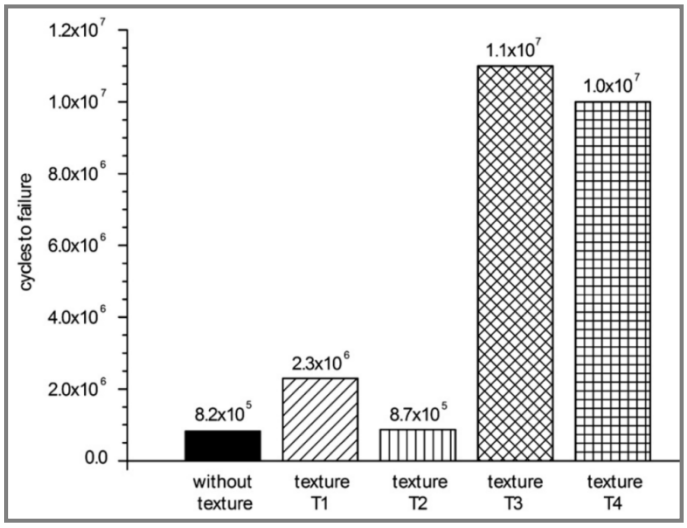

Fig. 2.54 Effect of surface texturing on contact fatigue life, T1 density: 9.2%; T2 area density: 31.6%; T3, T4 area density: 18.4% [87].

Ai et al. [84-85] revealed that under the pure sliding the effect of micro-dents on the stress is quite negligible and there are not noticeable benefits of using micro-dents to increase the contact fatigue life under sufficient lubrication conditions. When sliding is introduced the effect of micro-dent becomes pronounced and a significant pressure spike is generated which leads to a severe stress concentration on the edges of the micro-dent. The location of concentrated pressure depends on the direction of sliding. On the other hand, the fatigue life decreases with increasing load, indentation area-density and dent slope.

3 SUMMARY AND CONCLUSION OF STATE OF THE ART

The behavior of textured surfaces under different lubrication regimes has been studied by many researchers. Experimental and theoretical results showed that the tribological performance of textured interfaces is significantly related to the geometric dimensions, shape and orientation of micro-textures. The proper design of surface texturing has benefits in reducing friction and wear and increasing the load capacity of conformal surfaces under boundary and hydrodynamic lubrication. On the other hand, a lot of effort was exerted to investigate the benefits of surface texturing with non-conformal surfaces within the elastohydrodynamic lubrication (EHL). The results showed that the surface texturing leads to increase the film thickness in the contact between non-conformal surfaces because the micro-textures act as oil reservoirs or micro-bearings. Some experimental results recorded negative effects of deep micro-dented surfaces and a reduction of the film thickness. Indeed, micro-textures produce cavitations and pressure drop in the EHL contact as the depth of micro-textures is larger than the overall film thickness. The effect of operating conditions, particularly slide-to-roll ratio, on textured surfaces has been profoundly mentioned in the literature by many researchers. It was proven that increasing the slide-to-roll ratio increases the extraction of lubricant from micro-textures resulting in pressure and film thickness enhancement. On the other hand, the effect of micro-textures becomes negligible under conditions of pure rolling. Dumont et al. [81] investigated numerically the effect of micro pits under starved conditions on the film thickness and pressure of EHL point contacts. Their numerical results revealed that pits can improve the film thickness under starved lubrication.

However, the behavior of micro-texturing in EHL regime can be summarized by the following points:

- Micro-textures with proper dimensions and orientation could reduce the coefficient of friction and wear between rubbing surfaces.
- Micro-textures with a small size (in the scale of surface roughness) have a little effect on the pressure distribution and the film thickness profile in EHL contacts, because the micro-dimples will be completely absorbed by the elastic deformation.
- Micro-features with a large size cause a reduction in the film thickness in EHL contacts due to the cavitations.
- Micro- features with proper dimensions enhance the film thickness in non-conformal contacts.
- There is a very high concentrated stress around the edges of micro- features in the EHD Hertzian contact.
- The effect of micro-textures under pure rolling conditions is very little in comparison with the effect of same micro-textures under sliding conditions.
- Micro-textures bring into the contact additional lubricant by acting as oil reservoirs. However, lubricant is emitted into the contact under the effect of sliding and the elastic deformation.
- Shallow micro-dents have beneficial effects. On the contrary, deep micro-dents can cause negative effects on the film thickness.
- Micro-pits enhance the film thickness under poor lubrication or under starvation. On the contrary, micro-pits cause a reduction in film thickness under fully flooded conditions.
- Transverse and longitudinal micro-grooves increase traction and reduce the film thickness of EHL contacts due to the side leakage along the groove.

- Proper design of micro-dents could enhance the contact fatigue life by means of capturing wear debris or lift off the real roughness.
- Micro-dents are more active in enhancing the fatigue life under poor lubrication conditions than under fully flooded lubrication.

The most important parameters describing the efficiency of surface texturing are the friction and film thickness. The friction as well as film thickness determine the amount of wear and the loss of energy between rubbing surfaces. However, a lot of machine components have non-conformal contacts working under starved condition due to the severity of operating conditions and the increase of using grease lubricants. For this reasons it is necessary to find a method to prevent the metal-to-metal contact and reducing friction under extreme conditions. Surface texturing can offer the solution to avoid the failure of components under starved conditions. The biggest disadvantage of surface texturing is the fluctuation of pressure around dents and the concentration of stress on the edges of micro-textures in the EHD Hertzian contact. However, the proper design of micro-textures could bring some tribological benefits for mating surfaces. The literature review of surface texturing shows a lack of experimental study on micro-textures in starved EHL contacts. This thesis presents an attempt to fill this gap by highlighting the behavior of micro-textures under starvation and extreme conditions (thin film, reverse motion and high values of slid-to-roll ratio) in the EHL regime.

4 AIM OF THESIS

Based on the profound study of the literature and published papers concerning the modification of surface topography of lubricated contacts, the aim of the present thesis can be formulated by the following:

Experimental and numerical investigations on the effects of shallow micro-textures (micro-dents and micro-grooves) on the coefficient of friction and film thickness in EHL contacts (ball-on-disc) under extreme operating conditions and starved lubrication.

In practice, concentrated EHL contacts operate under poor lubrication in the presence of sliding motion. Therefore, it is important to understand the combined effect of extreme conditions and surface modification on the behavior of friction and film thickness in lubricated contacts. However, the aim of thesis is based on the hypothesis that, if the contact between starved lubricated non-conformal surfaces was modified by shallow micro textures then the friction between these surfaces will be less because micro textures work as lubricant reservoirs which support the film of lubrication in the contact and prevent the collapse of film lubrication. In addition, it is expected that micro-textures are more effective under starved conditions than under fully flooded conditions since the micro-amount of oil emitted from micro-dents can be more helpful in enhancing the starved thin film in comparison with enhancing the thick fully-flooded film. However, there is a possibility that micro textures lead to reduce the amount of lubricant in the contact under starved condition because the lubricant will be trapped in the micro textures resulting in reducing the feed rate of lubricant which leads to high friction.

Primary aims of thesis:

- Studying experimentally the effect of artificially produced micro-dents on reducing the coefficient of friction in sliding motion between non-conformal surfaces under starved lubrication.
- Comparing results with fully flooded conditions to ensure whether micro-dents are more effective under starved or fully flooded conditions.
- Experimental study of micro-dents effects on film thickness under starved conditions.
- Experimental study on the behavior of transverse limited micro-grooves with length less than Hertzian diameter through EHL contacts.
- Effect of transverse limited micro-grooves on friction and film thickness in sliding and reverse motion.
- Effect of transverse limited micro-grooves under starvation.
- Numerical simulation to the behavior of transverse limited micro-grooves in EHL point contacts and experimental verification.

Secondary aims of thesis:

- Studying the behavior of friction under starvation.
- Studying the effects of replenishment on friction and film thickness in EHL contacts.

5 METHODS

5.1 Methods and materials

Measurements are conducted using a tribometer shown in Figure 5.1. The system consists of three basic parts as the following:

- Simulator of the elastohydrodynamic contact represented by the contact between steel ball and glass disc. The steel ball AISI 52100 has a roughness about 10 nm and a diameter of 25.4 mm with the elastic modulus 210 GPa. The disc is made of chromium-coated glass with the elastic modulus 80 GPa.
- Microscope equipped with a high speed camera to capture interferograms of the lubricated contact. The contact is illuminated by high-power source of light.
- Software for processing data and control. The ball and disc are driven by servo-motors controlled by the computer with the ability to change the required slide-to-roll ratio in a wide range. The construction of the tribometer gives the ability of capturing interferometric images simultaneously with measuring the coefficient of friction.

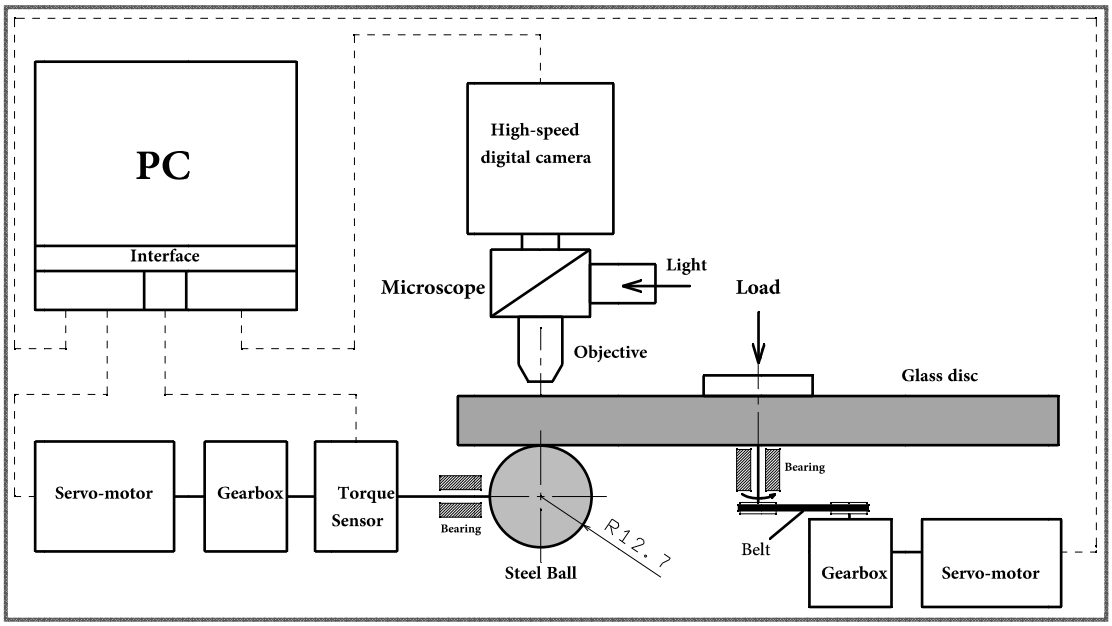

Fig. 5.1 Scheme of test rig.

When the surfaces of ball and disc are in relative motion, the entrainment speed u_e is given by:

$$u_e = (u_{disk} + u_{ball})/2$$

where u_{ball} $[m/s]$and $u_{disk}[m/s]$ are the linear speed of the ball and disc respectively. The slide-to-roll ratio SRR is given by the following formula:

$$SRR = (u_{disk} - u_{ball})/u_e$$

The sliding speed u_s is given by:

$$u_s = |u_{disk} - u_{ball}|$$

5.1.1 Friction measurements

The acquired signal from the torque sensor is processed by Digital/Analog card configured by the software LabVIEW. As shown in Figure5.2, the ball is driven by a servo-motor through torque sensor connected to the computer. The sensor has been well calibrated using static loads before all the tests. Also, compensation has been added to eliminate the effect of bearings on the ball shaft. However, the sensor has absolute error of ±0.2% according to the factory specifications.

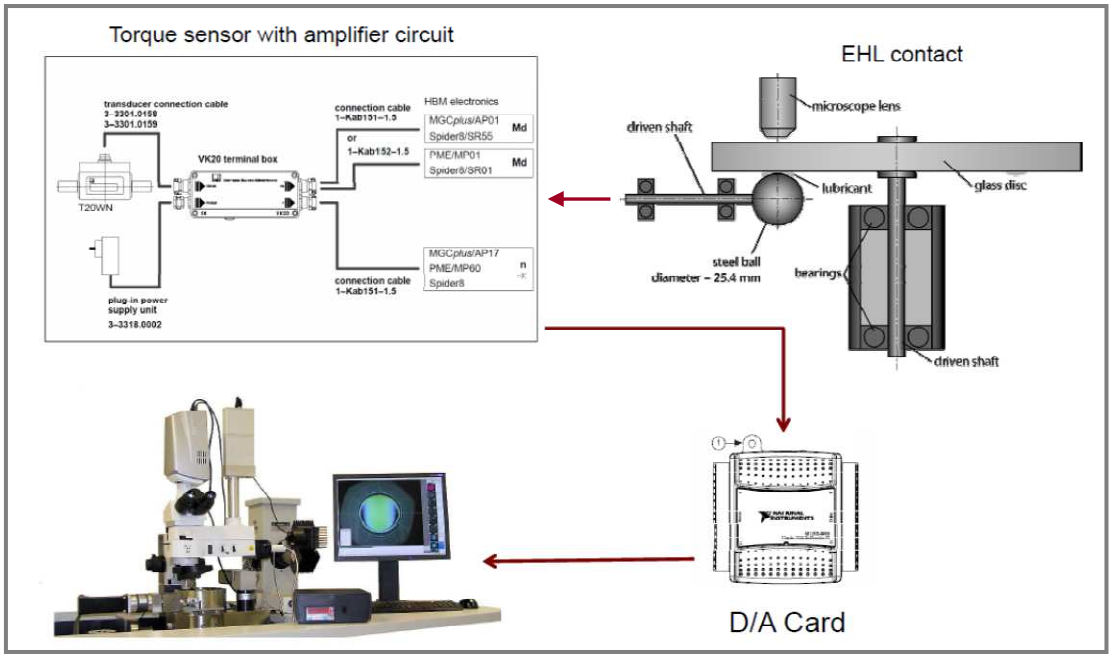

Fig. 5.2 Experimental setup for friction measurements using torque sensor.

Measuring of friction depends on determining the size of frictional forces in the contact between the rotating disc and ball using the torque sensor. Fig 5.3 shows the schematic representation of forces in the contact, where Fn is the load, Ft is the frictional force and Mt is torque. Measuring of torque using the sensor allows calculating friction by the following equations:

$$Mt = Ft\,\frac{d}{2}$$

where d is the diameter of ball.

$$\mu = \frac{Ft}{Fn} = \frac{2Mt}{d * Fn}$$

where μ is the coefficient of friction.

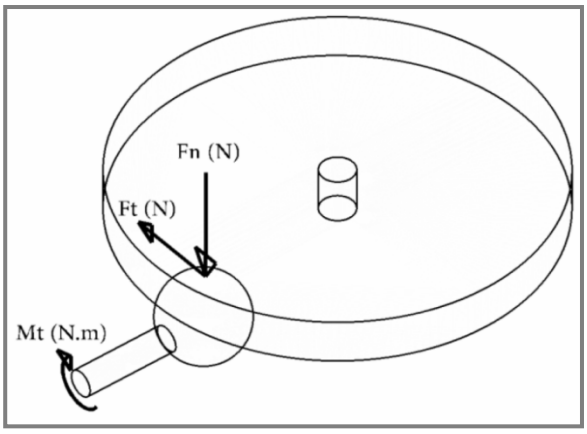

Fig. 5.3 Scheme of forces in the contact between ball and disc.

5.1.2 Film thickness measurements

The formation of the lubricating film is determined by colorimetric interferometry [88]. The principle of the method has been implemented in a comprehensive program that allows repeatedly determining the formation of the lubricating film of a large amount of chromatic interferograms obtained for different experimental conditions. Lubricated contacts are observed using a microscope imaging system. This method utilizes interference of light at the interface of contacting bodies and the lubricating film. Scheme of lubricant film thickness evaluation is shown in Figure5.4. The interferograms are converted into color model in which the colors are compared with the reference model. However, calibration is needed for proper evaluation of the lubricant film thickness from captured interferograms. Calibration consists of obtaining monochromatic and chromatic interferogram of static Hertzian contact. Monochrome image is used to establish the reference geometry, which is determined by the position of intensity maximum and minimum of the interference fringes. Subsequently, the color space CIELAB creates spatial curve, which gives the relationship between the lubricant film thickness and values coordinates in the color space. By analyzing the color of the scanned pixel interferogram during the experiment, each pixel according to the color is assigned to the thickness of the lubricating film.

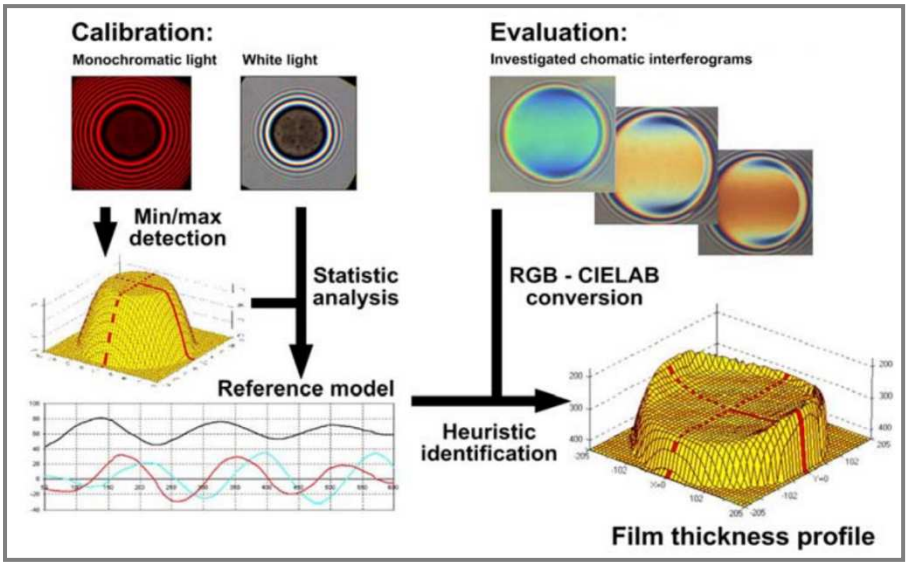

Fig. 5.4 Scheme of lubricant film thickness evaluation.

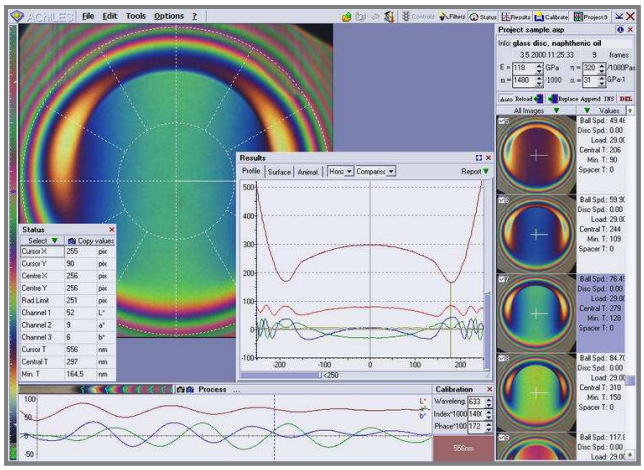

Fig. 5.5 Software for evaluation of chromatic interferograms colorimetric interferometry.

On the other hand, the method allows determining the distribution of film thickness in the entire region with 3D graphs for the resolution of 1 nm. Software Achilles is used for the evaluation of interference patterns (the interferogram). The user interface window of Achilles is shown in Figure5.5.

5.1.3 Micro-texturing

Micro-textures (micro-dents and micro-grooves) were made with a mechanical principle by using Rockwell indenter. The indenter has a diamond head with a radius of curvature of 0.2 mm. This allows creating indentations with very well defined geometry. Figure 5.6 shows the device for creating micro-textures. These parts are rigidly connected by threaded joints due maintenance or modification of the machine. This device is self-contained and not attached to any table.

Fig. 5.6 Device for creating micro-textures.

Rotational motion and axial displacement are completely automated and driven by stepper motors. Linear electromagnetic actuator is used for creating the impact between the Rockwell head and the surface of ball. The intensity of impact depends

on the value of volte and current in the electromagnetic actuator. Thus, the dimensions of micro-textures (depth and diameter) depend on the intensity of impact. The relationship between volt-current and micro-textures dimensions can be set by experimental iteration. The device is equipped also with two fans for cooling the stepper motor and electromagnet actuator. The total weight of the device without the control box is 26 kg. Maximum dimensions are 456x300x175 mm. Figure5.7 and Figure5.8 show the resulting micro-dents on the surface of ball. Geometry of indentation was defined by an optical profilometer. Actually, the devise is dedicated only for laboratory use.

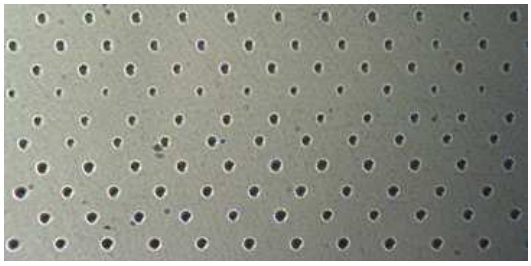

Fig. 5.7 Microscopic image of dented ball surface by Rockwell indenter.

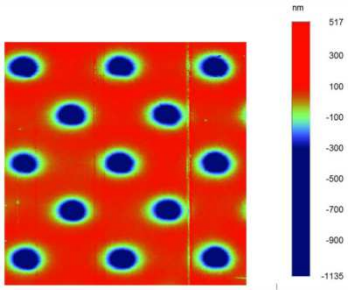

Fig. 5.8 Optical scanning of micro-dents by using profilometer.

5.1.4 Lubricants

Two different lubricants have been used in all experimental measurements. Tab.5.1 shows the properties of used lubricants.

Tab. 5.1 Properties of lubricants

Lubricant	type	Viscosity [Pas]	Viscosity-pressure coefficient [GPa^{-1}]
N 2400	Naphthenic	0.421 @ 40 °C	35
R 834/80	Mineral	0.215 @ 22 °C	21.85

6 RESULTS AND DISCUSSIONS

6.1 The degree of starvation in ball-disc machine based on the relative friction

This section focuses on analyzing the correlation between the degree of starvation and friction under the sliding motion in ball-disc machine. Thus, it can be stated that the approximate ratio of the film thickness reduction can be predicted based on accurate measurements of friction. The naphthenic base oil (N2400) with the dynamic viscosity $\eta = 0.412\ Pas$ at 40°C and the pressure-viscosity coefficient $\alpha = 35 GPa^{-1}$ was used in all the experiments introduced in this section.

6.1.1 Calculation of friction under starved lubrication

In each lubrication regime, the coefficient of friction is related to the film parameter $\lambda = h/\sigma$. Thus, the following equation by Sakaguchi et al. [89] can be adopted to calculate the coefficient of friction in the relative form:

$$\bar{\mu}_C = \frac{\mu_s}{\mu_{ff}} = \begin{cases} \mu_b/\mu_{ff} & if \quad \lambda_{st} < 0.01 \\ \dfrac{(\mu_b/\mu_{ff}) - \bar{\mu}_h}{(0.01-1.5)^6}(\lambda_{st}-1.5)^6 + \bar{\mu}_h & if \quad 0.01 \le \lambda_{st} < 1.5 \\ \bar{\mu}_h & if \quad 1.5 \le \lambda_{st} \end{cases} \qquad (6.1)$$

where $\bar{\mu}_c$ is the relative coefficient of friction through the different lubrication regimes, $\bar{\mu}_h$is the relative hydrodynamic coefficient of friction under starved lubrication, and μ_b is the boundary friction.

Experimental investigations show that the majority of lubricants exhibit a non-Newtonian behavior in the EHL contacts due to the non-linearity of the shear stress τ versus the shear rate. However, the shear stress is given by the Bair and Winer model as.

$$\bar{\tau} = 1 - e^{-(\gamma\eta/\tau_L)} \qquad (6.2)$$

with $\bar{\tau} = \tau/\tau_L$, η is the viscosity and$\dot{\gamma}$ is the shear rate.
The limiting shear stress is represented by the following (19).

$$\tau_L = \tau_{L0} + \beta p_m \qquad (6.3)$$

where τ_{L0} is the limiting shear stress at zero pressure, $\beta = \partial\tau_L/\partial p$ is the shear stress–pressure coefficient and p_m is the average Hertzian pressure.

For the most of mineral oils $\tau_{L0} \approx 15 MPa$ and $\beta \approx 0.052$ @ 40 $°c$, see references [90] and [91]. Under starved lubrication the film thickness tends to be flat which means that the central film thickness has a value nearly equal to the value of the minimum film thickness, see Chevalier [75]. Therefore, the pressure distribution can be approximated to the Hertzian pressure by the following:

$$p = p_h\sqrt{\left(1-(r_c/a)^2\right)} \qquad (6.4)$$

And the shear rate can be approximated by the following:

$$\gamma = \partial u/\partial h \approx \Delta u/h \qquad (6.5)$$

The ratio of the shear rate through the transition from fully flooded to starved conditions under a given steady state can be expressed by the following:

$$\gamma_s/\gamma_{ff} = h_{cff}/h_{cs} = 1/\Re \qquad (6.6)$$

Roelands equation [92] is adopted to define the viscosity by the following:

$$\eta = \eta_0 (\eta_\infty/\eta_0)^{\left(1-(1+P/P_r)^z\right)} \qquad (6.7)$$

with $\eta_\infty = 6.31\times10^{-5}$ Pa.s, $p_r = 1.962\times10^8$ Pa and p is given by equation (4).

The combination between equations (6.2) and (6.6) gives the relative hydrodynamic coefficient of friction under starved lubrication by the following:

$$\overline{\mu}_C = \overline{\mu}_h = \int_0^a \left(1-e^{-(\gamma_s\eta/\tau_L)}\right) r_c\, dr_c \Big/ \int_0^a \left(1-e^{-(\gamma_{ff}\eta/\tau_L)}\right) r_c\, dr_c = \int_0^a \left(1-e^{-(\gamma_{ff}\eta/\Re\tau_L)}\right) r_c\, dr_c \Big/ \int_0^a \left(1-e^{-(\gamma_{ff}\eta/\tau_L)}\right) r_c\, dr_c \qquad (6.8)$$

The slide-to-roll ratio SRR is given as:

$$SRR = 2*(u_{disk}-u_{ball})/(u_{disk}+u_{ball}) = u_s/u_e \qquad (6.9)$$

with u_s the sliding velocity and u_e the entraining velocity. The negative signal of SRR means that the ball is faster than the disc.

Equation (6.1) can be solved for $\Re \neq 0$ by applying a numerical integration to calculate $\overline{\mu}_h$ for an isothermal lubricated contact between a steel ball and a glass disc under steady state conditions. The central full film thickness h_{cff} can be calculated by the well known formula of Hamrock and Dowson [71]. Table 1 shows the parameters of contact for numerical calculations:

Tab.6.1 Parameters of contact for numerical calculations

Ambient temperature $t = 25\ ^\circ C$	Dynamic viscosity $\eta_0 = 0.421\ Pa.s\ @\ 40\ ^\circ C$
Modulus of elasticity $E_{ball} = 210 GPa$	Boundary friction $\mu_b = 0.12$
Modulus of elasticity $E_{disk} = 80\ GPa$	Pressure-viscosity index $z = 0.64$
Poisson's ratio $\upsilon_{ball} = 0.3$	Composite roughness $\sigma = 10.77\ nm$
Poisson's ratio $\upsilon_{disk} = 0.17$	Limiting stress $\tau_{L0} = 15 MPa @\ p = 0$
Reduced radius of the contact $R' = 6.35\times10^{-3}\ m$	Ellipticity parameter K=1

6.1.2 Effect of operating conditions

Equation (6.1) was numerically simulated using the adaptive *Simpson's* method with an error of 10^{-6} as shown in Figures 6.1, 6.2 and 6.3. It is necessary to take into consideration that the value of μ_{ff} changes with the load and the entraining velocity.

Hence, every single curve in Figures 6.1 and 6.2 represents a different steady state. Figure 6.1 shows that the increasing of the load in the starved contact of ball-disc under the same entraining velocity leads to reduce the sensitivity of friction versus the change of the starvation degree, whereas the critical degree of starvation $\Re_{cr}$ ($\Re_{cr} = 1.5\sigma/h_{cff}$ represents the transition from the full film regime to the mixed regime) is not significantly affected by the load since $h_{cs} = \Re^* h_{cff} \propto \Re^* w^{-0.073}$.On the other hand, Figure 6.2 shows the slight effect of the entraining velocity on the sensitivity of friction, whilst the value of $\Re_{cr}$ was noticeably reduced with the higher speed resulting in enlarging the range of the validity of equation (6.8) where $\bar{\mu}_C = \bar{\mu}_h$ for $\Re \in]\Re_{cr}, 1]$. Note that in this case $h_{cs} = \Re^* h_{cff} \propto \Re^* u_e^{0.68}$.

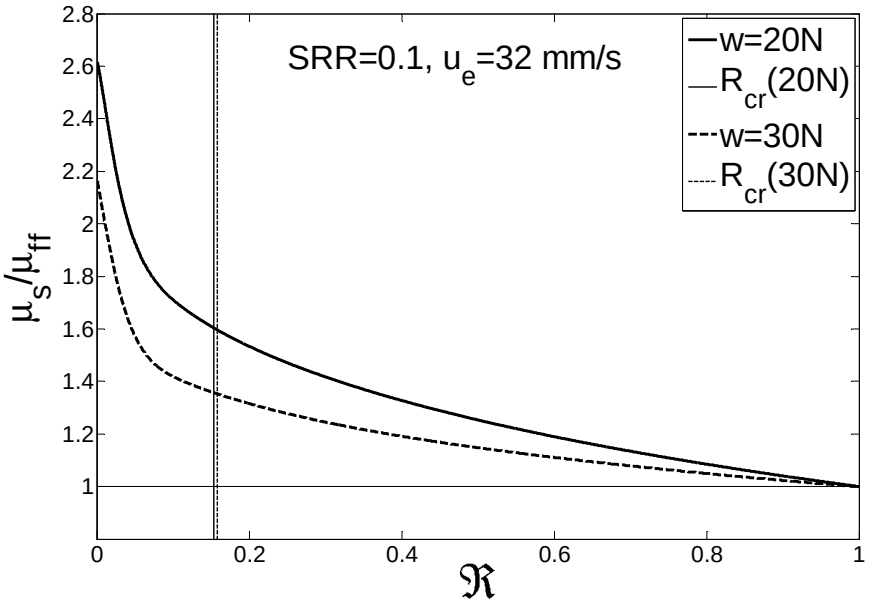

Fig.6.1 The simulation for the effect of the load on the non-Newtonian behavior of the relative coefficient of friction $\bar{\mu}_c = \mu_s/\mu_{ff}$ vs. the degree of starvation $\boldsymbol{\mathcal{R}}$ for SRR=0.1.

The large effect of load on the sensitivity of friction is attributed to the exponential change in the viscosity with load, see equation (6.7), while the effect of load on the limiting shear stress in equation (6.3) is linear and it is minor for low loads P<0.5 GPa. Therefore, the effect of τ_L on the sensitivity of friction is slight for low loads. The effect of speed is limited on the film thickness with the exponential factor 0.68. To investigate the influence of the slide-to-roll ratio SRR on the relative coefficient of friction, the entraining velocity and the load were kept constant in equation (6.1). Figure 6.3 shows the simulation of SRR effect on the non-Newtonian relative friction versus the degree of starvation in the steady state. In this simulation it was supposed that the critical degree of starvation is not related to the value of sliding $\Re_{cr} \neq f(SRR)$.

It is clear that increasing SRR leads to reduce the gradient of the relative coefficient of friction $\bar{\mu}_c = \mu_s/\mu_{ff}$ versus the degree of starvation $\boldsymbol{\mathcal{R}}$ although the larger SRR results in a larger μ_s. In other words, the starved coefficient of friction μ_s can be doubled more times under low slide-to-roll ratios than under high slide-to-roll ratios for the same degree of starvation. Hence, the lubricant tends to be more

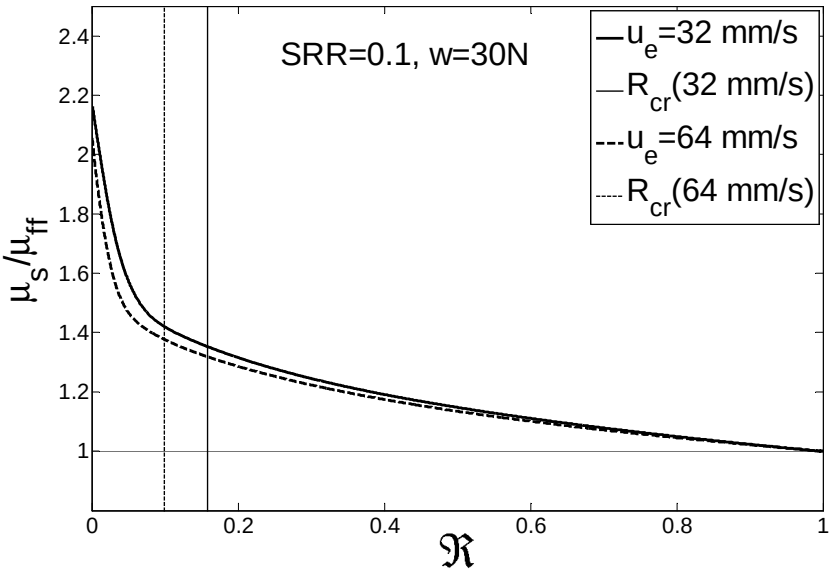

Fig.6.2 The simulation for the effect of the entraining velocity on the non-Newtonian behavior of the relative coefficient of friction $\bar{\mu}_c = \mu_s/\mu_{ff}$ vs. the degree of starvation $\mathcal{R}$ for SRR=0.1.

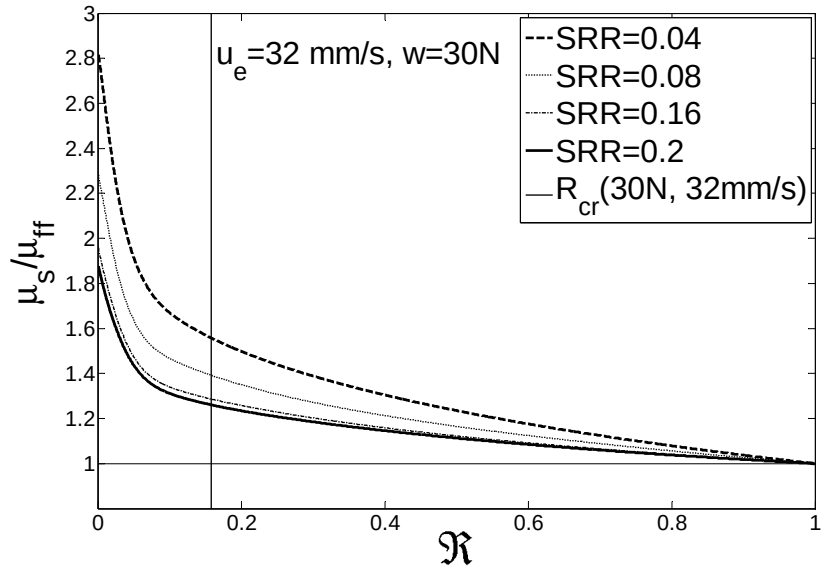

Fig.6.3 The simulation for the effect of the slide-to-roll ratio SRR on the relative coefficient of friction $\bar{\mu}_c = \mu_s/\mu_{ff}$ under starved conditions.

Newtonian (the transition from the Couette flow to the Poiseuille flow) with reducing the slide-to-roll ratio under the starved lubrication. This result is common in non-Newtonian shear stress models where the behavior of lubricants is Newtonian for low shear rates then it becomes gradually non-Newtonian with increasing the shear rate.

6.1.3 Experimental verification

Measurements were carried out to verify the theoretical models and to investigate experimentally the behavior of friction versus the degree of starvation under steady state operating conditions. The degree of starvation was modified from the fully flooded to extreme starvation by changing the oil amount available on the track. Indeed, the expression of the fully flooded is flexible because the same contact under the same steady state can be fully flooded for many different oil amounts. Thus, the concept of Q_{ff}, representing the minimum oil amount to make the contact fully flooded under a given steady state, is adopted. The value of Q_{ff} was adjusted for the minimum coefficient of friction measured by the sensor for the given steady state (load= 30N, the entraining velocity u_e=42mm/s and SRR=-0.2) and the oil amount Q_{ff} was iteratively defined by 60µL. For $Q > Q_{ff} = 60\mu L$ the contact is considered to be ultra fully flooded and a small increase of friction was observed. However, in experiments it was avoided to make the relative oil amount available on the track $Q_s/Q_{ff} \in [0,1]$ less than 20 % to avoid any possible damage of the contacting surfaces.

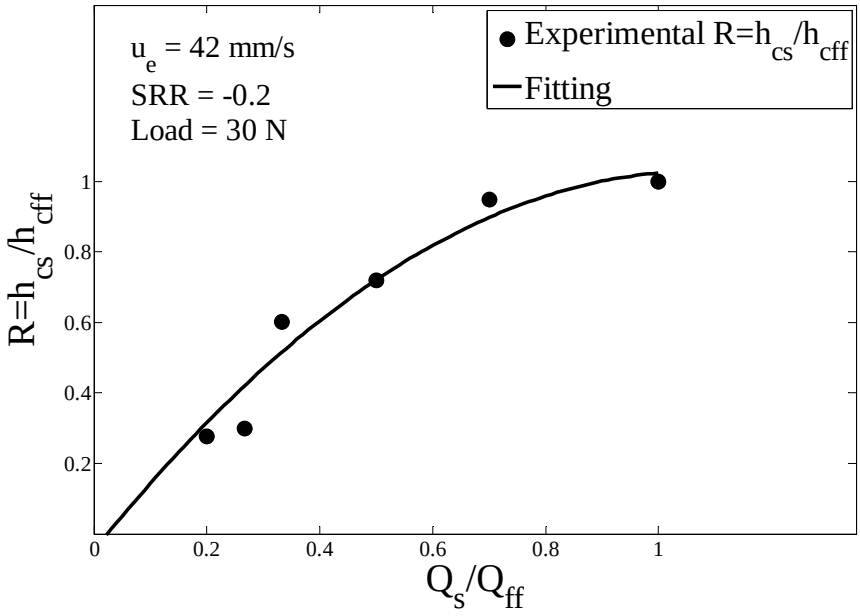

Fig.6.4 The degree of starvation $\mathcal{R} = h_{cs}/h_{ff}$ versus the relative oil amount reduction.

Figure 6.4 shows the measured degree of starvation $\mathcal{R} = h_{cs}/h_{ff}$ as a function of relative oil amount Q_s/Q_{ff}. On the other hand, Figure 6.5 shows a comparison between the calculated and the experimental ratio $\bar{\mu}_c = \mu_s/\mu_{ff}$ vs. the degree of starvation. It is clear that reducing the oil amount from $Q_{ff} = 60\,\mu L$ to $Q_s = 42\mu L$ caused a small increase in the friction but a smaller reduction in the oil amount from $16\mu L$ to $12\mu L$ resulted in a lager relative increase of friction coefficient. Therefore, the coefficient of friction becomes increasingly sensitive to the oil amount with increasing the severity of starvation, this result is in accord with Figures 6.1, 6.2 and 6.3.

Figure 6.5 shows that the theoretical model is slightly dependant on the value of τ_{L0} under low loads in the hydrodynamic range.

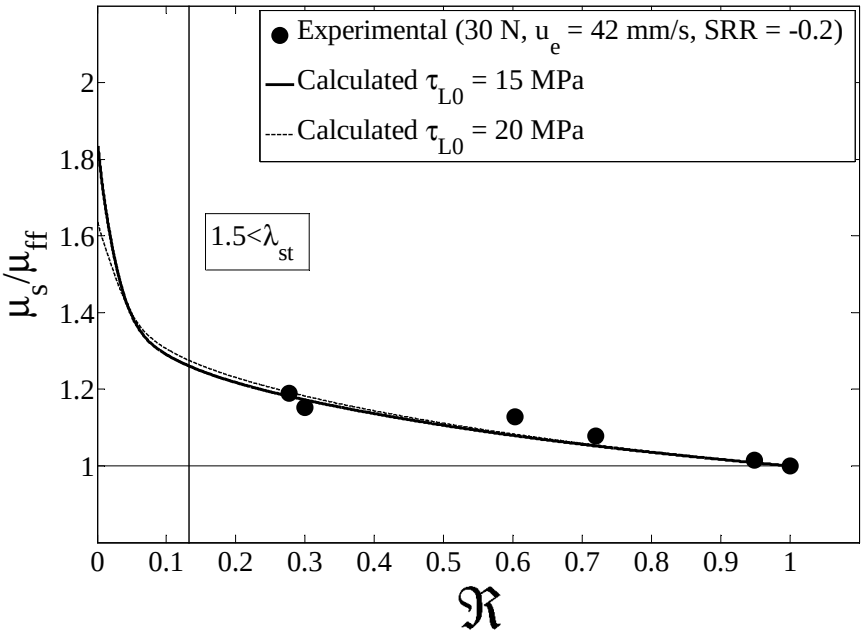

Fig.6.5 Comparison between the calculated and the experimental ratio $\bar{\mu}_c = \mu_s/\mu_{ff}$ vs. the degree of starvation.

Previous results in section 6.1 show that the degree of starvation can be defined approximately in the EHL contact based on measuring one parameter (the relative coefficient of friction). Such an approximate approach could be useful in cases of opaque contacts where the optical interferometry technique can't be used, e.g., steel ball on metal disc. This approach can be extended to some practical applications like ball bearings to predict the degree of starvation based on the value of friction which allows avoiding the failure.

6.2 Replenishment and starved EHL point contacts

Enhancing the film thickness of lubrication is the key to reduce friction and wear and to extend the lifecycle of concentrated conjunctions. However, the EHL theory is successfully valid for oil full film lubrication, while it fails in the case of starved or grease-lubricated contacts. Starvation is usually associated with a sharp reduction of the film thickness to just a few nanometres resulting in high friction and wear. Starvation is essentially due to the failure of lubricant to replenish the track after being displaced sideways by the repeated overrollings of the rolling element [93]. Grease lubrication is widely used in bearings to provide a sufficient and permanent separation between rolling elements and rings, which results in enhancing the lifecycle and reducing friction. In cases concerning the leakage, grease lubrication is preferred over oils lubrication since its stiffness creates a resistance against the leakage [68]. On the other hand, replenishment is strongly insufficient with grease lubrication because when the grease is pushed to the sides it can't readily flow back into the track leading to very thin films of lubrication and high temperatures in the contact [94, 95, 96, 97]. Cann [98] showed experimentally that the properties of the deposited thickener layer of grease determine friction and film thickness. However, the mechanism of replenishment for greases can be explained by the effect of base oil bleeding [99] and the shear degradation [100]. Such mechanisms are significantly insufficient.

6.2.1 Mechanism of artificially induced replenishment

Figure 6.6 shows the mechanism for generating the induced replenishment on the track of the ball. The mechanism consists of a slider (thin plastic sheet made of Polyethylene) with a micro-slot concentric with the over-rolled track. The thin plastic sheet is flexible with a tension force about 0.1N which ensures the permanent contact with the ball surface without fear of increasing friction or wear. The slider scrapes the lubricant on the surface and creates a forced and channeled reflow towards the centerline of the over-rolled track through the micro-slot.

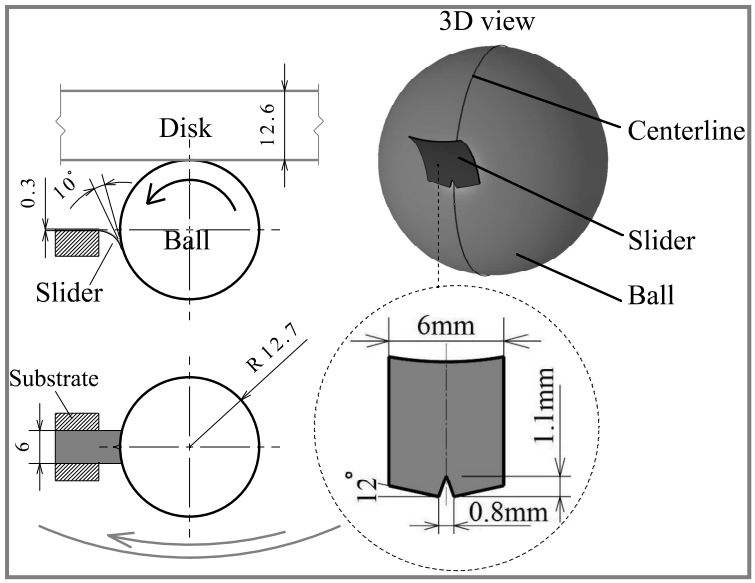

Fig.6.6 Scheme of the mechanism providing the artificially-induced replenishment in the ball-on-disc device.

6.2.2 Effect on film thickness

Figure 6.7 shows the effect of the induced replenishment on the distribution of lubricant along the over-rolled track and the resulting film thickness with grease lubrication. The interferometric images in Figure 6.7 are captured after 15 minute from the start with SRR = -0.51, u_e = 35.2 mm/s, w=30N and 100 mg of grease on the track. Figure6.7-a shows that the over-rolled track is severely depleted with the natural replenishment mechanisms. The width of the depleted track is approximately equal to the diameter of the Hertzian contact and the resulting central film thickness is about 80 nm after 15min from the start. That value of the central film thickness diminishes with time which is common with grease-lubricated contacts. The corresponding interferometric image in Figure 6.7-a shows the large intersection between the inlet air-oil meniscus and the Hertzian zone. This referees to an insufficient replenishment and severe starvation with a high risk of scuffing. On the other hand, Figure 6.7-b shows the distribution of grease on the track with the induced replenishment and it is clear that the over-rolled track is flooded by a thick and wide band of channelled grease. The resulting central film thickness is about 210 nm.

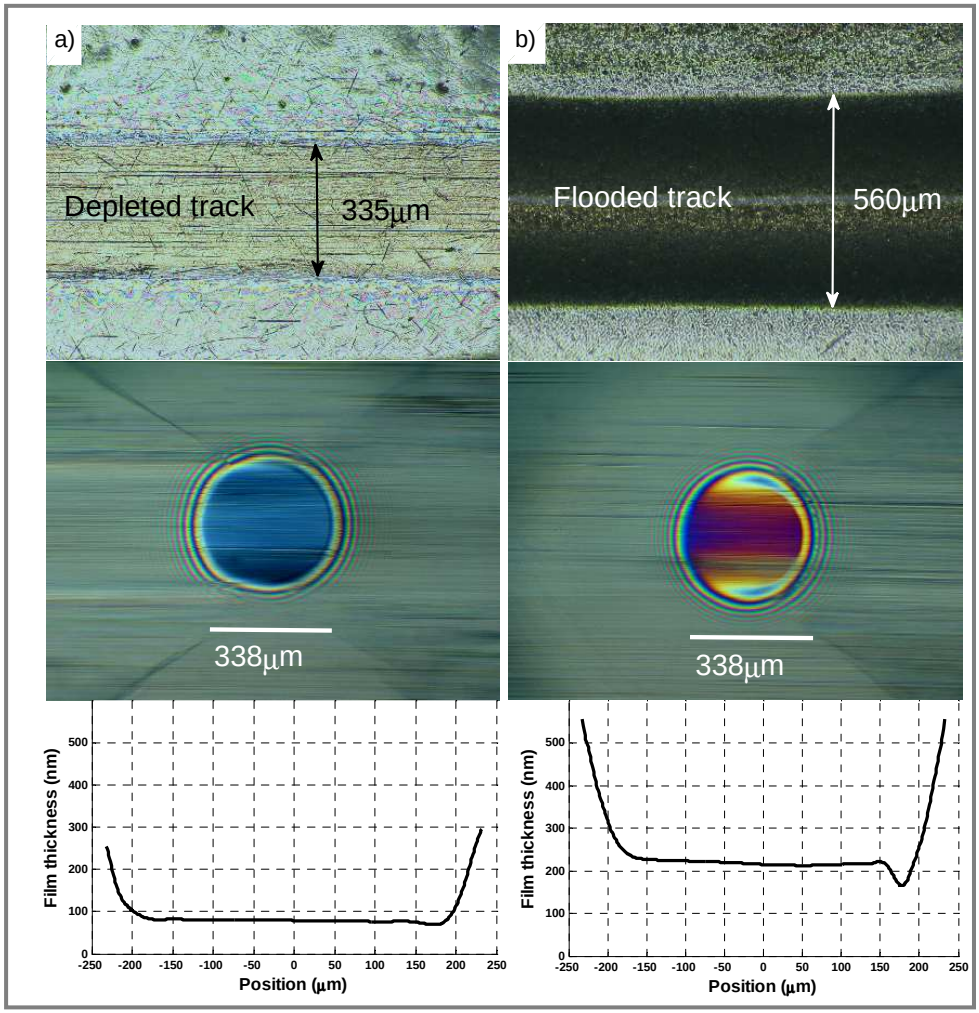

Fig.6.7 Optical microscope images of the overrolled track with the corresponding interferometric images and film thicknesses in the contact for grease lubrication with **a)** without induced replenishment **b)** with induced replenishment.

6.2.3 Effect on friction

Figure 6.8 shows a comparison of friction behavior of the contact with and without the mechanism of artificially induced replenishment under load 30 N, SRR=-1.85 and u_e=34.5 mm/s. The track is supplied by a very little amount of oil (8µl) and it is necessary to note that this amount of oil will be distributed on the tracks of the ball and disc due to the sliding. Although only the track of the ball is artificially replenished, it is clear that a significant reduction of friction about 31% has been occurred in the first 15 minute of the measuring (the percent of reduction increases with time). Figure 6.8 shows that the coefficient of friction (COF) for the starved contact with the natural replenishment increases with time due to the film thickness decay with the subsequent overrollings. On the other hand, the COF with the induced replenishment is stable over time.

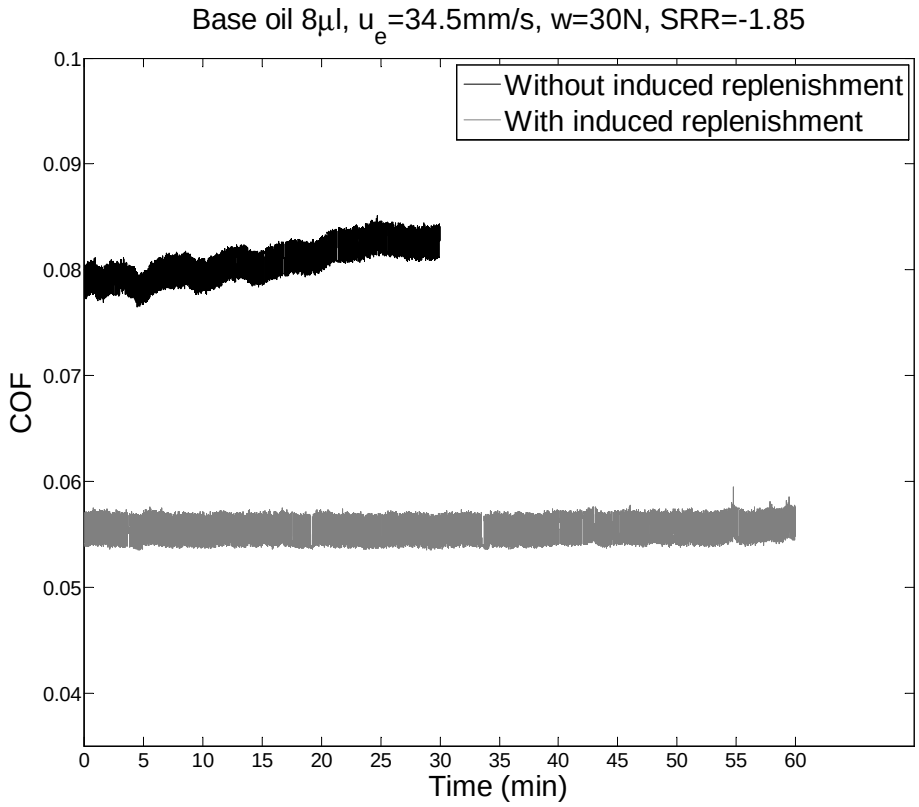

Fig.6.8 Coefficient of friction (COF) of the contact with and without induced replenishment with 8µl of base oil on the track.

Section 6.2 shows an approach of channeling lubricant (oil or grease) towards the centre of the depleted track. As a result, the displaced lubricant is recovered leading to a fully flooded contact even with a very little amount of lubricant and under extreme operating conditions. The mechanism of artificially channeled replenishment is proposed to operate in radial and thrust rolling bearings to recover the displaced lubricant into the raceway of bearings. The practical application of channeled replenishment in bearings is included in the appendix.

6.3 Behavior of micro-dents under starvation

Enhancing the film thickness between lubricated contacts is the first step to diminish friction and wear. Under starvation, the film thickness becomes shallower than under fully flooded conditions due to the delay of pressure build up. However, the presence of micro-features within EHL contacts can significantly influence the pressure distribution and film thickness. The tribological performance of surfaces with micro-dents was evaluated by comparing friction and film thickness with smooth surfaces under starvation in the presence of sliding motion. Measurements were carried out by using a ball-on-disc Tribometer shown in Figures 5.1 and 5.2. The naphthenic base oil (N2400) with the dynamic viscosity $\eta = 0.412\ Pas$ at 40°C and the pressure-viscosity coefficient $\alpha = 35GPa^{-1}$ was used in all experiments presented in this section.

6.3.1 Effect of micro-dents on friction under starvation

In order to investigate the effect of micro-dents on reducing friction, the surface of the ball was artificially dented by 4 rows of shallow micro-dents, see Figure 6. 9. The average diameter of the dent is about 35μm with a depth about 0.6μm. The interval step between dents is about 222μm while the offset between rows is about 110μm. Measurements were carried out under load 32 N, SRR=-1 and u_e=60 mm/s. The corresponding maximum Hertzian pressure is 0.521 GPa. In case of starvation, the contact has been supplied only by 14 μl of base oil (N400). Figures 6.10 and 6.11 show a comparison of the friction coefficient for smooth and textured surface under starved and fully flooded lubrication. The results show that the benefits of micro-dents under severe starved lubrication are relatively considered with a friction reduction about 9%. On the other hand, the benefits of micro-dents under fully flooded conditions are negligible and the value of average friction of smooth and textured surfaces is nearly the same. That effect is justified by the fact that the little amount of emitted fluid from micro-dents doesn't make a significant difference in enhancing the film thickness under fully flooded lubrication where the overall film thickness is originally large enough.

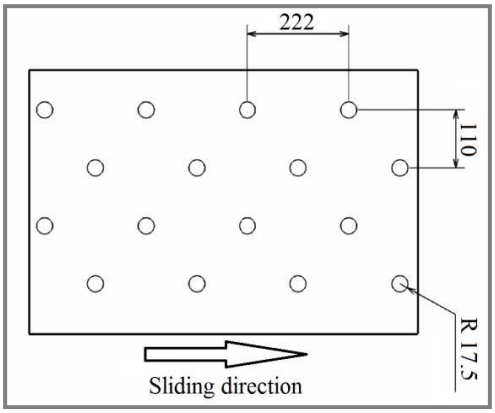

Fig.6.9 Distribution of micro-dents on the ball surface.

From Figures 6.10 and 6.11 we can also notice that the friction increases with the time under steady state for both textured and smooth surfaces under starved lubrication while the friction is stable with the time under fully flooded condition.

This behavior can be attributed to the thermal effect where the available amount of oil under fully flooded condition is larger in comparison with the starved condition which results in a larger heat capacity for fully flooded contact, for this reason the oil temperature for starved conditions is higher than the oil temperature for fully flooded conditions under the same operating conditions. It is well known that the higher temperature the lower viscosity of lubricant and film thickness.

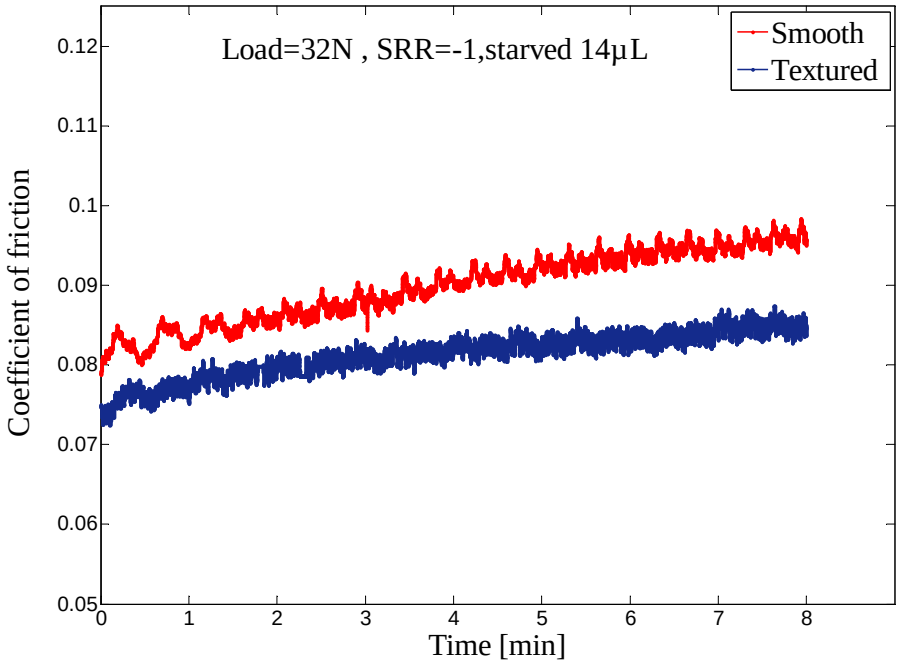

Fig. 6.10 Coefficient of friction for smooth and textured surfaces under starved conditions.

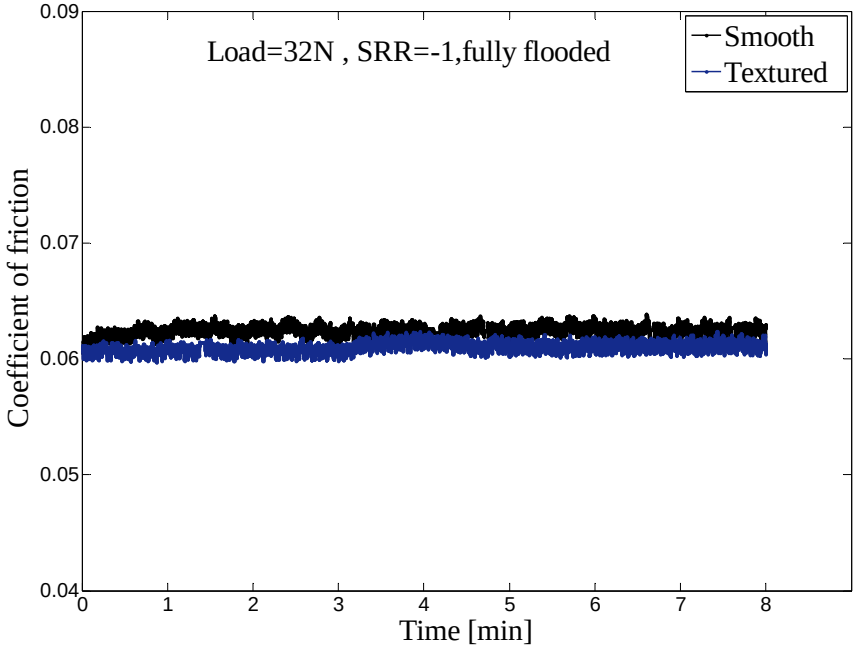

Fig. 6.11 Coefficient of friction for smooth and textured surfaces under fully flooded conditions.

6.3.2 Effect of micro-dents on film thickness under starvation

Figure 6.12 shows the profile and depth of micro-dents produced on the surface of ball for investigating the effect on the film thickness under starvation. The diameter of micro-dent is about 65 µm with average depth of 800 nm. The contact is lubricated with base oil (N2400) under load of 44 N, SRR=-1.66, u_e =4.8 mm/s and oil amount18 µl. In this case, the corresponding maximum Hertzian pressure is 0.58 GPa

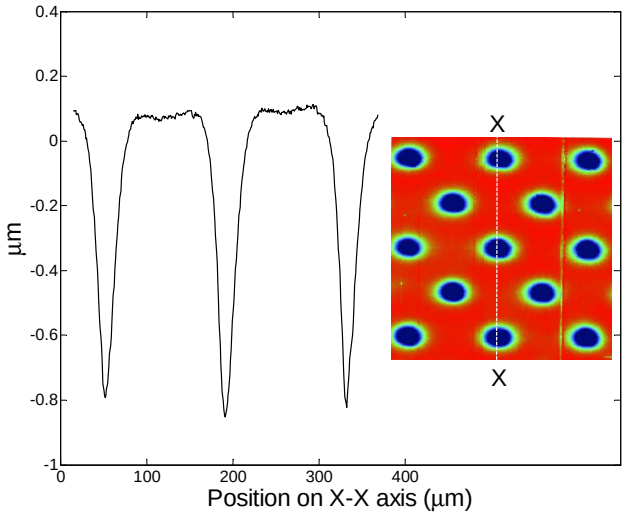

Fig. 6.12 Profile of micro-dents on X-X axis.

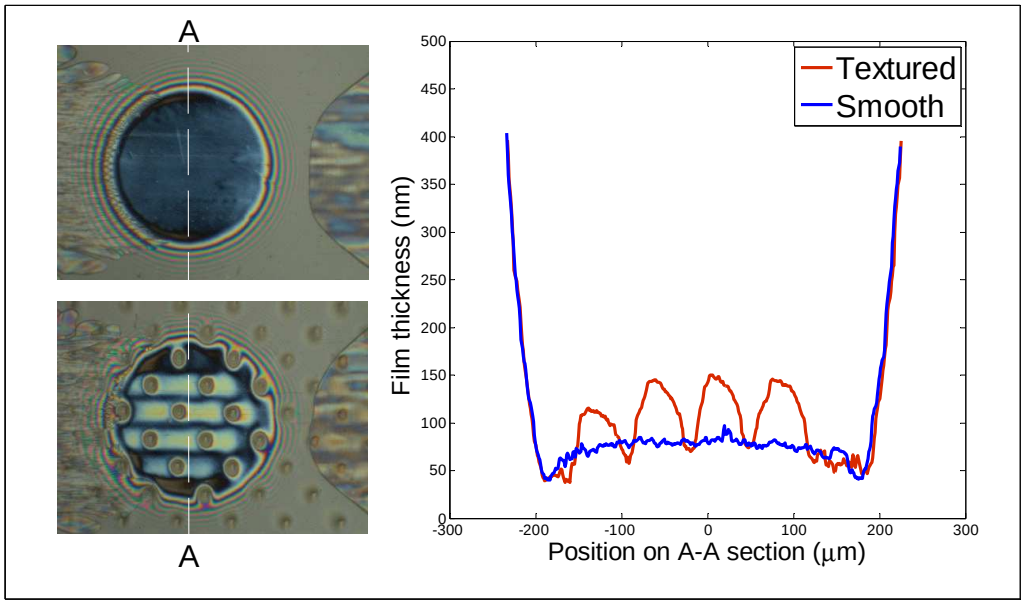

Fig. 6.13 The film thickness profile on A-A axis for smooth and textured surfaces under starved lubrication with SRR=-1.66, u_e =4.8 mm/s., w=44 N.

Figure 6.13 shows a film thickness comparison for smooth and textured surfaces with the corresponding interferogam images. Indeed, it would be difficult to capture

such images with high resolution without the high speed camera (700 pps). Starvation can be observed in interferogam images where the air-oil meniscus is localized very close to the Hertzian contact. On the other hand, interferogam images show a significant modification of lubrication film shape. The measured film thickness on A-A axis shows that the textured surface has a larger film thickness compared to the smooth one. This enhancement is attributed to the extraction of lubricant from micro-dents under the effect of the elastic deformation and the kinematic sliding. This implies that micro-dents are able to bring additional lubricant into the EHL contact even under starvation.

Section 6.3 shows experimental results on the effects of micro-dents on friction and film thickness under starvation. From Figures 6.10 and 6.13, one can note that the tribological performance of rubbing surfaces has been improved under starvation by introducing shallow micro-dents on the surface of ball. On the other hand, Figure 6.11 shows that the beneficial effect of micro-textures is lost as the contact becomes fully flooded. These results are in agreement with the numerical study of Dumont et al. [81].

6.4 Behavior of transverse shallow micro-grooves in EHL contacts

This section shows experimental investigation on the behavior of transverse shallow micro-grooves in concentrated non-conformal contacts. The tribological performance of micro-grooved surfaces has been assessed by measuring friction and film thickness under sliding, reverse and starvation conditions. The length of micro-grooves is considered as a crucial parameter to inhibit the side leakage.

Measurements have been carried out using a Tribometer equipped with a high-speed digital camera and torque sensor. The film thickness and friction have been measured in the contact between a steel ball and a glass disc under different values of the entraining velocity and slide-to-roll ratio $SRR = 2*(u_{disk} - u_{ball})/(u_{disk} + u_{ball})$. The negative signal of (SRR) means that the ball is faster than the disc. The steel ball AISI 52100 has a roughness about 10 nm and a diameter of 25.4 mm with the elastic modulus 210 GPa. The disc is made of glass with the elastic modulus 80 GPa and the lower surface of the disc is coated with a thin layer of Chromium. The ball and disc are driven by servo-motors controlled by the computer with the ability to change the required slide-to-roll ratio in a wide range. The construction of the Tribometer gives the possibility of capturing interferometric images simultaneously with measuring the friction. The base oil N2400 (dynamic viscosity $\eta = 0.412\ Pas$ at 40°C and the pressure-viscosity coefficient $\alpha = 35GPa^{-1}$ was used as lubricant in all the experiments in section 6.4.4.

6.4.1 Procedures of measuring the film thickness

The film thickness was evaluated by the colorimetric interferometry technique [101] for smooth and textured surfaces under a load of 35 N in the presence of sliding motion. The effects of three types of transverse micro-grooves have been investigated. These types are shown in Figure 6.14 as the following:

a) Large-sized micro-grooves with intersection with the outer Hertzian circle (depth h=1μm, width w=60 μm, length l>2*a*, where *a* is the radius of the Hertzian contact).
b) Small-sized micro-grooves with intersection with the outer Hertzian circle (h=0.4μm, w=42 μm, l>2*a*).
c) Small-sized micro-grooves without intersection with the outer Hertzian circle (h=0.4μm, w=42 μm, l<2*a*).

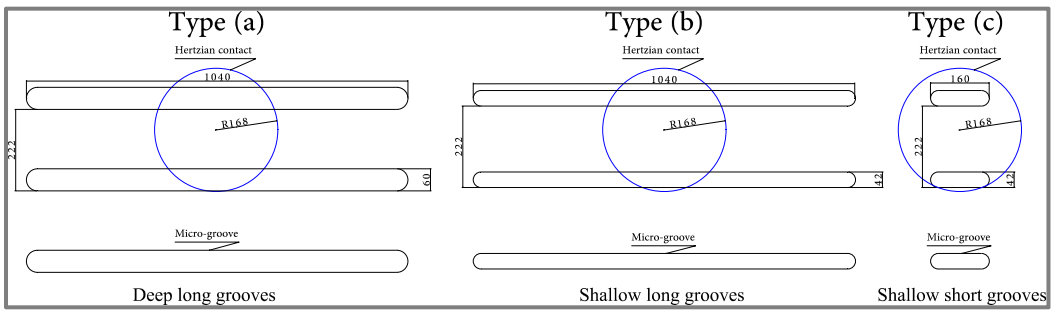

Fig. 6.14 Schematic representation of micro-grooves used to compare the effect on film thickness under load 35N (dimensions in μm).

Micro-grooves were made by using a Rockwell indenter with a head angle of 120 deg. The aim of the film thickness measurements is to show the effect of reducing the size on the mechanism of emitting the lubricant into the contact and side leakage.

6.4.2 Procedures of measuring the friction

Firstly, the coefficient of friction (COF) has been measured for a smooth ball under a load of 40 N for sliding and reverse motion. Please note that the load for measuring the friction is larger than for measuring the film thickness because the higher load results in a better sensitivity of the torque sensor and more accurate measurements.

Secondly, the friction was measured under the same conditions for the same ball with an array of micro-grooves, where only the small-sized micro-grooves with a length shorter than the diameter of the Hertzian contact have been adopted for measuring the friction. Figure 6.15 shows the profile, the distribution and dimensions of micro-grooves on the surface of the ball where only a single array on the whole circumference of the ball has been made by the Rockwell indenter. Note that the width (w) of the groove is taken at zero level on the surface of the ball; also the grooves are bounded with shoulders of 65 nm in the height. From Figure 6.15 it is clear that the small-sized micro-grooves dedicated for measuring the friction are transversely concentrated with the rolled track without intersection with the outer Hertzian circle. Therefore, the side leakage is inhibited across the groove. The interval step between grooves is taken as 222 μm along the direction of sliding, thus, in maximum only two grooves can be existed together in the contact, see Figure 6.15. Consequently, the relative surface density of micro-grooves in the contact for the given dimension in Figure 6.15 changes with time in the range $[5.9\% - 11.8\%]$ under the load 40 N.

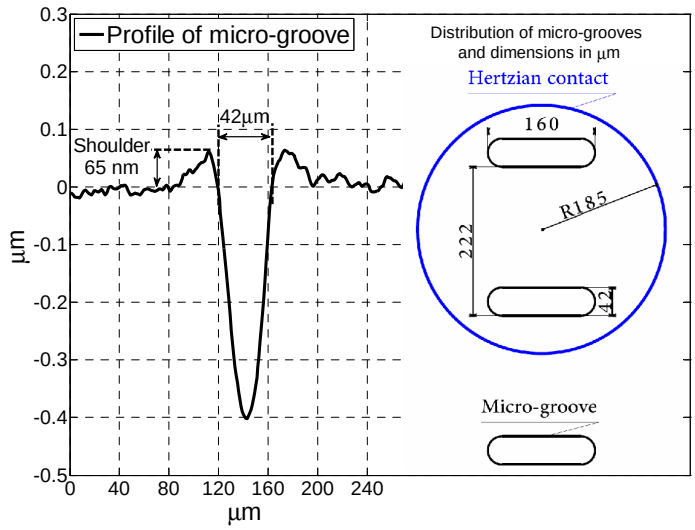

Fig. 6.15 Profile and distribution of micro-grooves used for comparing the friction under the load=40 N.

6.4.3 Effect of micro-grooves on the film thickness

The effect of micro-grooves passage through EHL point contacts is evaluated in comparison with smooth surfaces. Since the micro-grooved ball is faster than the disc

(SRR<0) in this experiment, the significant modification of film thickness is localized on the leading edge of the micro-groove, see reference [57]. Therefore, the film thickness is measured only on the trailing edge across an axis parallel to the micro-groove. Figure 6.16 shows the severe collapse of the film thickness as a large-sized micro-groove of type (a) passes the contact. The collapse is attributed to the side leakage across the micro-groove and it can be stated that the lubricant is displaced out of the Hertzian contact rather than to be emitted into the contact.

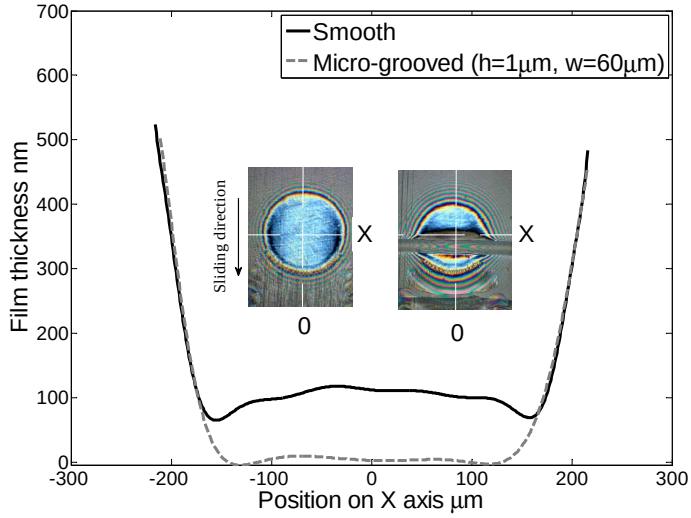

Fig. 6.16 The film thickness profile on X axis for the smooth and the textured surface with micro-grooves (h=1μm, w=60 μm, l>2a), F35 N, u_e4mm/s, SRR=-0.7.

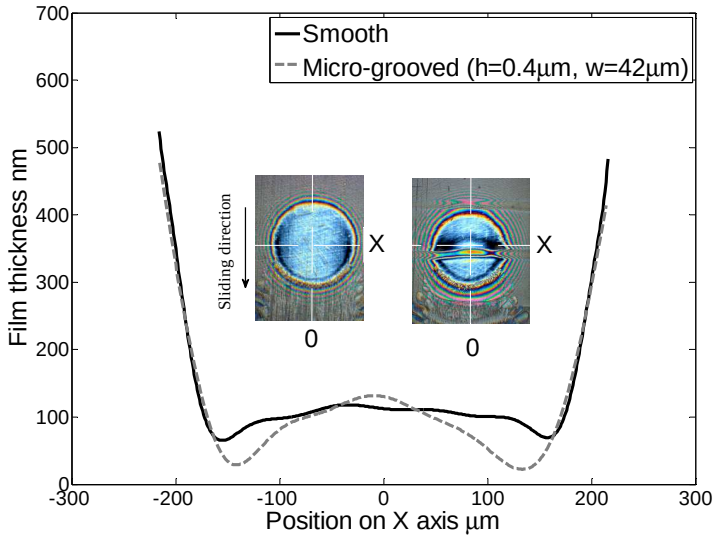

Fig. 6.17 The film thickness profile on X axis for the smooth and the textured surface with micro-grooves (h=0.4μm, w=42 μm, l>2a), F35 N, u_e4mm/s, SRR=-0.7.

Figure 6.17 shows that reducing the dimensions of the micro-groove (grooves of type (b)) does not solve the problem of the side leakage along the groove in the places where the groove is intersected with the outer circle of the Hertzian contact.

However, it is clear that the film thickness has been significantly enhanced only in the central region and it became larger than the film thickness of the smooth surface. Reducing the depth and width of the groove led to increase the pressure in the groove resulting in a higher viscosity and consequently the effect of the shear flow becomes less [57]. Thus, micro-groove with small depth and width can enhance the film thickness in the central region of the contact where the pressure is large enough to increase the viscosity of the lubricant. But even with the small size there is still a significant side leakage and film thickness reduction in the places where the pressure and viscosity are relatively low. From measurements in Figures 6.16 and 6.17 it is clear that the positive effect associated with the transversally-oriented micro-grooves is attributed basically to the side leakage which means that the lubricant is ejected out of the Hertzian contact across the groove. The amount of the expelled lubricant is influenced strongly by the dimensions of the groove.

Figure 6.18 shows the profile of the film thickness on the trailing edge of a transverse micro-groove without intersection with the border of the Hertzian contact. It is evident that the emitted lubricant enhanced strongly the film thickness in comparison with the smooth surface under the same operating conditions. In addition, the side leakage is completely absent since there is not any intersection with the outer circle of the Hertzian contact. However, a small reduction in the film thickness has been observed in the places where the shoulders of micro-grooves are longitudinally oriented; see the dashed circles in Figure 18. It is expected that as the shoulders of grooves are transversally-oriented on the sliding direction, they would be flattened (deformed) easier than the oblique or longitudinal shoulders under the effect of sliding [34]. Consequently, the shoulders of grooves induce a more of pressure fluctuation at the side edges of grooves because the orientation of shoulders tends to be oblique then longitudinal. The negative effects of shoulders can be minimized or eliminated by an effective polishing of the textured surfaces.

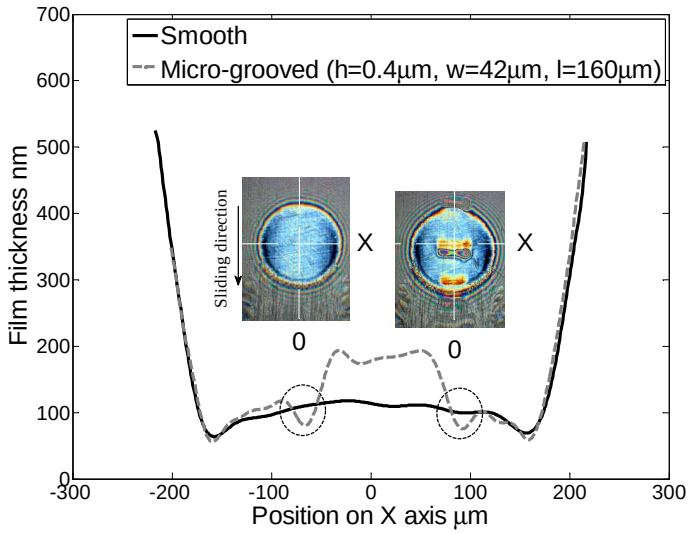

Fig. 6.18 The film thickness profile on X axis for the smooth and the textured surface with micro-grooves (h=0.4µm, w=42µm, l=160µm), F35 N, u_e4mm/s, SRR=-0.7.

Figure 6.9 shows the effects of grooves as the overall film thickness becomes thinner. The comparison between Figures 6.18 and 6.19 shows a similar behavior and the same negative reduction induced by the shoulders; see the dashed circles in Figure 6.19.

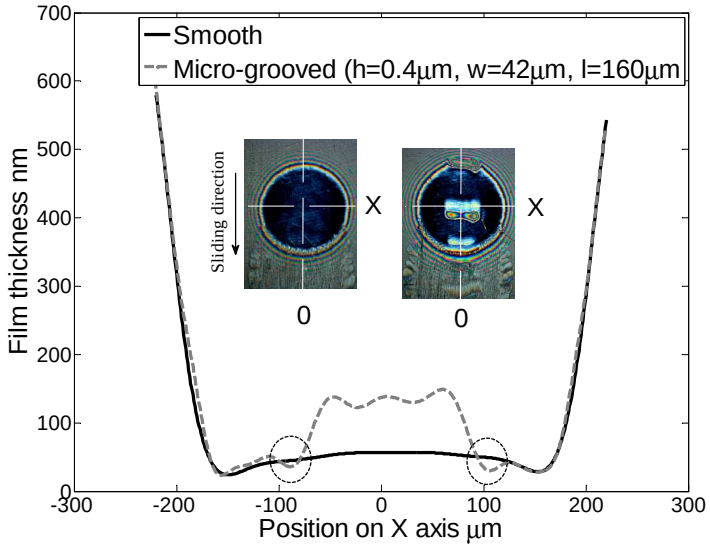

Fig. 6.19 The film thickness profile on X axis for the smooth and the textured surface with micro-grooves (h=0.4μm, w=42μm, l=160μm), F35 N, u_e1.6mm/s, SRR=-0.7.

However, some important points can be observed from the comparison between Figures 6.18 and 6.19 as the following:

- The film thickness has been enhanced by the same value (about 65 nm) on the trailing edge for the same slide-to-roll ratio SRR=0.7. Therefore, the absolute amount of lubricant emitted from the micro-groove is approximately the same regardless the value of the overall film thickness and the value of SRR determines quantitatively of the extracted lubricant.
- The relative enhancement of the film thickness is definitely larger and more appreciated for the thinner film thickness. Thus, relatively (not quantitatively) the benefits of micro-textures are more significant as the overall film thickness is less under the same SRR. Similar results are revealed experimentally and numerically in references [29] and [81].

6.4.4 Effect of micro-grooves on the friction in sliding and reverse motion

In Figures 6.18 and 6.19 is shown that the shallow transverse micro-grooves with a length shorter than the diameter of the Hertzian contact are helpful in enhancing the film thickness on the trailing edge as the ball is faster than the disc. On the other hand, a small reduction in the film is caused by the effect of shoulders. However, the coefficient of friction is crucial to evaluate the effect of the proposed design of micro-grooves shown in Figure 6.15 on the tribological performance of non-conformal contacts. The corresponding interferometric images in Figure 6.20 (captured in the 6th minute) show a significant enhancement of the film thickness for the textured surface in comparison with the smooth one. Nevertheless, Figure 6.20 shows that a small reduction of friction (about 4%) can be obtained for the surfaces textured with grooves under the given operating condition. The small reduction versus the large enhancement of the film thickness is attributed to the large overall film in the contact (central film= 150 nm) which results in a small relative enhancement. Furthermore, the large SRR=-1.58 increases the non-Newtonian behavior of the fluid (the shear stress becomes close the limiting shear stress) which

means that the friction becomes more dependent on the slide-to-roll ratio than the value of the film thickness. In references [102] it was proven that the sensitivity of friction to the change of film thickness becomes less with increasing the slide-to-roll ratio. In other words, the Couette friction is less sensitive to the change in the film thickness than the Poiseuille friction [103]. Consequently, high slide-to-roll ratios for textured surfaces reduce the benefits concerning the reduction of friction, despite the larger SRR improves the extraction of the lubricant from the Micro-textures.

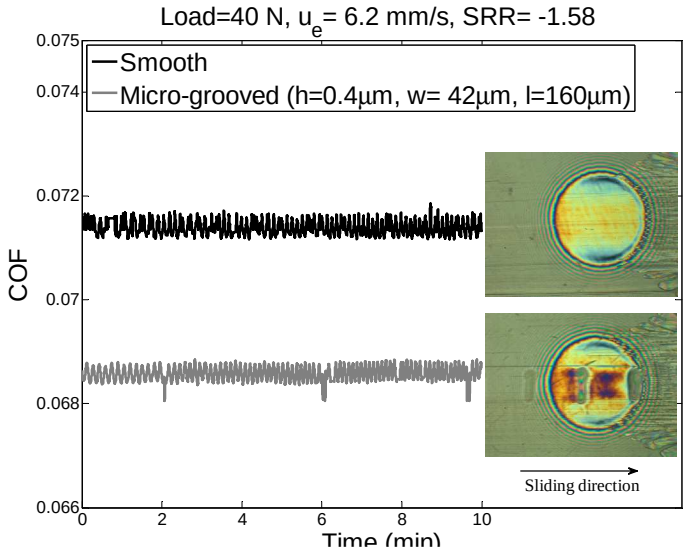

Fig. 6.20 The coefficient of friction (COF) for the smooth and the textured surface with micro-grooves (h=0.4µm, w=42µm, l=160µm) in the sliding motion with SRR=-1.58.

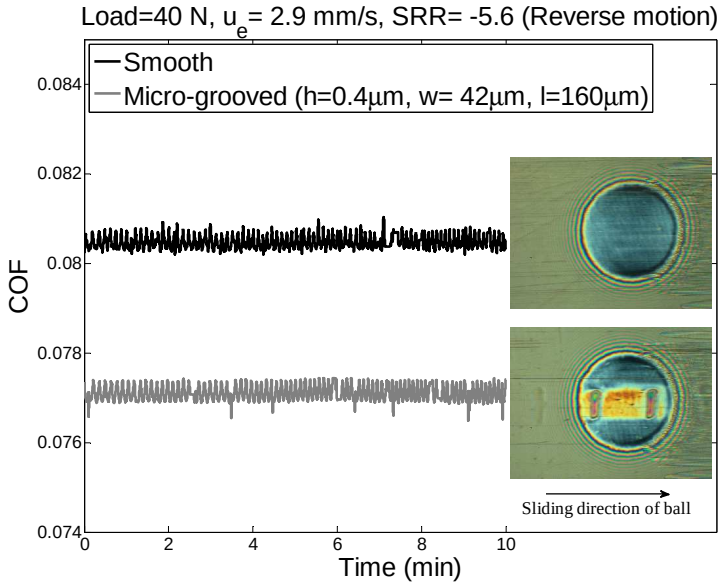

Fig. 6.21 The coefficient of friction (COF) for the smooth and the textured surface with micro-grooves (h=0.4µm, w=42µm, l=160µm) in the reversal motion with SRR=-5.6.

Figure 6.21 depicts the measurements of friction for smooth and textured surfaces in the reverse sliding motion for a large value of SRR=-5.6 with the corresponding

interferometric images captured in the 6th minute. Again, a small reduction of friction (about 4.2%) has been measured although the large relative enhancement of the film thickness. See Figures.6.22 and 6.23.

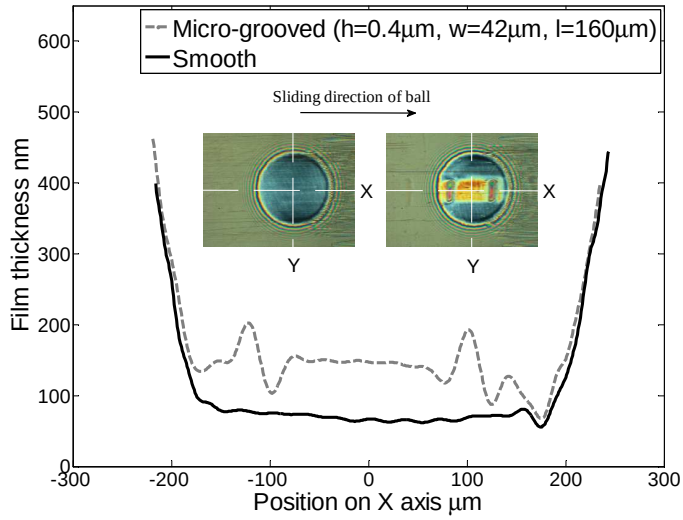

Fig. 6.22 The film thickness profile on X axis for the smooth and the textured surface in the reversal motion with SRR=-5.

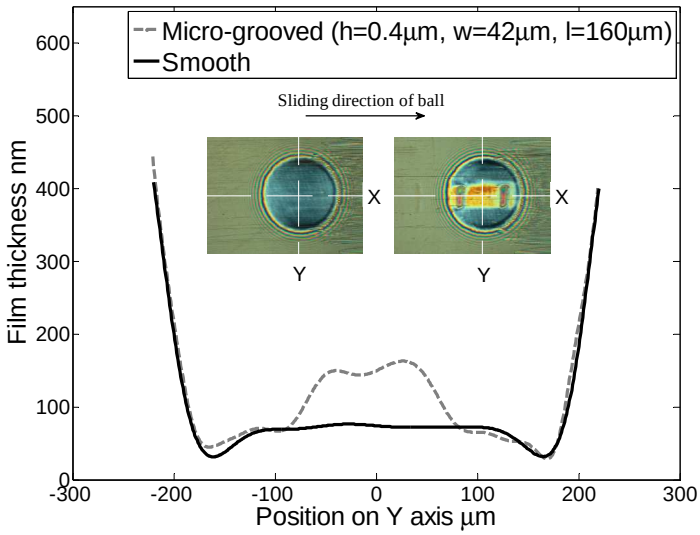

Fig. 6.23 The film thickness profile on Y axis for the smooth and the textured surface in the reversal motion with SRR=-5.6.

Indeed, the central film thickness has been increased about 2.1 times for textured surfaces. Nevertheless, the reduction of friction is too small. This can be attributed to the fact that the effect of the large relative enhancement of the film on the friction has been dissipated or damped by the high value of SRR in the reverse motion. However, the film thickness propagation becomes more pronounce in reverse motion due the effect of high value of SRR, see references [102] and [103]. As a result, increasing the slide-to-roll ratios improves the extraction of lubricant from micro-cavities but this does not necessarily result in a significant reduction of friction.

6.4.5 Behavior of micro grooves under starvation

Starvation can be encountered in EHL contacts under extreme operating conditions (high speeds and/or high viscosities) or in cases where greases are used to lubricate bearings. Starvation is caused basically by insufficient replenishment where the lubricant fails to reflow to the depleted track [73, 93]. However, enhancing the lubricating film thickness is the key to reduce friction and wear in starved EHL contacts. Dumont et al. [81] described numerically the behavior of micro-pits in the fully flooded and starved EHL point contacts. The benefits of micro-pits decrease as the degree of starvation decreases because the film thickness becomes larger and the emitted oil from micro-pits becomes negligible in comparison with the available amount of oil in the contact.

To investigate the effect of shallow micro grooves on the film thickness under starvation, measurements were conducted using a Tribometer equipped with a high-speed digital camera. Base oil (R 834/80) with the dynamic viscosity $\eta = 0.215\ Pas$ at 22°C and pressure-viscosity coefficient $\alpha = 22GPa^{-1}$ was used as lubricant. The film thickness was evaluated by the colorimetric interferometry technique [101].

Micro-grooves were made by using a Rockwell indenter with a head angle of 120 deg. The indentation process was fully automated by using steeper motors for linear and angular motion. An electromagnetic actuator was used to create the impact between the head of Rockwell indenter and the surface of the ball. Thus, the depth of micro-grooves depends on the volt and current supply to the electromagnetic motor. The profile of resulting micro-grooves was measured by optical profilometer.

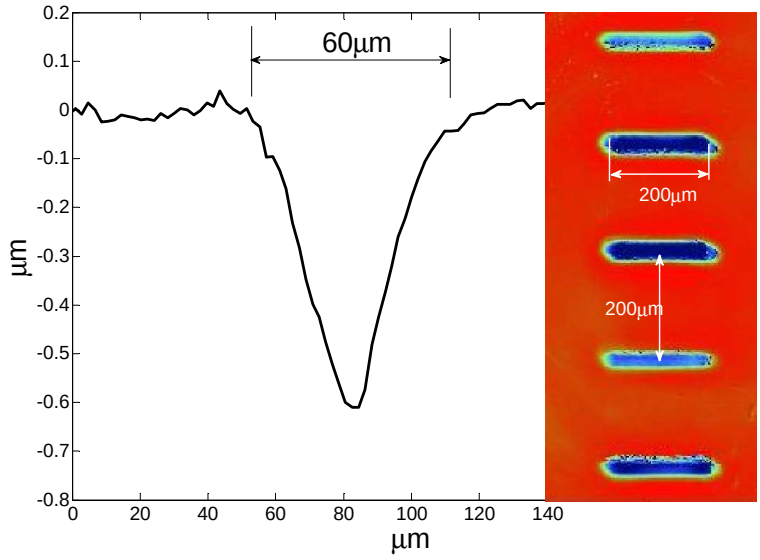

Fig. 6.24 Profile and distribution of micro-grooves on the surface of steel ball to investigate the effect on the film thickness under starvation.

Figure 6.24 shows the dimension and distribution of grooves on the surface of ball. The average depth of grooves is 600 nm, the width is about 60 µm and the transverse length is 200 µm. One row of 10 micro-grooves has been created on the surface of ball with angular pitch of 200 µm. All experiments presented in sub-section 6.4.5 were carried out at room temperature 22°C.

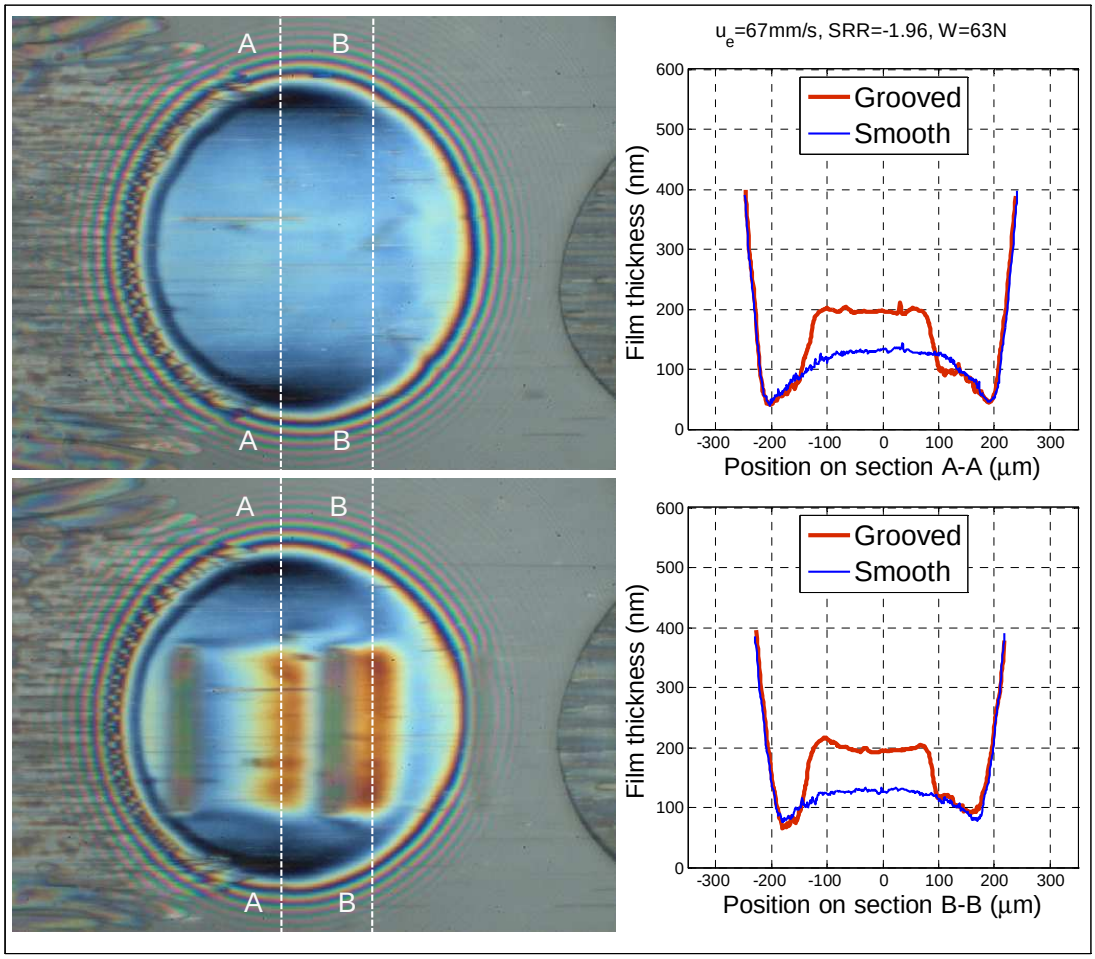

Fig. 6.25 Effect of transverse shallow micro-grooves on the film thickness under starvation.

Figure 6.25 depicts the behavior of transverse limited micro-grooves under starvation. The available amount of lubricant was only 8µl with entraining speed u_e = 67 mm/s, SRR=-1.96 and load w=63 N. In this case, the corresponding maximum Hertzian pressure and contact radius are 0.653 GPa and 215 µm, respectively. The Interferometry images shown in Figure 6.25 have been captured in the 20th minute after the start. Starvation can be easily observed from the oil-air meniscus in the inlet of the contact. The inlet cavitations are caused by the high speed and low amount of oil on the track. Indeed, these conditions with the high value of SRR=-1.96 represent extreme operating condition for EHL contacts. Although the contact is starved, Figure 6.25 shows that the transverse limited grooves are able to act as oil reservoirs and the film thickness of grooved surface is larger than for smooth surface. The enhancement of film thickness on the trailing edges of grooves is shown in Figure 6.25 along longitudinal sections A-A and B-B. However, acting as oil reservoirs means that the micro-grooves are filled with lubricant. But the micro-grooves are depleted after leaving the contact and the mechanism of replenishment is insufficient since the speed is high and the oil amount is very little. The inlet gap between the mating surfaces is filled by lubricant under full film lubrication. As a result, the depleted micro-grooves are filled in the inlet zone. The situation is different when the contact is starved because the inlet gap is occupied by oil-air cavitations with low pressure.

Nevertheless, Figure 6.25 shows that the micro-grooves are able to bring lubricant to the contact even after 20 minutes from the start. Probably, the depleted micro-grooves were filled with fresh lubricant in the inlet zone by the capillary forces. Jacod et al. [93] showed that the mechanism of capillary forces generates significant flows in the vicinity of the contact under starved lubrication. On the other hand, Dumont et al. [81] predicted in their numerical study that the emitted lubricant from micro-pits leads to enlarge the distance between the oil-air meniscus and the Hertzian contact. But they didn't explain how the depleted micro-pits can be filled after leaving the contact under starvation. Figure 6.25 shows the position of the oil-air meniscus is similar for smooth and grooved surfaces although the amount of emitted lubricant by micro-grooves is important. If micro-features (grooves, dents, pits) are filled in the inlet zone by capillary forces not by replenishment, then the amount of emitted lubricant by one micro-groove will be absorbed by the next depleted micro-groove. Consequently, the available amount of lubricant will be stable in the inlet zone without changing the position of the inlet oil-air meniscus.

6.4.6 Numerical simulation of micro-grooves passage through EHL point contact

The numerical simulation of the experiments was performed by assuming an isothermal Newtonian fluid. Therefore, the Reynolds equation is written as:

$$\frac{\partial}{\partial x}\left(\frac{\rho h^3}{12\eta}\frac{\partial p}{\partial x}\right)+\frac{\partial}{\partial y}\left(\frac{\rho h^3}{12\eta}\frac{\partial p}{\partial y}\right)=u_e\frac{\partial(\rho h)}{\partial x}+\frac{\partial(\rho h)}{\partial t} \qquad (6.10)$$

The boundary conditions of Eq.(6.10) are:

$$p(x_{in},y,t)=p(x_{out},y,t)=p(x,\pm y_{out},t)=0$$

$$p(x,y,t)>0 \quad (x_{in}<x<x_{out},\, y_{in}<y<y_{out}).$$

The film thickness equation reads:

$$h(x,y,t)=h_{00}(t)+\frac{x^2+y^2}{2R_x}+\frac{2}{\pi E'}\iint\frac{p(x',y',t)dx'dy'}{\sqrt{(x-x')^2+(y-y')^2}} \qquad (6.11)$$

The density-pressure and viscosity-pressure relations proposed by Dowson and Higginson [104] and Roelands et al. [105], respectively, are adopted, i.e.,

$$\rho=\rho_0\left[1+\frac{0.6\times10^{-9}p}{1+1.7\times10^{-9}p}\right] \qquad (6.12)$$

$$\eta=\eta_0\exp\left\{(\ln\eta_0+9.67)\left[-1+\left(1+5.1\times10^{-9}p\right)^{Z_0}\right]\right\} \qquad (6.13)$$

where $Z_0=\alpha/\left[5.1\times10^{-9}(\ln\eta_0+9.67)\right]$ and z_0 is the Barus' pressure-viscosity coefficient.

Figure 6.26 shows the numerical representation of micro-grooves used in the numerical simulation. The shape of the groove used in the experiments was assumed by the following equation:

$$\delta(x)=H\times10^{-12.5(x/60)^2}\cos(2\pi x/60) \qquad (6.14)$$

where H = - 0.6 μm.

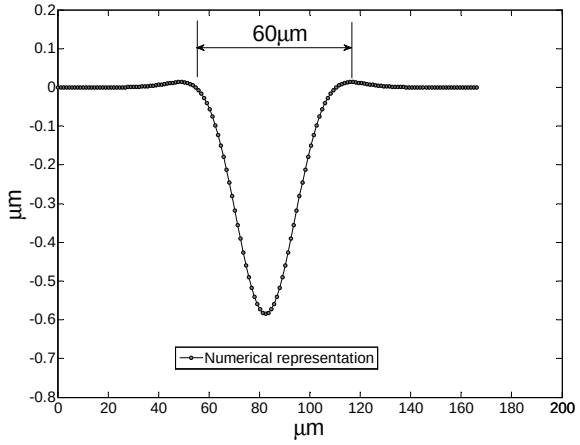

Fig. 6.26 Numerical representation of micro-grooves.

The Reynolds and film thickness equations are solved with the multi-level multi-integration technique [106]. The calculation domain was $-2.5a \le x \le 1.5a,\ 0 \le y \le 2.0a$, because of the symmetry with respect to the *x*-axis. Five levels of grids were used. On the finest level, 513 nodes were arranged in the *x*-direction and 257 nodes in the *y*-direction. Converged solutions were accepted when relative errors of pressure and load values became less than 10^{-4} simultaneously at the finest grid level.

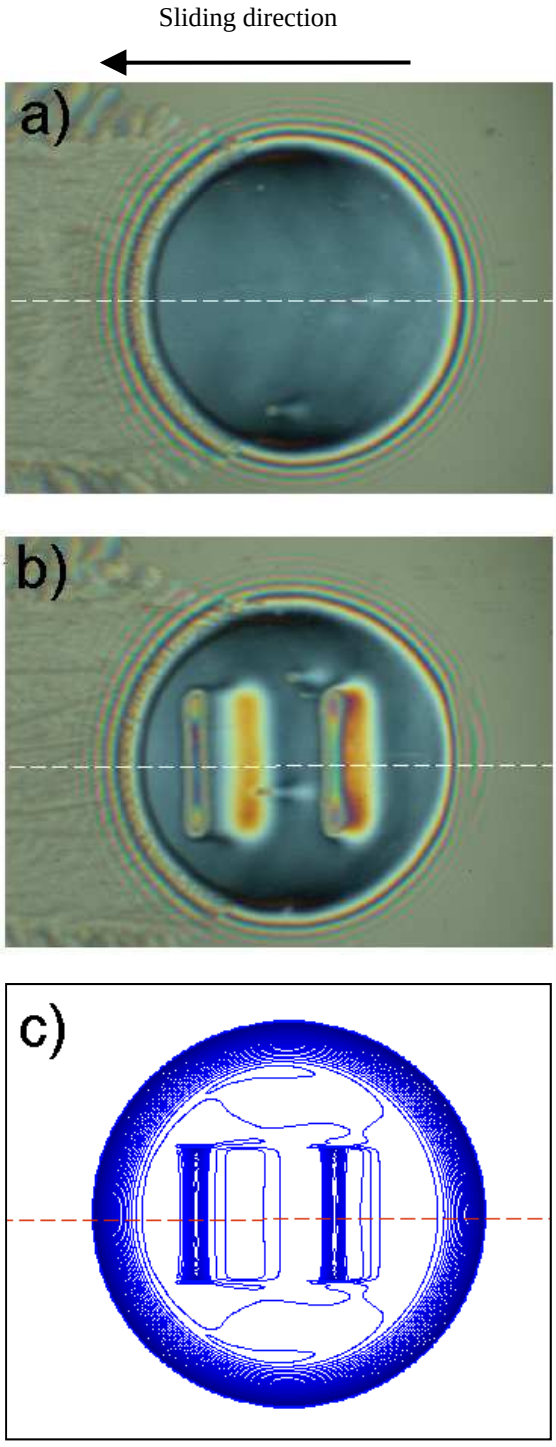

Fig. 6.27 Numerical and experimental comparison of the micro-grooves effects on film thickness formation (a) Interferometry image of smooth surface (b) Interferometry image of grooved surface (c) Numerical contour of film thickness.

The transient effect of the micro-grooves passage through the EHL contact is observed numerically and experimentally under sliding motion. This effect is compared with smooth surface film thickness. Measurements and simulation were carried out for entraining velocity u_e = 34 mm/s, slide-to-roll ratio SRR=-0.6 and load w=70 N. The corresponding maximum Hertzian pressure and contact radius are 0.68 GPa and 222 µm, respectively. Figure 6.27 shows an optical interferogarm comparison of smooth and micro-grooved surfaces with the numerical simulation. Optical interferometry images in Figure 6.27 are captured by high speed camera. Image (a) shows the film thickness formation of smooth surfaces while image (b) shows the transient effect of grooved surfaces. Image (c) represents the numerical simulation to the passage of micro-grooves for the same positions of micro-grooves in image (b). The central film thickness is measured along horizontal axes in the direction of sliding. These axes are shown in Figure 6.27 as dashed lines on images (a), (b) and (c). However, it is clear from Figure 6.28 that the passage of limited micro-grooves through the EHL contact created an enhancement of film thickness on the trailing edge of micro grooves. The film thickness on the trailing edge is about 178 nm while the average film thickness of smooth surface is about 88 nm.

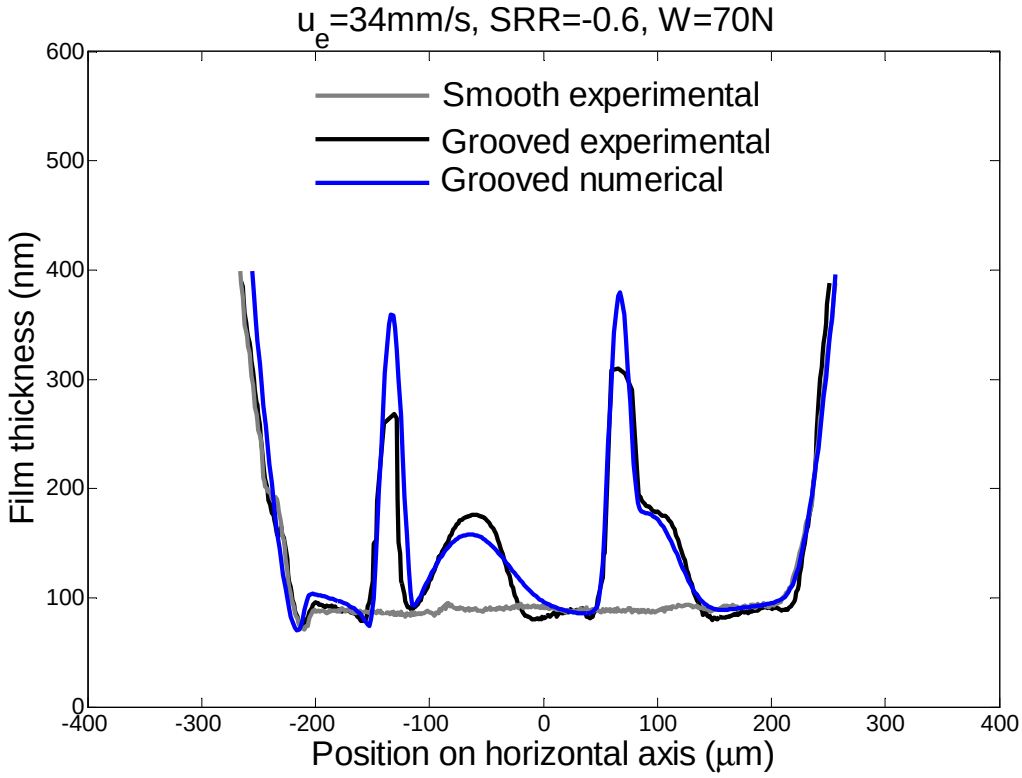

Fig. 6.28 Film thickness comparison for smooth and grooved contact with numerical simulation.

Figure 6.29 shows a 3-D visualization to the passage of micro-grooves through the contact of grooved surfaces for interval time T2-T1= 4.42 ms. During this time (4.42 ms) every micro-groove passes a distance about 196 µm since the linear speed of ball was 44.32 mm/s. The elastic deformation, caused by the emitted lubricant of micro-

groove, is clear on the trailing edge. The propagation of this elastic deformation increases as the groove passes a larger distance in the contact.

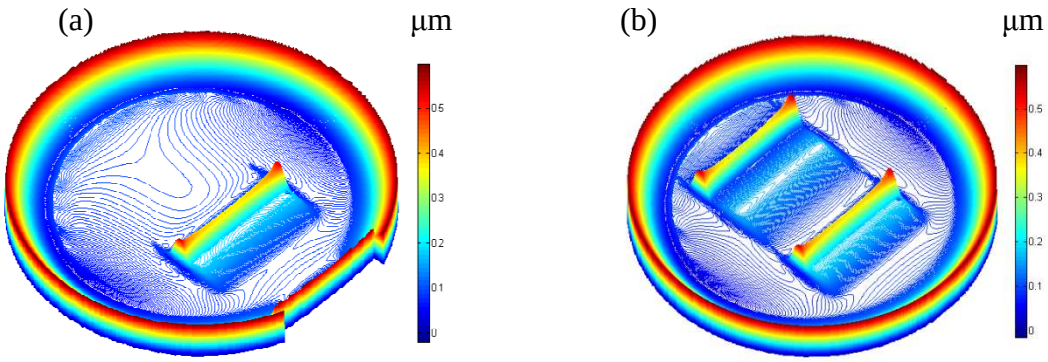

Fig. 6.29 3-D visualization to the passage of micro-grooves through the EHL contact, u_e= 34 mm/s, SRR=-0.6 and w=70 N. (a) at T1=0 (b) at T2=4.42 ms.

Section 6.4 introduced an innovative approach to obtain benefits from transverse shallow micro-grooves in EHL contacts. The approach depends on eliminating the side leakage along grooves by reducing the length of groove to be less than the diameter of the Hertzian contact. Consequently, micro-groves behave as closed texture cells with enough ability to maintain the hydrodynamic pressure leading to positive effects on the triblogical performance of EHL contacts. A significant enhancement in the film thickness can be induced by the passage of shallow short micro-grooves row in the EHL contact. In contrary, deep and shallow micro-grooves with a length larger than the diameter of Hertzian contact cause a reduction of film thickness due to the side leakage. The beneficial effect on the film thickness depends relatively on the overall film thickness and quantitatively on the slide-to-roll ratio. Surfaces with limited micro-grooves have a larger film thickness than smooth surfaces under starved lubrication. Such surface texturing approach is helpful to reduce friction and consequently wear of rubbing surfaces in the sliding and reversal motion. Increasing the slide-to-roll ratios improves the extraction of lubricant from micro-cavities but this does not necessarily result in a significant reduction of friction. Finally, the transient behavior of transverse limited micro-grooves is numerically simulated with good agreement with experimental measurements, see Figures 6.27 and 6.28.

7 CONCLUSIONS

This thesis focuses on studying the correlation between friction, lubricant replenishment, film thickness, and surface micro-textures under starved EHL contacts. The whole work presented in this thesis can be distinguished in the following three basic points:

Friction dependence on starvation in EHL contacts:

This topic is discussed in section 6.1. The coefficient of friction is relatively related to the increase of starvation due to the reduction of oil amount on the track, and this interaction between the friction and the degree of starvation can be generalized mathematically. However, the coefficient of friction is significantly sensitive to the change of load and starved conditions. This is attributed to the exponential change in the viscosity with load. Under low values of slide to roll ratios, the coefficient of friction is strongly influenced by the value of slide to roll ratios where the behavior of lubricant is Newtonian. The high values of slide to roll ratios produce large shear rates in the contact and lubricant shows very non-Newtonian properties. Therefore, the value of friction coefficient becomes more independent of slide to roll ratios in starved EHL contacts.

Lubricant replenishment under starved lubrication:

The results about Lubricant replenishment in starved EHL contacts are explained in section 6.2. A simple mechanism for channeling lubricant has been investigated by means of ball-on-disc device. The mechanism depends on recovering and channeling the displaced lubricant into the rolled track leading to enhanced replenishment. The results show a significant improvement of tribological performance of mating surfaces just by channeling the same amount of available lubricant. Indeed, the starved EHL contact transformed completely to the fully flooded regime (large film thickness and low friction) after applying the mechanism of induced replenishment. On the other hand, the mechanism operates efficiently over time with oil and grease lubrication. The channeling of lubricant leads to a significant reconditioning of fluid flow in the inlet zone of the contact. As a result, the onset of pressure buildup in lubricant is kept away from the Hertzian contact leading to enhanced film formation. Indeed, the channeling of lubricant is an effective approach to reduce the severity of starvation with grease lubrication and high viscosity oils. The results of this study can be easily implemented in practical applications such as radial and thrust rolling-element bearings.

Behavior of micro-textures under starved lubrication:

Sections 6.3 and 6.4 show experimental and numerical investigations on the behavior of micro-dents and micro-grooves in starved EHL contacts. The friction coefficient of non-conformal EHL point contacts was measured under starved and fully flooded conditions for smooth and textured surfaces. Shallow micro-dents (depth 600 nm and diameter 35 μm) have been applied on the surface of a steel ball. The results show that the modification of non-conformal mating surfaces by shallow micro-dents provide a considerable reduction of friction (about 9%) under severe starved lubrication compared to smooth surfaces. On the other hand, the benefits of micro-dents were negligible for fully flooded lubrication.

In the present thesis, the author introduced an optimized design of micro-grooves for improving the tribological performance of non-conformal contacts in the sliding and

reverse motion and under starvation. The design is based on creating shallow transverse micro-grooves with a length shorter than the diameter of the Hertzian contact resulting in eliminating the side leakage along the grooves. However, the importance of the study concerning behavior of micro-grooves can be concluded by the following:

- A significant enhancement in the film thickness can be induced by the passage of shallow limited micro-grooves row in the EHL contact.
- Deep and shallow micro-grooves with a length larger than the diameter of Hertzian contact cause a reduction of film thickness due to the side leakage.
- The beneficial effect on the film thickness depends relatively on the overall film thickness and quantitatively on the slide-to-roll ratio.
- Surfaces with micro-grooves of type (c) have a larger film thickness than smooth surfaces under starved lubrication.
- Such surface texturing approach is helpful to reduce friction and consequently wear of rubbing surfaces in the sliding and reversal motion.
- Increasing the slide-to-roll ratios improves the extraction of lubricant from micro-cavities but this does not necessarily result in a significant reduction of friction.
- Micro-grooves act as powerful oil reservoirs when they are introduced on the surface as closed texture cells with length less than the diameter of Hertzian contact.
- Transverse limited micro-grooves enhance significantly the film thickness of EHL contacts under thin film and starved conditions.
- The position of the oil-air meniscus is similar for smooth and grooved surfaces under same operating conditions.
- The behavior of limited micro-grooves in EHL contacts can be successfully predicted by numerical methods as shown in Figures 6.27, 6.28 and 6.29.

LIST OF FIGURES

Figure number and caption **page**

REFERENCES

[1] DOWSON, Duncan, et al. Elasto-Hydrodynamic Lubrication: A Survey of Isothermal Solutions. *Journal of Mechanical Engineering Science*, 1962, 4.2: 121-126.

[2] WANG, Shun, et al. Effects of surface roughness on sliding friction in lubricated-point contacts: Experimental and numerical studies. *Journal of Tribology*, 2007, 129.4: 809-817.

[3] WANG, Wen-zhong, et al. Simulations and measurements of sliding friction between rough surfaces in point contacts: from EHL to boundary lubrication.*Journal of tribology*, 2007, 129.3: 495-501.

[4] SOJOUDI, H.; KHONSARI, M. M. On the behavior of friction in lubricated point contact with provision for surface roughness. *Journal of Tribology*, 2010, 132.1: 012102.

[5] ETSION, Izhak. State of the art in laser surface texturing. *Journal of Tribology*, 2005, 127.1: 248-253.

[6] ZHOU, Yuankai, et al. Development of the theoretical model for the optimal design of surface texturing on cylinder liner. *Tribology International*, 2012, 52: 1-6.

[7] KOVALCHENKO, Andriy, et al. The effect of laser surface texturing on transitions in lubrication regimes during unidirectional sliding contact. *Tribology International*, 2005, 38.3: 219-225.

[8] TIAN, Hong; SAKA, Nannaji; SUH, Nam P. Boundary lubrication studies on undulated titanium surfaces. *Tribology Transactions*, 1989, 32.3: 289-296.

[9] SAKA, Nannaji; TIAN, Hong; SUH, Nam P. Boundary lubrication of undulated metal surfaces at elevated temperatures. *Tribology Transactions*, 1989, 32.3: 389-395.

[10] SUH, Nam P.; MOSLEH, Mohsen; HOWARD, Phillip S. Control of friction.*Wear*, 1994, 175.1: 151-158.

[11] PETTERSSON, Ulrika; JACOBSON, Staffan. Influence of surface texture on boundary lubricated sliding contacts. *Tribology International*, 2003, 36.11: 857-864.

[12] PETTERSSON, Ulrika; JACOBSON, Staffan. Friction and wear properties of micro textured DLC coated surfaces in boundary lubricated sliding. *Tribology letters*, 2004, 17.3: 553-559.

[13] RONEN, Aviram; ETSION, Izhak; KLIGERMAN, Yuri. Friction-reducing surface-texturing in reciprocating automotive components. *Tribology Transactions*, 2001, 44.3: 359-366.

[14] BURSTEIN, Leonid; INGMAN, Dov. Pore ensemble statistics in application to lubrication under reciprocating motion. *Tribology transactions*, 2000, 43.2: 205-212.

[15] BRIZMER, V.; KLIGERMAN, Y.; ETSION, I. A laser surface textured parallel thrust bearing. *Tribology Transactions*, 2003, 46.3: 397-403.

[16] WANG, Xiaolei, et al. The effect of laser texturing of SiC surface on the critical load for the transition of water lubrication mode from hydrodynamic to mixed.*Tribology International*, 2001, 34.10: 703-711.

[17] COSTA, H. L.; HUTCHINGS, I. M. Hydrodynamic lubrication of textured steel surfaces under reciprocating sliding conditions. *Tribology International*, 2007, 40.8: 1227-1238.

[18] RAMESH, Ashwin, et al. Friction characteristics of microtextured surfaces under mixed and hydrodynamic lubrication. *Tribology International*, 2013, 57: 170-176.

[19] HAN, Jing, et al. Hydrodynamic lubrication of surfaces with asymmetric microdimple. *Tribology Transactions*, 2011, 54.4: 607-615.

[20] HAMILTON, D. B.; WALOWIT, J. A.; ALLEN, C. M. A theory of lubrication by microirregularities. *Journal of Fluids Engineering*, 1966, 88.1: 177-185.

[21] RAHMANI, Ramin; SHIRVANI, Ayoub; SHIRVANI, Hassan. Optimization of partially textured parallel thrust bearings with square-shaped micro-dimples.*Tribology Transactions*, 2007, 50.3: 401-406.

[22] WANG, Xiaolei, et al. Loads carrying capacity map for the surface texture design of SiC thrust bearing sliding in water. *Tribology International*, 2003, 36.3: 189-197.

[23] MOURIER, Louis, et al. Transient increase of film thickness in micro-textured EHL contacts. *Tribology International*, 2006, 39.12: 1745-1756.

[24] WANG, Xiaolei, et al. Preliminary investigation of the effect of dimple size on friction in line contacts. *Tribology International*, 2009, 42.7: 1118-1123.

[25] BLATTER, A., et al. Lubricated friction of laser micro-patterned sapphire flats.*Tribology letters*, 1998, 4.3-4: 237-241.

[26] KŘUPKA, I.; HARTL, M. The effect of surface texturing on thin EHD lubrication films. *Tribology International*, 2007, 40.7: 1100-1110.

[27] KŘUPKA, I.; HARTL, M. Experimental study of microtextured surfaces operating under thin-film EHD lubrication conditions. *Journal of tribology*, 2007, 129.3: 502-508.

[28] VENNER, C. H.; LUBRECHT, A. A.; TEN NAPEL, W. E. Numerical simulation of the overrolling of a surface feature in an EHL line contact. *Journal of tribology*, 1991, 113.4: 777-783.

[29] AI, Xiaolan; CHENG, Herbert S. The influence of moving dent on point EHL contacts. *Tribology transactions*, 1994, 37.2: 323-335.

[30] VENNER, C. H.; LUBRECHT, A. A. Transient analysis of surface features in an EHL line contact in the case of sliding. *Journal of tribology*, 1994, 116.2: 186-193.

[31] ZHAO, Jiaxin; SADEGHI, Farshid. The effects of a stationary surface pocket on EHL line contact start-up. *Journal of tribology*, 2004, 126.4: 672-680.

[32] WEDEVEN, L. D.; CUSANO, C. Elastohydrodynamic film thickness measurements of artificially produced surface dents and grooves. *ASLE transactions*, 1979, 22.4: 369-381.

[33] MOURIER, Louis, et al. Action of a femtosecond laser generated micro-cavity passing through a circular EHL contact. *Wear*, 2008, 264.5: 450-456.

[34] GEIGER, M.; ROTH, S.; BECKER, W. Influence of laser-produced microstructures on the tribological behaviour of ceramics. *Surface and Coatings Technology*, 1998, 100: 17-22.

[35] ANDERSSON, P., et al. Microlubrication effect by laser-textured steel surfaces.*Wear*, 2007, 262.3: 369-379.

[36] WAKUDA, Manabu, et al. Effect of surface texturing on friction reduction between ceramic and steel materials under lubricated sliding contact. *Wear*, 2003, 254.3: 356-363.

[37] GALDA, Lidia; PAWLUS, Pawel; SEP, Jaroslaw. Dimples shape and distribution effect on characteristics of Stribeck curve. *Tribology International*, 2009, 42.10: 1505-1512.

[38] KOSZELA, Waldemar; PAWLUS, Pawel; GALDA, Lidia. The effect of oil pockets size and distribution on wear in lubricated sliding. *Wear*, 2007, 263.7: 1585-1592.

[39] PAWLUS, Pawel, et al. Abrasive wear resistance of textured steel rings. *Wear*, 2009, 267.11: 1873-1882.

[40] SCHRECK, S.; ZUM GAHR, K.-H. Laser-assisted structuring of ceramic and steel surfaces for improving tribological properties. *Applied surface science*, 2005, 247.1: 616-622.

[41] WAHL, Reiner; SCHNEIDER, Johannes; GUMBSCH, Peter. Influence of the real geometry of the protrusions in micro textured surfaces on frictional behaviour. *Tribology letters*, 2012, 47.3: 447-453.

[42] CHOUQUET, C., et al. Effect of DLC surface texturing on friction and wear during lubricated sliding. *Materials Chemistry and Physics*, 2010, 123.2: 367-371.

[43] ETSION, I.; SHER, E. Improving fuel efficiency with laser surface textured piston rings. *Tribology International*, 2009, 42.4: 542-547.

[44] ETSION, Izhak; KLIGERMAN, Y.; HALPERIN, G. Analytical and experimental investigation of laser-textured mechanical seal faces. *Tribology Transactions*, 1999, 42.3: 511-516.

[45] ETSION, Izhak; HALPERIN, Gregory. A laser surface textured hydrostatic mechanical seal. *Tribology Transactions*, 2002, 45.3: 430-434.

[46] NAKATSUJI, Takeshi; MORI, Atsunobu. The tribological effect of mechanically produced micro-dents by a micro diamond pyramid on medium carbon steel surfaces in rolling-sliding contact. *Meccanica*, 2001, 36.6: 663-674.

[47] NANBU, Toshikazu, et al. Micro-textures in concentrated conformal-contact lubrication: effects of texture bottom shape and surface relative motion.*Tribology Letters*, 2008, 29.3: 241-252.

[48] REN, Ning, et al. Micro textures in concentrated-conformal-contact lubrication: effect of distribution patterns. *Tribology Letters*, 2007, 28.3: 275-285.

[49] ZHU, D., et al. Model-based virtual surface texturing for concentrated conformal-contact lubrication. *Proceedings of the Institution of Mechanical Engineers, Part J: Journal of Engineering Tribology*, 2010, 224.8: 685-696.

[50] COULON, Sandrine, et al. Pressure profiles measured within lubricated contacts in presence of dented surfaces. Comparison with numerical models.*Tribology international*, 2004, 37.2: 111-117.

[51] NELIAS, Daniel; VILLE, Fabrice. Detrimental effects of debris dents on rolling contact fatigue. *Journal of tribology*, 2000, 122.1: 55-64.

[52] CANN, P. M.; SPIKES, H. A. Measurement of pressure distribution in EHL—development of method and application to dry static contacts. *Tribology transactions*, 2005, 48.4: 474-483.

[53] KŘUPKA, I.; VRBKA, M.; HARTL, M. Effect of surface texturing on mixed lubricated non-conformal contacts. *Tribology International*, 2008, 41.11: 1063-1073.

[54] KŘUPKA, I.; HARTL, M.; SVOBODA, P. Effects of surface topography on lubrication film formation within elastohydrodynamic and mixed lubricated non-conformal contacts. *Proceedings of the Institution of Mechanical Engineers, Part J: Journal of Engineering Tribology*, 2010, 224.8: 713-722.

[55] LUBRECHT, A. A. Influence of local and global features in EHL contacts.*Tribology Series*, 1997, 32: 17-25.

[56] MOURIER, Louis, et al. Lubrication mechanisms with laser-surface-textured surfaces in elastohydrodynamic regime. *Proceedings of the Institution of Mechanical Engineers, Part J: Journal of Engineering Tribology*, 2010, 224.8: 697-711.

[57] KANETA, M.; NISHIKAWA, H. Local reduction in thickness of point contact EHL films caused by a transversely oriented moving groove and its recovery.*Journal of tribology*, 1994, 116.3: 635-639.

[58] KANETA, M., et al. Abnormal phenomena appearing in EHL contacts. *Journal of tribology*, 1996, 118.4: 886-892.

[59] YANG, Peiran, et al. Influence of a surface bump or groove on the lubricating performance and dimple phenomena in simple sliding point EHL contacts.*Journal of tribology*, 2004, 126.3: 466-472.

[60] KANETA, M.; KANADA, T.; NISHIKAWA, H. Optical interferometric observations of the effects of a moving dent on point contact EHL. *Tribology Series*, 1997, 32: 69-79.

[61] JIANG, Xiaofei, et al. A mixed elastohydrodynamic lubrication model with asperity contact. *Journal of tribology*, 1999, 121.3: 481-491.

[62] AI, Xiaolan; LEE, Si C. Effect of slide-to-roll ratio on interior stresses around a dent in EHL contacts. *Tribology transactions*, 1996, 39.4: 881-889.

[63] JACKSON, A.; CAMERON, A. An interferometric study of the EHL of rough surfaces. *ASLE TRANSACTIONS*, 1976, 19.1: 50-60.

[64] SCARAGGI, Michele, et al. Friction properties of lubricated laser-microtextured-surfaces: an experimental study from boundary-to hydrodynamic-lubrication.*Tribology Letters*, 2013, 49.1: 117-125.

[65] NANBU, Toshikazu, et al. Increase of traction coefficient due to surface microtexture. *Tribology Letters*, 2008, 29.2: 105-118.

[66] YANG, Peiran, et al. Influence of two-sided surface waviness on the EHL behavior of rolling/sliding point contacts under thermal and non-Newtonian conditions. *Journal of Tribology*, 2008, 130.4: 041502.

[67] YAGI, Kazuyuki; KYOGOKU, Keiji; NAKAHARA, Tsunamitsu. Measurements of temperature distributions around longitudinally grooved rough surfaces in sliding elastohydrodynamic point contacts. *Tribology transactions*, 2006, 49.4: 482-489.

[68] LUGT, P. M.; MORALES-ESPEJEL, Guillermo E. A review of elasto-hydrodynamic lubrication theory. *Tribology Transactions*, 2011, 54.3: 470-496.

[69] VAN ZOELEN, Marco T. *Thin layer flow in rolling element bearings*. 2010. PhD Thesis. Ph. D. Thesis, University of Twente, the Netherlands, ISBN 978-90-365-2934-1.

[70] CANN, P. M. E.; DAMIENS, Bruno; LUBRECHT, A. A. The transition between fully flooded and starved regimes in EHL. *Tribology International*, 2004, 37.10: 859-864.

[71] HAMROCK, Bernard J.; DOWSON, Duncan. Isothermal elastohydrodynamic lubrication of point contacts: Part III—Fully flooded results. *Journal of Tribology*, 1977, 99.2: 264-275.

[72] WEDEVEN, Lavern D.; EVANS, D.; CAMERON, Alastair. Optical analysis of ball bearing starvation. *Journal of Tribology*, 1971, 93.3: 349-361.

[73] CHIU, Y. P. An analysis and prediction of lubricant film starvation in rolling contact systems. *ASLE transactions*, 1974, 17.1: 22-35.

[74] PEMBERTON, J.; CAMERON, A. A mechanism of fluid replenishment in elastohydrodynamic contacts. *Wear*, 1976, 37.1: 185-190.

[75] CHEVALIER, F., et al. Film thickness in starved EHL point contacts. *Journal of tribology*, 1998, 120.1: 126-133.

[76] DAMIENS, Bruno, et al. Starved lubrication of elliptical EHD contacts. *Journal of tribology*, 2004, 126.1: 105-111.

[77] GHOSH, M. K.; HAMROCK, B. J.; BREWE, D. E. Starvation effects on the hydrodynamic lubrication of rigid nonconformal contacts in combined rolling and normal motion. *ASLE transactions*, 1987, 30.1: 91-99.

[78] FARAON, I. C.; SCHIPPER, D. J. Stribeck curve for starved line contacts.*Journal of Tribology*, 2007, 129.1: 181-187.

[79] GELINCK, E. R. M.; SCHIPPER, D. J. Calculation of Stribeck curves for line contacts. *Tribology International*, 2000, 33.3: 175-181.

[80] QUERLIOZ, Emmanuelle, et al. Experimental investigations on the contact fatigue life under starved conditions. *Tribology International*, 2007, 40.10: 1619-1626.

[81] DUMONT, M.-LUGT; LUGT, P. M.; TRIPP, J. H. Surface feature effects in starved circular EHL contacts. *TRANSACTIONS-AMERICAN SOCIETY OF MECHANICAL ENGINEERS JOURNAL OF TRIBOLOGY*, 2002, 124.2: 358-366.

[82] CHENG, WHSLM; CHENG, H. S.; KEER, L. M. Experimental investigation on rolling/sliding contact fatigue crack initiation with artificial defects. *Tribology transactions*, 1994, 37.1: 1-12.

[83] ZHAI, Xuejun, et al. On mechanisms of fatigue life enhancement by surface dents in heavily loaded rolling line contacts. *Tribology transactions*, 1997, 40.4: 708-714.

[84] AI, Xiaolan; NIXON, Harvey P. Fatigue life reduction of roller bearings due to debris denting: Part I—Theoretical modeling. *Tribology Transactions*, 2000, 43.2: 197-204.

[85] AI, X. Effect of debris contamination on the fatigue life of roller bearings.*Proceedings of the Institution of Mechanical Engineers, Part J: Journal of Engineering Tribology*, 2001, 215.6: 563-575.

[86] VOLCHOK, A.; HALPERIN, G.; ETSION, I. The effect of surface regular microtopography on fretting fatigue life. *Wear*, 2002, 253.3: 509-515.

[87] VRBKA, M., et al. Effect of surface texturing on rolling contact fatigue within mixed lubricated non-conformal rolling/sliding contacts. *Tribology International*, 2010, 43.8: 1457-1465.

[88] HARTL, Martin; KRUPKA, Ivan; LISKA, Miroslav. Differential colorimetry: tool for evaluation of chromatic interference patterns. *Optical Engineering*, 1997, 36.9: 2384-2391.

[89] SAKAGUCHI, Tomoya; HARADA, Kazuyoshi. Dynamic analysis of cage behavior in a tapered roller bearing. *Journal of tribology*, 2006, 128.3: 604-611.

[90] JACOBSON, Bo O. *Rheology and elastohydrodynamic lubrication*. Elsevier, 1991.

[91] HÖGLUND, Erik. Influence of lubricant properties on elastohydrodynamic lubrication. *Wear*, 1999, 232.2: 176-184.

[92] ROELAND, C. J. A. *Correlation aspect of the viscosity–temperature–pressure relation of lubrication oils*. 1966. PhD Thesis. Ph. D. thesis, Delft University of Technology, Netherlands.

[93] JACOD, B., et al. An analysis of track replenishment mechanisms in the starved regime. *Tribology Series*, 1999, 36: 483-492.

[94] ÅSTRÖM, Henrik; ÖSTENSEN, Jan Ove; HÖGLUND, Erik. Lubricating grease replenishment in an elastohydrodynamic point contact. *Journal of tribology*, 1993, 115.3: 501-506.

[95] CANN, P. M. Starvation and reflow in a grease-lubricated elastohydrodynamic contact. *Tribology transactions*, 1996, 39.3: 698-704.

[96] CANN, P. M. E.; CHEVALIER, F.; LUBRECHT, A. A. Track depletion and replenishment in a grease lubricated point contact: a quantitative analysis.*Tribology Series*, 1997, 32: 405-413.

[97] LUGT, Piet M.; VELICKOV, Slavco; TRIPP, John H. On the chaotic behavior of grease lubrication in rolling bearings. *Tribology Transactions*, 2009, 52.5: 581-590.

[98] CANN, P. M.; HURLEY, I. S. Friction properties of grease in elastohydrodynamic lubrication. *NLGI spokesman*, 2002, 66.1: 6-15.

[99] BOOSER, E. R.; WILCOCK, D. F. Minimum oil requirements of ball bearings.*Lubrication Engineering*, 1953, 9.3.

[100] MÉRIEUX, J. S., et al. Shear-degradation of grease and base oil availability in starved EHL lubrication. *Tribology Series*, 2000, 38: 581-588.

[101] HARTL, MJIPMR, et al. Thin film colorimetric interferometry. *Tribology Transactions*, 2001, 44.2: 270-276.

[102] KUMAR, Punit; KHONSARI, M. M. Effect of starvation on traction and film thickness in Thermo-EHL line contacts with shear-thinning lubricants. *Tribology letters*, 2008, 32.3: 171-177.

[103] BIBOULET, Nans; COLIN, Francois; LUBRECHT, A. A. Friction in starved hydrodynamically lubricated line contacts. *Tribology International*, 2013, 58: 1-6.

[104] DOWSON, D.; HIGGINSON, G. R. *Elastohydrodynamic lubrication*, 1966. 1970.

[105] ROELANDS, C. J. A.; VLUGTER, J. C.; WATERMAN, H. I. The viscosity-temperature-pressure relationship of lubricating oils and its correlation with chemical constitution. *Journal of Fluids Engineering*, 1963, 85.4: 601-607.

[106] VENNER, Cornelis Henricus; LUBRECHT, Antonius A. (ed.). *Multi-level methods in lubrication*. Elsevier, 2000.

AUTHOR'S PUBLICATIONS

JOURNALS

1. **ALI, Fadi**; et al. Experimental and numerical investigation on the behavior of transverse limited micro-grooves in EHL point contacts. *Tribology International*, 2015, 84: 81-89. **IF=2.124 (2014)**
2. **ALI, Fadi**; KŘUPKA, Ivan; HARTL, Martin. An Approximate Approach to Predict the Degree of Starvation in Ball–Disk Machine Based on the Relative Friction.*Tribology Transactions*, 2013, 56.4: 681-686. **IF=1.081 (2013)**
3. **ALI, Fadi**; KŘUPKA, Ivan; HARTL, Martin. Enhancing the parameters of starved EHL point conjunctions by artificially induced replenishment. *Tribology International*, 2013, 66: 134-142. **IF=2.124 (2013)**
4. **ALI, Fadi**; KŘUPKA, Ivan; HARTL, Martin. Reducing the friction of lubricated nonconformal point contacts by transverse shallow micro-grooves. *Proceedings of the Institution of Mechanical Engineers, Part J: Journal of Engineering Tribology*, 2014, 1350650114543317. **IF=0.613 (2013)**
5. **ALI, Fadi**; KŘUPKA, Ivan; HARTL, Martin. Analytical and experimental investigation on friction of non-conformal point contacts under starved lubrication. *Meccanica*, 2013, 48.3: 545-553. **IF=1.747 (2012)**
6. **ALI, Fadi**; HARTL, Martin. Friction of non-conformal contacts under EHD lubrication. *MM Science Journal*, 2012, 12, 374-377.

CONFERENCES

1. **ALI, F.**; KŘUPKA, I.; HARTL, M. Friction of smooth and textured non-conformal surfaces under starved conditions 4th International Conference on Tribology and Design 2012. 3 - 5 September 2012, Kos, Greece.
2. **ALI, F.**; KŘUPKA, I.; HARTL, M. Overcoming starvation in EHL point contacts by enhanced replenishment. 16 Nordic Symposium on Tribology, 2014. Aarhus, Denmark.
3. Dipankar Choudhury, **Fadi Ali**, Martin Vrbka, Ivan Krupka, Martin Hartl. The influence of diamond like carbon coated surfaces on friction and film thickness to a bovine ceramic lubrication condition. 16 Nordic Symposium on Tribology, 2014. Aarhus, Denmark.

NOMENCLATURE

a = Radius of the Hertzian contact (m)

E' = Reduced modulus of elasticity (Pa)

h_{cff} = Fully flooded central film thickness (m)

h_{cs} = Starved central film thickness (m)

h_{00} = rigid central film thickness (m)

k = Ellipticity parameter

p = Hertzian pressure (Pa)

p_h = Maximum Hertzian pressure (Pa)

p_m = Average Hertzian pressure (Pa)

Q_{ff} = Fully flooded oil amount (μl)

Q_s = Starved oil amount (μl)

r_c = Radius of the contact (m)

$\Re$ = Degree of starvation

R' = Reduced radius of the contact (m)

$\Re_{cr}$ = Critical degree of starvation

u_e = Entraining velocity (m/s)

u_s = Sliding speed (m/s)

w = Load (N)

x,y = coordinates (m)

x_{out}, y_{out} = calculation domain (m)

z = Pressure-viscosity index

α = Pressure-viscosity coefficient (GPa^{-1})

β = Shear stress–pressure coefficient

$\dot{\gamma}$ = Shear rate (1/s)

$\dot{\gamma}_{ff}$ = Fully flooded shear rate (1/s)

$\dot{\gamma}_s$ = Starved shear rate (1/s)

λ_{st} = Starved film parameter

η = viscosity of lubricant (Pa s)

η_0 = ambient viscosity of lubricant (Pa s)

μ_b = Boundary coefficient of friction

μ_{ff} = Fully flooded coefficient of friction

μ_s = Starved coefficient of friction

$\overline{\mu}_C$ = Relative coefficient of friction

$\overline{\mu}_E$ = Relative experimental coefficient of friction

$\overline{\mu}_h$ = Relative hydrodynamic coefficient of friction

ρ = density of lubricant (kg/m^3)

ρ_0 = Ambient density of lubricant (kg/m^3)

σ = Composite roughness (m)

τ = Shear stress (Pa)

$\overline{\tau}$ = Non-dimensional shear stress

τ_L = Limiting shear stress (Pa)

τ_{L0} = Limiting shear stress at atmospheric pressure (Pa)

APPENDED PAPERS

This part of the thesis contains the full papers published by the author in relevant to the topics presented in this PhD thesis.

Tribology Transactions, 56: 681-686, 2013

ISSN: 1040-2004 print / 1547-397X online
DOI: 10.1080/10402004.2013.781722

STLE
Society of Tribologists
and Lubrication Engineers

An Approximate Approach to Predict the Degree of Starvation in Ball–Disk Machine Based on the Relative Friction

FADI ALI, IVAN KŘUPKA, and MARTIN HARTL
Faculty of Mechanical Engineering
Brno University of Technology
Technická 2896/2, 616 69 Brno, the Czech Republic

This article focuses on analyzing the correlation between the degree of starvation and friction under the sliding motion in a ball–disk machine. The objective of this study was to define approximately the degree of starvation in the contact based on measuring one parameter (the relative coefficient of friction). Such an approximate approach could be useful in cases of opaque contacts where the optical interferometry technique cannot be used; for example, a steel ball on a metal disk. Experimental measurements were conducted under different degrees of starvation using a tribometer equipped with a torque sensor and a high-speed digital camera. The results showed agreement between the theoretical equations and the experimental measurements. Thus, it can be stated that the approximate ratio of the film thickness reduction can be predicted based on accurate measurements of friction.

KEY WORDS

Relative Friction; Nonconformal Contacts; Starved Lubrication; Ball–Disk Machine

INTRODUCTION

In some practical measurements of friction it is necessary to simulate the contact of mating surfaces by a steel ball on a metal disk and to predict the degree of starvation to avoid scuffing risks of mating surfaces. In such cases, the optical interferometry technique cannot be used to estimate the ratio of the film thickness reduction in the contact. In addition, the elastohydrodynamic lubrication (EHL) theory (Dowson and Higginson *(1)*; Hamrock and Dowson *(2)*) efficiently predicts the film thickness under fully flooded conditions, but it is not recommended under poor lubrication conditions. However, the level of starvation and the position of the inlet meniscus are governed by many parameters, such as the film thickness, amount of lubricant available on the track, operating conditions, lubricant properties, and the replenishment (Lugt and Morales-Espejel *(3)*; Cann *(4)*). Therefore, it is quite difficult to determine the degree of starvation in opaque (nontransparent) EHL contacts.

Wedeven, et al. *(5)* and Wedeven *(6)* investigated the starvation of a ball bearing using optical interferometry. It was revealed that starvation inhibits the pressure buildup, resulting in a film thickness reduction and increase sliding friction due to the increase in the shear rate in the Hertzian contact. Chevalier, et al. *(7)* introduced a numerical study on starved EHL point contacts and the degree of starvation was defined by the amount of oil available on the track. A recent experimental study by Querlioz, et al. *(8)* indicated that the traction in point contacts depends on the degree of starvation. Faraon and Schipper *(9)* developed a model to predict the friction of starved line contacts. Cann, et al. *(10)* performed an experimental study describing the effect of operating conditions on the starved film thickness in nonconformal point contacts. The numerical results of starved elliptical EHL contacts by Damiens, et al. *(11)* showed that the degree of starvation depends on the operating conditions and the amount of oil available on the track. The effect of the replenishment on the degree of starvation has been recently investigated by Van Zoelen, et al. *(12)* and Gershuni, et al. *(13)*. Kumar and Khonsari *(14)* studied the effect of starvation on traction in thermo-EHL rolling–sliding line contacts. The results indicated that the effect of starvation on the traction coefficient increased with increasing speed and decreasing slide-to-roll ratio (SRR).

A study of the literature showed that the degree of starvation in EHL contacts has been predicted as a function of the inlet air–oil meniscus distance from the Hertzian contact or as a function of the inlet oil thickness instead of the meniscus position, which is difficult to measure in practice with nontransparent surfaces because the contact is hidden and it cannot be optically observed. For this reason, in this article, we propose to determine the approximate degree of starvation based on the experimental measurements of the coefficient of friction. This approach is applicable at least in the ball–disk machine with accurate measurements of friction.

CALCULATION OF FRICTION UNDER STARVED LUBRICATION

In each lubrication regime, the coefficient of friction is related to the film parameter $\lambda = h/\sigma$. Thus, the following equation by

Manuscript received October 4, 2012
Manuscript accepted February 27, 2013
Review led by Michael Khonsari

NOMENCLATURE

a = Radius of the Hertzian contact (m)
E' = Reduced modulus of elasticity (Pa)
h_{cff} = Fully flooded central film thickness (m)
h_{cs} = Starved central film thickness (m)
k = Ellipticity parameter
p = Hertzian pressure (Pa)
p_h = Maximum Hertzian pressure (Pa)
p_m = Average Hertzian pressure (Pa)
Q_{ff} = Fully flooded oil amount (μL)
Q_s = Starved oil amount (μL)
R' = Reduced radius of the contact (m)
$\Re$ = Degree of starvation
$\Re_{cr}$ = Critical degree of starvation
r_c = Radius of the contact (m)
u_e = Entraining velocity (m/s)
u_s = Sliding speed (m/s)
w = Load (N)
z = Pressure–viscosity index
α = Pressure–viscosity coefficient (GPa^{-1})
β = Shear stress–pressure coefficient
γ = Shear rate (1/s)
γ_{ff} = Fully flooded shear rate (1/s)
γ_s = Starved shear rate (1/s)
λ_{st} = Starved film parameter
μ_b = Boundary coefficient of friction
$\overline{\mu}_C$ = Relative coefficient of friction
$\overline{\mu}_E$ = Relative experimental coefficient of friction
μ_{ff} = Fully flooded coefficient of friction
$\overline{\mu}_h$ = Relative hydrodynamic coefficient of friction
μ_s = Starved coefficient of friction
σ = Composite roughness (m)
τ = Shear stress (Pa)
$\overline{\tau}$ = Nondimensional shear stress
τ_L = Limiting shear stress (Pa)
τ_{L0} = Limiting shear stress at atmospheric pressure (Pa)

Sakaguchi and Harada *(15)* can be adopted to calculate the coefficient of friction in the relative form:

$$\overline{\mu}_C = \frac{\mu_s}{\mu_{ff}} = \begin{cases} \mu_b/\mu_{ff} & \text{if } \lambda_{st} < 0.01 \\ \dfrac{(\mu_b/\mu_{ff}) - \overline{\mu}_h}{(0.01-1.5)^6}(\lambda_{st}-1.5)^6 + \overline{\mu}_h & \text{if } 0.01 \le \lambda_{st} < 1.5, \\ \overline{\mu}_h & \text{if } 1.5 \le \lambda_{st} \end{cases} \quad [1]$$

where $\overline{\mu}_C$ is the relative coefficient of friction through the different lubrication regimes, $\overline{\mu}_h$ is the relative hydrodynamic coefficient of friction under starved lubrication, and μ_b is the boundary friction.

Experimental investigations show that the majority of lubricants exhibit a non-Newtonian behavior in EHL contacts due to the nonlinearity of the shear stress τ versus shear rate. Nevertheless, some non-Newtonian models have been developed to characterize the rheological behavior of fluids in nonconformal conjunctions (Bair and Winer *(16)–(18)*). Indeed, the issue of lubricating EHL contacts is quite complex because many aspects are involved like, the thermal effect, waviness and roughness of mating surfaces, starvation and sliding velocity, and so on. Therefore, it is difficult to find a mathematical model able to simulate all of the involved parameters together. However, the shear stress is given by the Bair and Winer model as

$$\overline{\tau} = 1 - e^{-(\gamma\eta/\tau_L)}, \quad [2]$$

where $\overline{\tau} = \tau/\tau_L$, η is the viscosity, and γ is the shear rate.

The limiting shear stress is represented by the following (Jacobson *(19)*),

$$\tau_L = \tau_{L0} + \beta p_m, \quad [3]$$

where τ_{L0} is the limiting shear stress at zero pressure, $\beta = \partial\tau_L/\partial p$ is the shear stress–pressure coefficient, and p_m is the average Hertzian pressure.

For most mineral oils, $\tau_{L0} \approx 15$ MPa and $\beta \approx 0.052$ at 40°C; see Jacobson *(19)* and Hoglund *(20)*.

Under starved lubrication, the film thickness tends to be flat, which means that the central film thickness has a value nearly equal to the value of the minimum film thickness; see Chevalier, et al. *(7)*. Therefore, the pressure distribution can be approximated to the Hertzian pressure by the following:

$$p = p_h\sqrt{(1 - (r_c/a)^2)}, \quad [4]$$

and the shear rate can be approximated by the following:

$$\gamma = \partial u/\partial h \approx \Delta u/h. \quad [5]$$

The ratio of the shear rate through the transition from fully flooded to starved conditions under a given steady state can be expressed by the following:

$$\gamma_s/\gamma_{ff} = h_{cff}/h_{cs} = 1/\Re. \quad [6]$$

The Roelands equation (Roelands *(21)*) is adopted to define the viscosity by the following:

$$\eta = \eta_0\,(\eta_\infty/\eta_0)^{(1-(1+P/P_r)^z)}, \quad [7]$$

with $\eta_\infty = 6.31 \times 10^{-5}$ Pa.s, $p_r = 1.962 \times 10^8$ Pa, and p is given by Eq. [4].

Combining Eqs. [2] and [6] gives the relative hydrodynamic coefficient of friction under starved lubrication by the following:

$$\overline{\mu}_C = \overline{\mu}_h = \int_0^a \left(1 - e^{-(\gamma_s\eta/\tau_L)}\right) r_c\,dr_c \Big/ \int_0^a \left(1 - e^{-(\gamma_{ff}\,\eta/\tau_L)}\right) r_c\,dr_c = \int_0^a \left(1 - e^{-(\gamma_{ff}\,\eta/\Re\tau_L)}\right) r_c\,dr_c \Big/ \int_0^a \left(1 - e^{-(\gamma_{ff}\,\eta/\tau_L)}\right) r_c\,dr_c. \quad [8]$$

The SRR is given as:

$$SRR = 2 * (u_{\text{disk}} - u_{\text{ball}})/(u_{\text{disk}} + u_{\text{ball}}) = u_s/u_e, \quad [9]$$

where u_s is the sliding velocity and u_e is the entraining velocity. The negative signal of the SRR means that the ball is faster than the disk.

Equation [1] can be solved for $\Re \neq 0$ by applying a numerical integration to calculate $\overline{\mu}_h$ for an isothermal lubricated contact

TABLE 1—PARAMETERS OF CONTACT FOR NUMERICAL CALCULATIONS

Ambient temperature $t = 25\,^{\circ}\mathrm{C}$	Dynamic viscosity $\eta_0 = 0.421$ Pa.s at 40°C
Modulus of elasticity $E_{\mathrm{ball}} = 210\,\mathrm{GPa}$	Boundary friction $\mu_b = 0.12$
Modulus of elasticity $E_{\mathrm{disk}} = 80$ GPa	Pressure–viscosity index $z = 0.64$
Poisson's ratio $\upsilon_{\mathrm{ball}} = 0.3$	Composite roughness $\sigma = 10.77\,\mathrm{nm}$
Poisson's ratio $\upsilon_{\mathrm{disk}} = 0.17$	Limiting stress $\tau_{L0} = 15\,\mathrm{MPa}$ at $p = 0$
Reduced radius of the contact $R' = 6.35 \times 10^{-3}\,\mathrm{m}$	Ellipticity parameter $K = 1$

between a steel ball and a glass disk under steady-state conditions. The central full film thickness h_{cff} can be calculated by the well-known formula of Hamrock and Dowson *(22)*. In addition, the constants in Table 1 were used in the calculations.

EFFECT OF OPERATING CONDITIONS

Equation [1] was numerically simulated using the adaptive Simpson's method with an error of 10^{-6} as shown in Figs. 1–3. It is necessary to take into consideration that the value of μ_{ff} changes with the load and the entraining velocity. Hence, every single curve in Figs. 1 and 2 represents a different steady state. Figure 1 shows that increasing the load in the starved contact of ball–disk under the same entraining velocity led to reduce sensitivity of friction versus the change in the degree of starvation, whereas the critical degree of starvation $\Re_{cr}$ ($\Re_{cr} = 1.5\sigma/h_{cff}$ represents the transition from the full-film regime to the mixed regime) is not significantly affected by the load since $h_{cs} = \Re * h_{cff} \propto \Re * w^{-0.073}$. On the other hand, Fig. 2 shows the slight effect of the entraining velocity on the sensitivity of friction, but the value of $\Re_{cr}$ was noticeably reduced with the higher speed, resulting in enlarging the range of the validity of Eq. [8] where $\overline{\mu}_C = \overline{\mu}_h$ for $\Re \in]\Re_{cr}, 1]$. Note that in this case $h_{cs} = \Re * h_{cff} \propto \Re * u_e^{0.68}$.

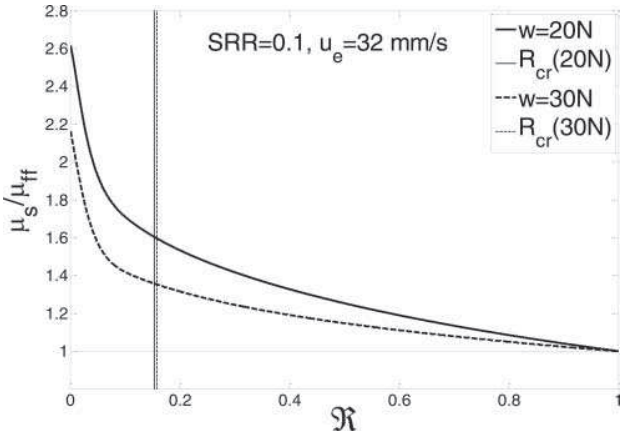

Fig. 1—Simulation of the effect of load on the non-Newtonian behavior of the relative coefficient of friction $\overline{\mu}_C = \mu_s/\mu_{ff}$ vs. the degree of starvation $\Re$ for SRR = 0.1.

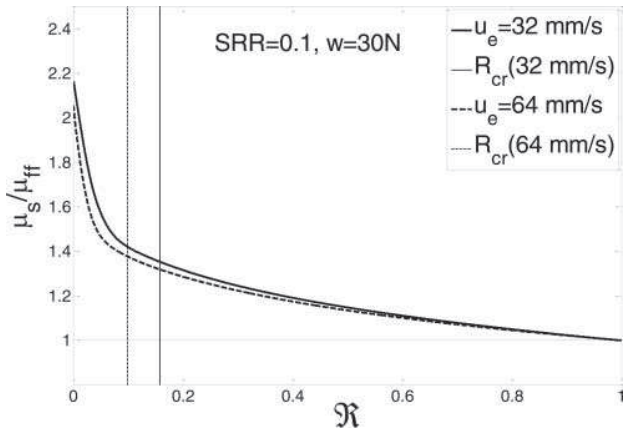

Fig. 2—Simulation of the effect of the entraining velocity on the non-Newtonian behavior of the relative coefficient of friction $\overline{\mu}_C = \mu_s/\mu_{ff}$ vs. the degree of starvation $\Re$ for SRR = 0.1.

The large effect of load on the sensitivity of friction was attributed to the exponential change in the viscosity with load (see Eq. [7]), and the effect of load on the limiting shear stress in Eq. [3] was linear and was minor for low loads, $p < 0.5$ GPa. Therefore, the effect of τ_L on the sensitivity of friction was slight for low loads. The effect of speed on the film thickness was limited with an exponential factor of 0.68.

To investigate the influence of the SRR on the relative coefficient of friction, the entraining velocity and the load were kept constant in Eq. [1]. Figure 3 shows the simulation of the SRR effect on the non-Newtonian relative friction versus the degree of starvation in the steady state. In this simulation, it was supposed that the critical degree of starvation was not related to the value of sliding $\Re_{cr} \neq f\,(SRR)$. It is clear that increasing SRR reduced the gradient of the relative coefficient of friction $\overline{\mu}_C = \mu_s/\mu_{ff}$ versus the degree of starvation $\Re$, although the larger SRR results in a larger μ_s. In other words, the starved coefficient of friction μ_s can be doubled more times under low SRRs than under high SRRs for the same degree of starvation.

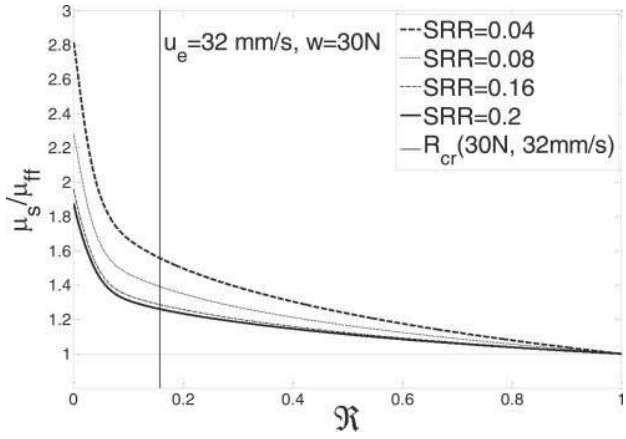

Fig. 3—Simulation of the effect of the SRR on the relative coefficient of friction $\overline{\mu}_C = \mu_s/\mu_{ff}$ under starved conditions.

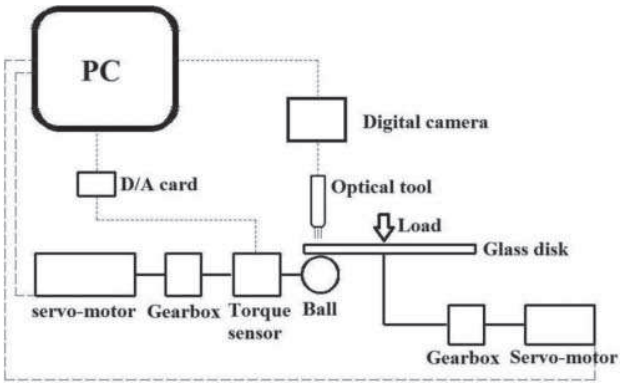

Fig. 4—Schema of experimental equipment.

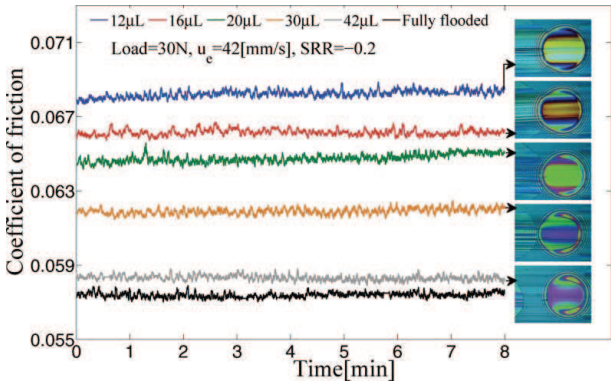

Fig. 5—Experimental gradient of friction coefficient vs. the reduction in the amount of oil on the track with the corresponding interferometric images captured in the sixth minute (color figure available online).

Hence, the lubricant tends to be more Newtonian (the transition from Couette flow to Poiseuille flow) with reducing SRR under starved lubrication. This result is common in non-Newtonian shear stress models where the behavior of lubricants is Newtonian for low shear rates and becomes gradually non-Newtonian with increasing shear rate.

EXPERIMENTAL EQUIPMENT

Measurements were carried out using a tribometer equipped with a torque sensor driven by the ball shaft; see Fig. 4. The acquired signal from the sensor was processed by a digital/analog card configured by the software LabVIEW. The ball and disk were driven by servomotors and gearboxes to reduce the frequency of the revolutions. The angular velocity of the servomotors was numerically controlled by the computer, which provided the ability to change the required SRR in a wide range. The steel ball AISI 52100 had a measured roughness (RMS) of about 10 nm and a diameter of 25.4 mm with an elastic modulus of 210 GPa.

The disk was made of a transparent glass with an elastic modulus of 80 GPa. The over-rolled track on the flat disk had a radius of 50 mm. The lower surface of the disk was coated with a thin layer of chromium. In addition, the apparatus was equipped with a digital camera and the contact between the ball and disk was illuminated by a high-power light source. This arrangement had the advantage of capturing interferometric images of the starved contact simultaneously with the friction measurements by the torque sensor; consequently, it was possible to experimentally observe the position of the air–oil meniscus in correspondence to the value of the friction coefficient. The amounts of lubricant for starved conditions were defined by a digital pipette. The naphthenic base oil (N2400) with a dynamic viscosity $\eta = 0.421$ Pa.s at 40°C and pressure–viscosity coefficient $\alpha = 35$ GPa^{-1} was used in all of the experiments introduced in this article. The contact was always loaded by 30 N with an entraining velocity 42 mm/s and SRR $= -0.2$, where the negative sign means that the ball was faster than the disk.

EXPERIMENTAL RESULTS

Measurements were carried out to verify the theoretical models and to experimentally investigate the behavior of friction versus the degree of starvation under steady-state operating conditions. The degree of starvation was modified from the fully flooded to extreme starvation by changing the oil amount available on the track. Indeed, the expression of the fully flooded was flexible because the same contact under the same steady state can be fully flooded for different amounts of oil. Thus, the concept of Q_{ff}, representing the minimum oil amount to make the contact fully flooded under a given steady state, was adopted. The value of Q_{ff} was adjusted for the minimum coefficient of friction measured by the sensor for the given steady state (load $= 30$ N, entraining velocity $u_e = 42$ mm/s, and SRR $= -0.2$) and the amount of oil Q_{ff} was iteratively defined by 60 μL. For $Q > Q_{ff} = 60\,\mu$L, the contact was considered to be ultra fully flooded and a small increase in friction was observed. However, the relative oil amount available on the track $Q_s/Q_{ff} \in [0, 1]$ has not been taken less than 20% to avoid any possible damage of the contacting surfaces. Figure 5 shows the measured friction versus the reduction in the amount of oil on the track; it is clear from the corresponding interferometric images, which were captured in the sixth minute of the measurement, that the coefficient of friction increased dramatically only as the air–oil meniscus intersected the Hertzian circle and the larger intersection resulted in a larger coefficient of friction. Moreover, reducing the amount of oil from $Q_{ff} = 60\,\mu$L to $Q_s = 42\,\mu$L caused a small increase in the friction but a smaller reduction in the oil amount from 16 to 12 μL resulted in a larger relative increase in the friction coefficient. Therefore, the coefficient of friction became increasingly sensitive to the amount of oil with increasing severity of starvation; this result is in accord with Figs. 1–3.

The degree of starvation $\Re = h_{cs}/h_{cff}$ versus the relative amount of oil available on the track Q_s/Q_{ff} was measured using optical interferometry. The film thickness reduction shown in Fig. 6 corresponds to interferometric images captured in the sixth minute, shown in Fig. 5.

Figure 7 shows a comparison between experimental measurements in Figs. 5 and 6 with the theoretical model in Eq. [1], which is based on the Bair and Winer model in calculating the friction. Good agreement was achieved in the hydrodynamic range for

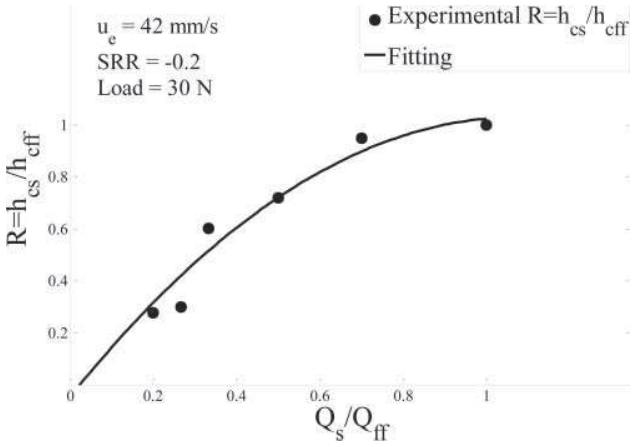

Fig. 6—Degree of starvation $\Re = h_{cs}/h_{cff}$ versus the relative reduction in the amount of oil.

$\Re \in]\Re_{cr}, 1]$. In addition, Fig. 7 shows that the theoretical model was slightly dependent on the value of τ_{L0} under low loads in the hydrodynamic range.

In Fig. 8 a simple algorithm was established to determine the approximate degree of starvation based on the measured value of $\overline{\mu}_E = \mu_s/\mu_{ff}$. In this algorithm, it is also assumed that the agreement between the theoretical Eq. [1] and experimental measurement is conserved, as shown in Fig. 7. However, this assumption may not be valid under extreme operating conditions, particularly at high sliding speeds, due to the increase in the thermal effect, which was not taken into account in this article. Furthermore, calculating the shear stress and pressure distribution based on solving the Reynolds equation and elastic deformation could lead to improved accuracy of this approximate approach. The convergence in the algorithm in Fig. 8 can be simply achieved as $|\overline{\mu}_C - \overline{\mu}_E| \to 0$.

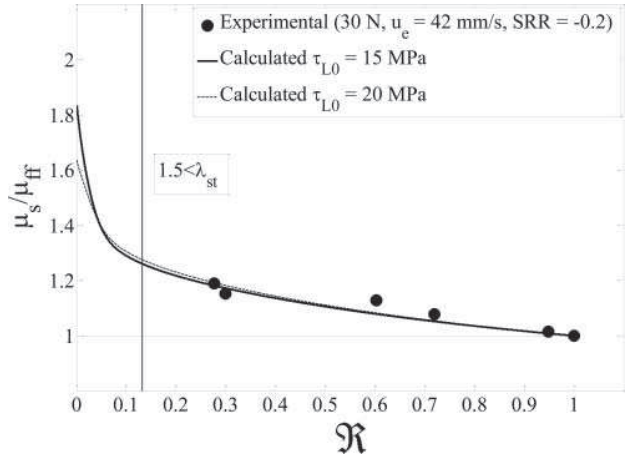

Fig. 7—Comparison between the calculated and experimental ratio $\overline{\mu}_C = \mu_s/\mu_{ff}$ vs. the degree of starvation.

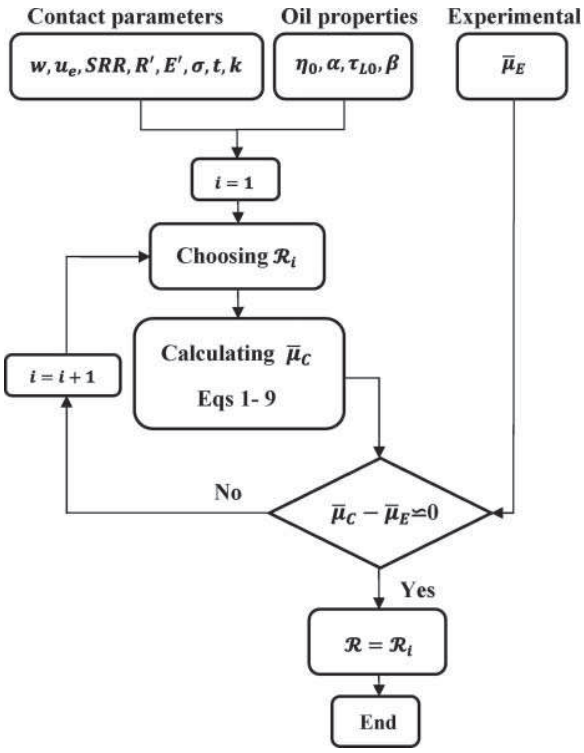

Fig. 8—Algorithm to determine the approximate degree of starvation based on the measured value of $\overline{\mu}_E = \mu_s/\mu_{ff}$.

CONCLUSIONS

The effect of operating conditions on the relative coefficient of friction $\overline{\mu}_C = \mu_s/\mu_{ff}$ and the critical degree of starvation $\Re_{cr}$ was introduced in this study using the Bair and Winer model. In addition, an approximate approach to predict the degree of starvation $\Re = h_{cs}/h_{cff}$ in a ball–disk machine was proposed. The approach was based on the assumption that the coefficient of friction is a reflection of the film thickness formation in the contact; thus, the relative change of friction due to starvation is related to a relative reduction of the film thickness under the same steady state. Hence, accurate measurements of friction and a reliable model of traction are required to obtain an accepted approximation of the predicted degree of starvation. The proposed approach is inexpensive and practical for a ball–disk machine in cases where the optical interferometry technique cannot be used.

ACKNOWLEDGEMENT

This research was financially supported by the Czech Science Foundation (Project No. GAP101/11/1115) and the European Regional Development Fund (Project No. CZ.1.07/2.3.00/20.0126).

REFERENCES

(1) Dowson, D. and Higginson, G. R. (1959), "A Numerical Solution to the Elastohydrodynamic Problem," *Journal of Mechanical Engineering and Sciences*, **1**, pp 6–15.

(2) Hamrock, B. J. and Dowson, D. (1976), "Isothermal Elastohydrodynamic Lubrication of Point Contacts, Part I, Theoretical Formulation," *Journal of Lubrication Technology*, **98**, pp 223–229.

(3) Lugt, P. M. and Morales-Espejel, G. E. (2011), "A Review of Elasto-Hydrodynamic Lubrication Theory," *Tribology Transactions*, **54**(3), pp 470–496.
(4) Cann, P. M. E. (1999), "Starved Grease Lubrication of Rolling Contacts," *Tribology Transactions*, **42**(4), pp 867–873.
(5) Wedeven, L. D., Evans, D., and Cameron, A. C. (1971), "Optical Analysis of Ball Bearing Starvation," *Journal of Lubrication Technology*, **93**, pp 349–363.
(6) Wedeven, L. D. (1975), "Traction and Film Thickness Measurements under Starved Elastohydrodynamic Conditions," *Journal of Lubrication Technology*, **97**, pp 321–329.
(7) Chevalier, F., Lubrecht, A. A., Cann, P. M. E., Colin, F., and Dalmaz, G. (1998), "Film Thickness in Starved EHL Point Contacts," *Journal of Tribology*, **120**, pp 126–133.
(8) Querlioz, E., Ville, F., Lenon, H., and Lubrecht, T. (2007), "Experimental Investigations on the Contact Fatigue Life under Starved Conditions," *Tribology International*, **40**, pp 1619–1626.
(9) Faraon, I. C. and Schipper, D. J. (2007), "Stribeck Curve for Starved Line Contact," *Journal of Tribology*, **129**, pp 181–187.
(10) Cann, P. M. E., Damiens, B., and Lubrecht, A. A. (2004), "The Transition between Fully Flooded and Starved Regimes in EHL," *Tribology International*, **37**, pp 859–864.
(11) Damiens, B., Venner, C. H., Cann, P. M. E., and Lubrecht, A. A. (2004), "Starved Lubrication of Elliptical EHD Contacts," *Journal of Tribology*, **126**, pp 105–111.
(12) Van Zoelen, M. T., Venner, C. H., and Lugt, P. M. (2010), "The Prediction of Contact Pressure–Induced Film Thickness Decay in Starved Lubricated Rolling Bearings," *Tribology Transactions*, **53**(6), pp 831–841.
(13) Gershuni, L., Larson, M. G., and Lugt, P. M. (2008), "Lubricant Replenishment in Rolling Bearing Contacts," *Tribology Transactions*, **51**, pp 643–651.
(14) Kumar, P. and Khonsari, M. M. (2008), "Effect of Starvation on Traction and Film Thickness in Thermo-EHL Line Contacts with Shear-Thinning Lubricants," *Tribology Letters*, **32**(3), pp 171–177.
(15) Sakaguchi, T. and Harada, K. (2006), "Dynamic Analysis of Cage Behavior in a Tapered Roller Bearing," *ASME Transactions*, **128**, pp 604–611.
(16) Bair, S. and Winer, W. O. (1979), "Shear Strength Measurements of Lubricants at High Pressure," *Journal of Lubrication Technology*, **101**, pp 251–257.
(17) Bair, S. and Winer, W. O. (1992), "The High Pressure High Shear Stress Rheology of Liquid Lubricants," *Journal of Tribology*, **114**, pp 1–13.
(18) Bair, S. and Winer, W. O. (1979), "A Rheological Model for Elastohydrodynamic Contacts Based on Primary Laboratory Data," *Journal of Lubrication Technology*, **101**, pp 258–265.
(19) Jacobson, B. J. (1991), *Rheology and Elastohydrodynamic Lubrication* (Vol 19), Elsevier: London.
(20) Hoglund, E. (1999), "Influence of Lubricant Properties on Elastohydrodynamic Lubrication," *Wear*, **232**(2), pp 176–184.
(21) Roelands, C. J. A. (1966), *Correlation Aspects of Viscosity–Temperature–Pressure Relationship of Lubricating Oils*, Ph.D. Thesis, Delft University of Technology: Delft, The Netherlands.
(22) Hamrock, B. J. and Dowson, D. (1977), "Isothermal Elastohydrodynamic Lubrication of Point Contacts, Part III—Fully Flooded Results," *Journal of Lubrication Technology*, **99**, pp 264–276.

Tribology International 66 (2013) 134–142

Contents lists available at SciVerse ScienceDirect

Tribology International

journal homepage: www.elsevier.com/locate/triboint

Enhancing the parameters of starved EHL point conjunctions by artificially induced replenishment

Fadi Ali *, Ivan Křupka, Martin Hartl

Faculty of Mechanical Engineering, Brno University of Technology, Technická 2896/2, 616 69 Brno, Czech Republic

ARTICLE INFO

Article history:
Received 1 February 2013
Received in revised form
24 April 2013
Accepted 8 May 2013
Available online 15 May 2013

Keywords:
Induced replenishment
EHL
Point contact
Starvation

ABSTRACT

The authors present in this paper a mechanism for enhancing the replenishment in EHL point contacts under extreme starvation. The mechanism of replenishment depends on channeling the available lubricant towards the centerline of the overrolled track by using a flexible slider (scraper) with a micro-slot concentric with the track. The slider accumulates the scraped lubricant to be hydrodynamically entrained through the micro-slot resulting in enriching the depleted track with fresh lubricant. The efficiency of induced replenishment is assessed by measuring the coefficient of friction (COF) and the film thickness over time in a ball-on-disc device. The results show a significant reduction of friction about 31% for oil lubrication and about 25% for grease lubrication after introducing the mechanism of artificially induced replenishment. On the other hand, the central film thickness has been doubled many times for oil and grease lubrication. The optical interferometric images show that the air–oil meniscus disappeared upstream far away from the Hertzian contact which means that the contact transformed from the severely starved to the fully flooded regime with a limited amount of lubricant. The reliability of this method is high since the observed benefits are stable over time.

1. Introduction

Enhancing the tribological performance of machine components has an increasing importance day after day. In practice, it is necessary to improve the properties of materials side by side with reducing friction and wear of rubbing surfaces to answer the economic and industrial requirements. Non-conformal contacts are common in machines (rolling-element bearings, gears, cams, etc.) and it is well known that enhancing the lubricating film thickness is the key to reduce friction and wear and to extend the lifecycle of concentrated conjunctions. However, the EHL theory is successfully valid for oil full film lubrication [1,2], while it fails in the case of starved or grease-lubricated contacts. The problem of starved lubrication can be encountered under extreme operating conditions (high speeds and viscosities) or in cases where greases are used to lubricate bearings [3,4]. Starvation is usually associated with a sharp reduction of the film thickness to just a few nanometers resulting in high friction and wear. However, starvation is essentially due to the failure of lubricant to replenish the track after being displaced sideways by the repeated overrollings, and without a mechanism to replenish the track with lubricant the reduction of the film thickness would inevitably lead to the failure of contacting surfaces [5]. In 1970s, the phenomenon of starvation was optically observed by Wedeven et al. [6,7] and it was found that the emergence of the inlet meniscus close to the Hertzian zone inhibits the pressure buildup in the contact resulting in a film thickness reduction and greater traction than under fully flooded regime for the same slide-to-roll ratio. Pemberton and Cameron [8] and Kingsbury [9,10] defined the degree of starvation as a function of the distance between the inlet meniscus and the Hertzian contact. Chevalier et al. [11–12] performed a numerical study of starved EHL point contacts and the amount of lubricant in the inlet was adopted to define the degree of starvation. Then, a similar study was conducted by Damiens et al. [13] for elliptical contacts. Lubrecht et al. [14] and Cann et al. [15] performed experimental studies to describe the effect of operating conditions on the starved film thickness in non-conformal point contacts. The mechanisms of replenishment have been studied by many authors. The analytical and experimental study of Chiu [16] showed that starvation in rolling contacts is related to the insufficiency of fluid replenishment on the track during the time interval between overrollings. Pemberton and Cameron [8] proposed that the balance between the entrained and the lost oil around the contact determines the position of the inlet meniscus. Guangteng et al. [17] performed experimental and theoretical investigations on EHL contacts with a limited amount of oil and it was revealed that starvation occurs at a critical rolling speed which is determined by the rate of flow-back of lubricant into the out-of-contact track due

* Corresponding author. Tel.: +420 773260784.
E-mail address: fa77f@yahoo.com (F. Ali).

0301-679X/$ - see front matter © 2013 Elsevier Ltd. All rights reserved.
http://dx.doi.org/10.1016/j.triboint.2013.05.003

to surface tension forces. However, the complete collapse of the film thickness does not occur even for speeds larger than the critical speed because of solid/liquid van der Waals forces. Jacod et al. [5] indicated that the mechanism of the out-of-contact replenishment under very thin film conditions is extremely insufficient; whilst the in-contact replenishment caused by the capillary forces produces a more significant reflow.

Grease lubrication is widely used in rolling bearings to provide a sufficient and permanent separation between rolling elements and rings, which results in enhancing the lifecycle and reducing friction. In cases concerning the leakage, grease lubrication is preferred over oil lubrication since its stiffness creates a resistance against the leakage [18]. On the other hand, replenishment is strongly insufficient with grease lubrication because as the grease is pushed to the sides it cannot readily flow back into the track leading to very thin films [19–21] and increasing the temperature in the contact [22]. Cann [23] showed experimentally that the properties of the deposited thickener layer of grease determine friction and film thickness. However, the mechanism of replenishment for greases can be explained by the effect of base oil bleeding [24] and the shear degradation [25]. The effect of centrifugal forces on the mechanism of replenishment in bearings was studied by Gershuni et al. [4] and Van Zoelen et al. [26–27]. Recent studies [28–30] focused on analyzing the correlation between friction and the degree of starvation in EHL sliding contacts. It was found that the effect of starvation on the traction coefficient increases with decreasing the slide-to-roll ratio and increasing speeds.

In fact, the tribology community focused in several references on understanding and modeling starvation instead of trying to overcome this problem. Therefore, the authors introduce in this paper an innovative solution to avoid the negative effects of starvation in EHL point contacts by means of channeling the lubricant on the track. The introduced approach can be efficiently integrated in practical applications such as radial and thrust rolling bearings.

2. Experimental

Measurements are conducted by using a tribometer equipped with a torque sensor driven by the ball shaft. The acquired signal from the sensor is processed by Digital/Analog card. The ball and disk are driven by servo-motors and gearboxes with a possibility of changing slide-to-roll ratios $SRR = 2 \times (u_{disk} - u_{ball})/(u_{disk} + u_{ball})$ in a wide range. The steel ball AISI 52,100 has roughness (RMS) about 15 nm and a diameter of 25.4 mm. The elastic modulus of the steel ball is 210 GPa while the disk is made of a transparent glass with an elastic modulus of 80 GPa. The lower surface of the disk is coated with a thin layer of chromium. The tribometer is equipped with a high-speed digital camera which enables capturing interferometric images of the starved contact simultaneously with measuring the friction. Consequently, it is possible to measure the film thickness in correspondence with the value of friction coefficient. The contact between the glass disk and steel ball is illuminated by a high-power source of light to capture interferometric images. The base oil (2400 N) with the dynamic viscosity $\eta = 0.421$ Pas at 40 °C and the commercial grease DIN-KPF2K-30 (lithium soaps and mineral oil with additives PTFE-Teflon) are used for investigating the effect of artificially induced replenishment on the film thickness formation and friction. The contact was always loaded by 30 N with different entraining velocities and slide-to-roll ratios SRR, where the negative signal of SRR means that the ball is faster than the disk. The micro amounts of lubricant for starved conditions were carefully measured and injected on the track by a digital pipette with high accuracy. Measurements were carried out after a short time (about 1 min) from the start to ensure that the lubricant is evenly distributed on the tracks of the ball and disk. The temperature in the laboratory room was strictly kept at 24 °C.

It is necessary to investigate the stability and the sustainability of the mechanism in replenishing the starved track over time. Therefore, friction and the corresponding film thickness are measured over time under the steady state to show how the mechanism is time dependant. Benefits are estimated in comparison with the measured values for the contact with natural replenishment (without slider).

2.1. Procedures of friction measurements

Measurements of friction for the starved contact without the mechanism of induced replenishment were carried out firstly and lasted a shorter time to avoid the possible damage of rubbing surface by excessive starvation. For base oil, the amount of lubricant on the track was 8 μl with entraining velocity $u_e = 34.5$ mm/s and SRR = −1.85. The same procedures were repeated for grease lubrication for 100 mg of grease on the track with entraining velocity $u_e = 25$ mm/s and SRR = −1.6.

2.2. Procedures of film thickness measurements

The film thickness is measured by the colorimetric interferometry technique [31]. Interferometric images were captured simultaneously with measuring friction. However, the film thickness is compared at $t1 = 5$ min and $t2 = 25$ min for oil and grease lubrication. Additional film thickness measurements were carried out for the contact with the mechanism of induced replenishment at $t3 = 60$ min for oil lubrication and $t3 = 40$ min for grease lubrication. Measurements of film thickness at $t3$ are dedicated only to show the reliability of the mechanism on enhancing the film thickness over time.

3. Results and discussion

3.1. Mechanism of artificially induced replenishment

Fig. 1 shows the mechanism for generating the induced replenishment on the track of the ball. The mechanism consists of a slider (thin plastic sheet made of polyethylene) with a micro-slot concentric with the overrolled track. The thin plastic sheet

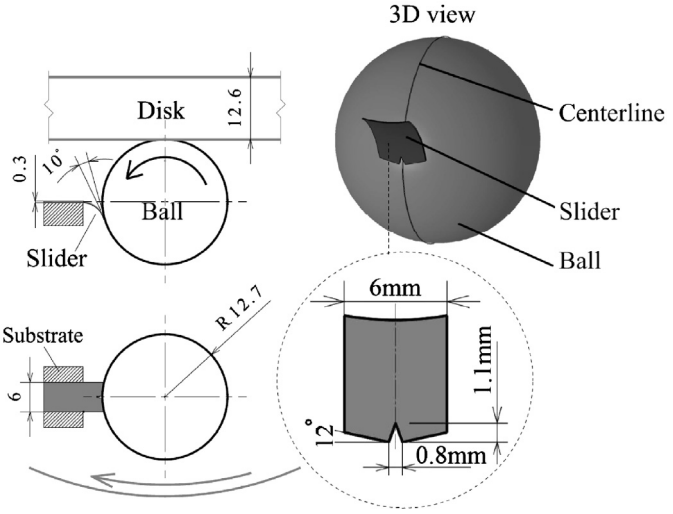

Fig. 1. Schema of the mechanism providing the artificially induced replenishment in the ball-on-disk device.

is flexible with a tension force about 0.1 N which ensures the permanent contact with the ball surface without fear of increasing friction or wear. The slider scrapes the lubricant on the surface and creates a forced and channeled reflow towards the centerline of the overrolled track through the micro-slot. The efficiency of scraping the track increases as the transverse width of the slider is large enough to collect all the displaced lubricant on the surface of the ball. On the other hand, the profile of the contact between the slider and the ball should generate a hydrodynamic resistance results in entraining the scraped fluid towards the centerline of the track. Therefore, the head of slider is chamfered upward with a small angle 12° on both sides, see Fig. 1. Hence, the profile of the contact between the slider and the ball takes the shape of a chevron oriented transversely on the sliding direction resulting in scraping the lubricant without side-leakage. Without chamfering, the contact between the slider and the ball becomes a transverse line leading to a significant leakage around the sides. The seal between the chamfered edges and the spherical surface of the ball is achieved because the plastic sheet tends to create conformity (coincident surfaces) with the opposite surface due to the flexibility and the tension force. In addition, the plastic sheet is prefolded along the centerline to create transverse tension forces to improve the seal. Increasing the angle of chamfering improves the hydrodynamic entraining but it worsens the seal on the sides of the slider because in this case the chamfered edges of the plastic sheet should coincide with a longer curve. However, for the given geometry of slider shown in Fig. 1, it was observed that the lubricant accumulates on the front surface of the slider head just after a few of overrollings. In general, grease tends to accumulate more than the oil due to its stiffness. The accumulated amount of lubricant is related to the viscosity, capillary forces (oil lubrication), the angle between the slider and the tangent surface of the ball, dimensions of the micro-slot, the sliding speed and the available amount of lubricant on the track. Nevertheless, the accumulated amount of lubricant stabilizes, if there is not side-leakage, in a short time (1–2 min) after the start and the scraped lubricant flows hydrodynamically (oil lubrication) through the micro-slot which is concentric with the centerline of the track

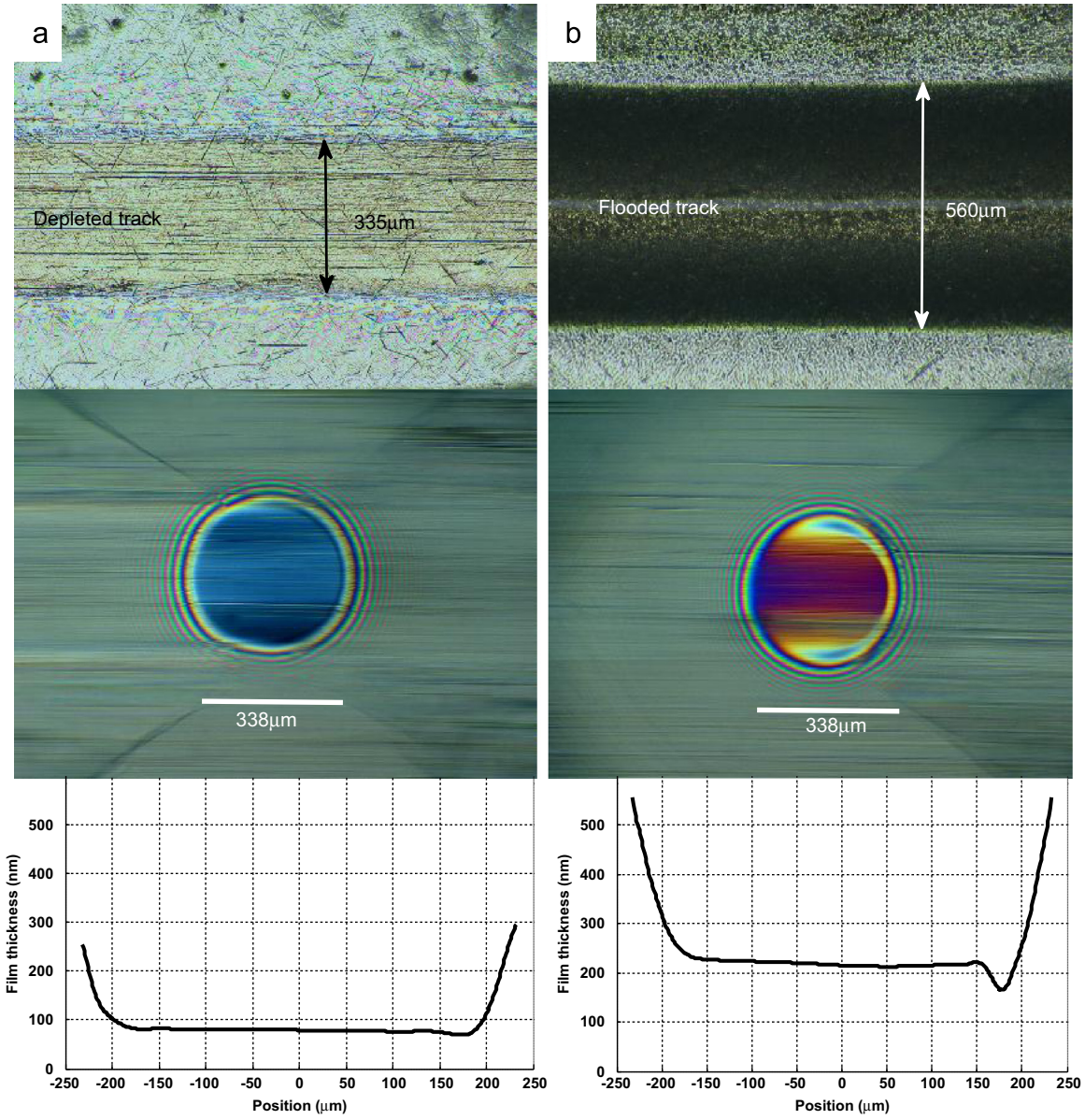

Fig. 2. Optical microscope images of the overrolled track with the corresponding interferometric images (inlet on the left) and central film thickness in the contact for grease lubrication with SRR=−0.51, u_e=35.2 mm/s and w=30 N (a) without induced replenishment (b) with induced replenishment.

leading to a significant replenishment. Indeed, grease is channeled through the micro-slot due to the squeeze between the slider and the surface of the ball. The squeeze effect depends basically on the speed, stiffness of grease and the angle between the slider and the surface of the ball. The profile and dimensions of the micro-slot influence the quantity of the channeled lubricant through the slot. Reducing the width of the micro-slot makes the channeled lubricant approaches more the centerline but the entrained amount through the slot could be less particularly with grease. Indeed, grease tends to accumulate on the slider rather than to flow though the slot as the width of slot becomes too small due to the semisolid behavior of grease. The excessive accumulation of lubricant on the front surface of the slider causes displacing the lubricant around the outer edges of the slider. Moreover, it is necessary to take into account that the virtual dimensions of the slot change after making the contact between the slider and the surface of the ball due to the flexibility of the plastic sheet and the ability of folding (bending) even under the small tension force. The tapered corners of the slot, see Fig. 1, deform (bend) elastically due to the tension force, therefore, the working width and height of the slot become less than the virtual values shown in Fig. 1. Furthermore, the channeled lubricant flows through a cross section equal to the projection of the working cross section thus, the angle between the slider and the surface of the ball has a significant effect. In this study the width and height of the micro-slot are taken as $w_s = 800\ \mu m$, $h_s = 1100\ \mu m$, respectively, see Fig. 1. The mentioned values have been chosen based on experimental iterations to obtain an adequate flow of grease through the slot without the excessive accumulation on the slider. The same values of w_s and h_s are used with oil lubrication, although the excessive accumulation on the slider has not been observed with oil even with smaller sizes of the slot. Nevertheless, definition of the optimum dimensions of the micro-slot still needs a lot of analytical and experimental investigations.

Fig. 2 shows the effect of the induced replenishment on the distribution of lubricant along the overrolled track and the resulting film thickness for grease lubrication. The interferometric images in Fig. 2 are captured after 15 min from the start with SRR = −0.51, $u_e = 35.2$ mm/s, $w = 30$ N and 100 mg of grease on the track. The optical microscope images of tracks are captured after a few more time (about 3–4 min) because an additional time was needed to remove the disk and adjusting the microscope over the track. The stiffness of grease keeps the distribution of grease on the track with a negligible change in the duration of removing the disk while the distribution of oil changes so much on the track by the surface tension forces during removing the disk. For this reason, the optical microscope images of the tracks were captured only for grease lubrication. However, similar effects are assumed to work with oil lubrication where the forced and entrained reflow induced by the slider results in enriching the depleted track with lubricant.

Fig. 2a shows that the overrolled track is severely depleted with the natural replenishment mechanisms. The width of the depleted track is approximately equal to the diameter of the Hertzian contact and the resulting central film thickness is about 80 nm after 15 min from the start. That value of the central film thickness diminishes with time which is common with grease-lubricated contacts [3,25,32,33,36]. The corresponding interferometric image in Fig. 2a shows the large intersection between the inlet air–oil meniscus and the Hertzian zone referring to an insufficient replenishment and severe starvation with a high risk of scuffing. On the other hand, Fig. 2b shows the distribution of grease on the track with the induced replenishment and it is clear that the overrolled track is flooded by a thick and wide band of channeled grease. The width of the band is about 560 μm which is larger than the diameter of the Hertzian contact 338 μm. However, this value is less than the virtual width of the micro-slot $w_s = 800\ \mu m$ because the plastic sheet folds (bends) elastically by the tension force resulting in reducing the working height and width of the

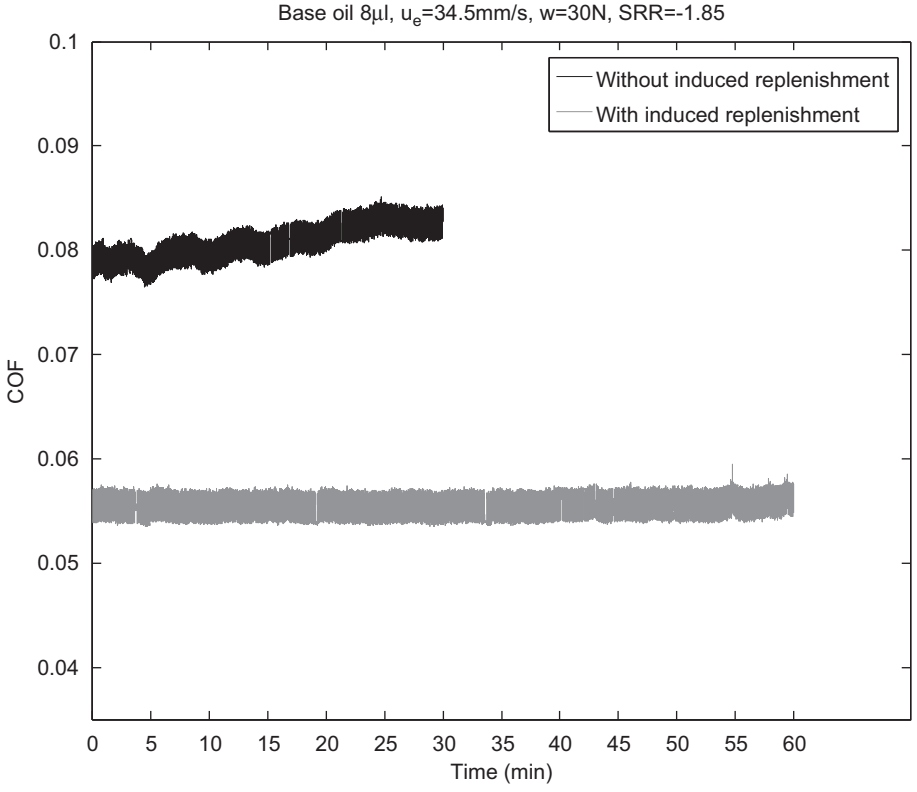

Fig. 3. Coefficient of friction (COF) of the contact with and without induced replenishment with 8 μl of base oil on the track.

micro-slot. The optical microscope image in Fig. 2b shows that the layer of grease squeezed through the slot is thicker on sides than on the centreline and it is bounded by wide scraped regions. Note that the scraped regions are not completely depleted but they are covered by a very thin layer of lubricant due to the micro-leakage through the interface between the slider and the ball. The interferometric image shows that the inlet air–oil meniscus has been completely disappeared upstream and the contact can be considered as fully flooded. Introducing the mechanism of artificially induced replenishment enhanced significantly the central film thickness from 80 nm to 215 nm under extreme operating conditions. The stability of the mechanism in replenishing the track over time is investigated in the next sections of this paper by measuring the coefficient of friction simultaneously with the film thickness for oil and grease lubrication.

3.2. Measurements for base oil

Fig. 3 shows a comparison of friction behavior of the contact with and without the mechanism of artificially induced replenishment. The track is supplied by a very little amount of oil (8 μl) and it is necessary to note that this amount of oil will be distributed on the tracks of the ball and disk due to the sliding. Although only the track of the ball is artificially replenished, it is clear that a significant reduction of friction about 31% has been occurred in the first 15 min of the measuring (the percent of reduction increases with time). Please remember that the measurements were carried out after a short time (about 1 min) from the start as it was explained in Section 2. Fig. 3 shows that the coefficient of friction (COF) for the starved contact with the natural replenishment increases with time due to the film thickness decay with the subsequent overrollings [5,10–13,37]. Fig. 4 shows the experimental film thickness decay for oil lubrication during 20 min (between $t1=5$ min and $t2=25$ min). On the other hand, introducing the mechanism of artificial replenishment resulted in a stable and lower coefficient of friction during 60 min. The reduction of friction is attributed to the significant enhancement of the film thickness on transverse and longitudinal axes. From Figs. 5 and 6 it is clear that the central film thickness has been doubled about five times at $t1=5$ min (the ratio increases with time) by introducing the artificially induced replenishment with a little amount of oil under extreme operating conditions. Moreover, interferometric images show the absence of the inlet air–oil meniscus. Measurements of friction and film thickness show a high stability and reliability of the artificially induced replenishment mechanism. Although the measurements lasted only 60 min, no signs show that the mechanism will fail easily later since the measured values of friction and film thickness are stable. Indeed, Figs. 5 and 6 show a small reduction of the central film thickness measured at the 60th minute with a negligible effect on the coefficient o friction (COF), see Fig. 3. The film thickness reduction was induced by an unexpected leakage observed only after removing the disk. A thin layer of oil was accumulated on the rear surface of the slider. This leakage probably grew up slowly over time due to the capillary forces. Thus, adding ridges on the rear surface of slider may help in reducing that leakage. However, the volume of the rear leakage is very small (the total amount present on the tracks is only 8 μl) and it tends to stabilize because it is retarded by the oil viscosity and surfaces tension forces but it results in removing an amount of oil from the service causing that mentioned small reduction of the film thickness in Figs. 5 and 6. On the other hand, the reduction of the film thickness in Figs. 5 and 6 could be attributed to the insistence of centrifugal forces to expel the lubricant on the disk.

3.3. Measurements for grease

In a similar way, measurements were repeated with grease lubrication to investigate the stability of the artificially induced replenishment mechanism over time. Fig. 7 shows that the mechanism of induced replenishment has significant benefits even with grease-lubricated contacts under sliding. Friction has been reduced

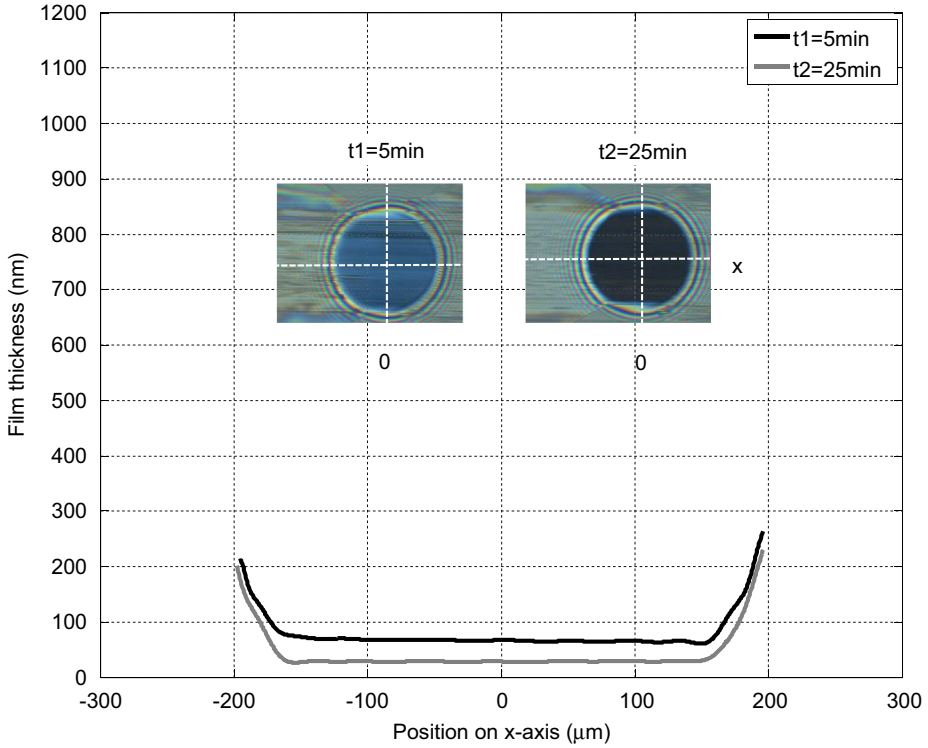

Fig. 4. Film thickness profile over time on x-axis with natural replenishment for oil amount 8 μl, $u_e=34.5$ mm/s, $w=30$ N and SRR=−1.85.

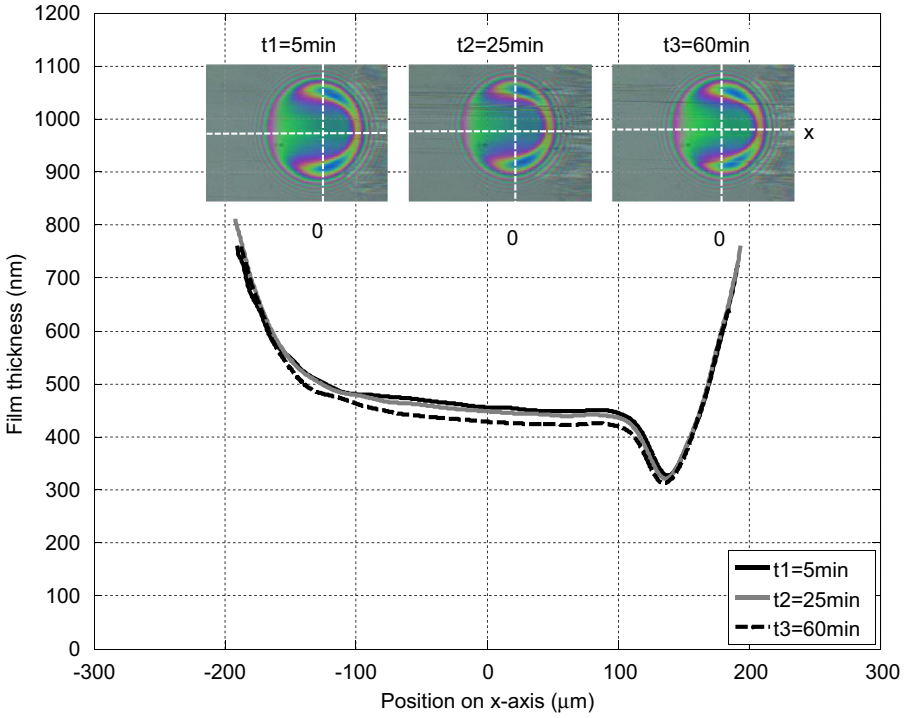

Fig. 5. Film thickness profile over time on x-axis with artificially induced replenishment for oil amount 8 μl, $u_e = 34.5$ mm/s, $w = 30$ N and SRR = −1.85.

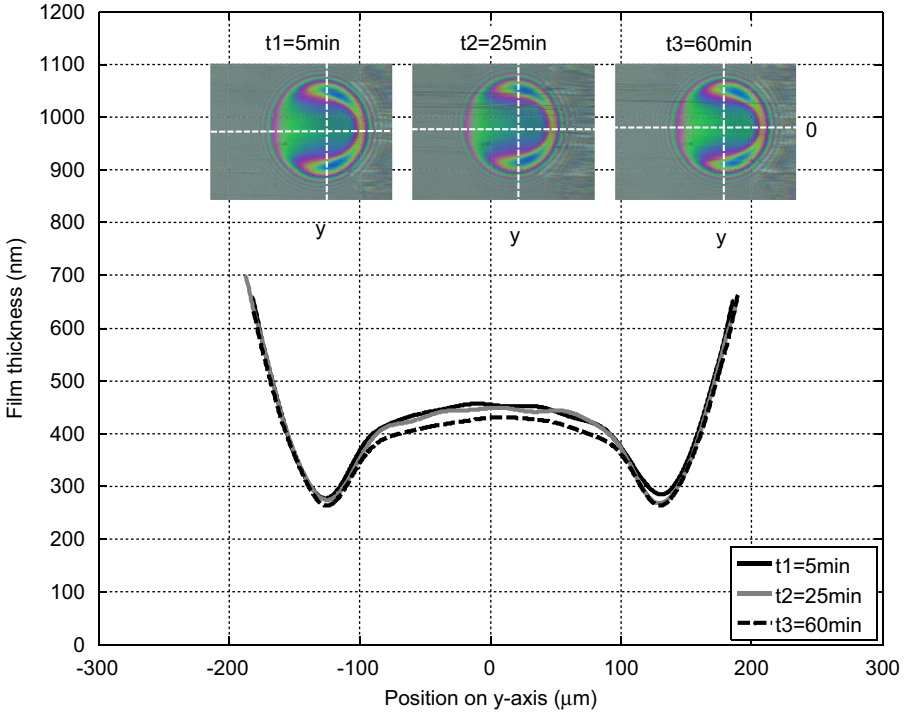

Fig. 6. Film thickness profile over time on y-axis with artificially induced replenishment for oil amount 8 μl, $u_e = 34.5$ mm/s, $w = 30$ N and SRR = −1.85.

about 25% in the first 15 min, see Fig. 7. The behavior of film thickness decay over time with natural replenishment is depicted in Fig. 8. Such behavior is common with grease-lubricated contacts where the initial film thickness is usually thick but it becomes thinner with time [3,25,32–33,36]. However, the comparison of the corresponding interferometric images in Figs. 8 and 9 shows that the air–oil meniscus is expelled out of the Hertzian circle and the contact is transformed from the severely starved to the fully flooded regime. The enhancement of the central film thickness is about 2.5 times at $t1 = 5$ min. Furthermore, Fig. 9 shows that the behavior of the film thickness over time is strongly stable and no explicit reduction has been observed during 40 min. The rear leakage mentioned in section 3.2 has not been observed with grease lubrication like in the case of oil lubrication because the stiffness of grease does not allow the capillary forces to grow. Thus, the mechanism of artificially induced replenishment provides a stable channeling of grease towards the

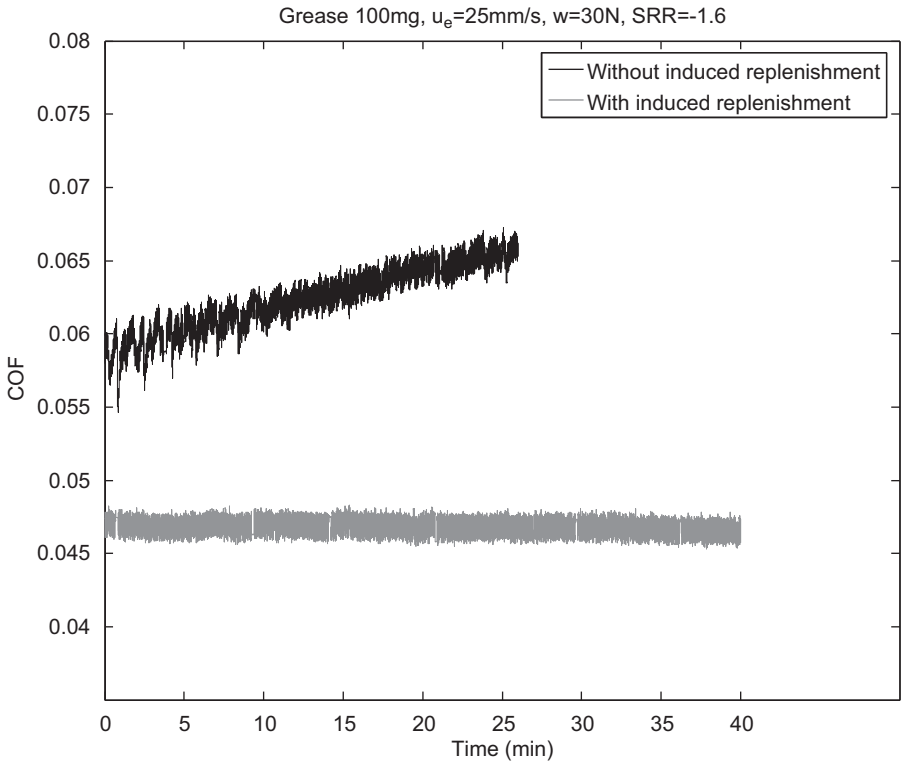

Fig. 7. Coefficient of friction (COF) of the contact with and without induced replenishment with 100 mg of grease on the track.

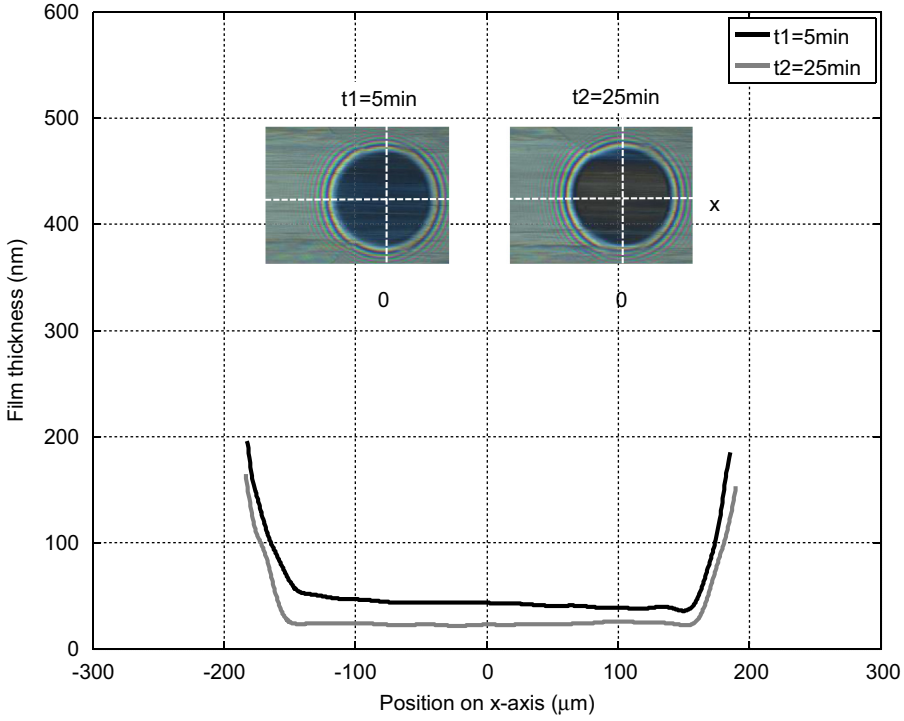

Fig. 8. Film thickness profile over time on x-axis with natural replenishment for grease amount 100 mg, $u_e = 25$ mm/s, $w = 30$ N and SRR $= -1.6$.

centerline by the continuous scraping of the expelled lubricant. Although the mechanism is stable in overcoming starvation, the replenishment could be affected over time by other loss mechanisms such as oxidation, polymerization evaporation [34] or by the degradation [35].

4. Practical application of the artificially induced replenishment mechanism

The mechanism of artificially induced replenishment is proposed to operate in radial and thrust rolling bearings with cage,

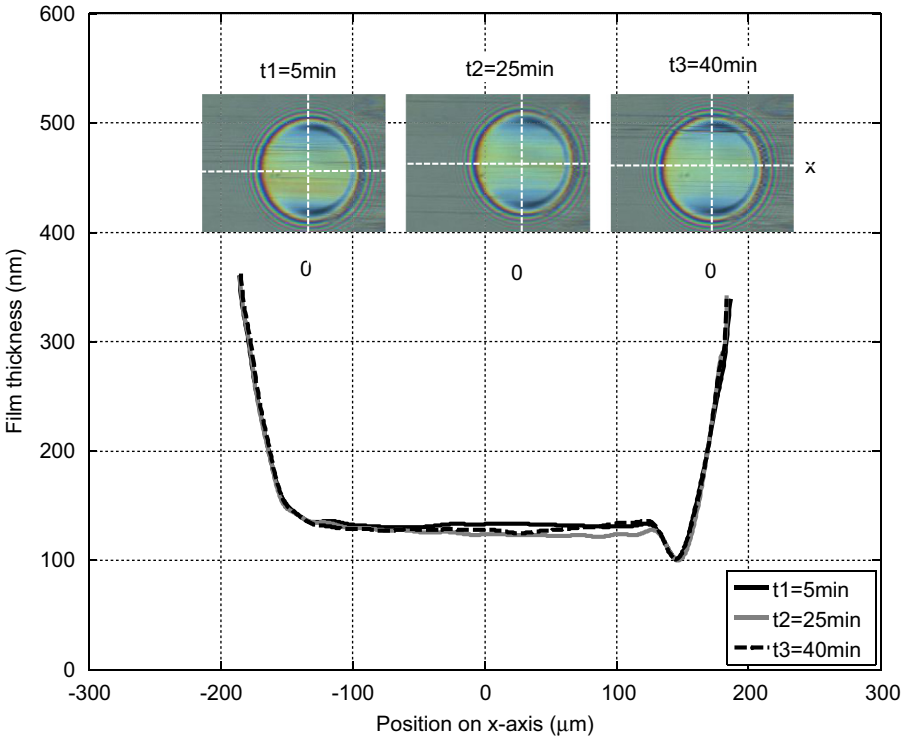

Fig. 9. Film thickness profile over time on x-axis with artificially induced replenishment for grease amount 100 mg, $u_e = 25$ mm/s, $w = 30$ N and SRR = −1.6.

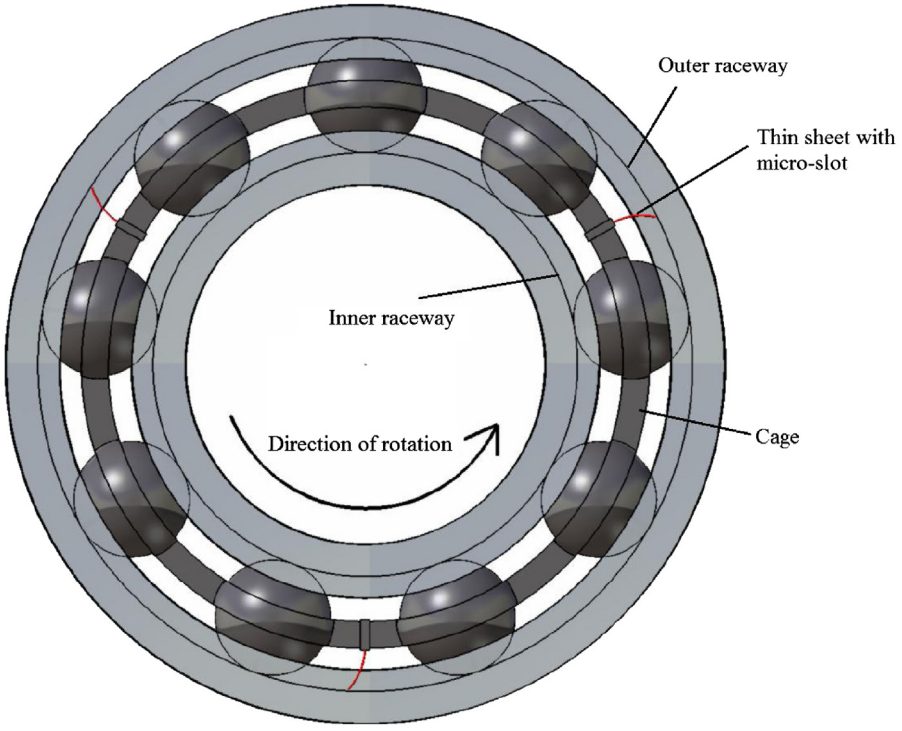

Fig. 10. The proposed mounting of sliders (thin plastic sheet with a micro-slot) in radial ball bearings with cage.

where the cage is assumed to provide the proper substrate for the sliders. However, the dimensions of the micro-slot should be modified to fit the possible displacement due to the clearance of the cage and vibrations. Fig. 10 shows the proposed mounting of sliders in a radial ball bearing for replenishing the outer raceway. The mechanism is expected to suffer from radial leakage on the body of the plastic sheet leading to negative effects. However, the leakage is inhibited by centrifugal forces in radial bearings and adding transverse ridges on the surface of the slider would minimize the radial leakage. Indeed, in radial ball bearings, centrifugal forces play a significant role because the accumulated lubricant on the slider will be pushed to track by centrifugal forces. Fortunately, in thrust ball bearings the problem of the radial leakage does not exist and the mechanism of artificially induced replenishment would operate efficiently for replenishing the lower raceway if the effects of radial centrifugal forces, cage

clearance and radial vibrations were taken into account. In the present study, the replenished surfaces is convex but the curvature of the outer raceway in radial ball bearings and the lower raceway in thrust ball bearings are concave which gives a positive effect for the induced replenishment in bearings because the scraped lubricant flows fluently towards the micro-slot the slider. Although the results in this study are promising for reducing friction and increasing the lifecycle of starved EHL contacts, the authors do not claim that the introduced results are enough to predict how the proposed mechanism would work in practice with reverse motion, vibrations, displacements, clearances, centrifugal forces, temperatures etc. Therefore, additional analytical and experimental investigations are required to understand the behaviour of the induced replenishment under the dynamic state. However, the ability of applying the artificially induced replenishment mechanism in roller bearings is the topic of future work for the authors.

5. Conclusions

An innovative mechanism was introduced in this paper to reduce or overcome the negative effects of starved lubrication in concentrated contacts. The proposed mechanism depends on enhancing the replenishment on the depleted track by channeling the lubricant towards the centerline of the overrolled track. Channeling the lubricant is performed by a flexible slider (scraper) with a micro-slot concentric with the track where the scraped lubricant accumulates on the front surface of the slider to be drained (oil) or squeezed (grease) through the micro-slot. Dimensions of the slider and micro-slot and the seal between the slider and the replenished surface are crucial for the stability and reliability of artificially induced replenishment over time. The results show a significant enhancement of the film thickness and a significant reduction of friction by introducing the mechanism of artificially induced replenishment. Interferometric images show that the inlet air–oil meniscus disappears upstream for oil and grease lubrication which means that the contact becomes in the fully flooded regime. The mechanism showed a high stability in improving the parameters of EHL conjunctions over time. Although the efficiency of induced replenishment is observed for a short time (60 min for oil and 40 min for grease), no signs indicate that the mechanism would fail easily since the observed parameters (friction and film thickness) are stable over time. Indeed, a small reduction of the oil film thickness was observed during 60 min due to a small leakage on the rear surface of the slider caused by capillary forces. The mechanism of induced replenishment is proposed to work in thrust ball bearings with cage to replenish the lower raceway, while in radial ball bearings the mechanism would suffer from radial leakage inhibited by the centrifugal forces. This approach can be negatively affected by the dynamic vibrations due to the increase of the eccentricity between the micro-slot and the centre of the Hertzian contact. Therefore, vibrations and the diameter of the Hertzian contact should be taken into account for the optimum dimensions of the micro-slot.

Acknowledgments

This research was financially supported by the Czech Science Foundation (Project No. GAP101/11/1115) and the European Regional Development Fund (Project No. CZ.1.07/2.3.00/20.0126).

References

[1] Dowson D, Higginson GR. Elasto-hydrodynamic lubrication—the fundamentals of roller and gear lubrication. Oxford: Pergamon Press; 235.
[2] Hamrock BJ, Dowson D. Isothermal elastohydrodynamic lubrication of point contacts, Part. I—Theoretical formulation. ASME, Journal of Lubrication Technology 1976;98:223–9.
[3] Cann PME. Starved grease lubrication of rolling contacts. Tribology Transactions 1999;42(4):867–73.
[4] Gershuni L, Larson MG, Lugt PM. Lubricant replenishment in rolling bearings contacts. STLE Tribology Transactions 2008;5(5):643–51, http://dx.doi.org/10.1080/10402000802192529.
[5] Jacod, B, Publier, F, Cann, PM, Lubrecht, AA. (1999), An analysis of track replenishment mechanisms in the starved regime. In: Proceedings of the 25th Leeds–Lyon symposium On Trib. p 483–492.
[6] Wedeven LD, Evans D, Cameron A. Optical analysis of ball bearing starvation,. ASME Journal of Online Learning and Training 1971;93:349–63.
[7] Wedeven LD. Traction and film thickness measurements under starved elastohydrodynamic conditions. ASME Journal of Online Learning and Training 1975;97:321–9.
[8] Pemberton J, Cameron A. A mechanism of fluid replenishment in elastohydrodynamic contacts. Wear 1976;37:185–90.
[9] Kingsbury E. Parched elastohydro-dynamic lubrication. Journal of Tribology 1985;107:229–36.
[10] Kingsbury E. Cross flow in a starved EHD contact. ASLE Transactions 1973;16:276–80.
[11] Chevalier F. Mode´lisation des conditions d'alimentation dans les contacts elastohydrodynamiques ponctuels. PhD thesis. INSA Lyon; 1996, 159p.
[12] Chevalier F, Lubrecht AA, Cann PME, Colin F, Dalmaz G. Film thickness in starved EHL point contacts. Transactions of the ASME 1998;120:126–33.
[13] Damiens B, Venner CH, Cann PME, Lubrecht AA. Starved lubrication of elliptical EHD contacts. Journal of Tribology: ASME 2004;126:105–11, http://dx.doi.org/10.1115/1.1631020.
[14] Lubrecht T, Mayuzer D, Cann P. Starved elastohydrodynamic lubrication theory: application to emulsions and greases. Comptes Rendus de l'Academie des Sciences. Serie IV Physique Astro-physique 2001;2(5):717–28.
[15] Cann PME, Damiens B, Lubrecht AA. The transition between fully flooded and starved regimes in EHL. Tribology International 2004;37:859–64.
[16] Chiu YP. An analysis and prediction of lubricant film starvation in rolling contact systems. ASLE Transactions 1974;17:22–8.
[17] Guangteng G, Spikes HA. The role of surface tension and disjoining pressure in starved and parched lubrication. Proceedings of the IMechE, Part J: Journal of Engineering Tribology 1996;210:113–24.
[18] Lugt. PM. A review on grease lubrication in rolling bearings. Tribology Transactions 2009;52(4):470–80.
[19] Astrom H, Ostenson JO, Ĥ oglund E. Lubricating grease replenishment in an elastohydrodynamic point contact. ASME, Journal of Tribology 1993;115:501–6.
[20] Cann PM. Starvation and reflow in a grease lubricated elastohydrodynamic contact. Tribology Transactions 1996;39:698–704.
[21] Cann PME, Chevalier F, Lubrecht AA. Track depletion and replenishment in a grease lubricated point contact: a quantitative analysis. In: Proceedings of the 23rd Leeds–Lyon symposium on tribology; 1996, p. 405–14.
[22] Lugt PM, Velickov S, Tripp JH. On the chaotic behavior of grease lubrication in rolling bearings. STLE Tribology Transactions 2009;52(5):581–90, http://dx.doi.org/10.1080/10402000902825713.
[23] Cann PM. Friction properties of grease in elastohydrodynamic lubrication. NLGI Spokesman 2002;66(1):6–15.
[24] Booster ER, Wilcock DF. Minimum oil requirements of ball bearings. Lubricant Engineering 1953;9(140-143):156–8.
[25] Merieux, JS, Hurley, S, Lubrecht, AA, Cann, PM. (2000), Shear-degradation of grease and base oil availability in starved EHL lubrication. In: Proceedings of the 26th Leeds–Lyon symposium on tribilogy, Tribology Series 38, Elsevier, p. 581–588.
[26] van Zoelen MT, Venner CH, Lugt PM. Free surface thin layer flow on bearing raceways. ASME Journal of Tribology 2008;130(2):021802–1-021802-10.
[27] Van Zoelen Marco T, Venner Cornelis H, Piet M. Lugt free surface thin layer flow in bearings induced by centrifugal effects. Tribology Transactions 2010;53:297–307 n3.
[28] Kumar P, Khonsari MM. Effect of starvation on traction and film thickness in Thermo-EHL line contacts with shear-thinning lubricants. Tribology Letters 2008;32(3):171–7.
[29] Ali F, Křupka I, Hartl M. An approximate approach to predict the degree of starvation in ball-disk machine based on the relative friction. Tribology Transactions 2013. http://dx.doi.org/10.1080/10402004.2013.781722.
[30] Ali F, Křupka I, Hartl M. Analytical and experimental investigation on friction of non-conformal point contacts under starved lubrication. Meccanica 2013;48(3):545–53.
[31] Hartl M, et al. Thin film colorimetric interferometry. Tribology Transaction 2001;44:270–6.
[32] Wilson AR. The relative film thickness of grease and oil films in rolling bearings,. Proceedings of the Institution of Mechanical Engineers 1979;193:185–92.
[33] Muennich HC, Gloekner HJR. Elastohydrodynamic lubrication of grease lubricated rolling bearings,. Transactions of the STLE 1979;23(1):45–52.
[34] Wikstrom V, Jacobson B. Loss of lubricant from oil lubricated near-starved spherical roller bearings,. IMechE Journal of Engineering Tribology, Part J: Journal of Engineering Tribology 1997;21(1):51–5.
[35] Cann PM, Webster MN, Doner JP, Wikstrom V, Lugt P. Grease degradation in R0F bearing tests. Tribology Transactions 2007;50(2):187–97.
[36] Venner CH, van Zoelen MT, Lugt PM. Thin layer flow and film decay modeling for grease lubricated rolling bearings. Tribology International 2012;47:175–87.
[37] Van Zoelen, MT, Venner, CH., Lugt, PM. Prediction of film thickness decay in starved EHL contacts using a thin layer flow model. Proceedings of the Institution of Mechanical Engineers—Part J:Journal of Engineering Tribology 2009, 223, 541–552.

Meccanica (2013) 48:545–553
DOI 10.1007/s11012-012-9614-6

Analytical and experimental investigation on friction of non-conformal point contacts under starved lubrication

Fadi Ali · Ivan Křupka · Martin Hartl

Received: 13 January 2012 / Accepted: 15 September 2012 / Published online: 5 October 2012

Abstract This paper presents an analytical and experimental study on the friction of non-conformal point contacts (ball-on-disk) under starved lubrication. Theoretical models were developed to simulate the behavior of friction and separation versus the degree of starvation while experimental measurements were conducted by using a Tribometer equipped with a torque sensor and a digital camera, which provided the possibility to use the optical interferometry technique simultaneously with measuring the friction. The effect of air-oil meniscus distance from the center of Hertzian contact on the friction between non-conformal surfaces was observed under starved conditions in sliding motion by capturing interferometric images. In addition, the reduction of friction by artificially-produced shallow micro-dents was investigated under severely starved and fully flooded conditions. Results show that the coefficient of friction increases dramatically when the air-oil meniscus starts to touch the circle of Hertzian contact and there is not such a significant difference in the friction between starved and fully flooded contacts since the air-oil meniscus is far away from the borders of Hertzian contact. In other words, the starvation of lubrication causes a high level of fatigue and wear of machine components when there is interference between the air-oil meniscus and the Hertzian contact. However, it was found that shallow micro-dents are helpful in reducing the friction under severe starvation conditions while the benefits of micro-dents are negligible for fully flooded conditions.

Keywords Friction · Non-conformal · Starved lubrication · Micro-dents

F. Ali (✉) · I. Křupka · M. Hartl
Department of Mechanical Engineering, Brno University of Technology, Brno, Czech Republic
e-mail: fa77f@yahoo.com

1 Introduction

A lot of machine components work with non-conformal point contacts such as gears, rolling-element bearings, cams, etc. The pressure in such concentrated contacts reaches high values according to the theory of Hertz in solid contacts, so that lubrication is needed to avoid wear and metal-to-metal contact. The separation between mating surfaces depends on the film thickness of lubrication and it is well known that the EHL regime is dominated in non-conformal point contacts where the theory of EHL can successfully predict the film thickness under fully flooded lubrication [1, 2]. In reality it is difficult to keep the rubbing surfaces under fully flooded lubrication, e.g., in cases of severe operating conditions (high speed, high load, high temperatures, start and reverse motion) or in cases where grease is used to lubricate rolling bearings. In previous cases the phenomenon of starved lubrication can be encountered and the film thickness may collapse to

just a few nanometers at high degrees of starvation, which in turn may result in component failure.

Wedeven *et al.* [3] used the technique of optical interferometry to investigate the phenomena of ball bearing starvation and the reduction of film thickness due to the failure of pressure build-up in the contact. The pressure in the inlet region of starved contact can be defined on the basis of a study that was performed by Elrod [4, 5], who developed a model using the parameter θ (fractional film content) representing the ratio between the oil thickness and the gap. Chiu [6] used a ball-flat rig test to study the starvation in roiling contact systems, obtained results showed that the starvation is attributed to the insufficiency of fluid replenishment on the track. Pemberton and Cameron [7] presented a study of fluid replenishment in EHL contacts and it was found that the balance between the entrained and the lost oil around the contact determines the position of inlet meniscus from the Hertzian contact. Chevalier *et al.* [8] performed a numerical study of starved EHL point contacts and the amount of oil on the surfaces was adopted to define the degree of starvation. Recent experimental studies about the effect of starvation on the film thickness of point contacts were carried out by Lubrecht *et al.* [9] and Cann *et al.* [10]. Numerical results by Damiens *et al.* [11] showed that the degree of starvation depends on operating conditions and the available amount of oil. The behavior of traction in starved EHL point contacts under rolling and sliding conditions was experimentally observed by Wedeven [12] and Querlioz *et al.* [13], the significance of these works is that the traction depends on the degree of starvation. Yang *et al.* [14] performed a numerical analysis on the traction of starved EHL line contacts and it was indicated that the traction increases rapidly at high degrees of starvation.

The proper modification of surface topography helps in reducing the friction between mating surfaces. For example, creating micro-dents on the surface, with proper dimensions and edges, reduces the interaction between asperities by emitting some amount of lubricant in the contact which results in enhancing the film thickness, contact fatigue life, wear resistance and reducing the friction. On the other hand, a reduction in film thickness with deep micro-dents was investigated under sliding motion due to the induction of cavitation and the increase of pressure fluctuation in the vicinity of micro-dent; see references [17–24]. Dumont *et al.* [25] described numerically the behavior of micro pits in the fully flooded and starved ball-on-disk contact and it was revealed that the benefits of micro pits decrease as the degree of starvation decreases because the film thickness becomes larger and the emitted amount of oil from micro-pits becomes negligible in comparison with the available amount of oil in the contact.

However, a lot of efforts focused on studying the effect of micro-dents on the film thickness formation and pressure distribution, while there is still a need to clarify the direct effect of micro-dents on the friction coefficient of non-conformal contacts under starved lubrication in sliding motion.

2 Theory

Many factors have an influence on the friction coefficient of EHL point contacts, such as rheological properties of lubricant, the slide-to-roll ratio, the thermal effect and so on. However, the Newtonian shear stress is given by;

$$\tau = \eta \Delta u / h \tag{1}$$

where τ is the shear stress [Pa], η is the dynamic viscosity of the lubricant [Pa s], Δu is the sliding velocity between the contacting surfaces [m/s] and h is the film thickness [m].

The traction force F is defined by the following;

$$F = \int_{r_c=0}^{r_c=a} \tau \, dA = \int_{r_c=0}^{r_c=a} \eta(\Delta u / h) 2\pi r_c dr_c \tag{2}$$

where F is the traction force [N], r_c is the radius of contact [m] and a is the radius of Hertzian contact [m].

The finite area dA of a circular point contact is given by;

$$dA = 2\pi r_c dr_c \tag{3}$$

The Barus equation in Ref. [15], predicts the viscosities as a function of pressure by the following form;

$$\eta = \eta_0 \exp(\alpha p_h) \tag{4}$$

where η_0 is the viscosity at atmospheric pressure [Pa s], α is the pressure-viscosity coefficient [1/Pa] and p_h is the Hertzian pressure [Pa s].

The Hertzian pressure is dominated in EHL point contacts and it is given by;

$$p_h = p_{\max}\left(1-(r_c/a)^2\right)^{1/2} = \left(3w/2\pi a^2\right)\left(1-(r_c/a)^2\right)^{1/2} \quad (5)$$

where $p_{\max}$ is the maximum pressure [Pa] and w is the normal load [N].

If we accept that the mating surfaces are parallel in the region of Hertzian contact ($h \neq f(r_c)$) and the sliding velocity is constant then the coefficient of friction μ can be defined as;

$$\mu = F/w = \left(2\pi\eta_0\Delta u/(wh)\right) \times \int_0^a r_c \exp\left(\left(3w\alpha/2\pi a^2\right) \times\left(1-(r_c/a)^2\right)^{1/2}\right)dr_c \quad (6)$$

Equation (6) can be simplified under steady-state load (w) by the following;

$$\mu = \overline{c}\,\overline{I}\,\Delta u/h \quad (7)$$

where $\overline{I} = \int_0^a r_c \exp((3w\alpha/2\pi a^2)(1-(r_c/a)^2)^{1/2})dr_c$ and $\overline{c} = 2\pi\eta_0/w$.

3 Model friction and separation under starved lubrication

Under starved conditions the shear stress in Eq. (1) increases with increasing the sliding velocity, which leads to increase both of the traction force and the coefficient of friction. From Eq. (7) the coefficient of friction under starved conditions can be given as;

$$\mu_s = \overline{c}\,\overline{I}\,\Delta u/h_{cs} \quad (8)$$

where μ_s is the coefficient of friction under starved conditions and h_{cs} is the central film thickness of starved contact [m].

Chevalier *et al.* [8] introduced an approximated relation representing the ratio between the central film thickness under starved conditions and the central film thickness under fully flooded conditions by the following equation;

$$R = h_{cs}/h_{cff} = r/\sqrt[\gamma]{1+r^\gamma} \quad (9)$$

where the parameter $r = H_{oil}/\overline{\rho}H_{cff}$, $\overline{\rho}$ is the compressibility, if $\overline{\rho}$ is not considered then $r = H_{oil}/H_{cff}$. The parameter γ varies from 2 to 5. From Eq. (9) we can notice that the ratio $R \in [0, 1]$ as r changes from 0 to ∞. By substituting Eq. (9) in Eq. (8) we obtain the following relation;

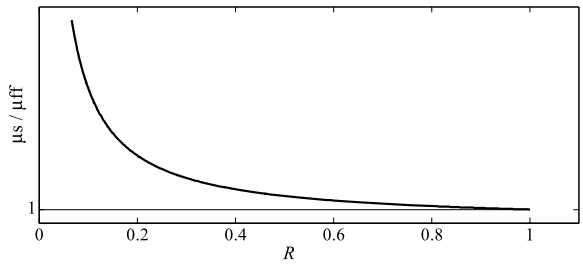

Fig. 1 The ratio μ_s/μ_{ff} versus the ratio $R = h_{cs}/h_{cff}$

$$\mu_s = \overline{c}\,\overline{I}\,\Delta u/Rh_{cff} \quad (10)$$

or

$$\mu_s = \mu_{ff}/R = \mu_{ff}\sqrt[\gamma]{1+r^\gamma}/r \quad (11)$$

where μ_{ff} and h_{cff} are respectively the coefficient of friction and the central film thickness under given operating conditions in the fully flooded lubrication.

Under steady state conditions, the coefficient of friction μ_{ff} has a constant value and the increase of starvation degree results in a nonlinear increase in the coefficient of friction μ_s under the same operating conditions according to Eq. (11).

Figure 1 shows the simulation of Eq. (11) and two asymptotes are observed. The first asymptote shows that the ratio μ_s/μ_{ff} tends to 1 as R tends to 1.

$$\lim_{R\to 1}(\mu_s/\mu_{ff}) = 1 \quad (12)$$

or

$$\lim_{R\to 1}(\mu_s) = \mu_{ff} \quad (13)$$

The other asymptote shows that the ratio μ_s/μ_{ff} tends to ∞ as R tends to 0. This situation represents the friction of dry contacts or boundary regime where the starved film thickness becomes 0.

$$\lim_{R\to 0}(\mu_s/\mu_{ff}) = \infty \quad (14)$$

Under severe starved lubrication, the film thickness may diminish to a few nanometers leading to the rise of air-oil meniscus in the inlet of contact. As the inlet meniscus approaches toward the circle of Hertzian contact, the gap between surfaces will be insufficiently filled by the fluid which inhibits the pressure build-up. If the contact is highly loaded and the pressure of fluid in the contact is low, then a part of the load will

be carried by the asperities and the regime of lubrication transforms from the EHD to the mixed lubrication (ML). However, the separation in the contact depends on the minimum film thickness and the roughness (RMS) of mating surfaces. To avoid the contact between asperities under starved lubrication, the film thickness parameter (λ) which was introduced by Tallian [16], should be larger than 1;

$$\lambda_{st} = h_{ms}/\sigma \geq 1 \tag{15}$$

where λ_{st} is the separation under starved conditions, h_{ms} is the minimum starved film thickness [m] and $\sigma = \sqrt{RMS_1^2 + RMS_2^2}$ where RMS_1, RMS_2 are the root mean square roughness of mating surfaces.

The ratio between central and minimum film thickness h_c/h_m tends to one under starved lubrication for all operating conditions. On the other hand, the ratio h_c/h_m tends to increase with load under fully flooded conditions, see Ref. [8] and references therein. We assume that $R' = h_{ms}/h_{mff}$ represents the ratio between the minimum film thickness of starved and fully flooded contact, where h_{mff} is the minimum film thickness of fully flooded contact. It is evident that the ratio $R' = (h_{ms}/h_{mff}) \in [0, 1]$ since the starved minimum film thickness cannot exceed the fully flooded minimum film thickness. By substituting $R' = h_{ms}/h_{mff}$ in Eq. (15) we obtain:

$$\lambda_{st} = R' h_{mff}/\sigma \geq 1 \tag{16}$$

$$\lambda_{st} = R' \lambda_{ff} \geq 1 \tag{17}$$

where λ_{ff} is the separation under fully flooded conditions. The last equation determines the conditions for keeping the contact under safe state against metal-to-metal contact through the transition from fully flooded to starved conditions. Equation (17) is simulated in Fig. 2 for different values of λ_{st}, where every curve in the figure represents a constant value of separation under starved lubrication conditions. Figure 2 shows that a constant starved separation ($\lambda_{st} = const$) results from a nonlinear relation between the degree of starvation and the fully flooded separation. For example, a fully flooded contact with a non-dimensional separation $\lambda_{ff} = 10$ can be starved to the degree $R' = 0.2$ which results in a starved separation $\lambda_{st} = 2$. On the other hand, the same starved separation $\lambda_{st} = 2$ can be obtained from a fully flooded separation $\lambda_{ff} = 4$ with the degree of starvation $R' = 0.5$.

However, in practical applications, safe operating conditions under starved lubrication require a minimum separation larger than the amplitude of surface

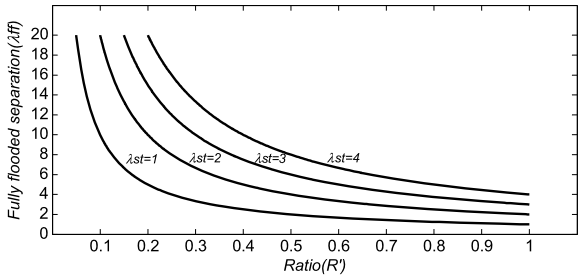

Fig. 2 Relation between the separation under starved and fully flooded conditions ($\lambda_{st}, \lambda_{ff}$) against $R' = h_{ms}/h_{mff}$

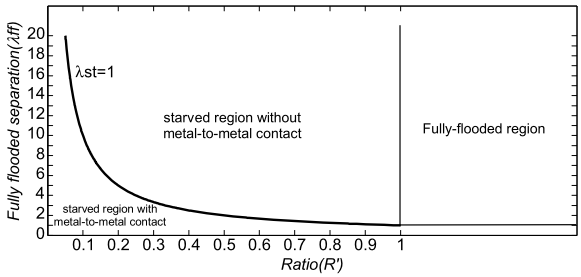

Fig. 3 Distribution of starved regions with and without metal-to-metal contact

asperities to avoid metal-to-metal contact; this case is defined in Fig. 3 where the region above the curve $\lambda_{st} = 1$ represents the safe separation whatever the degree of starvation was, and it can be stated that the friction in the region above the curve $\lambda_{st} = 1$ is basically due to the shear stress of the lubricant in sliding motion (see Eqs. (1), (6) and (7)) while the friction in the region under the curve $\lambda_{st} = 1$ is induced by the combined effect of the shear stress and metal-to-metal contacts.

4 Experimental

A tribometer modified by adding a torque sensor on the ball shaft was used for measuring the friction force between the ball and disk in the presence of base oil (2400 N) with a dynamic viscosity $\eta = 0.38$ [Pa s] at 40 °C. The torque sensor is integrated with a computer by using of Digital/Analog card (NI USB/6009) and the software LabVIEW receives the measurements as a digital signal to be processed and saved in the memory of the computer. The angular velocity of rotating parts is controlled by servo-motors where the velocity of ball can be independently changed in the

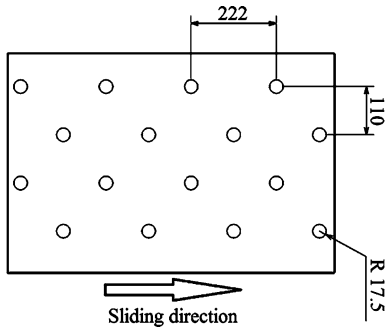

Fig. 4 Distribution of micro-dents on the surface of ball

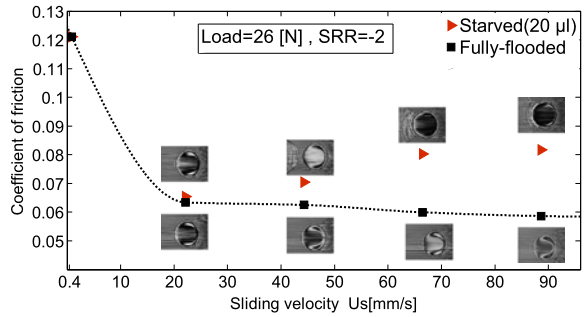

Fig. 5 Comparison of Stribeck curves for lubricated point contacts under starved and fully-flooded conditions

range −100 to +100 rpm, for disk the range is −150 to +150 rpm. This efficient mechanism provides the possibility of choosing the required slide-to-roll ratio under steady state and transient conditions. The diameter of ball is 25.4 [mm] and it is made of steel AISI 52100 with a measured roughness (RMS) about 15 nm, while the disk is made of a transparent glass and the lower surface of the disk is coated with a thin layer of Chromium. The elastic modulus of the steel ball and the glass disk is respectively 210 GPa and 80 GPa. On the other hand, the apparatus is equipped with a digital camera (Hitachi HV-F22) and the contact between the ball and disk is illuminated by a high-power source of light to improve the resolution of the images. This arrangement has the advantage of capturing interferometric images of the starved contact simultaneously with friction measurements by the torque sensor. The amounts of lubricant for starved conditions were calibrated by a digital micropipette.

For testing the effect of micro-dents on the coefficient of friction under starved conditions, the surface of the ball was manually indented by a Rockwell indenter. 4 rows were made along the whole ball circumference. Dents were made by applying a load of 8 N with the illustrated distribution in Fig. 4, where dimensions are in µm. The dent has an average diameter about 35 µm and a depth about 0.6 µm.

5 Results

The first part of results consists of experiments on friction under starved lubrication through non-steady state operating conditions (sliding velocity $u_s \neq const$) by establishing the Stribeck curve versus sliding velocity then experiments were conducted under steady state conditions by measuring the friction versus time, the effect of starvation on the position of inlet meniscus was investigated by optical interferometry. The second part provides an experimental comparison on the friction of textured and smooth non-conformal surfaces under starved and fully flooded conditions.

5.1 Stribeck curve

The coefficient of friction was measured versus the sliding velocity under pure sliding conditions ($SRR = 2 * (u_{disk} - u_{ball})/(u_{disk} + u_{ball}) = -2$, the disk is stationary $u_{disk} = 0$), the contact between the ball and disk was starved with oil amount 20 µl and it was loaded by 26 N. The measurements were repeated for the fully flooded contact with the same operating conditions and the position of the air-oil meniscus was simultaneously observed by digital camera. Figure 5 shows the measured Stribeck curves under starved and fully flooded conditions and it is evident that the air-oil meniscus approaches to the center of Hertzian contact as the sliding velocity increases because high velocities reduce the time needed to replenish the lubricant on the track where the oil is pushed out through sides by the over-rolling of the ball. The frequency of over-rolling determines the amount of oil that can flow back into the track, hence, the efficiency of oil replenishment on the track is inversely proportional to the frequency of over-rolling. In other words, high frequency of over-rolling at high sliding velocities leads to increase the degree of starvation and the reduction of film thickness due to the reduction of replenishment time. However, the comparison of the friction coefficient between starved and fully flooded conditions shows that the value of the friction coefficient increases strongly with increasing the sliding velocity

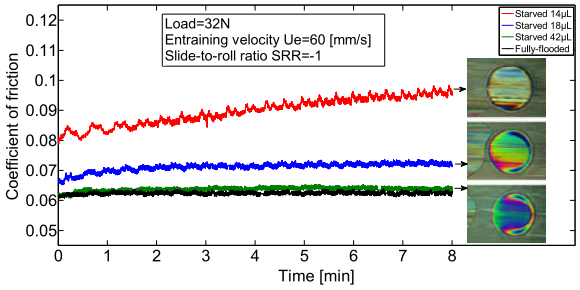

Fig. 6 Effect of oil amount on the coefficient of friction and the position of air-oil meniscus

under starved conditions, on the contrary, under fully flooded conditions, it is clear from Fig. 5 that high velocities enhance the film thickness and the separation according to the EHL theory, which results in low friction. The existence of the meniscus in the vicinity of the Hertzian contact reduces the pressure build-up of fluid and inhibits the formation of film lubrication in the contact which increases the contact between the asperities and the friction. Otherwise, it is observed that there is not such a large difference in the friction coefficient for starved and fully flooded conditions as the air-oil meniscus is far enough from the center of Hertzian contact at low sliding velocities.

5.2 Steady state

The effect of air-oil meniscus position on the coefficient of friction was observed under steady state operating conditions of the sliding and load ($SRR = -1$, entraining velocity $u_e = |u_s| = 60$ [mm/s], load = 32 N) and the degree of starvation was modified by changing the oil amount on the track, see Fig. 6 and please note that the images were captured in the 5th minute. Interferometric images show that the coefficient of friction increases significantly under starved conditions when the air-oil meniscus starts to touch the Hertzian contact. Otherwise, the coefficient of friction of starved and fully flooded contact is nearly the same for a sufficient amount of oil (42 µl) on the track. The rapid increase of the friction coefficient is attributed to the insufficient replenishment of fluid on the track for the little amount of lubricant which results in reducing the distance between the air-oil meniscus and the center of Hertzian contact. However, it is apparent that a little reduction of oil amount from 18 µl to 14 µl caused a large increase of friction, so it can be stated that, as the inlet meniscus is in touch with the Hertzian circle the gradient of friction becomes very sensitive and related to the oil amount on the track, while the effect of oil amount on the value of friction is quite fair since the inlet meniscus is out of the Hertzian circle. This result is in agreement with the theoretical model shown in Fig. 1, and it is clear from Fig. 1 that the gradient of the ratio μ_s/μ_{ff} is very little when the degree of starvation is low ($R \approx 1$) then the gradient starts to increase rapidly with increasing the degree of starvation ($R \ll 1$) and it is expected that the accelerated increase starts in the moment at which the air-oil meniscus starts to touch the Hertzian contact. If we assume that the degree of starvation at which the inlet meniscus starts to touch the Hertzian circle is the critical degree of starvation (R_{cr}) then we can explain mathematically the behavior of friction gradient versus the degree of starvation by the following;

$$\left|\Delta(\mu_s/\mu_{ff})/\Delta R\right| \approx 0 \quad \text{if } 1 \geq R \geq R_{cr} \tag{18}$$

$$\left|\Delta(\mu_s/\mu_{ff})/\Delta R\right| > 0 \quad \text{if } R < R_{cr} \tag{19}$$

Equation (18) represents the range of starvation where the inlet meniscus is far away from the contact, in this range of starvation, friction shows a low sensitivity against the small change of oil amount on the track, while Eq. (19) represents the range of starvation where the inlet meniscus is in interference with the Hertzian contact and the high sensitivity of friction against the small change of oil amount on the track.

In practical applications, it is difficult to determine the precise position of the inlet meniscus and the critical degree of starvation R_{cr} at which the inlet meniscus starts to touch the Hertzian circle, but on the basis of Eqs. (18) and (19) it is possible to determine approximately the fuzzy place of R_{cr} by using the coefficient of friction as indicator to the moment at which the air-oil meniscus makes the first contact with the Hertzian circle, see Fig. 7. However, the accuracy of determining the approximated place of R_{cr} depends on the ranges defined by Eqs. (18) and (19) in Fig. 7 and more expanded experimental tests are needed to precise correctly these ranges.

The experimental relation between the ratio μ_s/μ_{ff} and the amount of oil is represented in Fig. 8 where the values of μ_s and μ_{ff} were calculated from the mean value during 8 minutes of measuring. The experimental ratio μ_s/μ_{ff} tends to one as the degree of starvation reduces and we can clearly notice the accelerated increase of friction gradient at little amounts of oil (the jump of friction between values 18 µl and 14 µl).

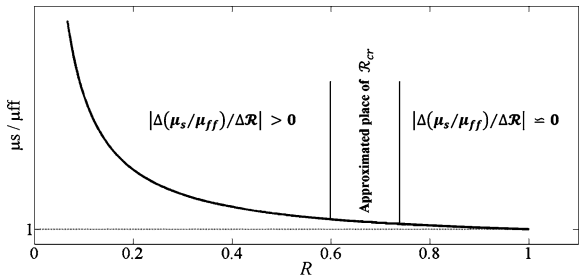

Fig. 7 Approximated approach to determine the critical degree of starvation R_{cr}

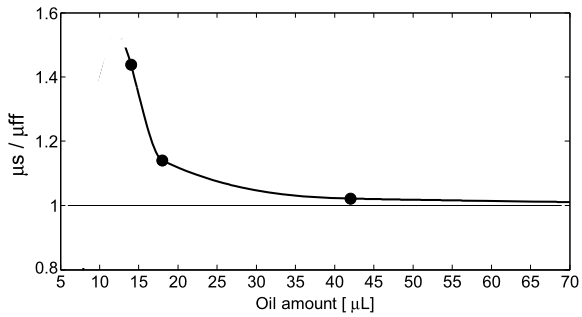

Fig. 8 Experimental relation between the ratio μ_s/μ_{ff} and the oil amount on the track

However, this result is in accord with Fig. 1 and Eqs. (12) and (13). The good agreement between the theoretical model in Fig. 7 and the experimental measurement in Fig. 8 is not absolute because the theoretical model was derived from the Newtonian model in the shear stress regardless rheological properties of the lubricant, for this reason, an optimized model which takes in account the non-Newtonian behavior of oil can be more realistic. In addition to that, the theoretical model is correct under steady state operating conditions but it cannot be adopted for non-steady states or transient cases.

5.3 Friction of textured surfaces

The study above indicated that the coefficient of friction becomes very sensitive to the little change of oil amount when the degree of starvation is large; this region is presented in Fig. 7 by the formula $|\Delta(\mu_s/\mu_{ff})/\Delta R| > 0$. According to this result, it is expected that the surface texturing to be efficient in this region because the little amount of oil emitted from micro-dents can play a significant role in reducing the friction. In contrast, it is not recommended to apply the surface texturing under fully

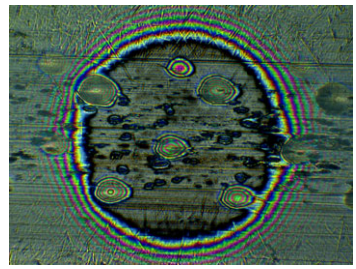

Fig. 9 Micro-dents on the ball surface

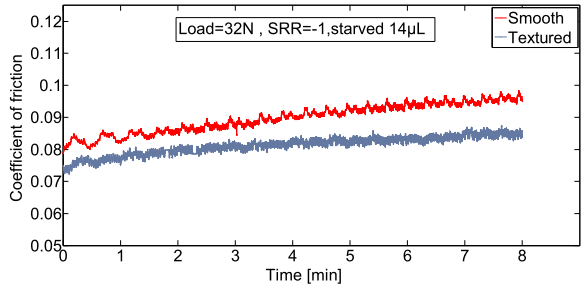

Fig. 10 Coefficient of friction for smooth and textured surfaces under starved conditions

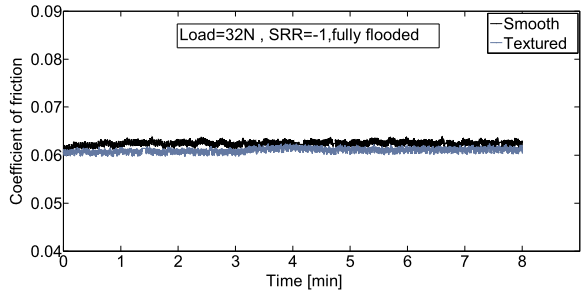

Fig. 11 Coefficient of friction for smooth and textured surfaces under fully flooded conditions

flooded or fairly starved conditions where the coefficient of friction is insensitive to small changes of oil amount, this case is presented in Fig. 7 by the formula $|\Delta(\mu_s/\mu_{ff})/\Delta R| \approx 0$.

However, in order to investigate the effect of micro-dents in reducing the friction, the surface of the ball was artificially modified by 4 rows of shallow micro-dents, see Fig. 9. The average diameter of the dent is about 35 μm with a depth about 0.6 μm.

Figures 10 and 11 show a comparison of the friction coefficient for smooth and textured surface under starved and fully flooded lubrication. Results show that the benefits of micro-dents under severe starved

lubrication are proportionally considered and the reduction of friction is about 9 %. On the other hand, the benefits of micro-dents under fully flooded conditions are negligible and the value of average friction of smooth and textured surfaces is nearly the same; this is justified by the fact that the little amount of emitted fluid from micro-dents doesn't make a significant difference in enhancing the film thickness under fully flooded lubrication where the film is originally large enough. In addition to that, it was mentioned in the context of this study that coefficient of friction is insensitive against the micro-change in oil amount under fairly starved and fully flooded conditions.

From Figs. 10 and 11 we can also notice that the friction increases with the time under steady state for both textured and smooth surfaces under starved lubrication while the friction is stable with the time under fully flooded condition and this can be attributed to the thermal effect where the available amount of oil under fully flooded condition is larger in comparison with the starved condition which results in a larger heat capacity for fully flooded contact, for this reason the oil temperature for starved conditions is higher than the oil temperature for fully flooded conditions under the same operating conditions.

6 Conclusions

The friction coefficient of non-conformal EHL point contacts was measured under starved and fully flooded conditions and the benefits of surface texturing were also investigated. Results show that the friction coefficient of non-conformal point contacts increases dramatically and non-linearly under starved conditions when the sliding velocity increases; this action is accompanied by reducing the time to replenish the lubricant on the track which results in minimizing the distance between the air-oil meniscus and the center of Hertzian contact. Under steady state conditions, the coefficient of friction depends strongly on the oil amount on the track, particularly at high degrees of starvation. On the other hand, the value of the friction coefficient was almost the same for fully flooded and starved contacts when the air-oil meniscus was far away from the Hertzian contact. Results showed a good agreement between the theoretical model of friction under starved lubrication and experimental measurements, this theoretical model can be used to predict approximately the position of inlet meniscus. Finally, the modification of non-conformal mating surfaces by shallow micro-dents provided a considerable reduction of friction (about 9 %) under severe starved lubrication while the benefits of micro-dents were negligible for fully flooded lubrication.

Acknowledgement This research was supported by Czech Science Foundation (project No. GA101/11/1115) and European Regional Development Fund (project No. CZ.1.07/2.3.00/20.0126) financed.

References

1. Hamrock BJ, Dowson D (1977) Isothermal elastohydrodynamic lubrication of point contacts. Part III—fully flooded results. J Lubr Technol 99:264–276
2. Dowson D, Higginson GR (1959) A numerical solution to the elastohydrodynamic problem. J Mech Eng Sci 1:6–15
3. Wedeven LD, Evans D, Cameron AC (1971) Optical analysis of ball bearing starvation. ASME J Lubr Technol 93:349–363
4. Elrod HG (1981) A cavitation algorithm. ASME J Lubr Technol 103:350–354
5. Elrod HG, Adams ML (1974) A computer program for cavitation and starvation problems. In: Proceedings of the 1st Leeds-Lyon symposium on tribology, pp 37–41
6. Chiu YP (1974) An analysis and prediction of lubricant film starvation in rolling contact systems. ASLE Trans 17:22–35
7. Pemberton J, Cameron AC (1976) A mechanism of fluid replenishment in elastohydrodynamic contacts. Wear 37:185–190
8. Chevalier F, Lubrecht AA, Cann PME, Colin F, Dalmaz G (1998) Film thickness in starved EHL point contacts. ASME J Tribol 120:126–133
9. Lubrecht T, Mayuzer D, Cann P (2001) Starved elastohydrodynamic lubrication theory: application to emulsions and greases. C R Acad Sci, Sér IV Phys Astrophys 2(5):717–728
10. Cann PME, Damiens B, Lubrecht AA (2004) The transition between fully flooded and starved regimes in EHL. Tribol Int 37:859–864
11. Damiens B, Venner CH, Cann PME, Lubrecht AA (2004) Starved lubrication of elliptical EHD contacts. ASME J Tribol 126:105–111. doi:10.1115/1.1631020
12. Wedeven LD (1975) Traction and film thickness measurements under starved elastohydrodynamic conditions. Trans ASME J Lubr Technol 97:321–329
13. Querlioz E, Ville F, Lenon H, Lubrecht T (2007) Experimental investigations on the contact fatigue life under starved conditions. Tribol Int 40:1619–1626
14. Yang P, Wang J, Kaneta M (2006) Thermal and non-Newtonian numerical analyses for starved EHL line contacts. ASME J Tribol 128:282–290
15. Barus C (1893) Isothermals, isopiestics and isometrics relative to viscosity. Am J Sci 45:87–96

16. Tallian TE (1967) On competing failure modes in rolling contact. ASLE Trans 10:418–439
17. Nakatsji T, Mori A (2001) The tribological effect of mechanically produced micro-dents by a micro diamond pyramid on medium carbon steel surfaces in rolling-sliding contact. Meccanica 36:663–674
18. Coulon S, Jubault I, Lubrech AA, Ville F, Vergne P (2004) Pressure profiles measured within lubricated contacts in presence of dented surfaces. Comparison with numerical models. Tribol Int 37:111–117
19. Nelias D, Ville F (2000) Detrimental effects of debris dents on rolling contact fatigue. Trans ASME J Tribol 122:55–64
20. Mourier L, Mazuyer D, Lubrecht AA, Donnet C (2006) Transient increase of film thickness in micro-textured EHL contacts. Tribol Int 39:1745–1756
21. Ai XL, Cheng HS (1994) The influence of moving dent on point EHL contacts. Tribol Trans 37:323–335
22. Krupka I, Hartl M (2007) The effect of surface texturing on thin EHD lubrication films. Tribol Int 40:1100–1110
23. Vrbka M, Křupka I, Šamánek O, Svoboda P, Vaverka M, Hartl M (2011) Effect of surface texturing on lubrication film formation and rolling contact fatigue within mixed lubrication. Meccanica 46:491–498
24. Galada L, Dzierwa A, Pawlus P, Reizer R (2011) Improvement of tribological properties of co-elements by oil pockets creation on sliding surfaces. Meccanica 46:523–534
25. Dumont M, Lugt PM, Tripp JH (2002) Surface feature effects in starved circular EHL contacts. Trans ASME J Tribol 124:358–366

Original Article

Institution of MECHANICAL ENGINEERS
Journal of ENGINEERING TRIBOLOGY

Proc IMechE Part J:
J Engineering Tribology
0(0) 1–9

DOI: 10.1177/1350650114543317
pij.sagepub.com
SAGE

Reducing the friction of lubricated nonconformal point contacts by transverse shallow micro-grooves

Fadi Ali, Ivan Křupka and Martin Hartl

Abstract

This study focuses on the effects of transverse shallow micro-grooves on the film thickness and friction of nonconformal contacts under relative motion. Experiments were conducted using a ball-on-disc tribometer equipped with high speed camera and torque sensor. The lubricated contact between the steel ball and glass disc represents a nonconformal point contact with elastohydrodynamic lubrication. The measurements of the film thickness were carried out using the optical interferometry technique while the friction was measured by a torque sensor on the ball shaft. The results reveal that the rubbing surfaces with transverse shallow micro-grooves with a length less than the diameter of the Hertzian contact have an improved tribological performance in comparison with smooth surfaces in the elastohydrodynamic lubrication regime. Indeed, a significant enhancement of film thickness has been observed using such design of micro-grooves. On the other hand, the transverse deep and shallow micro-grooves with a length larger than the diameter of the Hertzian contact suffer from the side leakage and the lubricant is ejected out of the contact by sideways leading to a pressure drop and film thickness collapse. Moreover, the measured friction of surfaces textured with shallow micro-grooves without intersection with the outer Hertzian circle is less than the friction of smooth surfaces in sliding and reversal motion.

Keywords

Elastohydrodynamic lubrication, film thickness, friction, surface texturing, micro-grooves

Date received: 5 November 2013; accepted: 10 June 2014

Introduction

Concentrated nonconformal contacts such as rolling-element bearings, gears, and cams are common as machine components. Usually, concentrated contacts operate under high pressure and thin film lubrication (less than 1 μm). Therefore, improving the tribological performance of nonconformal surfaces is required to avoid the failure of machine components and to minimize the loss of energy. The modification of surface topography by artificially produced micro-features was introduced as a promising approach to reduce the friction and wear between rubbing surfaces.[1] However, the obtained benefits depend quantitatively and qualitatively on the proper design of the shape and the size of micro-features.[2] Also, the regime of lubrication in combination with the operating conditions should be taken into account to optimize the design of micro-futures.[3] The mechanisms of how micro-cavities can bring benefits to the lubricated contacts are explained in the literature by the following:

1. Entrapment of wear debris: This mechanism operates efficiently in the boundary or dry regime where the micro-cavities help in minimizing the plowing friction caused by the wear particles.[4–6] Generally, a pattern of transversely oriented fine micro-grooves are helpful to get benefits in the boundary lubrication.[4–8]
2. Increasing the load-carrying capacity: This effect can be observed basically in the hydrodynamic

Faculty of Mechanical Engineering, Brno University of Technology, Brno, Czech Republic

Corresponding author:
Ivan Křupka, Faculty of Mechanical Engineering, Brno University of Technology, Technická 2896/2, 616 69 Brno, Czech Republic.
Email: krupka@fme.vutbr.cz

regime where the artificially produced micro-features (dents, grooves, or dimples) generate additional separating forces and a hydrodynamic lift between sliding surfaces resulting in reducing the friction and enhancing the film thickness.[9–18]

3. Acting as oil reservoirs: Shallow micro-cavities can store the lubricant to be emitted in the contact under the effect of the sliding motion and the elastic deformation resulting in a significant increase in the film thickness in the elastohydrodynamic lubrication (EHL) regime. However, micro-features with improper design can aggravate the tribological performance of rubbing surfaces.[19–29]

Kaneta and Nishikawa[30] and Kaneta et al.[31] investigated optically the passage of transverse micro-grooves through EHL contacts. They found that the local reduction in film thickness is essentially caused by the side leakage along the groove. The side leakage is attributed to the relative low viscosity in the groove due to the low pressure. However, the amount of the side leakage decreases with reducing the size (width and depth of micro-groove) and increasing the overall film thickness. Yang et al.[32] proved numerically the results of Kaneta. Nakano et al.[33] stated that groove patterns have higher fiction coefficients than the flat surfaces because groove patterns have not enough ability to keep the hydrodynamic pressure. On the other hand, the dimples keep the hydrodynamic pressure because of the closed shape. Similarly, Costa and Hutchings[13] showed that textured samples with features larger than the width of the contact give a film thickness smaller than for smooth samples. They attributed that effect to the channeling of the lubricant away from the contact.

Although the negative effects observed numerically and experimentally with micro-grooves in the literature,[13,30–33] the authors introduce in this paper an innovative approach to obtain benefits from transverse shallow micro-grooves in EHL contacts. The approach depends on eliminating the side leakage along grooves by reducing the length of groove to be less than the diameter of the Hertzian contact. Consequently, micro-groves behave as closed texture cells with enough ability to maintain the hydrodynamic pressure leading to positive effects on the tribological performance of EHL contacts. Moreover, micro-grooves are preferred over micro-dents or dimples for the low cost of machining.

Experimental

Measurements have been carried out using a ball-on-disc tribometer equipped with a high-speed digital camera and torque sensor (see Figure 1). The film thickness and friction have been measured in the contact between a steel ball and a glass disc under different values of the entraining velocity and slide-to-roll ratios (SRR). The negative signal of SRR means that the ball is faster than the disc. The steel ball AISI 52100 has a roughness of about 10 nm and a diameter of 25.4 mm with the elastic modulus 210 GPa. The disc is made of chromium-coated glass with the elastic modulus 80 GPa. The ball and disc are driven by servomotors controlled by the computer with the ability to change the required SRR in a

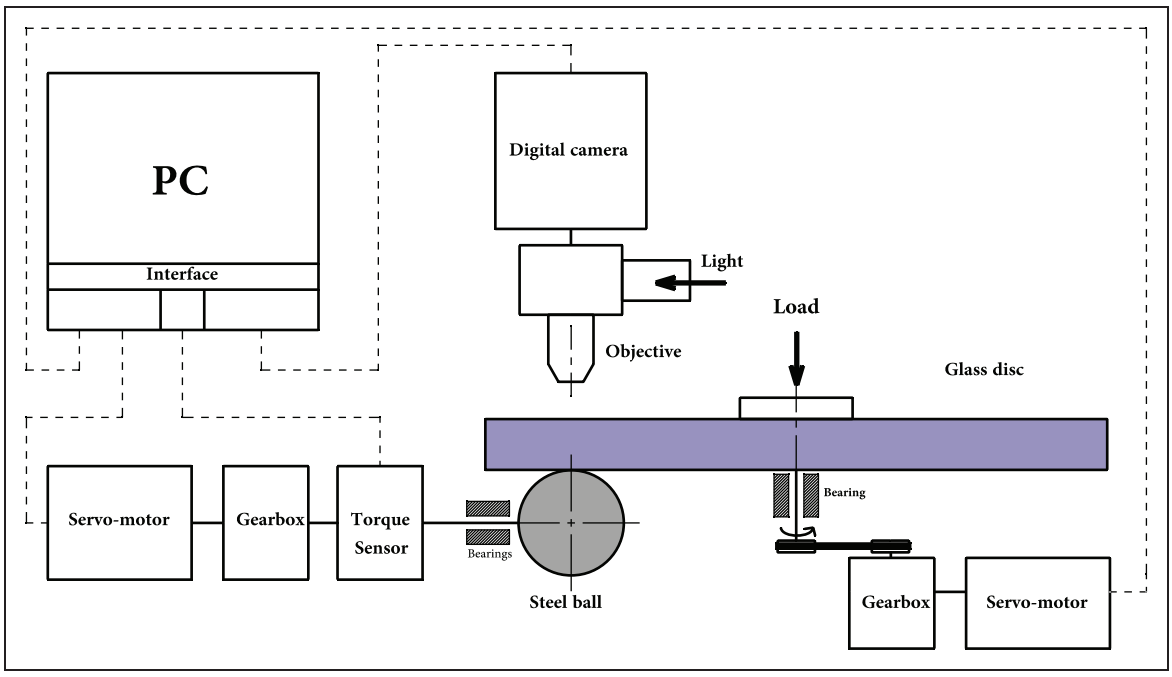

Figure 1. Schema of test rig.

wide range. The construction of the tribometer gives the possibility of capturing interferometric images simultaneously with measuring the friction. The base oil N2400 (dynamic viscosity $\eta = 0.421$ Pas at 40 °C and pressure–viscosity coefficient $\alpha = 35\,\mathrm{GPa}^{-1}$) was used as lubricant in all experiments in this paper. All measurements were carried out at room temperature of 22 °C.

Procedures of film thickness measurements

The film thickness was evaluated by the thin film colorimetric interferometry technique[34] (error is less than 1 nm) for smooth and textured surfaces under sliding motion and under starved conditions. The contact was loaded by 35 N corresponding to a maximum Hertz pressure of 0.537 GPa and radius of the Hertzian contact a = 168 μm. Micro-grooves were made by using a Rockwell indenter with a head angle of 120°. Three types of transverse micro-grooves have been used to investigate the effects on the film thickness. Figure 2 shows schematically the relative size of micro-grooves and the Hertzian contact for load 35 N. However, the types of micro-grooves can be distinguished according to the size as the following:

1. Type (a): Large-sized micro-grooves with intersection with the outer Hertzian circle (depth h = 1 μm, width w = 60 μm, length l = 1040 μm > 2a = 2*168 μm, where a is the radius of the Hertzian contact).
2. Type (b): Small-sized micro-grooves with intersection with the outer Hertzian circle (h = 0.4 μm, w = 42 μm, l = 1040 μm > 2a = 2*168 μm).
3. Type (c): Small-sized micro-grooves without intersection with the outer Hertzian circle (h = 0.4 μm, w = 42 μm, l = 160 μm < 2a = 2*168 μm).

Procedures of friction measurements

As shown in Figure 1, the ball is driven by a servomotor through torque sensor integrated with the computer. The sensor has been well calibrated using static loads before the testing. Also compensation has been added to eliminate the effect of bearings on the ball shaft. However, the sensor has absolute error of ± 0.2% according to the factory specifications. The coefficient of friction (COF) was measured in the lubricated contact between the steel ball and flat disc as the following:

First stage: The COF has been measured for a smooth ball under a load of 40 N corresponding to a maximum Hertz pressure of 0.561 GPa and radius of the Hertzian contact a = 185 μm. Friction coefficient was measured for 10 min in sliding and reversal motion. Simultaneously with friction measurements, interferometric images have been captured in the 6th min after the start for the film thickness evaluation.

Second stage: One single array of small-sized micro-grooves of type (c) has been made on the whole circumference of the ball. Figure 3 shows the resulting profile, distribution, and dimensions of micro-grooves on the surface of the ball. It is clear from Figure 3 that the micro-grooves are bounded with shoulders of 65 nm in the height. The interval

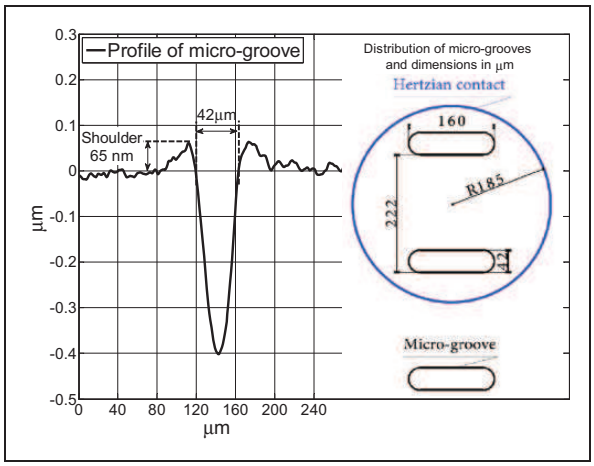

Figure 3. Profile and distribution of micro-grooves of type (c) used for comparing the friction under the load=40 N.

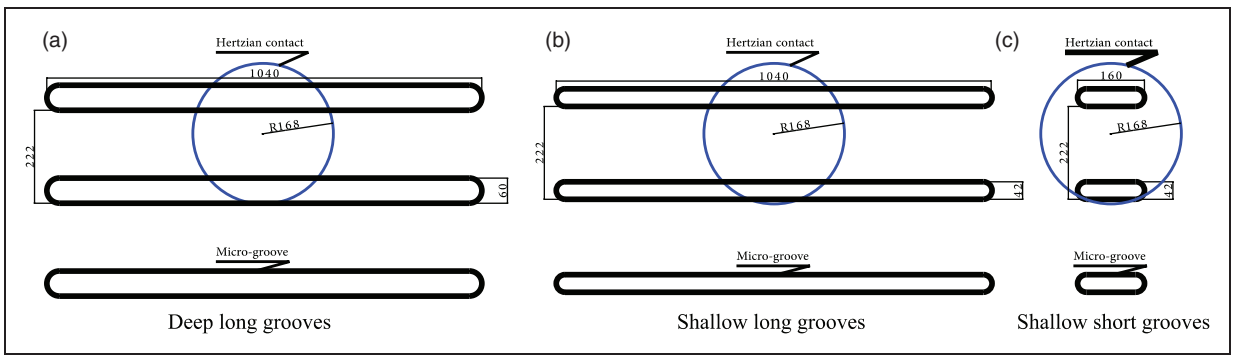

Figure 2. Schematic representation of micro-grooves used to compare the effect on film thickness under load 35 N (dimensions in μm). (a) Type (a), (b) (b) type (b), and (c) type (c).

pitch between grooves is 222 μm along the direction of sliding. This means that there are 360 grooves on the whole circumference of the ball. But only one or two grooves can be existed in the contact at once since the interval pitch is 222 μm see (Figure 3). Consequently, the relative surface density of micro-grooves in the contact for the given dimensions in Figure 3 changes with time in the range (5.9 – 11.8%) under the load 40 N. The friction was measured for the textured ball under the same operating conditions mentioned in the first stage. Also, interferometric images have been captured in the 6th min after the start for the film thickness comparison.

Results and discussion

Effect of micro-grooves on the film thickness in sliding motion

The effect of passing micro-grooves through point EHL contacts is tested in comparison with smooth surfaces under sliding motion. The behavior of the three types of micro-grooves shown in Figure 2 has been investigated for entraining speed $u_e = 4$mm/s, load $F = 35$ N, and SRR = –0.7. The negative signal of SRR means that the ball is faster than the disc. Therefore, there will not be any significant effect on the leading edge (downstream) of the micro-groove while the substantial film thickness modification will be localized on the trailing edge (upstream), see Kaneta and Nishikawa.[30] Thus, the film thickness is measured only on the trailing edge on axis parallel to the micro-groove. Theses axes are shown in all figures as dashed lines on the interferometric images. Measurements show a significant difference in the behavior of film thickness related to the size and length of grooves. Figure 4 shows the severe collapse of the film thickness as a deep long groove of type (a) passes the contact. The collapse is attributed to the side leakage across the micro-groove and it can be stated that the lubricant is channeled away out of the Hertzian contact along the groove. Figure 5 shows the film thickness on the trailing edge for micro-grooves of type (b). It is clear from Figure 5 that reducing the dimensions of the micro-groove does not solve the problem of the side leakage along the groove in the places where the groove is intersected with the outer circle of the Hertzian contact. However, the film thickness has been slightly enhanced only in the central region and it became larger than the film thickness of the smooth surface. Reducing the depth and width of the groove leads to increase the pressure in the groove resulting in a higher viscosity, consequently, the effect of the shear flow becomes less.[30] Thus, micro-grooves of type (b) with small depth and width can enhance the film thickness in the central region of the contact where the pressure is large enough to increase the viscosity of the lubricant. But even with the small size there is still

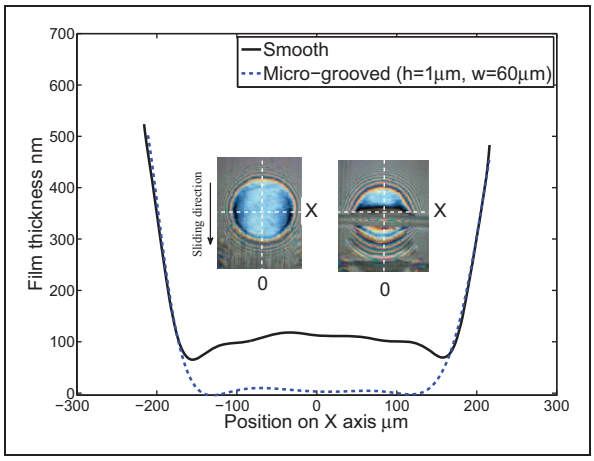

Figure 4. The film thickness profile on X axis for the smooth and the textured surface with micro-grooves (h = l μm, w = 60 μm, l > 2a), $F = 35$ N, $ue = 4$ mm/s, SRR = −0.7.

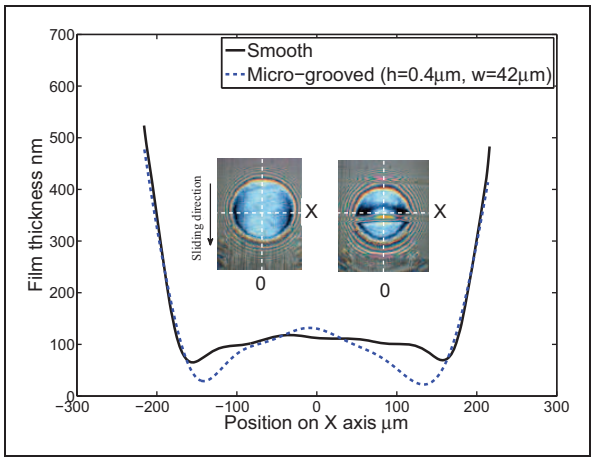

Figure 5. The film thickness profile on X axis for the smooth and the textured surface with micro-grooves (h = 0.4 μm, w = 42 μm, l > 2a), $F = 35$ N, $ue = 4$ mm/s, SRR = −0.7.

a significant side leakage and film thickness reduction in the places where the pressure and viscosity are relatively low. Measurements in Figures 4 and 5 show that micro-grooves of type (a) and (b) cannot keep the hydrodynamic pressure of lubricant and the resulting film thickness is smaller than for smooth surfaces. On the other hand, the reduction in film thickness is more pronounced as the dimensions of the groove are larger.

Figure 6 shows the profile of the film thickness on the trailing edge of a transverse micro-groove of type (c). In this case, the side leakage is restricted since there is not any intersection with the outer circle of the Hertzian contact. Figure 6 shows that the emitted lubricant from the groove caused a larger film thickness in comparison with the smooth surface under the same operating conditions. Indeed, micro-grooves act as oil reservoir when they are introduced as closed

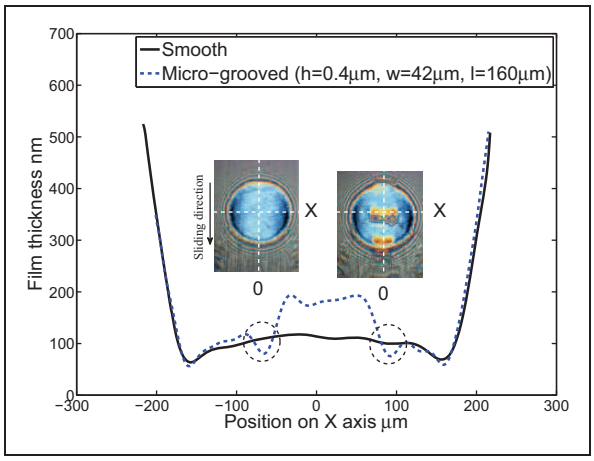

Figure 6. The film thickness profile on X axis for the smooth and the textured surface with micro-grooves (h = 0.4 μm, w = 42 μm, l = 160 μm), $F = 35$ N, $ue = 4$ mm/s, SRR = −0.7.

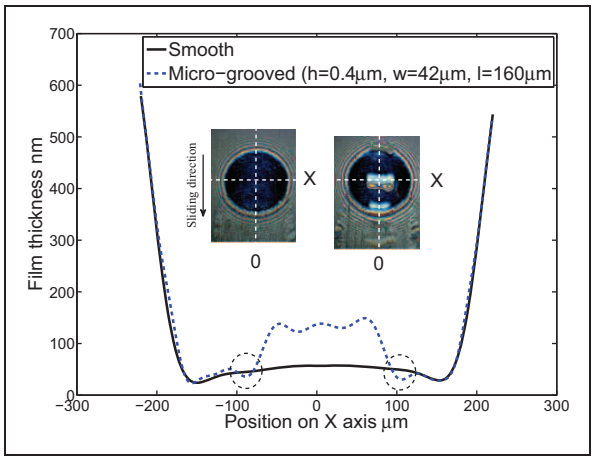

Figure 7. The film thickness profile on X axis for the smooth and the textured surface with micro-grooves (h = 0.4 μm, w = 42 μm, l = 160 μm), $F = 35$ N, $ue = 1.6$ mm/s, SRR = −0.7.

texture cells without access to the low pressure zone around the Hertzian contact. However, a small reduction in the film thickness has been observed in the places where the shoulders of micro-grooves are longitudinally oriented; see the dashed circles in Figure 6. The transversally oriented shoulders of grooves would be flattened (deformed) easier than the oblique or longitudinal shoulders under the effect of sliding.[35] Consequently, the shoulders induce a pronounced pressure fluctuation at the side edges of grooves where the shoulders tend to be longitudinal. The negative effects of shoulders can be minimized or eliminated by an effective polishing of the textured surfaces.

Figure 7 depicts the effect of micro-grooves of type (c) under low entraining speed $u_e = 1.7$ mm/s and thin film conditions. The comparison between Figures 6 and 7 shows a similar behavior of the film thickness and the emitted lubricant from the micro-groove increases the separation of rubbing surfaces. The dashed circles in Figure 7 show also the same negative reduction of film thickness induced by the shoulders. However, some important points can be observed from the comparison between Figures 6 and 7 as the following:

1. The film thickness has been enhanced by the same value (about 65 nm) on the trailing edge for the same SRR = 0.7. Therefore, the absolute amount of lubricant emitted from the micro-groove is approximately the same regardless the value of the overall film thickness and entraining speed. But the value of SRR determines the amount of extracted lubricant.
2. The relative enhancement of the film thickness is definitely larger and more appreciated for the thinner film thickness. Thus, relatively (not quantitatively) the benefits of micro-textures are more pronounced as the overall film thickness is less under the same SRR. Similar results are revealed experimentally and numerically in the literature.[25,36,37]

Behavior of micro-grooves under starvation

Starvation can be encountered in EHL contacts under extreme operating conditions (high speeds and/or high viscosities) or in cases where greases are used to lubricate bearings.[38] Starvation is caused basically by insufficient replenishment where the lubricant fails to reflow to the depleted track.[39,40] However, enhancing the lubricating film thickness is the key to reduce friction and wear in starved EHL contacts. Dumont et al.[37] described numerically the behavior of micro-pits in the fully flooded and starved EHL point contacts. The benefits of micro-pits decrease as the degree of starvation decreases because the film thickness becomes larger and the emitted oil from micro-pits becomes negligible in comparison with the available amount of oil in the contact. Figure 8 depicts the behavior of micro-grooves of type (c) under starvation where the available amount of oil was only 6 μl with $u_e = 3.7$ mm/s and SRR = −1.6. The interferometric images shown in Figure 8 have been captured in the 15th min after the start and starvation can be easily observed from the oil–air meniscus in the inlet of the contact. Although the contact is starved, Figure 8 shows that the closed grooves of type (c) are able to act as oil reservoirs. Consequently, the oil squeezed out of the micro-groove results in a film thickness larger than for smooth surfaces. Indeed, the enhancement of film formation shown in Figure 8 would not occur unless the micro-groove was filled with lubricant. But the micro-grooves are depleted after leaving the contact. The inlet gap between the mating surfaces is filled by lubricant under full film lubrication. As a result, the depleted micro-grooves are filled in the inlet zone; this is valid for cases in Figures 6 and 7. The situation is different when the contact is starved because the inlet gap is occupied by oil–air cavitations

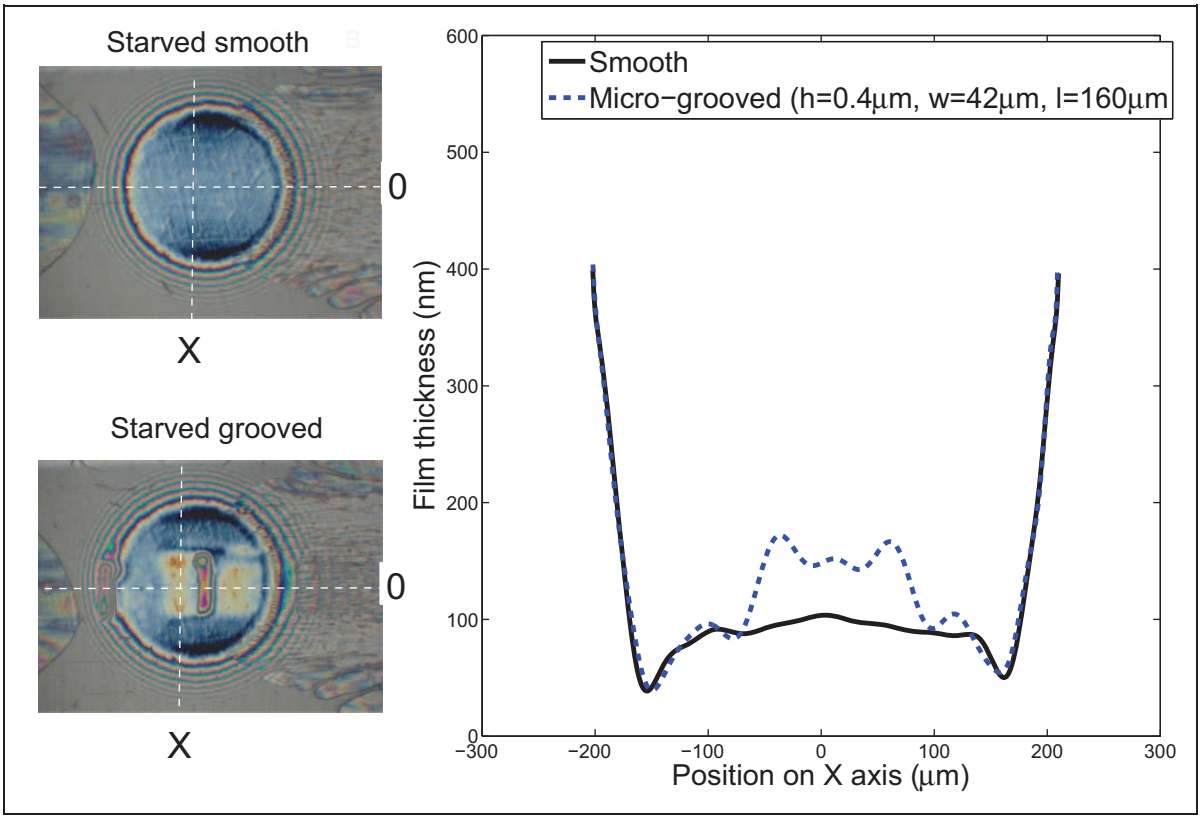

Figure 8. Film thickness for smooth and textured surfaces under starved conditions (available oil amount = 6 μl), F = 35 N, ue = 3.7 mm/s, SRR = −1.6.

with low pressure (see Figure 8). Nevertheless, Figure 8 shows that the micro-grooves are able to bring lubricant to the contact even after 15 min from the start. Surely micro-grooves have not been filled by the out-of-contact replenishment since this mechanism is insufficient for a very little amount available on the track (only 6 μl). Probably, the depleted micro-grooves were filled with lubricant in the inlet zone by the capillary forces. Jacod et al.[39] showed that the mechanism of capillary forces generates significant flows in the vicinity of the contact under starved lubrication. However, the mechanism of filling micro-features entering a starved contact is a topic for future study.

Effect of micro-grooves on the friction in sliding and reverse motion

Figures 6 to 8 show that shallow transverse micro-grooves with a length shorter than the diameter of the Hertzian contact are helpful in enhancing the film thickness under sliding and starved conditions. On the other hand, a small reduction in the film is caused by the effect of shoulders. However, the COF is crucial to evaluate the tribological performance of textured surfaces. Figure 9 shows a comparison of friction coefficient for smooth and textured surfaces under sliding motion. Interferometric images (captured in the 6th min after the start) in Figure 9 show a significant modification of the film

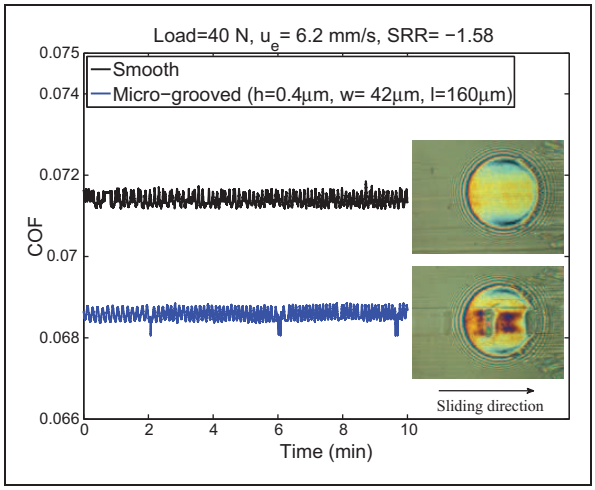

Figure 9. The coefficient of friction (COF) for the smooth and the textured surface with micro-grooves (h = 0.4 μm, w = 42 μm, l = 160 μm) in the sliding motion with SRR = −1.58.

thickness for the textured surface along the contact in the direction of sliding. Indeed, the COF has been reduced about 4% by introducing the micro-groves of type (c) on the surface of the ball. On the other hand, the COF was measured for reversal motion where the risk of surface damage increases. Reversal motion with EHL contacts can be encountered in many mechanical applications operating with reciprocating motion such as cams and seals. The value of

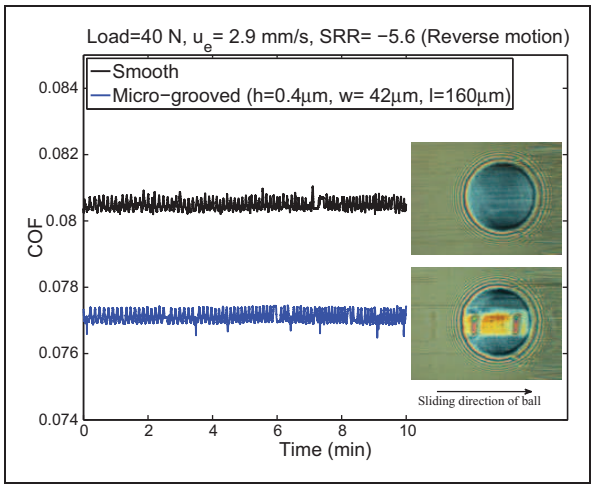

Figure 10. The coefficient of friction (COF) for the smooth and the textured surface with micro-grooves (h = 0.4 μm, w = 42 μm, l = 160 μm) in the reversal motion with SRR = –5.6.

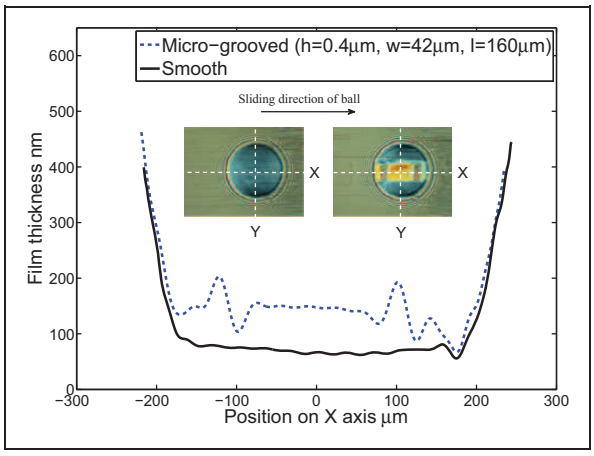

Figure 11. The film thickness profile on X axis for the smooth and the textured surface in the reversal motion with SRR = –5.6.

SRR is high in reversal motion leading to high friction and high shear stress in the contact. Under such extreme conditions the buildup of lubricating film is inhibited.[38,39,41] Figure 10 shows the measurements of friction for smooth and textured surfaces in the reversal motion for SRR = –5.6. The friction has been measured for 10 min under steady state conditions. A small reduction of friction (about 4%) has been observed for surfaces textured by micro-grooves of type (c) in the reversal motion. On the other hand, Figures 11 and 12 show the measured film thickness on axes transverse and parallel to the sliding direction. The central film thickness has been increased to about 2.1 times for textured surfaces. The small reduction of friction (about 4%)) versus the large enhancement of the film thickness (about 2.1 times) is attributed to the large value of SRR in the reversal motion. In Gershuni et al.[38] and Jacod et al.[39] it was proven that the sensitivity of friction to the change of film thickness becomes less with increasing the SRR.

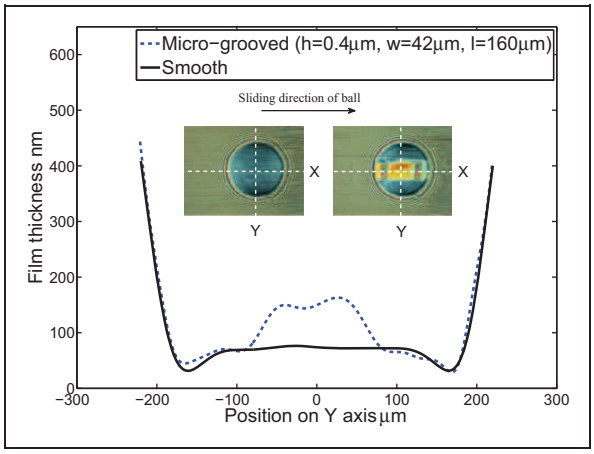

Figure 12. The film thickness profile on Y axis for the smooth and the textured surface in the reversal motion with SRR = –5.6.

In other words, the Couette friction is less sensitive to the change in the film thickness than the Poiseuille friction.[42] Since the Couette friction is dominant in the sliding motion, the high SRRs reduce the benefits concerning the reduction of friction for textured surfaces. On the other hand, the larger SRR improves the extraction of the lubricant from the micro-cavities resulting in a larger enhancement of the film thickness. Therefore, the beneficial effect on the friction from the film thickness enhancement has been dissipated or damped by the high value of SRR in the reversal motion. Furthermore, Figure 12 shows that the negative effect of shoulders has been strongly diminished on the axis perpendicular to the sliding direction in comparison with Figures 6 and 7. This is attributed to the high SRR in the reversal motion which means a larger flattening of shoulders.

Conclusions

In the present study the authors introduced an optimized design of micro-grooves for improving the tribological performance of nonconformal contact in the sliding and reversal motion. The design is based on creating shallow transverse micro-grooves with a length shorter than the diameter of the Hertzian contact resulting in eliminating the side leakage along the grooves. However, the importance of this study can be concluded by the following:

1. A significant enhancement in the film thickness can be induced by the passage of shallow short micro-grooves row in the EHL contact.
2. Deep and shallow micro-grooves with a length larger than the diameter of Hertzian contact cause a reduction of film thickness due to the side leakage.
3. The beneficial effect on the film thickness depends relatively on the overall film thickness and quantitatively on the SRR.

4. Surfaces with micro-grooves of type (c) have a larger film thickness than smooth surfaces under starved lubrication.
5. Such surface texturing approach is helpful to reduce friction and consequently wear of rubbing surfaces in the sliding and reversal motion.
6. Increasing the SRRs improves the extraction of lubricant from micro-cavities but this does not necessarily result in a significant reduction of friction.

Funding

This research was carried out under the project NETME CENTRE PLUS (LO1202) with financial support from the Ministry of Education, Youth and Sports under the National Sustainability Programme I and project P101/11/1115 from Czech Science Foundation.

Conflict of interest

None declared.

References

1. Etsion I. State of the art in laser surface texturing. *Trans ASME J Tribol* 2005; 127: 248–253.
2. Nanbu T, Ren N, Yasuda Y, et al. Micro-textures in concentrated conformal-contact lubrication: Effects of texture bottom shape and surface relative motion. *Tribol Lett* 2008; 29: 241–252.
3. Kovalchenko A, Ajayi O, Erdemir A, et al. The effect of laser surface texturing on transitions in lubrication regimes during unidirectional sliding contact. *Tribol Int* 2005; 38: 219–225.
4. Tian H, Saka N and Suh NP. Boundary lubrication studies on undulated titanium surfaces. *STLE Tribol Trans* 1989; 32: 289–296.
5. Saka N, Tian H and Suh NP. Boundary lubrication of undulated metal surfaces at elevated temperature. *STLE Tribol Trans* 1989; 32: 389–395.
6. Suh NP, Mosleh M and Howard PS. Control of friction. *Wear* 1994; 175: 151–158.
7. Pettersson U and Jacobson S. Influence of surface texture on boundary lubricated sliding contacts. *Tribol Int* 2003; 36: 857–864.
8. Pettersson U and Jacobson S. Friction and wear properties of micro textured DLC coated surfaces in boundary lubricated sliding. *Tribol Lett* 2004; 17: 553–559.
9. Ronen A, Etsion I and Kligerman Y. Friction-reducing surface-texturing in reciprocating automotive components. *Tribol Trans* 2001; 44: 359–366.
10. Burstein L and Ingman D. Pore ensemble statistics in application to lubrication under reciprocating motion. *Tribol Trans* 2002; 43: 205–212.
11. Brizmer V, Kligerman Y and Etsion I. A laser surface textured parallel thrust bearing. *Tribol Trans* 2003; 46: 397–403.
12. Wang X. The effect of laser texturing of SiC surface on the critical load for the transition of water lubrication mode from hydrodynamic to mixed. *Tribol Int* 2001; 34: 703–711.
13. Costa HL and Hutchings IM. Hydrodynamic lubrication of textured steel surfaces under reciprocating sliding conditions. *Tribol Int* 2007; 40: 1227–1238.
14. Ramesh A, Akram W, Mishra SP, et al. Friction characteristics of microtextured surfaces under mixed and hydrodynamic lubrication. *Tribol Int* 2013; 57: 170–176.
15. Han J, Fang L, Sun J, et al. Hydrodynamic lubrication of surfaces with asymmetric microdimple. *Tribol Trans* 2011; 54: 607–615.
16. Hamilton DB, Walowit JA and Allen CM. A theory of lubrication by micro-irregularities. *Trans ASME J Basic Eng* 1966; 88: 177–185.
17. Rahmani R, Shirvani A and Shirvani H. Optimization of partially textured thrust bearings with square-shaped micro-dimples. *Tribol Trans* 2007; 50: 401–406.
18. Wang XL, Kato K, Adachi K, et al. Loads carrying capacity map for the surface texture design of SiC thrust bearing sliding in water. *Tribol Int* 2003; 36: 189–197.
19. Mourier L, Mazuyer D, Lubrecht AA, et al. Transient increase of film thickness in micro-textured EHL contacts. *Tribol Int* 2006; 39: 1745–1756.
20. Wang XL, Liu W, Zhou F, et al. Preliminary investigation of the effect of dimple size on friction in line contacts. *Tribol Int* 2009; 42: 1118–1123.
21. Blatter A, Maillat M, Pimenov SM, et al. Lubricated friction of laser micro-patterned sapphire flats. *Tribol Lett* 1998; 4: 237–241.
22. Krupka I and Hartl M. The effect of surface texturing on thin EHD lubrication films. *Tribol Int* 2007; 40: 1100–1110.
23. Krupka I and Hartl M. Experimental study of micro-textured surfaces operating under thin-film EHD lubrication conditions. *Trans ASME J Tribol* 2007; 129: 502–508.
24. Venner CH, Lubrecht AA and ten Napel WE. Numerical simulation of the over-rolling of a surface feature in an EHL line contact. *Trans ASME J Tribol* 1991; 113: 777–783.
25. Ai X and Cheng HS. The influence of moving dent on point EHL contacts. *STLE Tribol Trans* 1994; 37: 323–335.
26. Venner CH and Lubrecht AA. Transient analysis of surface features in an EHL line contact in the case of sliding. *Trans ASME J Tribol* 1994; 116: 186–193.
27. Zhao J and Sadeghi F. The effects of a stationary surface pocket on EHL line contact start-up. *Trans ASME J Tribol* 2004; 126: 672–680.
28. Wedeven LD and Cusano C. Elastohydrodynamic film thickness measurements of artificially produced surface dents and grooves. *ASLE Trans* 1979; 22: 369–381.
29. Mourier L, Mazuyer D, Lubrecht AA, et al. Action of a femtosecond laser generated micro-cavity passing through a circular EHD contact. *Wear* 2008; 264: 450–456.
30. Kaneta M and Nishikawa H. Local reduction in thickness of point contact EHL films caused by transversely oriented moving groove and its recovery. *Trans ASME J Tribol* 1994; 116: 635–639.
31. Kaneta M, Nishikawa H, Kanada T, et al. Abnormal phenomena appearing in EHL contacts. *Trans ASME J Tribol* 1996; 118: 886–892.
32. Yang P, Cui J, Kaneta M, et al. Influence of a surface bump or groove on the lubricating performance and dimple phenomena in simple sliding point EHL contacts. *Trans ASME J Tribol* 2004; 126: 466–472.

33. Nakano M, Korenaga A, Korenaga A, et al. Applying micro-texture to cast iron surfaces to reduce the friction coefficient under lubricated conditions. *Tribol Lett* 2007; 28: 131–137.
34. Hartl M, Krupka I, Poliscuk R, et al. Thin film colorimetric interferometry. *Tribol Trans* 2001; 44: 270–276.
35. Venner CH and Lubrecht AA. Numerical analysis of the influence of waviness on the film thickness of a circular ehl contact. *Trans ASME J Tribol* 1996; 118: 153–161.
36. Ali F, Křupka I and Hartl M. Analytical and experimental investigation on friction of non-conformal point contacts under starved lubrication. *Meccanica* 2013; 48: 545–553.
37. Dumont ML, Lugt PM and Tripp JH. Surface feature effects in starved circular EHL contacts. *Trans ASME J Tribol* 2002; 124: 358–366.
38. Gershuni L, Larson MG and Lugt PM. Lubricant replenishment in rolling bearings contacts. *STLE Tribol Trans* 2008; 5: 643–651.
39. Jacod B, Publier F, Cann PM, et al. An analysis of track replenishment mechanisms in the starved regime. In: *Proceedings of the 25th Leeds–Lyon symposium on tribology*, Lyon, France, 8–11 September 1998. *Tribology and Interface Engineering Series*, vol. 36, 1999, pp.483–492.
40. Ali F, Křupka I and Hartl M. Enhancing the parameters of starved EHL point conjunctions by artificially induced replenishment. *Tribol Int* 2013; 66: 134–142.
41. Sugimura J, Jones WR Jr and Spikes HA. EHD film thickness in non-steady state contacts. *Trans ASME J Tribol* 1998; 120: 442–452.
42. Kudish LI. On formulation of a non-steady lubrication problem for a non-conformal contact. *Tribol Trans* 1999; 43: 53–57.
43. Ali F, Krupka I and Hartl M. An approximate approach to predict the degree of starvation in ball-disk machine based on the relative friction. *Tribol Trans*, Epub ahead of print 2013. DOI: 10.1080/10402004.2013.781722.
44. Kumar P and Khonsari MM. Effect of starvation on traction and film thickness in thermo-EHL line contacts with shear-thinning lubricants. *Tribol Lett* 2008; 32: 171–177.
45. Biboulet N, Colin F and Lubrecht AA. Friction in starved hydrodynamically lubricated line contacts. *Tribol Int* 2013; 58: 1–6.

Appendix

Notation

a	radius of the Hertzian contact (m)
F	load (N)
h	depth of micro-groove (m)
l	length of micro-groove (m)
SRR	$2 * (u_{disc} - u_{ball})/(u_{disc} + u_{ball})$ slide-to-roll ratio
u_e	$(u_{disc} + u_{ball})/2$ entraining speed (m/s)
u_s	$u_{disc} - u_{ball}$ sliding speed (m/s)
w	width of micro-groove (m)
α	pressure–viscosity coefficient (GPa^{-1})
η	dynamic viscosity (Pa s)

Tribology International 84 (2015) 81–89

Contents lists available at ScienceDirect

Tribology International

journal homepage: www.elsevier.com/locate/triboint

Experimental and numerical investigation on the behavior of transverse limited micro-grooves in EHL point contacts

Fadi Ali, Motohiro Kaneta, Ivan Křupka *, Martin Hartl

Institute of Machine and Industrial Design, Faculty of Mechanical Engineering, Brno University of Technology, Technická 2896/2, 61669 Brno, Czech Republic

ARTICLE INFO

Article history:
Received 5 September 2014
Received in revised form
12 November 2014
Accepted 27 November 2014
Available online 6 December 2014

Keywords:
Elastohydrodynamic (EHL)
Limited micro-grooves
Film thickness
Reciprocating motion

ABSTRACT

This study presents experimental and numerical investigations on the effects of transverse limited micro-grooves on the behavior of film thickness and friction in EHL point contacts. The tribological performance has been compared for smooth and textured surfaces in sliding and reciprocating motion and under starvation. The measurements were conducted by using a ball-on-disk tribometer equipped with a high speed camera and torque sensor. The results show that the transverse shallow micro-grooves with a length less than the diameter of the Hertzian contact are efficiently able to enhance the film thickness under different operating conditions. The beneficial effect under starved lubrication requires a mechanism for filling the depleted micro-grooves entering the contact with fresh lubricant. This mechanism can be attributed to the capillary effect in the inlet zone under starvation. The numerical simulation of the transient behavior of transverse limited micro-grooves shows agreement with experimental results. On the other hand, introducing micro-grooves as closed texture cells on one of rubbing surfaces results in a friction reduction in the reciprocating motion. The reduction of friction is substantially attributed to the film thickness enhancement.

1. Introduction

Reducing the friction and wear of lubricated mechanical interfaces is crucial for extending the service life of machine components. Extreme operating conditions with high friction values and thin lubrication films aggravate the wear rate over time. Usually, wear begins when there is a plastic deformation due to metal-to-metal contacts. The modification of surface topography by artificially produced micro-textures patterns influences the behavior of lubrication films significantly, consequently, wear and friction of rubbing surfaces. However, micro-textures are presented in many shapes and sizes to improve the tribological performance of mechanical interfaces. Many researchers studied the behavior of longitudinal and transverse micro-grooves in EHL conjunctions. Wedeven and Cusano [1,2] used optical EHD rig to investigate the passage of parallel and longitudinal grooves through EHL point contacts under rolling and sliding conditions. They revealed that both types of grooves reduce the film thickness compared to a smooth surface under pure rolling conditions. Also by using of optical interferometry, Jackson and Cameron [3] observed cavitation between transverse asperity pairs in the elastohydrodynamic lubrication. Suh et al. [4] studied the effects of geometrical parameters of micro-grooved crosshatch pattern on friction in mixed and elastohydrodynamic lubrication. They observed that the decrease of groove aspect ratio and the increase of groove sliding length show friction reduction performance. Pettersson et al. [5,6] showed that the performance of surface texture depends significantly on the orientation of micro-textures in boundary lubricated sliding. Furthermore, samples with parallel grooves and crossed groove have less friction fluctuations than polished samples. Yuan et al. [7] showed that surfaces textured with perpendicular grooves could reduce friction up to 38.2% compared to the untextured surfaces under a low contact pressure. On the other hand, under a relative high contact pressure, parallel grooves cause a larger friction reduction than grooves with perpendicular orientation. Costa et al. [8] stated that textured samples with features larger than the width of the contact give a film thickness smaller than that for smooth samples. This is attributed to the channeling of lubricant away from the contact. Similarly, Nakano et al. [9,10] showed that groove patterns have higher friction coefficients than flat surfaces because groove patterns do not have enough ability to keep the hydrodynamic pressure while dimples keep the hydrodynamic pressure because of the closed shape. Kaneta et al. [11,12] optically investigated a local reduction in film thickness through the passage of transverse micro-grooves EHL contacts. The local reduction in film thickness

* Corresponding author. Tel.: +420 54114 2723.
E-mail address: krupka@fme.vutbr.cz (I. Křupka).

http://dx.doi.org/10.1016/j.triboint.2014.11.025
0301-679X/

Nomenclature

A	radius of Hertzian contact circle (m)
E_1, E_2	elastic moduli of glass and steel
E'	$2\{(1-\nu_1^2)/E_1+(1-\nu_2^2)/E_2\}^{-1}$, equivalent elastic modulus (Pa)
h	film thickness (m)
h_{00}	rigid central film thickness (m)
p	film pressure (Pa)
R_x	radius of steel ball (m)
u_e	rolling velocity (m s^{-1})
x, y	coordinates (m)
x_{out}, y_{out}	calculation domain (m)
α	pressure–viscosity coefficient (Pa^{-1})
ν_1, ν_2	Poisson's ratios of glass and steel
η	viscosity of lubricant (Pa s)
η_0	ambient viscosity of lubricant (Pa s)
δ	groove shape
ρ	density of lubricant (kg m^{-3})
ρ_0	ambient density of lubricant (kg m^{-3})
H	depth of groove (m)

is essentially caused by the side leakage along the groove due to the relative low viscosity in the groove. However, the amount of the side leakage decreases with reducing the size (width and depth of micro-groove) and increasing the overall film thickness. Yang et al. [13] proved numerically the results of Kaneta. Scaraggi et al. [14] showed by means of pin-on-disk test rig that the regular array of micro-holes reduces friction in the different lubrication regimes. On the contrary, the parallel micro-grooves lead to an increase of friction compared to the flat control surface because the oil easily flows along the parallel microgrooves leading to increased friction. Jiang et al. [15] studied numerically the effect of asperity orientation as well as the effect of rolling–sliding condition on the film thickness and pressure in the mixed EHL. The study simulated the behavior of asperity under sliding conditions for longitudinal and transverse orientation with respect to the rolling direction. Nanbu et al. [16] used 4-roller tester to show the influence of the surface micro-texture orientation on the traction coefficient. Their experiments were performed under high pressure and rolling speed conditions. It was found that the grooves with orientation parallel to the rolling direction reduce the metal-to-metal contact and increase the traction coefficient. Yang et al. [17] studied the influence of surface waviness on the EHL behavior of point contacts. The results show that the thermal and non-Newtonian effects can be enlarged significantly by the surface waviness, and the worst configuration of the surface topography is that both surfaces are with longitudinal waviness. Yagi et al. [18] studied the effect of longitudinal groove on the temperature field in the EHL conjunction between steel ball and a sapphire disk under high slip conditions. An infrared technique has been used to measure the temperatures of the oil film. The results show that the temperature of the grooved ball surface increased considerably compared with that of a non-grooved ball. Under starved boundary lubrication conditions, the successful textures were the grooves with an orientation perpendicular to the sliding direction. Dumont et al. [19] studied numerically the behavior of micro-pits in fully flooded and starved ball-on-disk contact. They revealed that micro-pits improve the film thickness under starvation but not under fully flooded conditions. These results have been proved experimentally in reference [20]. The main inconvenience with surface texturing is the risk of contact fatigue due to the increase of pressure fluctuation and stresses around the micro-cavity [21–23]. However, some possible beneficial effects of surface texturing on rolling contact fatigue have been observed by Zhai et al. [24], Akamatsu et al. [25] and Vrbka et al. [26].

Negative effects have been observed numerically and experimentally with micro-grooves in lubricated non-conformal contacts [8,9–13]. Therefore, there is a tendency of applying surface textures as micro-dents or spherical dimples in EHL contacts to avoid the side leakage associated with micro-grooves. In addition, spherical dimples are indifferent to the directionality of the relative velocity between the mating surfaces. However, this study introduces an innovative approach of micro-grooves design for EHL contacts. This approach depends on eliminating the side leakage by introducing grooves as closed texture cells in the contact. In this case, the length of micro-groove should be less than the diameter of the Hertzian contact. Such surface texturing approach is helpful also to reduce friction and consequently wear of rubbing surfaces and it could be extended to some engineering applications.

2. Numerical procedures

The numerical simulation of the experiments was performed by assuming an isothermal Newtonian fluid. Therefore, the Reynolds equation is written as

$$\frac{\partial}{\partial x}\left(\frac{\rho h^3}{12\eta}\frac{\partial p}{\partial x}\right)+\frac{\partial}{\partial y}\left(\frac{\rho h^3}{12\eta}\frac{\partial p}{\partial y}\right)=u_e\frac{\partial(\rho h)}{\partial x}+\frac{\partial(\rho h)}{\partial t} \tag{1}$$

The boundary conditions of Eq. (1) are

$$p(x_{in},y,t)=p(x_{out},y,t)=p(x,\pm y_{out},t)=0$$
$$p(x,y,t)>0\ \ (x_{in}<x<x_{out},y_{in}<y<y_{out}).$$

The film thickness equation reads

$$h(x,y,t)=h_{00}(t)+\frac{x^2+y^2}{2R_x}+\frac{2}{\pi E'}\iint\frac{p(x',y',t)dx'\,dy'}{\sqrt{(x-x')^2+(y-y')^2}} \tag{2}$$

The density–pressure and viscosity–pressure relations proposed by Dowson and Higginson [27] and Roelands et al. [28], respectively, are adopted, i.e.,

$$\rho=\rho_0\left[1+\frac{0.6\times10^{-9}p}{1+1.7\times10^{-9}p}\right] \tag{3}$$

$$\eta=\eta_0\exp\left\{(\ln\eta_0+9.67)\ \left[-1+\left(1+5.1\times10^{-9}p\right)^{Z_0}\right]\right\} \tag{4}$$

where $Z_0=\alpha/\left[5.1\times10^{-9}(\ln\eta_0+9.67)\right]$ and α is the Barus' pressure–viscosity coefficient.

The Reynolds and film thickness equations are solved with the multi-level multi-integration technique [29]. The calculation domain was $-2.5a\le x\le1.5a$, $0\le y\le2.0a$, because of the symmetry with respect to the x-axis. Five levels of grids were used. On the finest level, 513 nodes were arranged in the x-direction and 257 nodes in the y-direction. Converged solutions were accepted when relative errors of pressure and load values became less than 10^{-4} simultaneously at the finest grid level.

The shape of the groove used in the experiments was assumed by the following equation:

$$\delta(x)=H\times10^{-12.5(x/60)^2}\cos(2\pi x/60) \tag{5}$$

where $H=-0.6$ μm.

The numerical representation of micro-grooves profile is shown in Fig. 1 with the corresponding measured profile.

3. Experimental

3.1. Test rig

Measurements were conducted using a Tribometer equipped with a high-speed digital camera and torque sensor. Fig. 2 shows a schematic representation of ball-on-disk test rig. The film thickness and friction have been measured in the contact between a steel ball and a glass disk under different values of the entraining velocity $u_e = (u_{disk} + u_{ball})/2$ and slide-to-roll ratio $SRR = 2(u_{disk} - u_{ball})/(u_{disk} + u_{ball})$. The negative sign of SRR means that the ball is faster than the disk. The steel ball AISI 52100 has a diameter of 25.4 mm with an elastic modulus of 210 GPa. The disk is made of glass with an elastic modulus of 80 GPa and the lower surface of the disk is coated with a thin layer of chromium. Base oil with a dynamic viscosity $\eta = 0.215$ Pa s at 22 °C and a pressure–viscosity coefficient $\alpha = 22\ \mathrm{GPa}^{-1}$ was used in all experiments presented in this study. The film thickness was evaluated by the colorimetric interferometry technique [30].

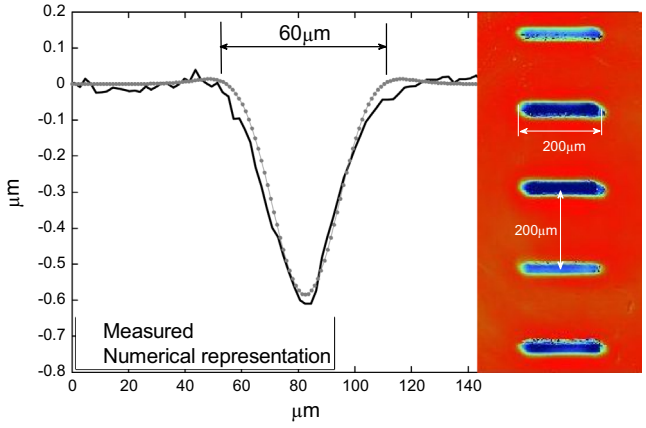

Fig. 1. Numerical and measured profiles of limited micro-grooves on the surface of ball.

3.2. Micro-texturing

Micro-grooves were made by using a Rockwell indenter with a head angle of 120° The indentation process was fully automated by using stepper motors for linear and angular motion. An electromagnetic motor was used to create the impact between the head of Rockwell indenter and the surface of the ball. Thus, the depth of micro-grooves depends on the volt and current supply to the electromagnetic motor. An experimental interpolation has been used to obtain the corresponding values of volt and current to produce the desired depth of micro-grooves. This device was made just for laboratory purposes. Indeed, a post-texturing treatment (polishing) was needed to remove piled-up material following the indentation. Thus, the whole surface of the ball had a homogeneous roughness about 10 nm after the polishing process. The profile of resulting micro-grooves was measured by optical profilometer. Fig. 1 shows the measured profile of micro-grooves (and the numerical representation of these grooves) and its distribution on the surface of the ball. The average depth of grooves is about 600 nm, the width is about 60 μm and the transverse length is 200 μm. One row of 10 micro-grooves has been created on the surface of the ball with axial pitch of 200 μm corresponding to angular pitch about 0.9°.

3.3. Reciprocating motion

The frictional behavior of smooth and grooved surfaces has been investigated in reciprocating motion. The reciprocating motion was created by the numerical control of servo-motors benefiting from a closed loop. The frequency of ball has been fixed at 0.5 Hz while the speed of disk was constant over time ($0.96\ \mathrm{mm\ s}^{-1}$). The maximum speed of ball is $\pm 3.146\ \mathrm{s}^{-1}$. Fig. 3 shows a simplified profile to the relative speed of ball and disk in the reciprocating motion. Indeed, the profile of ball speed is subjected to the acceleration and deceleration rate of stepper motor. In this study, authors are interested only in determined points at the maximum speed of ball. Points A and B in Fig. 3 show the places in which the film thickness has been measured during the reciprocating motion. Such measurements of the film thickness in correspondence with friction helps to better understand the mechanism of friction modification. The stroke of reciprocating motion has a total length of about 3.55 mm and angle of 16°.

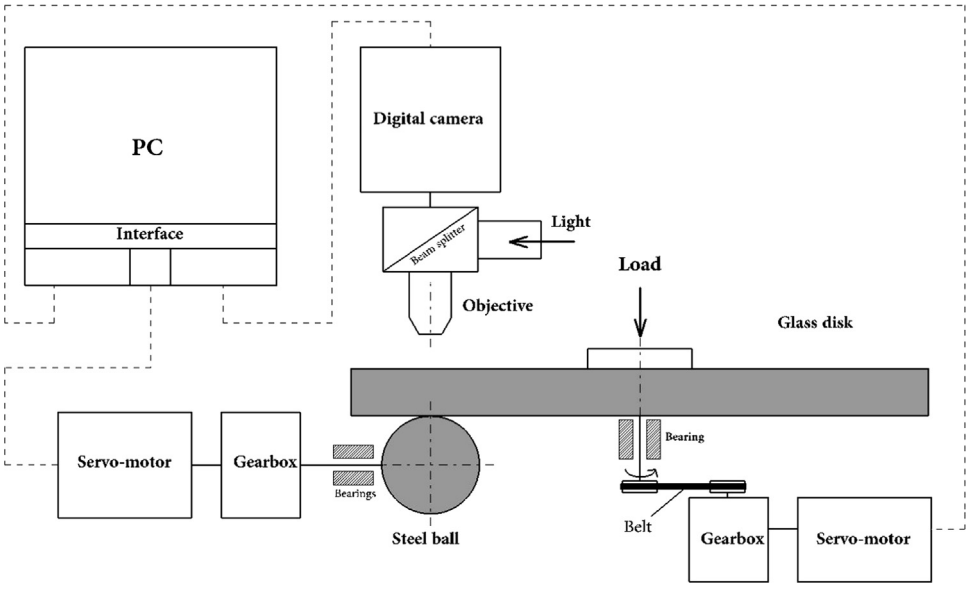

Fig. 2. Schematic representation of ball-on-disk test rig.

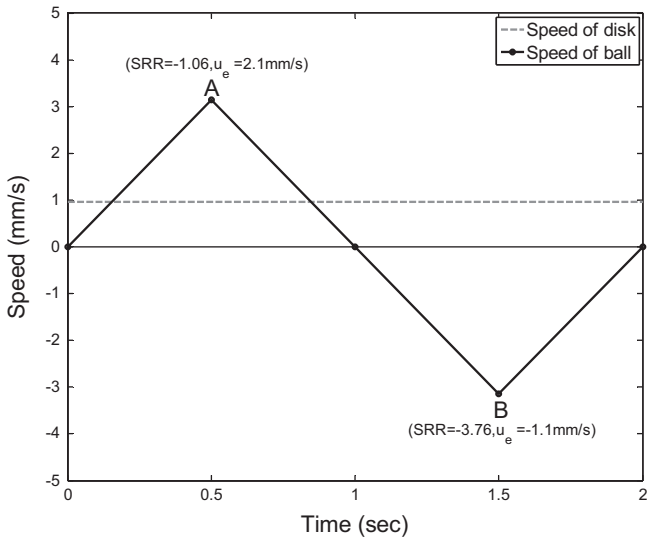

Fig. 3. The relative speed of ball and disk in the reciprocating motions, points A and B show the positions in which the film thickness has been measured for comparison.

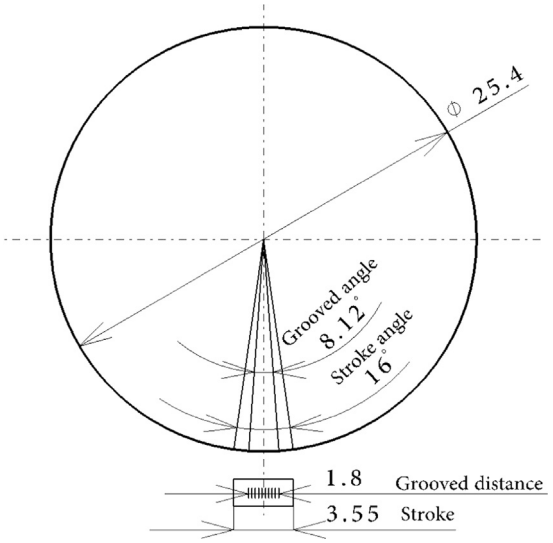

Fig. 4. Dimensions of the stroke and the grooved distance with corresponding angles for reciprocating motion (dimensions are in mm).

Therefore, the grooved distance (length 1.8 mm, angle 8.12°) is about 51% from the total stroke. Fig. 4 shows the relative length of the stroke and the grooved distance for reciprocating motion and the corresponding angles. Friction of smooth surfaces was measured with the same ball but in non-grooved track. Thus, the degree of polishing and the surface roughness are the same for grooved and smooth zones. All experiments presented in this paper were carried out at room temperature of 22 °C.

4. Results and discussion

4.1. Numerical simulation and experimental verification

In this section, the transient effect of the micro-grooves passage through the EHL contact is observed numerically and experimentally under sliding motion. This effect is compared with smooth surface film thickness. Measurements and simulation were carried out for entraining velocity $u_e = 34$ mm s^{-1}, slide-to-roll ratio SRR $= -0.6$ and load $w = 70$ N. The corresponding maximum Hertzian pressure and contact radius are 0.68 GPa and 222 μm, respectively. Figs. 5 and 6 show a film thickness comparison of smooth and micro-grooved surfaces with numerical simulation. Optical interferometry images in Figs. 5 and 6 are captured by high speed camera. Images (a) show the film thickness formation of smooth surfaces while images (b) show the transient effect of grooved surfaces for interval time T2 − T1 = 4.42 ms. During this time (4.42 ms) every micro-groove passes a distance about 196 μm since the linear speed of ball is 44.32 mm s^{-1}. Images (c) in Figs. 5 and 6 represent the numerical simulation to the passage of micro-grooves for the same positions of micro-grooves in images (b). The central film thickness is measured along horizontal axes in the direction of sliding. These axes are shown in Figs. 5 and 6 as dashed lines on images (a), (b) and (c). However, it is clear that the passage of limited micro-grooves through the contact created an enhancement of film thickness on the trailing edge. The film thickness on the trailing edge is about 178 nm while the average film thickness of smooth surface is about 88 nm. On the other hand, Fig. 5 shows a reduction of film thickness as the micro-groove enters the contact. This reduction is predicted also by the numerical simulation. Indeed, Figs. 5 and 6 show agreement of experimental measurements and numerical simulation to the transient behavior of limited micro-grooves through the EHL point contact. It is well known that the passage of micro-features though EHL contacts is associated with pressure fluctuation as shown in Figs. 5 and 6. The mid-plane pressure along the moving direction is larger at both the edges of the groove than the maximum Hertzian pressure (0.68 GPa). These high pressures may give some effects on the fatigue life depending on the applied load and sliding velocity. However, the resulting effect of micro-features is a combination of positive effects (film thickness enhancement) and negative effects (pressure fluctuation). Fig. 7 shows a 3-D visualization to the passage of micro-grooves through the contact. This visualization simulates the position of grooves in images (b) in Figs. 5 and 6. The elastic deformation, caused by the emitted lubricant of micro-groove, is clear on the trailing edge. The propagation of this elastic deformation increases as the groove passes a larger distance in the contact. The significance of this section is that the behavior of limited micro-grooves in EHL contacts can be successfully predicted by numerical methods.

4.2. Limited micro-grooves under thin films

Thin films are common in EHL contacts with low speeds, low oil viscosity, in start/stop and oscillating motion. Under such conditions, the film thickness becomes in the scale or less than the surface roughness amplitude and the risk of metal-to-metal contacts increases. Therefore, enhancing the separation under thin film conditions is significantly appreciated to avoid the fatigue and wear initiation. In order to investigate the effect of limited micro-grooves on thin films, measurements were carried out for a low entraining velocity $u_e = 8.2$ mm s^{-1} with slide-to-roll ratio SRR $= -0.58$ and load $w = 70$ N. The corresponding maximum Hertzian pressure and contact radius are 0.68 GPa and 222 μm, respectively. Under these operating conditions, the average resulting central film thickness of the smooth surfaces is about 28 nm. Fig. 8 shows a comparison of film thickness for smooth and grooved surfaces. The film thickness is measured on longitudinal and parallel axes to the sliding direction. These axes are shown in Fig. 8 as crossed dashed lines on the interferometry images. Introducing limited micro-grooves on the surface of ball resulted in film thickness of about 105 nm on the trailing edge. Moreover, no significant film thickness reduction is observed as the micro-groove becomes entirely encircled by the Hertzian contact. The amplitude of groove reduces as it approaches the center of the contact where the maximum pressure is localized. Therefore, the elastic deformation of micro-grooves in the contact

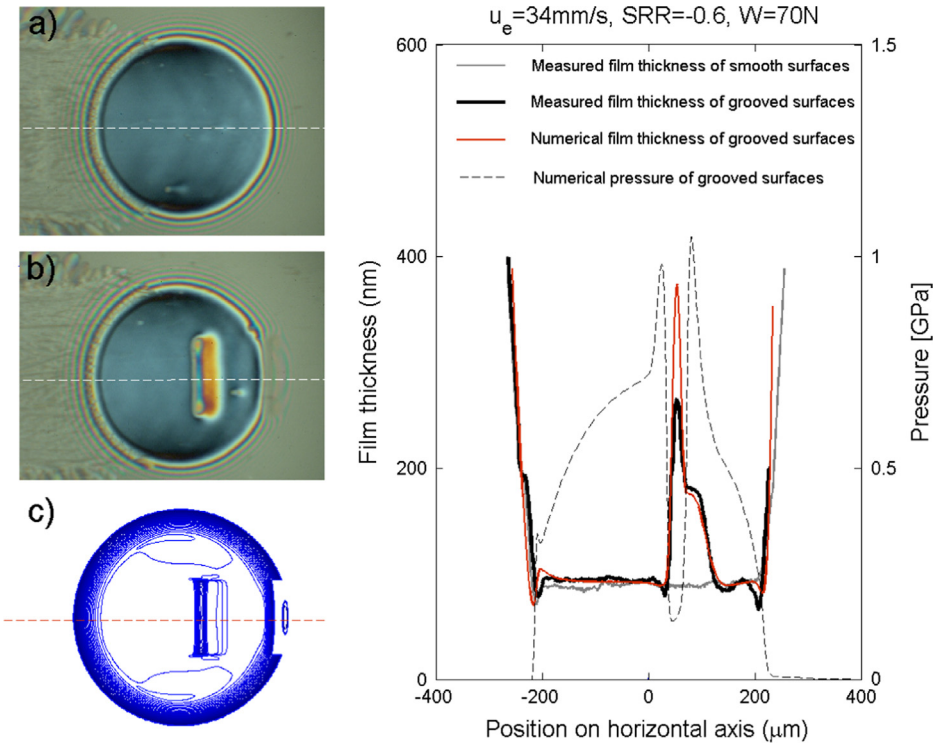

Fig. 5. Numerical and experimental comparison of the micro-grooves effects on film thickness at time T1 = 0 (a) interferometry image of smooth surface (b) interferometry image of grooved surface (c) and numerical contour of film thickness for case (b).

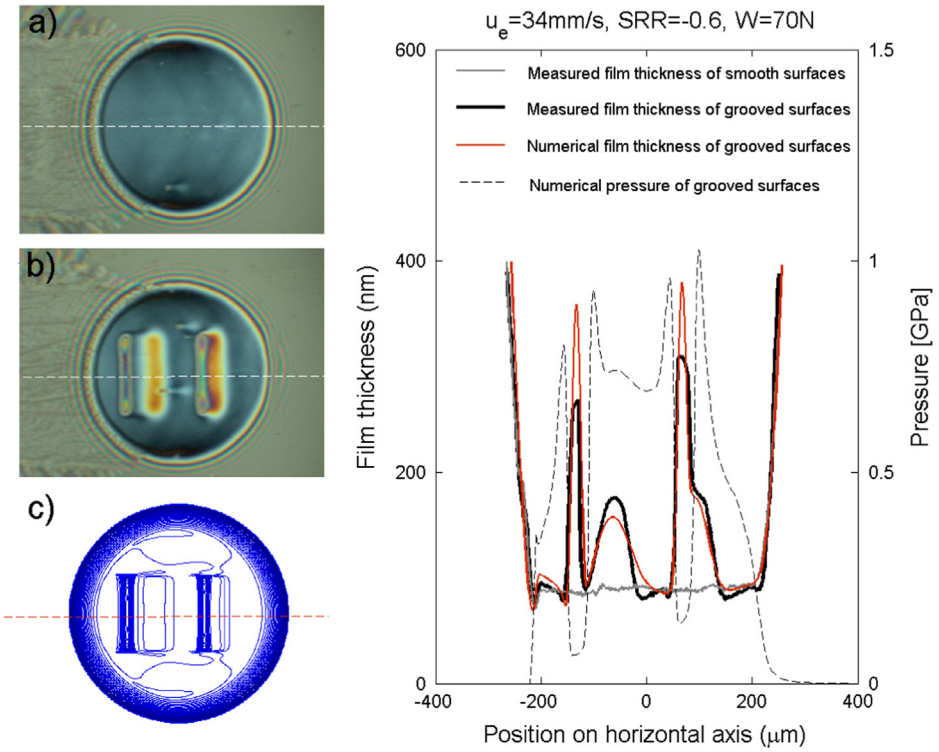

Fig. 6. Numerical and experimental comparison of the micro-grooves effects on film thickness at time T2 = 4.42 ms (a) interferometry image of smooth surface (b) interferometry image of grooved surface (c) and numerical contour of film thickness for case (b).

does not occur instantly, but some milliseconds are necessary until the micro-groove reaches the maximum value of deformation. Indeed, this elastic deformation results in emitting the lubricant out of the micro-groove. The presence of sliding helps in propagating the emitted lubricant upstream in case the grooved surface is faster than the opposite one.

4.3. Limited micro-grooves under starved conditions

Starvation is common in EHL contacts under extreme operating conditions (high speeds and/or high viscosities) or in cases where greases are used to lubricate bearings [31]. Starvation is caused basically by insufficient replenishment where the lubricant fails to

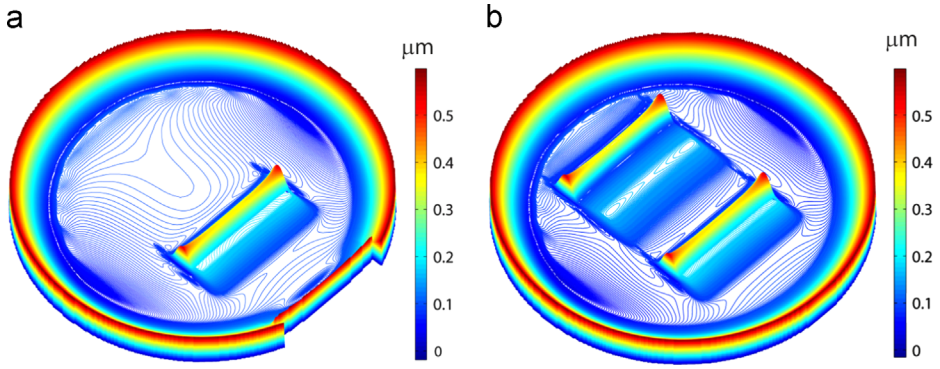

Fig. 7. 3-D visualization to the passage of micro-grooves through the EHL contact, $u_e=34$ mm/s, SRR$=-0.6$ and $w=70$ N. (a) At T1$=0$ (b) at T2$=4.42$ ms.

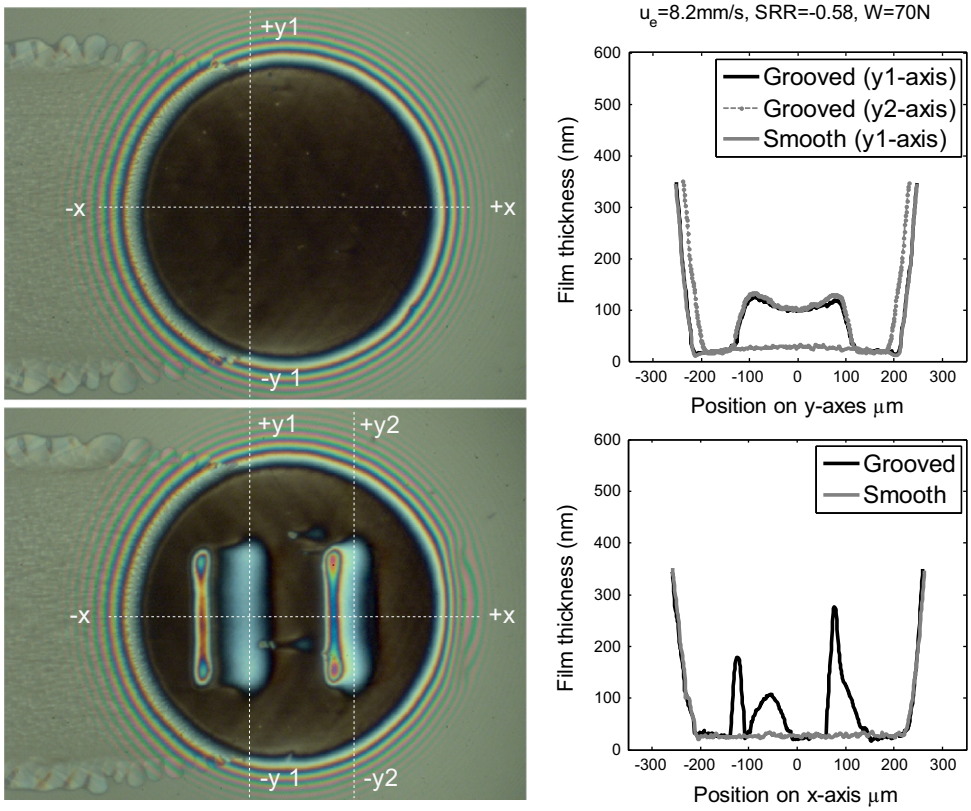

Fig. 8. Experimental comparison of the micro-grooves effects on film thickness under thin film conditions.

reflow to the depleted track [32,33]. Fig. 9 depicts the behavior of transverse limited micro-grooves under starvation. The available amount of lubricant was only 8 μl with entraining speed $u_e=67$ mm s^{-1}, SRR$=-1.96$ and load $w=63$ N. In this case, the corresponding maximum Hertzian pressure and contact radius are 0.653 GPa and 215 μm, respectively. The interferometry images shown in Fig. 9 have been captured in the 20th minute after the start. Starvation can be easily observed from the oil–air meniscus in the inlet of the contact. The inlet cavitation is caused by the high speed and low amount of oil on the track. Indeed, these conditions with the high value of SRR$=-1.96$ represent extreme operating condition for EHL contacts. Although the contact is starved, Fig. 9 shows that the transverse limited grooves are able to act as oil reservoirs and the film thickness of grooved surface is larger than that for smooth surface. The enhancement of film thickness on the trailing edges of grooves is shown in Fig. 9 along longitudinal sections A–A and B–B. However, acting as oil reservoirs means that the micro-grooves are filled repeatedly with lubricant. But the micro-grooves are depleted after leaving the contact and the mechanism of replenishment is insufficient since the speed is high and the oil amount is very little. Probably, the depleted micro-grooves have been filled with fresh lubricant in the inlet zone by the capillary forces and/or by inducing some kind of local flow reconditioning. Jacod et al. [32] showed that the mechanism of capillary forces generates significant flows in the vicinity of the contact under starved lubrication. In addition, Scaraggi [34] showed that optimized patterns of surface textures induce a local flow reconditioning.

Dumont et al. [19] predicted in their numerical study that the emitted lubricant from micro-pits leads to enlarge the distance between the oil–air meniscus and the Hertzian contact. Nevertheless, Fig. 9 shows that the position of the oil–air meniscus is similar for smooth and grooved surfaces although the amount of emitted lubricant by micro-grooves is important. If micro-features (grooves, dents, pits) are filled in the inlet zone by capillary forces not by replenishment, then the emitted lubricant from one micro-groove

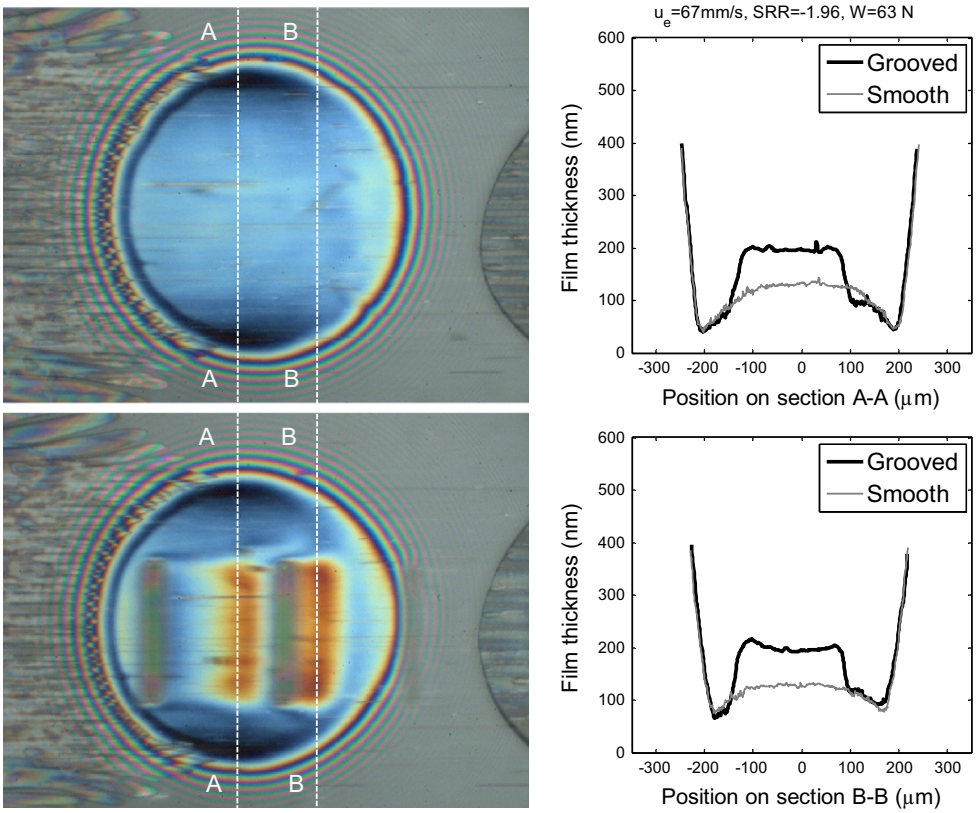

Fig. 9. Experimental comparison of the micro-grooves effects on film thickness under starved conditions.

will be absorbed by the next depleted micro-groove. Consequently, the available amount of lubricant will be stable in the inlet zone without changing the position of the inlet oil–air meniscus.

4.4. Limited micro-grooves in reciprocating motion

This section shows a comparison of the tribological performance of smooth and micro-grooved surfaces in the reciprocating motion under a constant load of 70 N. The corresponding maximum Hertzian pressure and contact radius are 0.68 GPa and 222 μm, respectively. The parameters of this reciprocating motion are explained in Section 3. The film thickness and friction are measured by optical interferometry technique and a torque sensor, respectively. The results show that the behavior of micro-textures varies significantly according to the direction of motion and the relative speed of mating surfaces. Fig. 10 shows a reduction of friction amplitude to about 20% by introducing the limited micro-grooves on the surface of the ball as shown in Fig. 4. It is clear that the textured distance (1.8 mm) is shorter than the length of stroke (3.55 mm) of reciprocating motion. Thus, there are no grooves at points of zero ($u_{ball}=0$and $u_e=0$). In order to understand the mechanism of friction reduction, the film thickness has been measured in points A and B, see Fig. 3. The values of entraining speeds (u_e) and slide-to-roll ratio (SRR) in points A and B are shown in Fig. 3. From Figs. 11 and 12, it can be stated that shallow micro-grooves enhance the film thickness in positions where the sliding speed is high, particularly, in the reverse motion phase (ball and disk have opposite directions). The propagation of emitted lubricant becomes larger in the reverse phase due to the high value of SRR since the high SRRs lead to a larger shear flow. The flow in EHL conjunctions is dominated basically by the shear flow not by the pressure flow due to the very high viscosity [35]. Therefore the propagation and the extraction of oil from micro-grooves is influenced by the kinematics conditions, particularly,

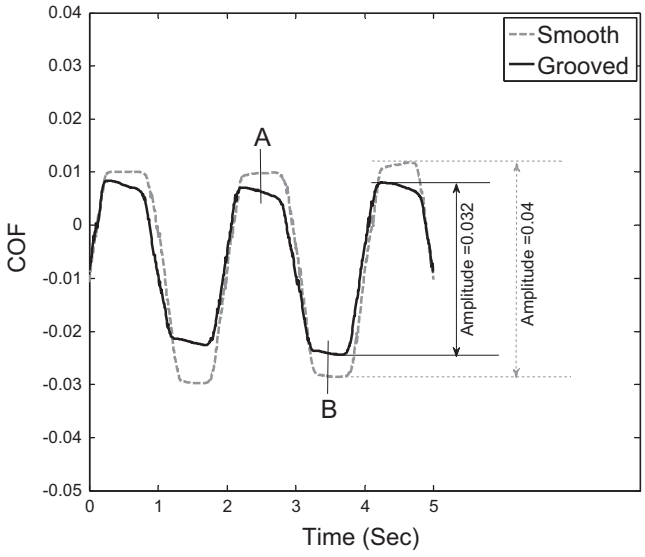

Fig. 10. Friction coefficient comparison for smooth and micro-grooved surfaces in reciprocating motion.

SRR [36]. The behavior of transverse limited micro-grooves in reverse motion has been explained profoundly by the authors in reference [37]. The authors believe that the reduction of the coefficient of friction results from the thick film exhausted from the grooves, not by the decrease of area contact. In the boundary and mixed lubrication regime, the decrease of area contact by micro-features could reduce friction since roughness of mating surfaces is in direct contact. For sliding EHL conditions, friction is caused basically by the shear stress in the fluid squeezed between the rubbing surfaces. Thus, any enhancement of film thickness results in reducing the hydrodynamic shear stress. On the other

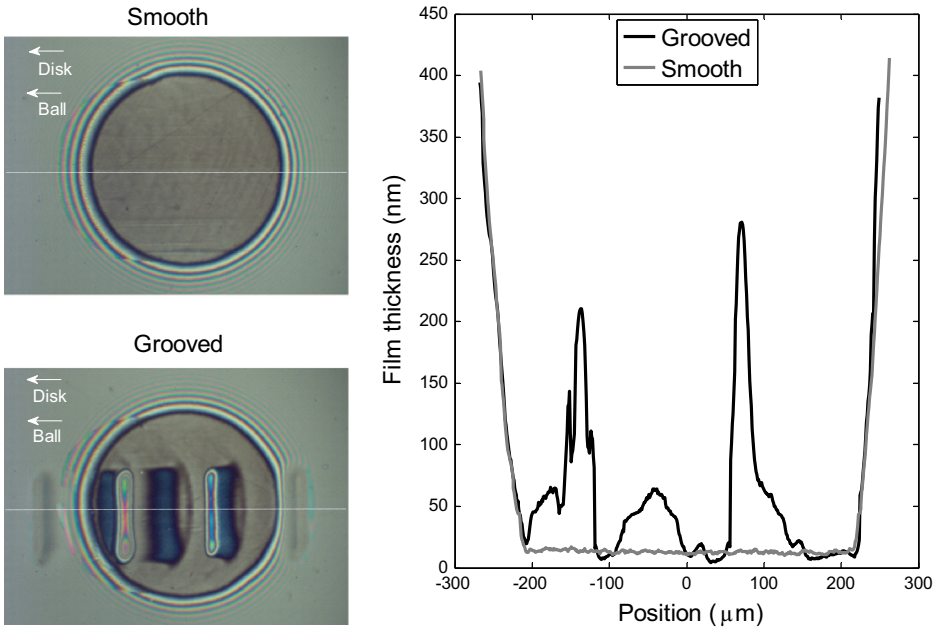

Fig.11. Film thickness comparison for smooth and micro-grooved surfaces in point A.

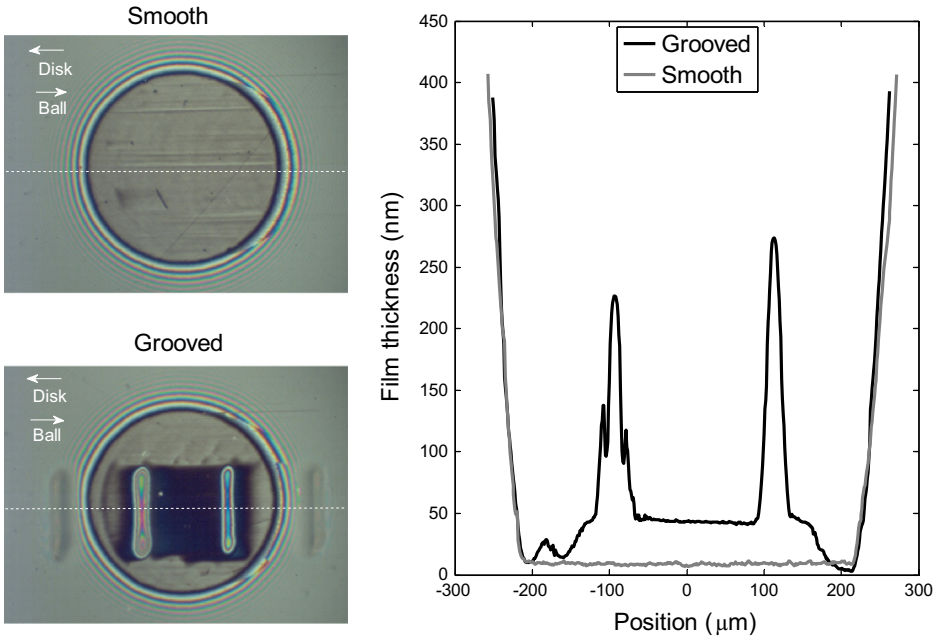

Fig.12. Film thickness comparison for smooth and micro-grooved surfaces in point B.

hand, as shown in Figs. 5 and 6, the pressure at the position of groove is low and that at both the edges of groove is high, so that the authors think that the effect of pressure on the coefficient of friction is not so large.

5. Conclusion

The behavior of transverse limited micro-grooves in EHL point contacts has been investigated in this study. The film thickness was measured for smooth and grooved surfaces in sliding motion under different conditions (thin films due to low speed and under starvation). Friction and film thickness have been compared for smooth and grooved surfaces under reciprocating motion. The significance of this study can be concluded by the following points:

- The transient behavior of transverse limited micro-grooves is numerically simulated in good agreement with experimental measurements.
- Micro-grooves act as powerful oil reservoirs when they are introduced on the surface as closed texture cells with length less than the diameter of Hertzian contact.
- Transverse limited micro-grooves enhance significantly the film thickness of EHL contacts under thin film and starved conditions.
- Surfaces with transverse limited micro-grooves show less friction and larger film thickness in reciprocation motion compared to smooth surfaces.

Acknowledgments

This research was carried out under the project NETME CENTRE PLUS (LO1202) with financial support from the Ministry of Education, Youth and Sports (LO1202) under the "National Sustainability Programme I" and Project P101/11/1115 from Czech Science Foundation. The authors would like to express their thanks to Prof. Jing Wang of Qingdao Technological University for her valuable discussion on this work.

References

[1] Wedeven LD, Cusano C. Elastohydrodynamic film thickness measurements of artificially produced surface dents and grooves. ASLE Trans 1979;22:369–81.
[2] Cusano C, Wedeven LD. Elastohydrodynamic film thickness measurements of artificially produced nonsmooth surfaces. ASLE Trans 1980;24:1–14.
[3] Jackson A, Cameron A. An interferometric study of the EHL of rough surfaces. ASLE Trans 1975;19:50–60.
[4] Suh M-s, Chae Y-h, Kim S-s, Hinoki T, Kohyama A. Effect of geometrical parameters in micro-grooved crosshatch pattern under lubricated sliding friction. Tribol Int 2010;43:1508–17.
[5] Pettersson U, Jacobson S. Friction and wear properties of micro textured DLC coated surfaces in boundary lubricated sliding. Tribol Lett 2004;17:553–9.
[6] Pettersson U, Jacobson S. Textured surfaces for improved lubrication at high pressure and low sliding speed of roller/piston in hydraulic motors. Tribol Int 2007;40:355–9.
[7] Yuan S, Huang W, Wang X. Orientation effects of micro-grooves on sliding surfaces. Tribol Int 2011;44:1047–54.
[8] Costa HL, Hutchings IM. Hydrodynamic lubrication of textured steel surfaces under reciprocating sliding conditions. Tribol Int 2007;40:1227–38.
[9] Nakano M, Korenaga A, Korenaga A, Miyake K, Murakami T, Ando Y, et al. Applying micro-texture to cast iron surfaces to reduce the friction coefficient under lubricated conditions. Tribol Lett 2007;28:131–7.
[10] Nakano M, Miyake K, Korenaga A, Sasaki S, Ando Y. Tribological properties of patterned NiFe-covered Si surfaces. Tribol Lett 2009;35:133–9.
[11] Kaneta M, Nishikawa H. Local reduction in thickness of point contact EHL films caused by transversely oriented moving groove and its recovery. ASME J Tribol 1994;116:635–9.
[12] Kaneta M, Nishikawa H, Kanada T, Matsuda K. Abnormal phenomena appearing in EHL contacts. ASME J. Tribol 1996;118:886–92.
[13] Yang P, Cui J, Kaneta M, Nishikawa H. Influence of a surface bump or groove on the lubricating performance and dimple phenomena in simple sliding point EHL contacts. Trans ASME J Tribol 2004;126:466–72.
[14] Scaraggi M, Mezzapesa FP, Carbone G, Ancona A, Tricarico L. Friction properties of lubricated laser-microtextured-surfaces: an experimental study from boundary- to hydrodynamic lubrication. Tribol Lett 2013;49:117–25.
[15] Jiang X, Hua DY. A mixed elastahydrodynamic lubrication model with asperity contact. J Tribol—T ASME 1999;121:481–91.
[16] Nanbu T, Yasuda Y, Ushijima K, Watanabe J, Zhu D. Increase of traction coefficient due to surface microtexture. Tribol Lett 2008;29(2):105–18. http://dx.doi.org/10.1007/s11249-007-9287-9.
[17] Yang P, Cui J, Jin ZM, Dowson D. Influence of two-sided surface waviness on the EHL behavior of rolling/sliding point contacts under thermal and non-newtonian conditions. J Tribol 2008;130:041502 (12 pp.).
[18] Yagi K, Kyogoku K, Nakahara T. Measurements of temperature distributions around longitudinally grooved rough surface in sliding elastohydrodynamic point contacts,. Tribol Trans 2006;49(4):482–9.
[19] Dumont ML, Lugt PM, Tripp JH. Surface feature effects in starved circular EHL contacts. Trans ASME J Tribol 2002;124:358–66.
[20] Ali F, Křupka I, Hartl M. An approximate approach to predict the degree of starvation in ball-disk machine based on the relative friction. Tribol Trans 2013;56(4):681–6. http://dx.doi.org/10.1080/10402004.2013.781722.
[21] Ai X, Lee SC. Effect of slide-to-roll ratio on interior stresses around a dent in EHL contacts. Tribol Trans 1996;39:881–9.
[22] Nelias D, Ville F. Detrimental effects of debris dents on rolling contact fatigue. ASME J Tribol 2000;122:55–64.
[23] Coulon S, Jubault I, Lubrecht AA, Ville F, Vergne P. Pressure profiles measured within lubricated contacts in presence of dented surfaces. Comparison with numerical models. Tribol Int 2004;37:111–7.
[24] Zhai X, Chang L, Hoeprich MR, Nixon HP. On mechanisms of fatigue life enhancement by surface dents in heavily loaded rolling line contacts. Tribol Trans 1997;40:708–14.
[25] Akamatsu Y, Tsushima N, Goto T, Hibi K. Influence of surface roughness skewness on rolling contact fatigue life. Tribol Trans 1992;35:745–50.
[26] Vrbka M, Samanek O, Sperka P, Navrat T, Krupka I, Hartl M. Effect of surface texturing on rolling contact fatigue within mixed lubricated non-conformal rolling/sliding contacts. Tribol Int 2010;43:1457–65.
[27] Dowson D, Higginson GR. Elastohydrodynamic lubrication. Oxford: Pergamon; 1966.
[28] Roelands CJA, Vlugter JC, Waterman HI. The viscosity–temperature–pressure relationship of lubricating oils and its correlation with chemical constitution. ASME J Fluids Eng 1963;85:601–7.
[29] Venner CH, Lubrecht AA. Multilevel methods in lubrication. Amsterdam: Elsevier; 2000.
[30] Hartl M, Krupka I, Poliscuk R, Liska M, Molimard J, Querry M, et al. Thin film colorimetric interferometry. Tribol Trans 2001;44:270–6.
[31] Gershuni L, Larson MG, Lugt PM. Lubricant replenishment in rolling bearings contacts. STLE Tribol Trans 2008;5(5):643–51. http://dx.doi.org/10.1080/10402000802192529.
[32] Jacod, B, Publier, F, Cann, PM, Lubrecht, AA. An analysis of track replenishment mechanisms in the starved regime. In: Proceedings of the 25th Leeds–Lyon symposium on tribology; 1999. p. 483–92.
[33] Ali F, Krupka I, Hartl M. Enhancing the parameters of starved EHL point conjunctions by artificially induced replenishment. Tribol Int 2013;66:134–42.
[34] Scaraggi, Michele. Partial surface texturing: a mechanism for local flow reconditioning in lubricated contacts. Proc Inst Mech Eng Part J: J Eng Tribol 2014. 1350650114539935.
[35] Venner CH. Multilevel solution of the EHL line and point contact problems. (Ph.D.thesis). Netherlands: Twente University; 1991.
[36] Kaneta M, Kanada T, Nishikawa H. Optical interferometric observations of the effects of a moving dent on point contact EHL. Tribology series, vol. 32. Amsterdam: Elsevier; 1997 p. 69–79.
[37] Ali Fadi, Ivan Křupka, Martin Hartl. Reducing the friction of lubricated nonconformal point contacts by transverse shallow micro-grooves. Proc Inst Mech Eng Part J: J Eng Tribol 2014. 1350650114543317.